To the Graduate Council:

I am submitting herewith a dissertation written by Youn Eung Lee entitled "Process Property Studies of Melt Blown Thermoplastic Polyurethane Polymers." I have examined the final electronic copy of this dissertation for form and content and recommend that it be accepted in partial fulfillment of the requirements for the degree of Doctor of Philosophy, with a major in Materials Science and Engineering.

Larry C. Wadsworth
Major Professor

We have read this dissertation
and recommend its acceptance:

Randy Bresee

Gajanan Bhat

Roberto Benson

Donald W. Dareing

Accepted for the Council:
Anne Mayhew
Vice Chancellor and Dean of
Graduate Studies

(Original signatures are on file with additional student records.)

PROCESS PROPERTY STUDIES OF MELT BLOWN THERMOPLASTIC POLYURETHANE POLYMERS

A Dissertation
Presented for the
Doctor of Philosophy
Degree
The University of Tennessee, Knoxville

Youn Eung Lee
August 2004

ACKNOWLEDGEMENTS

I would like to thank all those who helped me to achieve the Doctor of Philosophy degree in Textile Science program. I would like to express my deepest appreciation to Dr. Larry C. Wadsworth for his precious guidance and encouragement in the past three years as my major professor. I wish to thank to Dr. Randy Bresee, Dr. Gajanan Bhat, Dr. Robert Benson, and Dr. Donald W. Dareing for taking time to serve on my committee and the helpful suggestions during this research.

I am also very thankful to the TANDEC faculty and engineers for their valued assistances and suggestions: Dr. David Garner, Dr. Allen Stahl, Dr. Peter Tsai, Dr. Dong Zhang, Dr. Christine Sun, Mr. Van Brantley, Mr. James Murphy, Mr. Jack Wyrick, Mr. Chris Eash and Mrs. Lisa Salamie.

I would like to give my special thanks to Dr. Chang Whan Joo for his inestimable assistances and advice for my resolutions. The financial supports from the University of Tennessee are most greatly appreciated. Finally, I would like to thank my family for enormous support, sacrifices and understanding. Without family's special encouragement, this work would have taken a substantially longer time for completion.

ABSTRACT

The primary goal of this research was to determine optimum processing conditions to produce commercially acceptable melt blown (MB) thermoplastic polyurethane (TPU) webs. The rheological/thermal properties of TPU pellets and the morphological/mechanical properties of MB TPU fibers and webs were characterized by Advanced Rheometric Expansion System (ARES), Differential Scanning Calorimetry (DSC), Fourier Transform Infrared Spectroscopy (FTIR) and etc.

The 6-inch MB line and the 20-inch wide Accurate Products MB pilot line at the Textiles and Nonwovens Development Center (TANDEC), The University of Tennessee, Knoxville, were utilized for this study. Preliminary MB studies were performed with Noveon ESTANE® 58277 on the 6-inch MB line to identify some of the process-properties relationships that needed to be addressed in this dissertation.

The MB TPU trials were performed in four different phases: Phase 1 focused on the envelope of the MB operating conditions for different TPU polymers; Phase 2 focused on the production of commercially acceptable MB TPU webs; Phase 3 focused on the optimization of the processing conditions of MB TPU webs, and the determination of the significant relationships between processing parameters and web properties utilizing statistical analyses; Based on the first three phases, a more extensive study of fiber and web formation in the MB TPU process was made and a multi liner regression model for the MB TPU process versus properties was also

developed in Phase 4.

The first phase (Phase 1) of the MB studies in this dissertation was performed with one polyester-based TPU polymer: ESTANE® 58238 (TPU_{238}) and three different polyether-based TPU polymers: ESTANE® 58237 (TPU_{237}), ESTANE® 58245 (TPU_{245}) and ESTANE® 58280 (TPU_{280}) on the 6-inch MB line. Based on the results of 6-inch MB line trials, TPU_{245} and TPU_{280} were melt blown on the 20-inch line in the first phase of this research. However, both webs were coarse with large fiber diameters and the webs were spotty in appearance.

Based on the knowledge of MB TPU processing in Phase 1, MB TPU webs, which had improved uniformity and better mechanical properties than Phase 1, were achieved in the next phase of the 20-inch MB line trials (Phase 2) with TPU_{245} and TPU_{280}.

In Phase 3, uniform webs of MB TPUs were produced having good mechanical properties in the 20-inch MB line trials with TPU_{245} and TPU_{280}. The MB TPU fibers and webs from the spinneret were characterized by DSC, FTIR, SEM (scanning electron microscope), optical microscopy and etc.

In Phase 4, the fiber and web formation study of the MB TPU process was expanded to include fiber diameter, fiber orientation and fiber entanglement of MB TPUs depending on DCD. Furthermore, the velocity of MB TPU fiber in the spin-line was estimated based on the air velocity and air temperature. In addition, multi liner regression models were introduced to optimize the MB TPU process for predicting

and evaluating MB TPU fiber and web properties.

In conclusion, the basic MB process was fundamentally valid for the MB TPU process; however, the MB process was more complicated for TPU than PP, because web structures and properties of MB TPUs are very sensitive to MB process conditions: Furthermore, different TPU grades responded very differently to MB processing and exhibited different web structure and properties.

In Phase 3 and Phase 4, small fiber diameters of less than 5μm were produced from TPU_{237}, TPU_{245} and TPU_{280} pellets, and the mechanical strengths of MB TPU webs including the tensile strength, tear strength, abrasion resistance and tensile elongation were notably good. In addition, the statistical model showed useful interaction regarding trends for processing parameters versus properties of MB TPU webs. Die and air temperature showed multicollinearity (a case of multiple regression in which the predictor variables are themselves highly correlated) problems and fiber diameter was notably affected by air flow rate, throughput and die/air temperature. It was also shown that most of the MB TPU web properties including mechanical strength, air permeability and fiber diameters were affected by air velocity and die temperature.

TABLE OF CONTENTS

CHAPTER 1: INTRODUCTION …….. 1

1.1 The Background ……1

1.2 The Goal of This Research ……... 3

CHAPTER 2: LITERATURE REVIEW …….. 7

2.1 Thermoplastic Polyurethane Elastomer …… 7

2.2 Rheology ……...16

2.3 Melt Blowing Process …….. 21

2.4 Modeling and Analyses of MB Process Using

Statistical Methods ……28

CHAPTER 3: EXPERIMENTAL ……..... 33

3.1 Phase 1 …… 33

3.1.1 Preliminary Research ….…….....33

3.1.2 The 6-inch and 20-inch MB Line Trials ……... 36

3.2 Phase 2 ……... 38

3.3 Phase 3 ……... 41

3.4 Phase 4 …… 44

3.4.1 Fiber and Web Formation Studies …… 44

3.4.2 The 20-inch MB Line Trials ……..... 45

3.5 Polymer Materials ……..... 52

3.6 Characterizations of Polymer Resins ……53

3.6.1 Viscoelastic Properties…..……..53

3.6.2 Differential Scanning Calorimetry ..…….....54

3.7 Characterizations of Fiber and Web ……..55

3.7.1 Fiber Diameter ….……. 55

3.7.2 Fiber Bundle Size and Orientation ……56

3.7.3 Basis Weight and Thickness ……..57

3.7.4 Air Permeability ….…….. 57

3.7.5 Tensile Strength and Elongation ……..... 57

3.7.6 Abrasion Resistance ……..58

3.7.7 Fourier Transform Infrared Spectroscopy ……..... 58

CHAPTER 4: RESULTS AND DISCUSSION …….....60

4.1 Phase 1 …….. 60

4.1.1 Preliminary Research …… 60

4.1.2 The 6-inch and 20-inch MB Lines …… 60

4.2 Phase 2 ……..... 61

4.3 Phase 3 …….. 68

4.3.1 Rheological Properties of Polymers …….....68

4.3.2 Thermal Properties of Polymers

and MB Webs ……77

4.3.3 Molecular Compositions of MB TPU Webs …..... 81

4.3.4 Mechanical Properties of
MB TPU Fibers and Webs ……..... 88
4.4 Phase 4 …….. 106
4.4.1 Fiber and Web Formation Studies ……106
4.4.2 Mechanical Properties of
MB TPU Fibers and Webs …… 118
4.4.3 Multi Liner Regression Models ……..... 167
CHAPTER 5: CONCLUSIONS AND RECOMMENDATIONS ……..... 182
REFERENCES …….....186
APPENDICES ……...…….....193
APPENDIX I …… 194
APPENDIX II …..…….....203
APPENDIX III ……...218
VITA …….....240

LIST OF TABLES

Table 3-1. Melt blown processing conditions of first trials on the 6-inch and 20-inch line in Phase 1 ……..... 37

Table 3-2. Melt blown processing conditions of second trials on the 20-inch line in Phase 2 ……..... 40

Table 3-3. Melt blown processing conditions on the 20-inch line in Phase 3 ……..... 43

Table 3-4. Melt blown processing conditions of TPU_{237} on the 20-inch line in Phase 4 ……..... 46

Table 3-5. Melt blown processing conditions of TPU_{245} on the 20-inch line in Phase 4 ……..... 47

Table 3-6. Melt blown processing conditions of TPU_{280} on the 20-inch line in Phase 4 ……..... 48

Table 4-1. Melt blown web properties of the 20-inch line in Phase 2 63

Table 4-2. Melt blown web properties of the 20-inch line in Phase 3 …..... 89

Table 4-3. Abrasion resistance of MB TPU webs ……..... 103

Table 4-4. Melt blown web properties of TPU_{237} on the 20-inch line in Phase 4 …… 122

Table 4-5. Melt blown web properties of TPU_{245} on the 20-inch line in Phase 4 ……..... 123

Table 4-6. Melt blown web properties of TPU_{280} on the 20-inch line in Phase 4 124

LIST OF FIGURES

Figure 2-1. Schematic diagram of TPUs composed of diisocyanate, long-chain diol and chain extender …….. 8

Figure 2-2. Structures of the diisocyanates ……..... 10

Figure 2-3. Schematic representations of polyurethane structures at various temperatures ……..... 12

Figure 2-4. Schematic diagram of cross-section of coat-hanger type die …..... 23

Figure 3-1. The schematic diagram of air gap and setback in an MB die …... 35

Figure 3-2. Schematic diagram of the 20-inch Accurate MB Products line …….. 39

Figure 3-3. The experimental design for TPU_{237} ……..…….. 49

Figure 3-4. The experimental design for TPU_{245} ……..…….. 50

Figure 3-5. The experimental design for TPU_{280} ……..…….. 51

Figure 4-1. Optical fiber diameters of MB TPU_{245} webs depending on the volumetric air flow rate …….. 67

Figure 4-2. Apparent viscosity of TPU resins depending on the apparent shear rates …….....69

Figure 4-3. Storage and loss modulus (G' and G") depending on angular velocity of TPU resins ……..... 71

Figure 4-4. Tangent delta ($\tan\delta$) depending on angular velocity of TPU resins 73

Figure 4-5. Complex viscosity depending on angular velocity of TPU resins 76

Figure 4-6. DSC curves of TPU pellets 78

Figure 4-7. DSC curves of MB TPU webs 80

Figure 4-8. FTIR spectra from the middle of the MB TPU_{245} web..... 82

Figure 4-9. FTIR spectra from the edge of the MB TPU_{245} web..... 85

Figure 4-10. FTIR spectra from the middle of the MB TPU_{280} web..... 86

Figure 4-11. FTIR spectra from the edge of the MB TPU_{280} web..... 87

Figure 4-12. Relationship between time and pressure after pump for TPU_{245} and TPU_{280} 91

Figure 4-13. Relationship between the volumetric air flow rate and fiber diameter of TPU_{245} and TPU_{280} 92

Figure 4-14. The morphological features of TPUs 94

Figure 4-15. Relationship between the volumetric air flow rate and basis weight of TPU_{245} and TPU_{280} 95

Figure 4-16. Relationship between basis weight and thickness and air permeability of TPUs 97

Figure 4-17. Relationship between basis weight and tear strength and tensile strength of TPUs 99

Figure 4-18. MB TPU_{280} and MB PP specimens after abrasion ……. 102

Figure 4-19. Loss in peak tensile force of MB TPU webs after abrasion …….. 104

Figure 4-20. Cycling test of extension and relaxation ……..... 107

Figure 4-21. Air temperature and velocity profiles
at various DCDs 109

Figure 4-22. The air/fiber velocity of MB PP and TPU process
at various DCDs 112

Figure 4-23. The MB TPU fibers collected at various DCDs
with maximum speed (100mpm) of collector …… 113

Figure 4-24. The fiber diameters of MB TPU_{280} webs collected
at various DCDs ……. 115

Figure 4-25. The optical microscopy of MB TPU_{280} fiber bundle
collected at various DCDs ……..... 116

Figure 4-26. The mean fiber bundle diameter of MB TPU_{280} collected
at various DCDs …… 117

Figure 4-27. Fiber diameter and coefficient of variation of MB TPU_{280}
collected at various DCDs ……..119

Figure 4-28. The mean fiber bundle angle of MB TPU_{280} collected
at various DCDs ……. 120

Figure 4-29. The mean fiber bundle degree and MD/CD ratio of MB TPU_{280}
collected at various DCDs ……..121

Figure 4-30. The fiber diameter and air permeability of MB TPU_{237} webs produced by various die temperatures……..... 127

Figure 4-31. The tear and tensile strength of MB TPU_{237} webs produced by various die temperatures ……..... 129

Figure 4-32. The fiber and web properties of MB TPU_{237} webs produced with various extrusion rates ……... 131

Figure 4-33. The tear and tensile strength of MB TPU_{237} webs produced with various extrusion rates……..... 132

Figure 4-34. The fiber and web properties of MB TPU_{237} webs produced at various air temperatures…….. 133

Figure 4-35. The tear and tensile strength of MB TPU_{237} webs produced at various air temperatures…….. 134

Figure 4-36. The fiber and web properties of MB TPU_{237} webs produced with various air velocities……..... 136

Figure 4-37. The tear and tensile strength of MB TPU_{237} webs produced with various air velocities……..... 137

Figure 4-38. The fiber diameter and air permeability of MB TPU_{237} webs collected at various DCDs ……..139

Figure 4-39. The tear and tensile strength of MB TPU_{237} webs collected at various DCDs.....140

Figure 4-40. The fiber diameter and air permeability of MB TPU_{245} webs produced by various die temperatures……..... 142

Figure 4-41. The fiber and web properties of MB TPU_{245} webs produced with various extrusion rates ……... 143

Figure 4-42. The tear and tensile strength of MB TPU_{245} webs produced with various extrusion rates ……..... 145

Figure 4-43. The fiber and web properties of MB TPU_{245} webs produced at various air temperatures…….. 146

Figure 4-44. The tear and tensile strength of MB TPU_{245} webs produced at various air temperatures…….. 148

Figure 4-45. The fiber and web properties of MB TPU_{245} webs produced with various air velocities ……..... 149

Figure 4-46. The tear and tensile strength of MB TPU_{245} webs produced with various air velocities ……..... 150

Figure 4-47. The fiber and web properties of MB TPU_{245} collected at various DCDs ……..152

Figure 4-48. The tear and tensile strength of MB TPU_{245} webs collected at various DCDs.....153

Figure 4-49. The fiber diameter and air permeability of MB TPU_{280} webs produced by various die temperatures ……..... 154

Figure 4-50. The tear and tensile strength of MB TPU_{280} webs produced by various die temperatures ……..... 156

Figure 4-51. The fiber and web properties of MB TPU_{280} webs produced with various extrusion rates ……... 157

Figure 4-52. The tear and tensile strength of MB TPU_{280} webs produced with various extrusion rates ……..... 158

Figure 4-53. The fiber and web properties of MB TPU_{280} webs produced at various air temperatures…….. 160

Figure 4-54. The tear and tensile strength of MB TPU_{280} webs produced at various air temperatures…….. 161

Figure 4-55. The fiber and web properties of MB TPU_{280} webs produced with various air velocities ……..... 162

Figure 4-56. The tear and tensile strength of MB TPU_{280} webs produced with various air velocities ……..... 164

Figure 4-57. The fiber diameter and air permeability of MB TPU_{280} webs collected at various DCDs ……..165

Figure 4-58. The tear and tensile strength of MB TPU_{280} webs collected at various DCDs..... 166

Figure 4-59. Prediction profiles of MB TPUs basis weight depending on the processing conditions ……... 169

Figure 4-60. Prediction profiles of MB TPUs air permeability depending on the processing conditions …….. 172

Figure 4-61. Prediction profiles of MB TPUs fiber diameters depending on the processing conditions …….. 174

Figure 4-62. Prediction profiles of MB TPUs tear strength depending on the processing conditions …….. 176

Figure 4-63. Prediction profiles of MB TPUs peak tensile force depending on the processing conditions ……...178

Figure 4-64. Prediction profiles of MB TPUs peak elongation depending on the processing conditions …….. 180

CHAPTER 1

INTRODUCTION

1.1 The Background

Melt blowing is a one-step process and one of the most practical processes for producing microfiber nonwovens directly from thermoplastic polymers, in which hot/high velocity air blows the extruded filament from a die tip towards moving a conveyer belt on a cylinder. Melt blown (MB) nonwovens have an inherent advantage over spunbond (SB) nonwovens and other conventional fabrics made from melt or solution spun fibers in that MB fabrics typically have average fiber diameters ranging from 2-6μm compared to 12-50μm with SB webs and conventional textiles.

The concept of the MB process was first introduced in 1956 through a Naval Research Laboratory project initiated by Van. A. Wente [1956]. MB technology was originally developed to produce filters composed of microfibers to collect radioactive particles from the atmosphere during the early years of the cold war. Since then there has been a renaissance of research, development and commercial production in the past few years for addressing a variety of applications using MB fabrics in the nonwoven products.

Zhao [2001] reported that only 20 US Patents were granted from 1950s to 1970s related to MB technologies and products, but the numbers of patents have remarkably increased to 64 and 236 during the 1980s and 1990s, respectively. The

increased understanding and requirement for high technological end-uses have accelerated MB research and development, resulting in an increasing number of applications, such as filtration, thermal insulators, battery separators, oil absorbents, hygiene products and composites for protective apparel.

The most important advantage of the MB process is that fundamentally all thermoplastics polymers can be processed by MB technology [Wadsworth, 1991]. Recently, elastomers including thermoplastic polyurethane (TPU) have been a focus of MB research because of their unique properties such as high elasticity in all directions, good shore hardness for a given modulus, high abrasion/chemical resistance, excellent mechanical/elastic properties, low stress relaxation and resistance to long-term cyclic flex failure. Furthermore, TPUs have blood/tissue compatibility, structural versatility and hydrophilic compatibility [Hsieh, 1997].

Many processing methods such as melt spinning, injection molding, coating, film blowing, melt blowing and sealing work well with TPU materials. However, the consumption of TPU elastomers is still much less than conventional polyurethanes which must be solvent spun to produce fibers, because the melt spinning process of elastic fibers is more difficult than other polymers due to their tendency to snap back during attenuation of the spin-line [Wadsworth, 2002].

This is even more challenging with MB since the filaments are attenuated by aerodynamic skin friction and form drag, and the filaments may be discontinuous and are not positively held by a take-up spindle or nip while in flight to the collector. But

the fact that TPUs still can be melt spun into fibers makes them much more versatile for replacing natural rubber thread, solvent spun polyurethane, and other more conventional materials for use in biomedical devices, implants, medical applications, and protective clothing field [Wadsworth, 2002]. Furthermore, the products of MB TPU webs with average fiber diameters in the range of 2-6μm provide high filtration and barrier protection with the additional advantages such as good mechanical strength and stretchability.

1.2 The Goal of This Research

This research has concentrated on determining optimum processing conditions to produce commercially acceptable MB TPU webs for protective apparel and durable elastic textiles based on preliminary MB work performed at The University of Tennessee in cooperation with the U. S. Army Natick Soldier Center and Noveon Inc. [Wadsworth, 2002].

The MB process has many processing parameters such as melt/die temperature, throughput, die geometry, air flow rate, air temperature, die-to-collector distance (DCD) and collector speed. The MB TPU process to produce elastic and durable nonwoven fabric is even more complex in that high elongational viscosity, high shear viscosity and narrow acceptable processing temperature ranges in melt and air temperature versus thermal degradation, and in air and polymer flow rates must be taken into account.

Although numerous studies have been performed in determining the relationships between the MB process and product parameters of polyolefin polymers, additional studies were needed to understand the melt blowing of TPUs to make further improvements in MB TPU web performance properties.

In addition, response surface methodology (RSM) was applied in this research for determining the effect of multi-control variables for the response parameters with fewer experimental runs, and RSM has been demonstrated in other recent MB studies [Zhang, 2002].

The general forms of the RSM statistical model included mathematical terms, response variables and random errors. The predictors and coefficient parameters of the mathematical terms were observed along with the response variables and estimated during the modeling process, respectively.

The MB process parameters were designated as predictor variables, and the primary desired fiber/web properties of the MB nonwovens were selected as response variables in the statistical analysis for optimum results via the RSM process. For this research, five main processing parameters: polymer throughput (TP), die temperature (DT), air temperature (AT), airflow rate (AIR) and die-to-collector distances (DCD) were referred to as predictors. Fiber diameter and major web properties were taken as the responses.

In determining the random errors, the relationships between the predictor and response variables represents a statistical relation rather than a perfect deterministic

relation, because in addition to the major parameters such as melt/die temperature, polymer throughput, die geometry, air flow rate, air temperature, DCD and collector speed (CS), there are minor parameters which have not been considered in the statistical model such as moisture content of resins and unknown effects. Thus, the adjustment of variance between the statistical model and actual MB TPU process was calibrated by random errors.

The primary objectives of this dissertation are:

1. To study the rheological properties of TPU polymers, evaluate viscoelastic properties of TPUs such as steady shear viscosity, normal force, shear modulus, complex viscosity, storage modulus and loss modulus to provide more complete information concerning the melt extrusion process for improving MB TPUs processing.

2. To study the fiber formation of the MB TPU process, evaluate fiber diameter, fiber orientation, fiber entanglement and fiber crystallization depending on the DCD, air temperature and air velocity that will provide understanding of the MB TPU fiber formation process.

3. To study the web formation of the MB TPU process and investigate the effect

of operational conditions on MB TPU nonwovens properties. The extruded MB TPU webs from the spinneret were characterized by DSC, FTIR, SEM and optical microscopy. Analyses of chemical compositions, physical morphologies and mechanical properties included fiber diameter and tensile strength to provide information of MB TPU web formation.

4. To optimize the operational conditions of the MB TPU process by statistical analyses based on the information learned in accomplishing the first three objectives. The understanding of the essential interrelationship between predictors and responses variables of MB TPU process provided fundamental processing guidelines of TPU polymers for the desired MB fiber/web properties.

CHAPTER 2

LITERATURE REVIEW

2.1 Thermoplastic Polyurethane Elastomer

Thermoplastic polyurethane (TPU) elastomers were the first homogeneous, thermoplastically processable elastomers, and TPUs have been used in various engineering applications due to their advantageous mechanical properties such as elasticity, toughness, strength, and low temperature flexibility [Oertal, 1993].

The elastomeric properties of TPUs result from the arrangement of the soft and hard segments, and their elasticity is influenced by physical cross-linking and their hetero-phase microstructures. The soft segment is derived from flexible oligomers with low glass transition temperatures, thus the soft segments of TPUs are viscous at room temperature and impart flexibility to the TPUs. The hard segments function as a thermally reversible physical cross-linking mechanism between molecular domains, contributing to elasticity, mechanical strength, and dimensional stability to the TPUs. Typical compositions of TPU segments are presented on Figure 2-1 [Seymour, 1973].

Bruins [1969] noted that the essential properties of TPUs depend on the types of soft segments. Ester-based TPUs usually show better tensile/tear strength and abrasion/cut resistance than ether-based TPUs. Ester-based TPUs also swell less in oil, grease and water than ether-based TPUs.

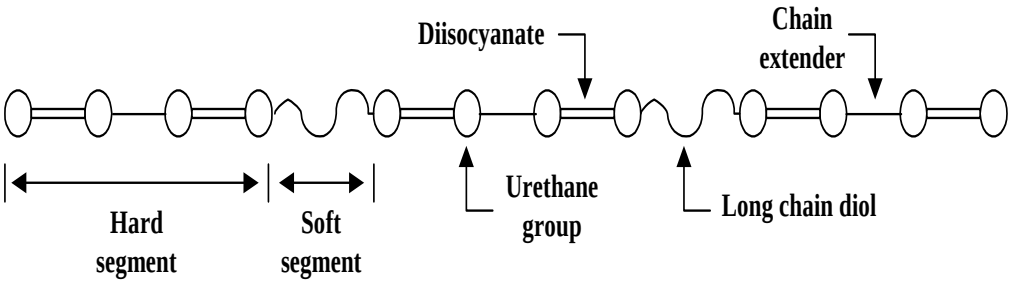


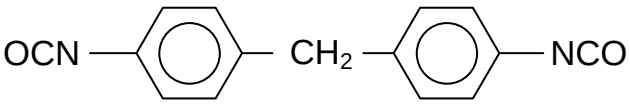
Figure 2-1. Schematic diagram of TPUs composed of diisocyanate, long-chain diol and chain extender [Oertal, 1993].

On the other hand, Dombrow [1965] noted that ether-based TPUs could be recommended if special properties such as resistance to hydrolysis and microbiological degradation or low-temperature flexibility are required.

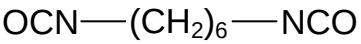
Szycher [1999] studied hard segments of TPUs, and provided fundamental information about diisocyanate and chain extenders. Szycher and his colleagues suggested that diphenylmethane-4,4'-diisocyanate (MDI) is the most important diisocyanate, and other diisocyanates such as hexamethylene diisocyanate (HDI), 3,3'-dimethyl-4,4'-biphenyl diisocyanate (TODI), 1,4-benzene diisocyanate, trans-cyclohexane-1,4-diisocyanate and 1,5-naphthalene diisocyanate (NDI) were also studied. Figure 2-2 shows the different structures of the diisocyanates for hard segments of TPUs.

For the morphological features of TPUs, Xiao and Frisch [1995] reported that hydrogen bonding between adjacent polymer chains significantly increases the physical properties of TPUs. Hydrogen bonding gives rise to a three-dimensional "virtually cross-linked" molecular domain structure. Inter-chain attractive forces between rigid segments are far greater than those present in the soft segments due to the high concentration of polar groups and the possibility of extensive hydrogen bonding.

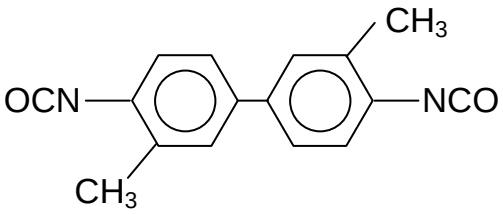
Cooper [1966] described that the strength and high elasticity of TPUs are due to hard domains stabilized by hydrogen bonding between hard segments and the degree of phase separation.



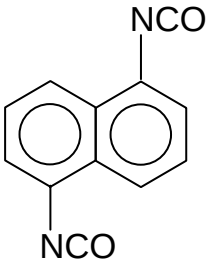
(a) diphenylmethane-4,4'-diisocyanate (MDI)



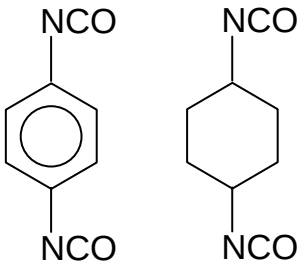
(b) hexamethylene diisocyanate (HDI)



(c) 3,3’-dimethyl-4,4’-biphenyl diisocyanate (TODI)



(d) 1,5-naphthalene diisocyanate (NDI)



(e) 1,4-benzene diisocyanate and trans-cyclohexane-1,4-diisocyanate,

Figure 2-2. Structures of the diisocyanates.

In the ether-based TPUs, hydrogen bonding between the N-H and C=O groups is first formed at the hard domain, and then hydrogen bonding of the N-H group is dispersed in the C-O-C group of the soft domain [Tanaka, 1968].

Lee [1987] studied the properties of hydrogen bonding about urethane functional groups using the Fourier transform infrared (FTIR) spectroscopic technique to better understand the phase separated structures of polyurethanes. As a function of temperature, IR spectra have been obtained for TPUs and unique spectroscopic features in the N-H and C=O stretching regions were found for rapidly cooled samples. Lee also reported the change of hydrogen bonding characteristics in soft and hard domains by the macroscopic phase transformations analysis as a function of temperature using Differential Scanning Calorimetry (DSC) and FTIR.

Schematic representations of phase separated morphology at three different temperatures are given in Figure 2-3, and characteristics of hydrogen bonded species are explained by Lee and his colleagues as each diagram depending on the temperature [1987].

By increasing the temperature above the melting point of the hard domain, homogeneous structure (Figure 2-3(b)) is obtained accompanied by the disassociation of the hard segment-hard segment hydrogen bonding.

If it is quenched, most of high-temperature structure is frozen resulting in a significant number of interactions between the hard and soft segments as shown Figure 2-3(c).

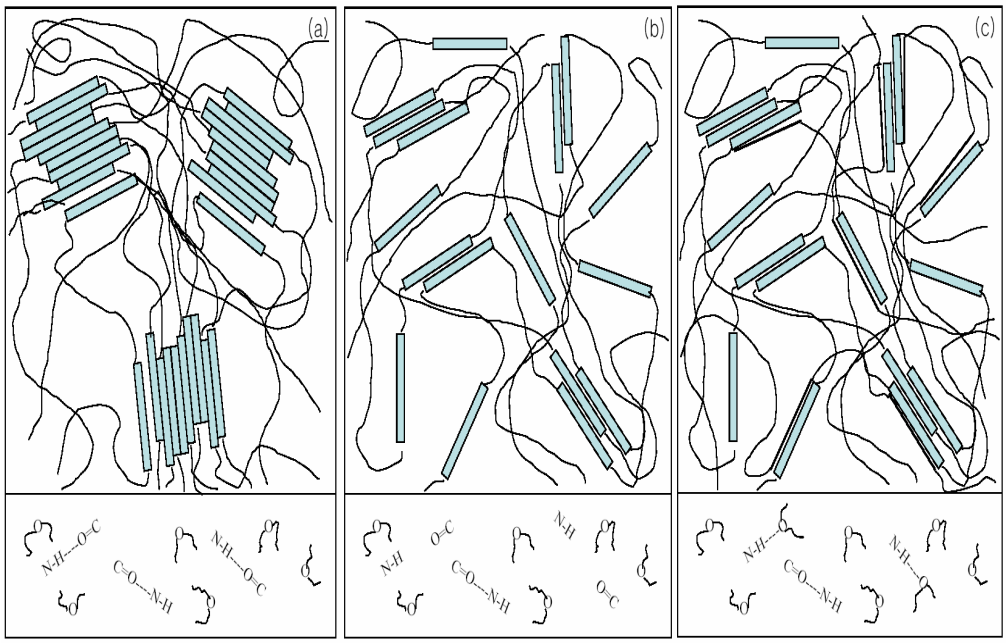


Figure 2-3. Schematic representations of polyurethane structures at various temperatures.

(a) Room temperature phase separated morphology,

(b) most disassociated structures at high temperature,

(c) dispersed phase “trapped” at extremely low temperature [Lee, 1987].

The low temperature structure below the glass transition temperature of the soft segment undergoes phase separation to a room temperature structure when the temperature is raised. In this way, direct correlation between microscopic evidence for hydrogen bonding characteristics in soft and hard domains and macroscopic phase transformation was obtained by Lee and his colleagues [1987]. Recently, studies of phase separation of the hard segment and soft segment in the TPUs have focused on more than hydrogen bonding studies because of the close relationship between mechanical and chemical properties of TPUs.

Seymour and Cooper [1973] described the thermal properties of polyurethane block polymers using DSC. A DSC endotherm in the region of 80^{o}C has been described as the dissociation of the urethane soft segment hydrogen bonds, while an endotherm around 150-170^{o}C is related to the breakup of inter-urethane hydrogen bonds. They found that the observed DSC endotherms result from short and long range ordering of the hard segments rather than from hydrogen-bond dissociation. The thermal behavior of the hydrogen bonds is insensitive to the degree of ordering and primarily affected above the glass transition temperature of the hard segments. The presence of hydrogen bonds serves to increase the overall cohesion of the materials, as hydrogen bonds are stronger and more directional than other intermolecular forces. The good mechanical properties of segmented polyurethanes must be attributed to the incompatibility of the segments resulting in phase separation rather than to the presence of hydrogen bonds [Seymour, 1973].

Interpretation of structure-property relationships should be placed more on the morphological analysis. Woods [1990] noted that phase separation of TPUs with soft segment materials that ether-based TPUs showed a higher degree of phase separation than the ester-based TPUs in his research because of the lower degree of compatibility of polyethers with MDI. As the chain length of the soft segments increases, phase separation increases in both ether- and ester-based TPUs.

On the other hand, Crawford and his colleagues [1998] studied the strain effects on thermal transitions and mechanical properties of TPU elastomers. In their research, strain aging disrupts the domain structure enough to cause a reduction in abrasion resistance. This disruption in the domain structure involved phase mixing concerned with hydrogen bonding taking place between the hard and soft domains, a breaking up of the hard domain microstructure and dispersion of hard segments within the soft domain, or plastic deformation of the hard domains. The strain effects indicated that it is possible that the ester- and ether- based polyurethanes exhibit different domain reordering mechanisms [Crawford, 1998].

The effect of hard and soft segment structure on tensile properties were more specifically studied by Petrovic and Ferguson [1991] and physical properties of TPUs such as high tensile strength and elongation were studied by Holden [1996]. Depending on their chemical structures and the types of chain extenders, the tensile strengths of TPUs vary from 25 to 70MPa. Comparison of the effect of diol chain extenders on tensile strength shows the order as follows: 1,4-butanediol (BD) >

ethanediol (ED) > 1,5-pentanediol > 1,6-hexanediol (HD) > 1,3-propanediol.

Li and his colleague [1992] provided information about thermal properties of TPUs, which can be used over a wide range of temperatures. The products made from TPUs can be used from –40^{o}C up to 80^{o}C for both long and short term applications. The hard segment is the main contributor to high service temperature performance of TPUs. However, the ratio of chain extenders to diisocyanate and types of chain extenders in hard segments greatly affect performance of TPUs at high temperature.

Hydroquinone bis (2-hydroxyethyl) ether yields TPUs with higher service temperature than BD or HD, and the type of diisocyanate also affects the high temperature performance. So, the hard segments produced from different diisocyanates and chain extenders show different melting points.

Processing studies of TPUs are described by Dieterich and Uhlig [2001]. TPUs easily become wetted; therefore, TPUs must be dried prior to processing. Moist granules should be dried at 100 to 110^{o}C in a circulating air oven or in a flash drier for 1 to 2 hours. The moisture content of the granules should be below 0.1 wt. %.

Hepburn [1982] reported some parameters for the injection molding process of TPUs such as compression ratio, screw speed and processing temperatures. Hepburn also strongly cautioned about overheating during the process. If the TPU polymers are processed above 230^{o}C, which is above the normal processing range (170–220^{o}C), the polymers quickly degrade and loose their mechanical properties. Volatiles evolved during overheating, combustion, or decomposition have not been

fully determined, but would be expected to be a primary hazard because these gases may include irritating or toxic substances such as CO, CO_2, hydrogen cyanide, oxides of nitrogen, hydrocarbons, isocyanates, and water vapor.

Much research has been performed for modifying mechanical properties of TPUs. Koichi [1983] disclosed soft resinous compositions containing 5 to 70 wt. % TPU and 30 to 95% of polyolefins modified with functional groups such as carboxyl, carboxylic acid anhydride, carboxylate salt, hydroxyl and epoxy. This leads to their prime utility in the coextrusion, extrusion coating, extrusion laminating of polymer laminates.

Hlavacek and Wolf [1975] showed that blends of 80:20 to 20:80 weight ratio of chlorinated polyethylenes with polyurethanes result in improved processibility, particularly in the manufacture of films or sheets by milling or calendering, and these blends are more economical than polyurethane alone.

2.2 Rheology

Rheology plays a significant role in polymer processing. Shear flow and elongational (extensional) flow are two primary flow modes in polymer processing. For Newtonian fluids, the shear viscosity (η_o) is independent from shear rate ($\dot{\gamma}$) and the shear stress (τ). Therefore, shear viscosity can be expressed as equation (2-1).

$$\frac{\tau}{\dot{\gamma}} = \eta_o \tag{2-1}$$

For Non-Newtonian fluids, which are the flows of pseudo-plastic fluid (shear thinning) such as polymers, paint, paper pulp and dilatant fluid (shear thickening) such as latex, the ratio of the shear stress to shear rate are not constant. So, the shear viscosity can be explained by a power-law equation (2-2).

$$\tau = K(\dot{\gamma})^n \tag{2-2}$$

Where, K is a consistency coefficient, n is a flow index (power law index). In equation (2-2), when $n = 1$, this denotes Newtonian fluids and $K = \eta_o$, when $n < 1$, this indicates pseudo-plastic fluid, and $n > 1$ indicates a dilatant fluid.

The changes of viscosity depend on the variation of shear rate of Non-Newtonian fluids and the relationship between n and K can be expressed as equation (2-3).

$$\eta_a = \frac{\tau}{\dot{\gamma}} = \frac{K(\dot{\gamma})^n}{\dot{\gamma}} = K(\dot{\gamma})^{n-1} \tag{2-3}$$

Where, η_a is an apparent viscosity.

The shear stress can be calculated from storage modulus (G', in phase) and loss modulus (G'', out of phase). Tangent delta ($\tan\delta$), the ratio of loss modulus to storage modulus, also express fluid properties. A value of $\tan\delta > 1$ indicates more viscous than elastic properties, and materials having $\tan\delta < 1$ denotes more elastic than viscous properties.

The complex viscosity (η^*) is defined as equation (2-4).

$$\left|\eta^*\right| = \frac{\left|G^*\right|}{\omega} = \sqrt{\eta'^2 + \eta''^2} \qquad (2\text{-}4)$$

Where, η' is dynamic and η'' is elastic part of the complex viscosity, ω is an angular viscosity, and G^* ($G^* = \sqrt{(G')^2 + (G'')^2}$) is a complex shear modulus.

The measurements of viscosity have been demonstrated in many different ways. For shear viscosity, capillary rheometry is widely used. Flow through a capillary is a unidirectional flow, and the viscosity is measured from the fluid near the wall with assumption that the fluid at the wall is representative of the properties of the fluid. However, parallel-plate rheometry and cone-and-plate rheometry are preferred for the study of small quantities of materials or materials that would be adversely affected by the severe contractions at the inlet of a capillary die [Morrison, 2001].

On the other hand, elongational flow is more important in polymer processing such as extrusion, injection molding, film stretching, fiber spinning and melt blowing. The measurement of elongational viscosity is difficult because of the difficulty in maintaining a uniaxial elongational flow to reach a steady state for steady elongational viscosity, but the homogeneous stretching method and the constant stress method are known as direct methods for the measurement of elongational viscosity [Barnes et al., 1989, Morrison, 2001].

Recently, Collier and colleagues [1998] studied elongational rheological properties of polymer melts and solutions using non-lubricated flow characteristics through a semihyperbolic converging conical die. The elongational strain rate is constant in the dies and determined by the die geometry and volumetric flow rate because the flow is dominated by the orientation developing in the fluid. Therefore, a skin layer of a lower viscosity fluid is neither necessary nor does the data require correction for shearing effects. The fluids are being transformed from an isotropic state to a metastable oriented state. Retention of this orientation after the dies would depend on the relative rates of relaxation versus the induced phase change. Because of the above mentioned experimental problems for determining elongational viscosity, theoretical models have been developed to predict elongational viscosity through shear viscosity.

For the MB process, which is the uniaxial stretching operation, where elongational viscosity (η_e) is a critical property for better understanding the process,

estimating elongational viscosity from the Newtonian shear viscosity was first attempted by Trouton using equation (2-5).

$$\eta_e = 3\eta_o \tag{2-5}$$

This relation was previously found not to be rigorously correct for many cases. By assuming a Newtonian flow behavior, Haynes used equation (2-6) for elongational viscosity of PP in his MB process.

$$\eta_e = 2\eta_o \tag{2-6}$$

However, Hayne's equation is not the best model for the MB process for different types of polymer. Thus, Zhao [2003] combined shear viscosity of Patel's data for PP (35 MFR) and equation (2-6). Then the Arrhenius model of elongational viscosity was introduced as equation (2-7).

$$\eta_{e,PP} = 2.56\times10^{-4}\exp\left(\frac{7316}{T+273}\right) \tag{2-7}$$

The elongational viscosity of PET is also given in equation (2-8) as a function of temperature and molecular weight.

$$\eta_{e,PET} = 0.3[\eta_i]^{5.1} \exp\left[2.303\left(\frac{3280}{T+273}\right) - 1.54\right] \quad (2\text{-}8)$$

Where, η_i is an intrinsic viscosity.

2.3 Melt Blowing Process

The main advantage of the MB process is its ability to handle a wide variety of fiber forming polymers and blends of polymers. Basically, any fiber forming polymer having an acceptably low melt viscosity at a suitable processing temperature can be melt blown into fine fibered webs and can solidify before landing on the collector screen.

Wente [1956] first showed the concept of thermoplastics MB to form fibers with diameters as low as 0.3μm by operating at air temperatures around 454^{o}C and nozzle temperature around 380^{o}C with polytrifluorochloroethylene.

Since then, DuPont, Freudenberg and Monsanto produced nonwovens having fine fibers for filter media of fine aerosols, which is based on converting polymer into continuous cold drawn filaments and integrating the conversion of these filaments into a randomly laid bonded nonwoven fabric [McCulloch, 1999].

Different aspects of the MB process were discussed by Wadsworth and McCulloch [1991], who defined the process and explained the general MB process.

McCulloch [1999] presented detailed information about the type of extruder required in the MB process. During the MB process, the extrusion process can be divided into feed, transition, and metering zones. The polymer moves along the barrel, and then the polymer melts primarily from the heat/friction of the viscous flow, the mechanical action between the screw and barrel, and from the electrical heaters around the barrel. The metering pump ensures the consistent flow of polymer melt with uniform pressure and temperature.

The die assembly is the most important element of the MB process, which consists of three distinct components: polymer feed distribution having a typically coat-hanger design, die nosepiece containing the spinneret nozzles and air manifolds.

There are basically two types of feed distribution that have been employed in the MB die, T type and coat-hanger type. The coat-hanger die gives both uniform polymer flow and even residence time across the full width of the die [Mastubara, 1983].

Mastubara [1980] studied the geometry design and residence time of a coat-hanger die. Figure 2-4 shows the schematic diagram of coat-hanger die. Volumetric flow rate in the manifold and residence time can be decided by coat-hanger design, if the fluid can be assumed to be a Non-Newtonian fluid, fluid temperatures are constant, and laminar flow. The residence time corresponding to a flow stream can be expressed as equation (2-9) [Matsubara, 1980].

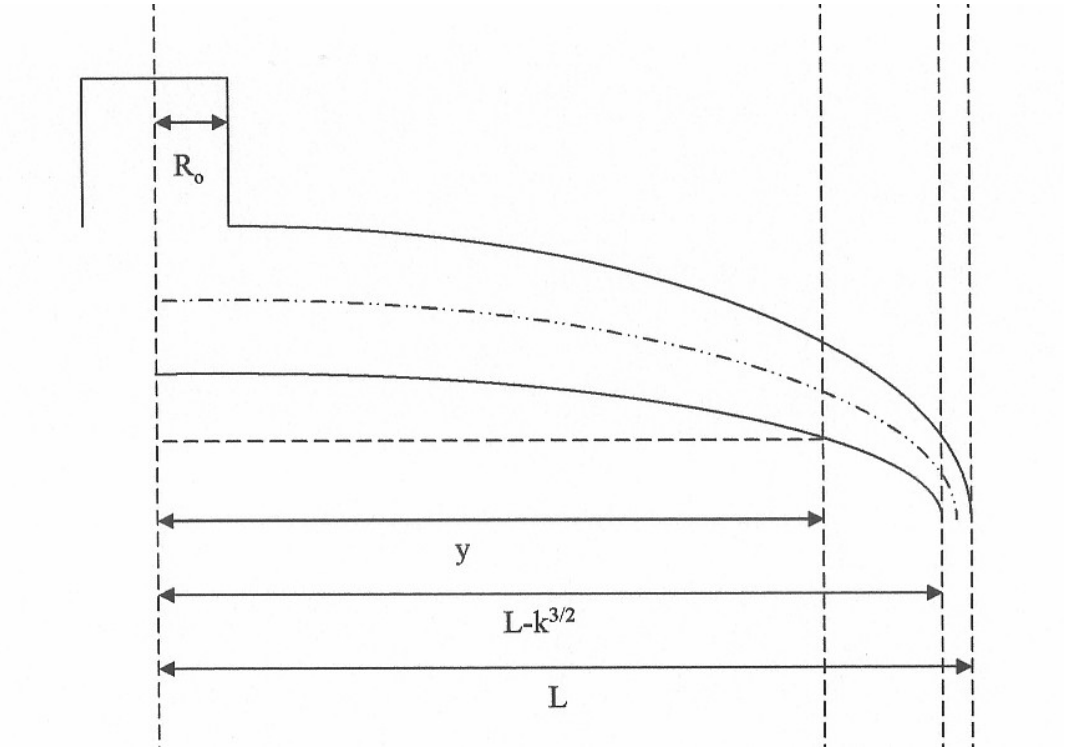


Figure 2-4. Schematic diagram of cross-section of coat-hanger type die [Matsubara, 1980].

$$T = \frac{LH}{Q_o}\{z_c + (m-1)z\} \tag{2-9}$$

Where, L is half of the coat-hanger width, H represents the gap of coat-hanger section, Q_o is half of the total volumetric flow, m is the differential residence time distribution (ratio of residence time in the manifold to residence time in the coat-hanger slot through distance), and z and z_c represents as equation (2-10) and equation (2-11), respectively.

$$z = \int_0^y \left\{ \frac{k'}{(L-y)^{2/3} - k'} \right\}^{1/2} dy \tag{2-10}$$

$$z_c = \int_0^{L-k'^{\frac{3}{2}}} \left\{ \frac{k'}{(L-y)^{2/3} - k'} \right\}^{1/2} dy \tag{2-11}$$

Where, $k' = m^{\frac{-2(3n+1)}{3(n+1)}} (\pi H)^{2/3} \left\{ \frac{(3n+1)}{2(2n+1)} \right\}^{\frac{4n}{3(n+1)}}$

Zhao and Wadsworth adjusted the coat-hanger die temperature for improving the polymer distribution across the PP/PET bicomponent (bico) MB web and evaluated three different cases of die temperature profiles in their studies. The distribution of PP and PET ratio in the PP/PET bico webs were different for all cases,

but the weight uniformity of the PP/PET bico MB web at the left side and right side from the middle of the die was almost the same.

Zhao et al suggested that the uniformity of the PP/PET ratio across the bico web could be improved by adjusting die temperature, so that the lower viscosity of PP could displace the higher viscosity of PET on the edge of the die. The best uniformity was achieved with a die temperature profile of 299-304-315-304-299^{o}C for 15% PP/85% PET polymer ratio [Zhao et al, 2002].

On the other hand, the relationship between nosepiece and web uniformity was reported by McCulloch [1999]. A typical MB die nosepiece has holes which are approximately 0.4mm diameter orifices spaced at 1 to 4 per mm, and are either mechanically drilled hole type or made by electric deposition machining (EDM) [Wadsworth, 1991].

During the MB process, the air manifolds supply the hot and high velocity air through the slots to the top and bottom sides of the die nosepiece. Air streams attenuate the polymer jet streams to form the microfibers after the molten polymer is extruded from the die holes, and then form a self-bonded nonwoven web.

Milligan and Haynes [1995] determined an empirical model for the MB process based on experimental correlations between processing parameters. The data was given for single-hole and multi-hole in terms of mass flux ratio and momentum flux ratio. Equation (2-12) is the empirical correlation expressed in terms of mass flux ratio, Γ, for a single-hole.

$$\delta = 0.0047 + 0.0149\Gamma^{-1.49}\beta^{-0.65}\phi^{-1.12}\theta^{-3.47}\xi^{-0.92} \quad (2\text{-}12)$$

Where, δ is diameter ratio, β is polymer throughput ratio, ϕ is die face width ratio, θ is the polymer temperature ratio, and ξ represents the air temperature ratio. The correlation in terms of momentum flux ratio, ψ, is given by equation (2-13) for single-hole.

$$\delta = 0.00646 + 3.373\psi^{-0.81}\beta^{-0.74}\phi^{-1.14}\theta^{-3.78}\xi^{-0.62} \quad (2\text{-}13)$$

Equation (2-14) is the empirical correlation expressed in terms of mass flux ratio for multi-hole.

$$\delta = 0.0044 + 0.0053\Gamma^{-1.49}\beta^{-0.65}\phi^{-1.12}\theta^{-3.47}\xi^{-0.92} \quad (2\text{-}14)$$

The correlation in terms of momentum flux ratio is given by equation (2-15) for multi-hole.

$$\delta = 0.0044 + 1.5444\psi^{-0.81}\beta^{-0.74}\phi^{-1.14}\theta^{-3.78}\xi^{-0.62} \quad (2\text{-}15)$$

Khan [1993] discussed the variables of MB process as two comprehensive aspects: set constants such as die hole size, die setback, air gap, air angle, web collection type, and polymer/air distribution, which can only be changed when the production line is not in operation, and operational constants such as polymer and air throughput, polymer/die and air temperatures, DCD, and quench environment, which can be changed during production by requirement.

Sun and colleagues [2000] showed that fiber diameters, fiber entanglements on the web and the extended zone of attenuation were basically controlled by the polymer and air throughput rates. Sun also explained how the die/air temperature and air flow rate affect the appearance and tactile handle of the fabric, fabric uniformity and fabric defects such as shot, rope and fly formation. The DCD generally affects the openness of the fabric, fiber-to-fiber thermal bonding and fiber orientation [Sun et al, 2000].

The air gap is known to affect air exit pressure and the degree of fiber breakage. The air angle controls the nature of air flow; when the air angle approaches 90^{o}, a high degree of fiber separation or turbulence results, and the most random fiber distribution was developed in the product. However, when an air angle of 30^{o}, yielded a high proportion of roped or paralleled fibers deposited as loosely coiled bundles, which are considered undesirable in a finished product [Staff report, 1989].

Bresee [2002] showed that the filaments were attenuated most quickly at a distance of 2 or 3 inches from the die tip, and after that fiber diameters did not change

as notably. Bresee also explained that the fiber orientation of the MB webs depends on the die to collector distance (DCD) by flapping motion and the fibers are generally laid randomly because of the turbulence in the air stream, but there is a small bias in the machine direction due to some directionality imparted by the moving collector.

Malkan and Wadsworth [1991] reported that fiber attenuation is a function of air flow rate as well as the other mechanisms which take place between the die and the collector after fibers travel a certain distance from the die, and the drawing of fiber segments between entanglement points as fiber network is stressed during its flight.

The combination of fiber entanglement and fiber to fiber bonding produces enough MB web cohesion so that the web can be used without further bonding. However, the webs may be subsequently thermally calendered with a smooth or patterned for a smooth or patterned finish or they may be thermally laminated with other substrates. Smooth roll calendering at somewhat low temperature is employed to reduce the pore sizes of the MB webs and to stiffen the webs to form pleated filters [Wadsworth, 2002].

2.4 Modeling and Analyses of MB Process Using Statistical Methods

Statistical modeling and analysis are critical in engineering processes and products. The statistical modeling process using response surface method (RSM) has proven to be reliable in predicting the affect of process variables on product

properties by employing multi-factorial methodology for complicated processes such as melt blowing [Sun et al, 2000].

The general forms of the statistical model include the mathematical term, response variable and random errors. The predictors and coefficient parameters of the mathematical term are observed and estimated along with the response variables during the modeling process. Any MB process parameters can be predictor variables, and the main desired properties of the MB products are normally selected as response variables in the statistical analysis.

Desired responses such as smallest fiber diameters are optimized by processing conditions. However, the optimized conditions for the MB process are more complex than conventional melt spinning. For example, optimum processing conditions for fine fiber diameter can not always be the optimum processing conditions for desired web properties, although web properties are significantly affected by fiber size.

Therefore, additional MB process optimization studies may be required for each desired web property. The random error component is included in the statistical model for determining the relationship between the response and the predictor variables. Thus, a statistical relation rather than a perfect deterministic relation is obtained because the functional relationship between the response and predictors is only an indication of the average effect on the populations. Many processing parameters, not only major parameters such as melt/die temperature, throughput, die

geometry, air flow rate, air temperature, DCD, and collector speed, but also minor parameters which are not considered in the statistical model such as polymer grade, moisture content of resins and ambient temperature may also affect final MB properties. Therefore, the adjustment of variance between the statistical model and actual MB process should be calibrated by random errors. The statistical modeling process is mainly divided into the following sequences:

Estimation – Prediction – Calibration – Optimization

The estimation process determines the average value of the response variable such as fiber diameter and other desired fiber or web properties, which is associated with a specific combination of predictor variable. Regression function values can be estimated for any combination of predictor variable values, including values for which no data have been measured or observed. A critical part of estimation is an assessment of how much estimated value will fluctuate due to the noise in the data. Without that information there is no basis for comparing an estimated value to a target value or to another estimate.

The prediction determines either the value of a new observation of the response variable or the values of a specified proportion of all future observations of the response variable for a particular combination of the values of the predictor variables. As a result, any method used for the prediction should include an

assessment of the uncertainty in the predicted values. It is often the case that the data used to fit the model to a process can also be used to compute the uncertainty of predictions from the model. Therefore, the prediction of the response variance will be possible based on statistical analysis with a confidence of 95% or 99%.

The calibration is to quantitatively convert measurements made on one of two measurement scales to the other measurement scales. A process model describing the relationship between the two measurement scales provides the means for conversion.

The statistical modeling using RSM is the link that ties the inputs and output together, successful optimization requires a cause-and-effect relationship between the predictors and the response variable. So designed experiments, run in a randomized order, will be used to ensure that the process model represents a cause-and-effect relationship between the variables.

Zhao [2001] used RSM for estimating the final web properties of the PP/PET bicomponent (bico) MB process. The important operational parameters such as melt temperature, throughput, air temperature, airflow rate, and DCD were used as predictors under a particular condition assuming freedom of interaction between the response variables and the fixed factors. Zhao indicated that the smallest fiber might be produced at higher temperature, lower throughput, higher airflow rate and a DCD of 8 inches. In his research, the effect of air temperature was less significant, since it was nearly constant. Even though, the effect of air temperature on fiber diameter was

minimal at low melt temperature, as the melt temperature increased to 300°C, the effect of air temperature appeared more significant.

Zhang and his colleagues [2001] also suggested RSM for process and product optimization with designed trials, which not only efficiently covered the wide multi-variable operating range of the process, but also tremendously reduced the run sampling number [Zhang, 2001].

CHAPTER 3

EXPERIMENTAL

This research was performed in four phases. The objective of Phase 1, which was conducted on the 6-inch and 20-inch MB line, was to establish an envelope of MB operating conditions versus web performance properties. Phase 2 was focused on the production of MB TPU webs on the 20-inch MB line having commercially acceptable appearance and mechanical properties. The objective of Phase 3 was to optimize the MB TPU processing conditions of the 20-inch MB line through the evaluation of the web barrier and strength properties. The design of the statistical model using RSM based on the results from Phase 1 and Phase 2 was employed in this phase. On the other hand, fiber and web formation processes were studied in Phase 4; and furthermore, more data was obtained on the morphological and mechanical properties of MB TPU fibers and webs for the multi liner regression model.

3.1 Phase 1

3.1.1 Preliminary Research

Preliminary MB TPU studies using ESTANE® 58277 were performed on the 6-inch line at TANDEC. The 6-inch MB line was used in the preliminary study with a minimal 5kg quantity of the TPU, although edge effects reduced the useable width of

the web produced for testing. This preliminary study was undertaken to identify processing parameters and scale up guidelines for future processing.

MB TPU webs were produced with light, medium and heavy basis weights of 23.9, 75.4 and 164.9 g/m^2, three different air flow rates and die-to-collector distances of 25, 30, 36, 46 and 61cm.

The MB spinneret with orifice diameters of 0.508mm, 10/1 L/D, and 20 holes per inch was used. The air knife slot widths on each side of the 60 degree angle nose tip was 0.152cm and setback of the nose tip from the inside edge of the air knives was also 0.152cm.

Air gap refers to the distance between the walls of the die tip and the inner walls of the air knives; the setback is the distance from outer edges of die nose tip to the outer edges of the air knives, as shown in Figure 3-1 [Zhao, 2001].

The polymer throughput rate was set to 0.48 g/hole/min, die temperature was held at 204^{o}C, while air temperature was varied from 203^{o}C to 259^{o}C. Melt pressures after the metering pump varied from 1,227 to 2,124KPa, die air pressures ranged from 48 to 97KPa depending on the desired volume of air flow to the die, and web collection speeds varied from 61 to 488 cm/min.

All fabrics were tested for basis weight, thickness, air permeability, tear strength and tensile properties. Selected fabrics were also evaluated for the effect of thickness upon moisture vapor transmission rates to optimize breathability [Wadsworth, 2001].

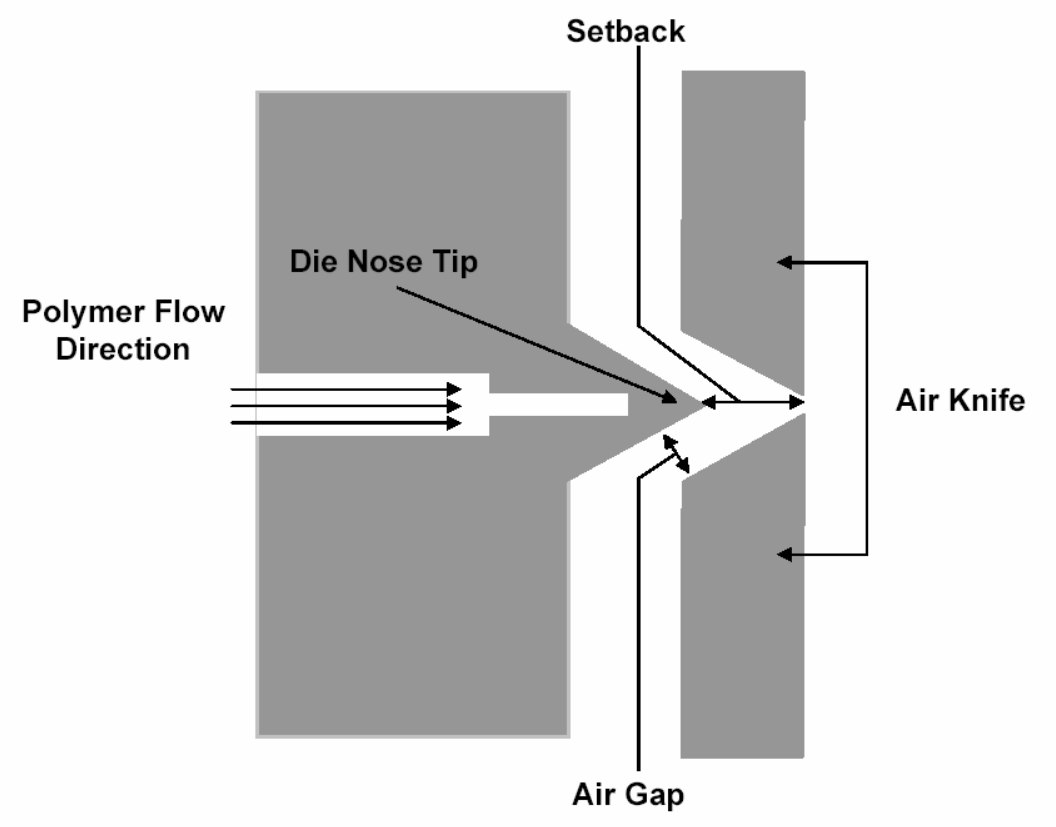


Figure 3-1. The schematic diagram of air gap and setback in an MB die [Zhao, 2001].

3.1.2 The 6-inch and 20-inch MB Line Trials

The processing conditions of first 6-inch and 20-inch MB line trials in preliminary research are presented on Table 3-1. TPU_{237}, ESTANE® 58238 (TPU_{238}), TPU_{245} and TPU_{280} pellets were obtained from Noveon. According to Noveon, TPU_{237} and TPU_{245} are produced from a similar class of ESTANE® polymers, which have lower elasticity than TPU_{238} and TPU_{280}, but the TPU_{237} and TPU_{245} have higher breathability with TPU_{245} having higher breathability than TPU_{237}. TPUs with higher breathability are better at absorbing moisture and transferring it through the film or fiber for greater thermal comfort. TPU_{237} and TPU_{245} were developed as breathable films to compete with Gore-Tex® membranes, whereas, TPU_{238} and TPU_{280} were designed to compete with Lyrca® fiber. The four ESTANE® TPUs were dried for 12 hr at 105 ºC in a Conair Franklin Compu-Dry CD 60 hopper dryer to a moisture content <0.02%.

As shown on Table 3-1, the first six MB trials (TPU_{237}, TPU_{245}, TPU_{238} and TPU_{280}) were performed on the 6-inch MB line at TANDEC. After the 6-inch MB trials, the 20-inch MB line was utilized based on previous results. For these trials, a MB spinneret with 0.457mm diameter orifices, 4.5/1 L/D, and 20 holes/inches was used. The air knife slot widths on each side of the 60^{o} angle nose tip and setback were 0.152cm. The polymer throughput rate was 0.5-0.7 g/hole/min. The die temperature was kept between 193 to 199^{o}C and the primary air temperature in the die varied from 196 to 214^{o}C [Wadsworth, 2001].

Table 3-1. Melt blown processing conditions of first trials on the 6-inch and 20-inch line in Phase 1.

Description			Weight (g/m^2)	DCD (cm)	Collector speed (mpm)	Die-Temp. (°C)	Air-Temp. (°C)	Pump (KPa)
Resin		Sample No.						
6-inch	58237	1.1	NA*	48.3	1.52	193	198	3,599
		1.2	NA*	48.3	4.57	193	196	2,213
		1.3	150	48.3	4.57	193	196	1,903
	58245	1.4	NA*	48.3	4.57	193	206	3,482
	58238	1.5	NA*	25.4	1.52	193	198	3,730
	58280	1.6	NA*	43.2	1.22	193	212	NA*
20-inch	58245	2.1	17.5	25.4	2.44	199	214	25,510
	58280	2.2	71.25	25.4	6.71	199	213	25,510
	58280	2.3	100	25.4	3.96	199	214	25,510

NA*: Data is not available due to failure of producing MB TPU webs

3.2 Phase 2

The information gained from first 6-inch MB line and 20-inch MB line trials was useful in the next series of trials on the 20-inch wide Accurate Products MB pilot line at TANDEC. A schematic diagram of the 20-inch MB pilot line is shown in Figure 3-2 [Wadsworth, 2002].

Although progress was made in producing MB webs on the 20-inch MB line in the first trials, it had been observed that the TPU filaments were often traveling horizontally from MB die only a few inches or more, depending on air flow rates before dropping vertically towards the floor.

From earlier work, it was found that the large hole die diameter of 0.457mm compared to the standard hole diameter of 0.368mm and larger air knife gap of 2.286mm actually results in finer fibers and softer webs with high melt viscosity polymers such as polyesters and nylons.

However, in the second phase of this research, the standard die tip with 0.368mm diameter holes and with an L/D of 8.5/1 and a hole density of 25 holes/inch was used. The air knife gap on both sides of the nose tip and die tip setback was reduced to 0.762mm. For the second phase of preliminary research, TPU_{237}, TPU_{245} and TPU_{280} pellets were obtained from Noveon and were dried for 12 hr at 105ºC to a moisture content <0.02% [Wadsworth, 2002].

As shown in Table 3-2, a series of MB webs were produced with different basis weights with different air flow rates and die-to-collector distances (DCD).

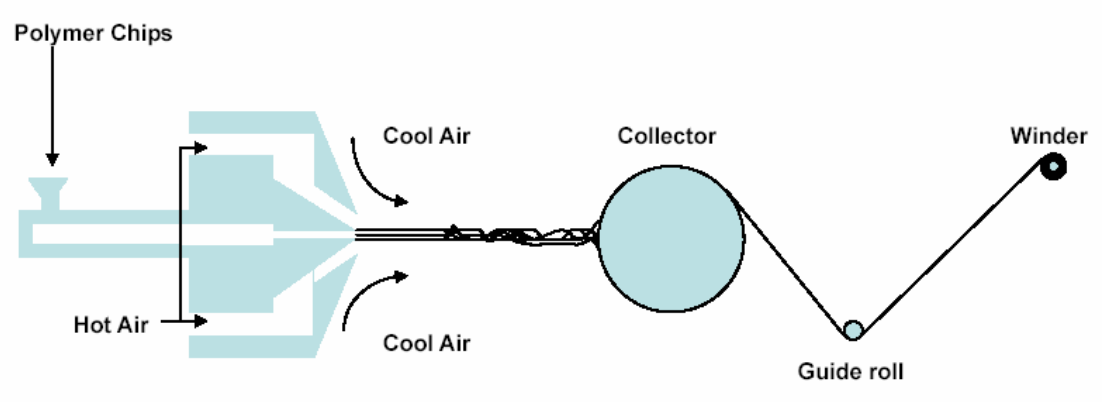


Figure 3-2. Schematic diagram of the 20-inch Accurate MB Products line [Wadsworth, 2002].

Table 3-2. Melt blown processing conditions of second trials on the 20-inch line in Phase 2.

Description		Weight (g/m^2)	DCD (cm)	Collector speed (mpm)	Polymer Thru-put		Press after pump (KPa)	Die-Temp. (^oC)	Air-Temp. (^oC)	Air flow rate (m^3/min, SCFM)
Resin	Sample No.				Gear Pump (rpm)	Extrusion rate (g/h/min)				
58245	1.1	79	91.4	4.57	75	0.13	4,619	204	209	3.46 (121)
	1.2	131	91.4	1.52	75	0.13	5,516	204	207	3.46 (121)
	1.3	124	91.4	1.52	75	0.13	6,688	204	206	3.46 (121)
	1.4	136	91.4	1.52	75	0.13	6,550	204	210	3.71 (130)
	1.5	97	30.5	1.52	75	0.13	6,757	204	207	3.46 (121)
	1.6	120	48.3	1.52	75	0.13	6,895	204	207	3.71 (130)
58280	1.7	110	33.0	NA	47.5	NA*	10,618	204	206	3.46 (121)
58237	2.1	68	30.5	1.52	75		6,895	204	208	3.49 (122)
	2.2	NA*	45.7	1.52	75		7,791	204	211	3.83 (134)
	2.3	118	35.6	1.52	67.5		8,274	204	214	4.26 (149)
58245	2.4	273	55.9	1.52	67.5		8,274	204	216	4.34 (152)
	2.5	145	55.9	2.44	67.5		8,274	204	216	4.34 (152)

Die temperature was held at 204°C, while air temperature in the die manifold was varied from 206°C to 216°C. Web collection speeds varied from 1.52 to 4.57 m/min. Melt pressures after the metering pump varied from 4,619 to 10,618KPa. The polymer throughput of Trials #1.1 through #1.6 (TPU_{245}) was very low at 0.13 g/hole/min in an effort to obtain the small fiber diameters. The polymer throughput based on the gear pump should be reasonably constants during the MB process since the Zenith Nichols gear pump (Single Steam Type H, Model HLB-5592, 10 cc/rev/port) is a positive displacement pump, although the melt densities of the TPU polymers would be expected to differ slightly from PP and PET.

The MB TPU webs were laminated with Kraft paper immediately after the collector to prevent deformation of webs from tension of winding and to avoid blocking causing by adhesion of the wound web. The Kraft paper was wound up with the webs during winding [Wadsworth, 2002].

3.3 Phase 3

To utilize the information learned from Phase 1 and Phase 2. The 20-inch MB line was used with TPU_{245} and TPU_{280} for continuous and uniform webs having commercially acceptable mechanical properties. The 20-inch MB line provides relatively accurate and precise control of die/air temperatures and polymer throughput, compared to 6-inch line, because of a positive displacement gear pump.

The 20-inch MB die, which is a single row of drilled hole type, was inserted

into a nose tip with an angle of 60^{o} angle, a linear hole density of 30 holes/inch and an average nozzle hole diameter of 0.368mm. The MB die was configured with an air gap and setback of 0.762mm.

Experimental processing conditions of Phase 3 were given on Table 3-3. Die temperature was varied from 207^{o}C to 210^{o}C, while air temperature in the die manifold was varied from 210^{o}C to 221^{o}C. Web collection speed was kept at 3.35 m/min. Melt pressures after the metering pump varied from 5,929 to 7,929KPa for TPU_{245}.

On the other hand, die and air temperature of TPU_{280} was set higher than TPU_{245}, Die temperature was held at 232^{o}C, and air temperature in the die manifold was maintained from 241^{o}C to 242^{o}C. Web collection speeds varied from 1.52 to 16.15 m/min. Melt pressures after the metering pump varied from 6,136 to 6,895KPa for TPU_{280}. The MB TPU_{280} webs were not sticky and did not have to wound with Kraft paper.

As shown in Table 3-3, the polymer throughput in Trials 2.1 through 2.5 with TPU_{245} was very low at 0.14 g/hole/min in an effort to obtain small fiber diameters, and then was increased to 0.30 g/hole/min. The throughput rate of TPU_{280} was 0.34 g/hole/min. The MB TPU fibers and webs were characterized by DSC, FTIR, SEM, optical microscopy and etc for the determination of chemical compositions, fiber diameter and morphology. Mechanical strength was determined from the standpoint of molecular bonding, percent crystallinity and tensile/tear strength.

Table 3-3. Melt blown processing conditions on the 20-inch line in Phase 3.

Description		Weight (g/m^2)	DCD (cm, inch)	Collector Speed (m/min)	Polymer Thru-put		Press after pump (KPa)	Air flow rate (m^3/min, SCFM)	Temp. (^oC, ^oF)	
Resin	No.				Gear Pump (rpm)	Extrusion Rate (g/h/min)			Die	Air
TPU_{245}	1.1	45	51 (20)	3.35	84	0.14	5,998	3.37 (118)	207 (405)	219 (427)
	1.2	52	51 (20)	3.35	104	0.29	5,929	3.37 (118)	207 (405)	221 (429)
	1.3	82	64 (25)	3.35	104	0.30	6,136	3.71 (130)	210 (410)	218 (425)
	1.4	88	64 (25)	3.35	104	0.30	7,584	4.03 (141)	210 (410)	210 (410)
	1.5	76	64 (25)	3.35	104	0.30	7,929	4.11 (144)	210 (410)	210 (410)
TPU_{280}	2.1	615	58 (23)	1.52	79.5	0.34	6,895	3.37 (118)	232 (450)	241 (465)
	2.2	139	58 (23)	7.01	79.5	0.34	6,550	3.37 (118)	232 (450)	241 (465)
	2.3	52	58 (23)	16.15	79.5	0.34	6,136	3.37 (118)	232 (450)	242 (467)
	2.4	161	58 (23)	7.01	79.5	0.34	6,136	3.94 (138)	232 (450)	242 (467)
	2.5	79	58 (23)	7.01	79.5	0.34	6,136	4.29 (150)	232 (450)	242 (467)

3.4 Phase 4

3.4.1 Fiber and Web Formation Studies

To understand the fiber and web formation process, experimental measurements were made to provide phenomenological insights into MB TPU process. TPU_{237}, TPU_{245} and TPU_{280} were supplied by Novoen, and processed on the 20-inch MB die. The MB die geometry consisted of a 60^{o} nose tip, a linear hole density of 30 holes/inch, and an average nozzle hole diameter of 0.368mm. The MB die was configured with an air gap and setback of 0.762mm.

For Phase 4, air temperature and air speed were measured by a Series 471 Digital Thermo-anometer produced by Dwyer®, which has a measuring range from -17 to 100^{o}C and 0 to 70 m/s. On the other hand, die temperature was measured by an infrared thermometer MX2™ provided by Rasytek® with the measuring range of -50 to 500^{o}C without polymer extrusion. The TPU fiber speed and fiber temperature during the MB process was calculated based on the PP fiber velocity and air velocity spin-line study by Bresee [2002].

Furthermore, the morphological change of MB TPU_{280} fibers and the orientation of fiber bundles on the MB TPU_{280} webs with different DCDs was investigated, for this purpose, MB TPU_{280} webs were collected at different DCDs with a high collector speed of 100 m/min, polymer throughput rate of 0.14 g/h/min, and die and air temperatures were set at 216^{o}C and 227^{o}C, respectively.

3.4.2 The 20-inch MB Line Trials

In phase 4, MB TPU_{237}, TPU_{245} and TPU_{280} nonwoven fabrics were also produced by different processing parameters to achieve more complete information for the statistical modeling process. The detailed experimental processing conditions of TPU_{237}, TPU_{245} and TPU_{280} are given on Table 3-4, Table 3-5 and Table 3-6, and the experimental designs of TPU_{237}, TPU_{245} and TPU_{280} are given on Figure 3-3, Figure 3-4 and Figure 3-5, respectively. For all TPUs, three different set points of die temperature, air temperature, air valve opening (air velocity), extrusion rate and DCD were applied. Also different basis weight webs of TPU_{245} were collected for the same processing condition using different collector speeds.

The die temperature of TPU_{237} was set on 203-210^{o}C, and air temperature in the die manifold was kept on 210-232^{o}C. Collector speeds were set at 7.3 and 16 m/min, extrusion rates were 0.20, 0.31, 0.38, and 0.49 g/h/min and DCD was varied from 33 to 52.7cm. The die temperature of TPU_{245} was set on 203-207^{o}C, and air temperature in the die manifold was kept on 204-224^{o}C. Collector speeds were varied from 3.2 to 9.6 m/min, extrusion rates were 0.09, 0.16 and 0.24 g/h/min and DCD was varied from 29.2 to 63.5cm. On the other hand, die temperature of TPU_{280} was set on 210-220^{o}C, and air temperature in the die manifold was kept between 227-245^{o}C. Collector speeds were set at 4.8 m/min, extrusion rate were 0.14, 0.19 and 0.24 g/h/min and DCDs were varied from 30.1 to 52.7cm. For the study of heat shrinkage, cooling water was applied for #3.4, #3.5 and #3.6, during the MB process.

Table 3-4. Melt blown processing conditions of TPU_{237} on the 20-inch line in Phase 4.

Sample No.	DCD (cm, inch)	Collector Speed (m/min)	Gear Pump (rpm)	Extrusion Rate (g/h/min)	Air Valve Opening (%)	Temperature (^{o}C, ^{o}F)	
						Die	Air
1.1	52.7 (20.8)	16	100	0.49	50	203 (397)	216 (420)
1.2	52.7 (20.8)	16	100	0.49	50	210 (410)	216 (420)
1.3	52.7 (20.8)	16	100	0.49	50	205 (401)	216 (420)
1.4	52.7 (20.8)	16	60	0.31	50	205 (401)	216 (420)
1.5	52.7 (20.8)	16	40	0.20	50	205 (401)	216 (420)
1.6	33.0 (13.0)	16	40	0.20	50	205 (401)	216 (420)
1.7	63.5 (25.0)	16	40	0.20	50	205 (401)	216 (420)
1.8	52.7 (20.8)	16	40	0.20	40	205 (401)	216 (420)
1.9	52.7 (20.8)	16	40	0.20	60	205 (401)	216 (420)
1.10	52.7 (20.8)	16	40	0.20	50	205 (401)	210 (410)
1.11	52.7 (20.8)	16	40	0.20	50	205 (401)	216 (420)
1.12	52.7 (20.8)	16	40	0.20	50	205 (401)	221 (430)
1.13	52.7 (20.8)	16	80	0.38	50	205 (401)	232 (450)
1.14	52.7 (20.8)	16	100	0.49	50	205 (401)	232 (450)
1.15	52.7 (20.8)	7.3	100	0.49	50	203 (397)	216 (420)

Table 3-5. Melt blown processing conditions of TPU_{245} on the 20-inch line in Phase 4.

Sample No.	DCD (cm, inch)	Collector Speed (m/min)	Gear Pump (rpm)	Extrusion Rate (g/h/min)	Air Valve Opening (%)	Temp. (°C, °F)	
						Die	Air
2.1	52.7 (20.8)	7.3	100	0.24	50	203 (397)	216 (420)
2.2	52.7 (20.8)	7.3	100	0.24	50	207 (405)	216 (420)
2.3	52.7 (20.8)	7.3	100	0.24	50	205 (401)	216 (420)
2.4	52.7 (20.8)	9.6	100	0.24	50	205 (401)	216 (420)
2.6	52.7 (20.8)	3.2	100	0.24	50	205 (401)	216 (420)
2.7	29.2 (11.5)	7.3	100	0.24	50	205 (401)	216 (420)
2.8	35.6 (14.0)	7.3	100	0.24	50	205 (401)	216 (420)
2.9	63.5 (25.0)	7.3	100	0.24	50	205 (401)	216 (420)
2.10	52.7 (20.8)	7.3	100	0.24	40	205 (401)	216 (420)
2.11	52.7 (20.8)	7.3	100	0.24	60	205 (401)	216 (420)
2.12	52.7 (20.8)	7.3	80	0.16	50	205 (401)	216 (420)
2.13	52.7 (20.8)	7.3	60	0.09	50	205 (401)	216 (420)
2.14	52.7 (20.8)	7.3	100	0.24	50	205 (401)	204 (400)
2.15	52.7 (20.8)	7.3	100	0.24	50	205 (401)	224 (435)

Table 3-6. Melt blown processing conditions of TPU_{280} on the 20-inch line in Phase 4.

Sample No.		DCD (cm, inch)	Collector Speed (m/min)	Gear Pump (rpm)	Extrusion Rate (g/h/min)	Air Valve Opening (%)	Temp. (°C, °F)	
							Die	Air
3.1		52.7 (20.8)	4.8	80	0.14	40	220 (430)	245 (473)
3.2		52.7 (20.8)	4.8	80	0.14	40	216 (420)	232 (450)
3.3		52.7 (20.8)	4.8	80	0.14	40	210 (410)	232 (450)
3.4	D	52.7 (20.8)	4.8	80	0.14	40	216 (420)	232 (450)
	W							
3.5	D	30.1 (12.0)	4.8	80	0.14	40	216 (420)	232 (450)
	W							
3.6	D	73.7 (29.0)	4.8	80	0.14	40	216 (420)	232 (450)
	W							
3.7		52.7 (20.8)	4.8	80	0.14	30	216 (420)	232 (450)
3.8		52.7 (20.8)	4.8	80	0.14	50	216 (420)	232 (450)
3.9		52.7 (20.8)	4.8	90	0.19	40	216 (420)	232 (450)
3.10		52.7 (20.8)	4.8	100	0.24	40	216 (420)	232 (450)
3.11		52.7 (20.8)	4.8	80	0.14	40	216 (420)	235 (455)
3.12		52.7 (20.8)	4.8	80	0.14	40	216 (420)	227 (440)

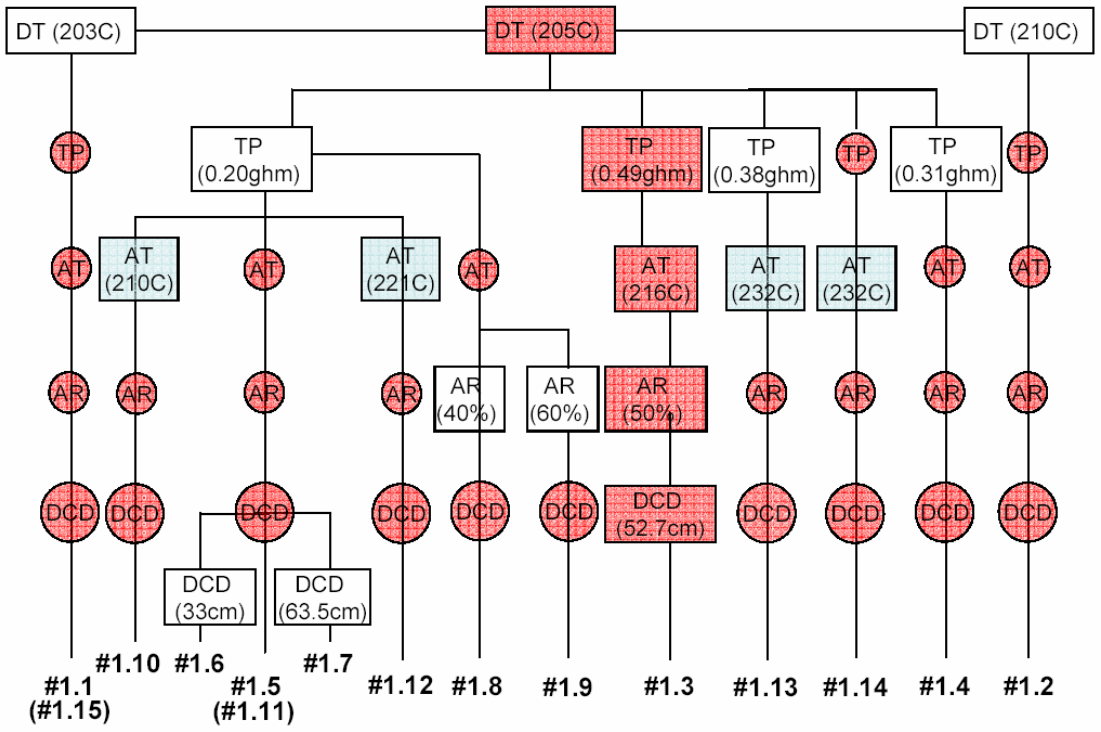


Figure 3-3. The experimental design for TPU_{237} (Phase 4).

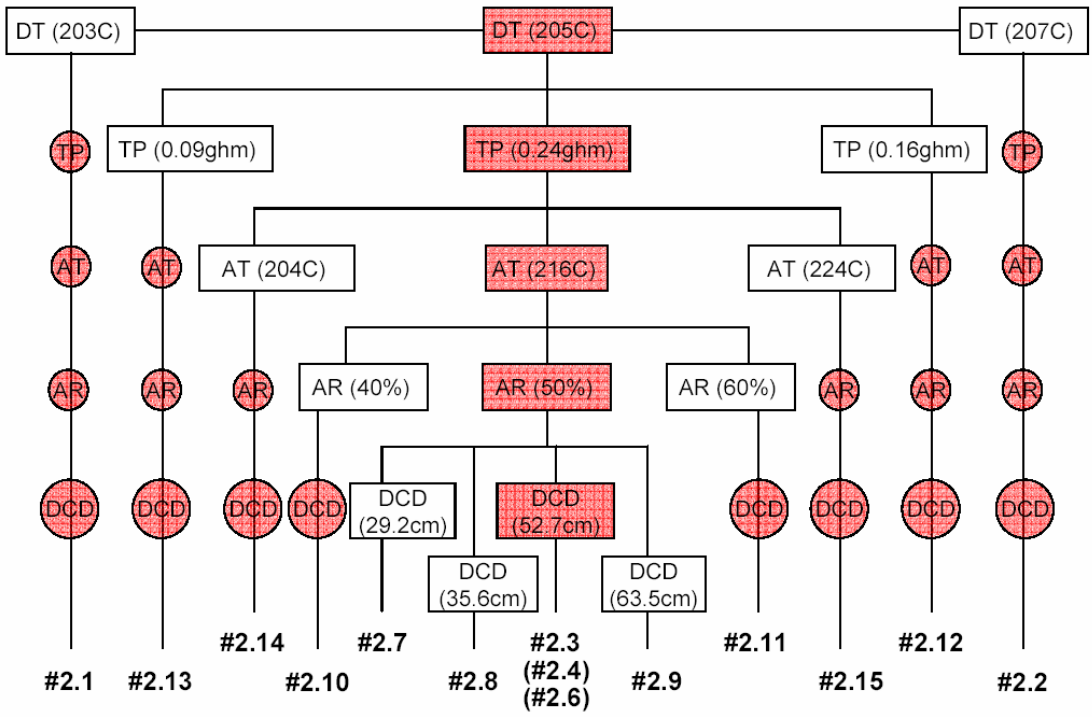


Figure 3-4. The experimental design for TPU_{245} (Phase 4).

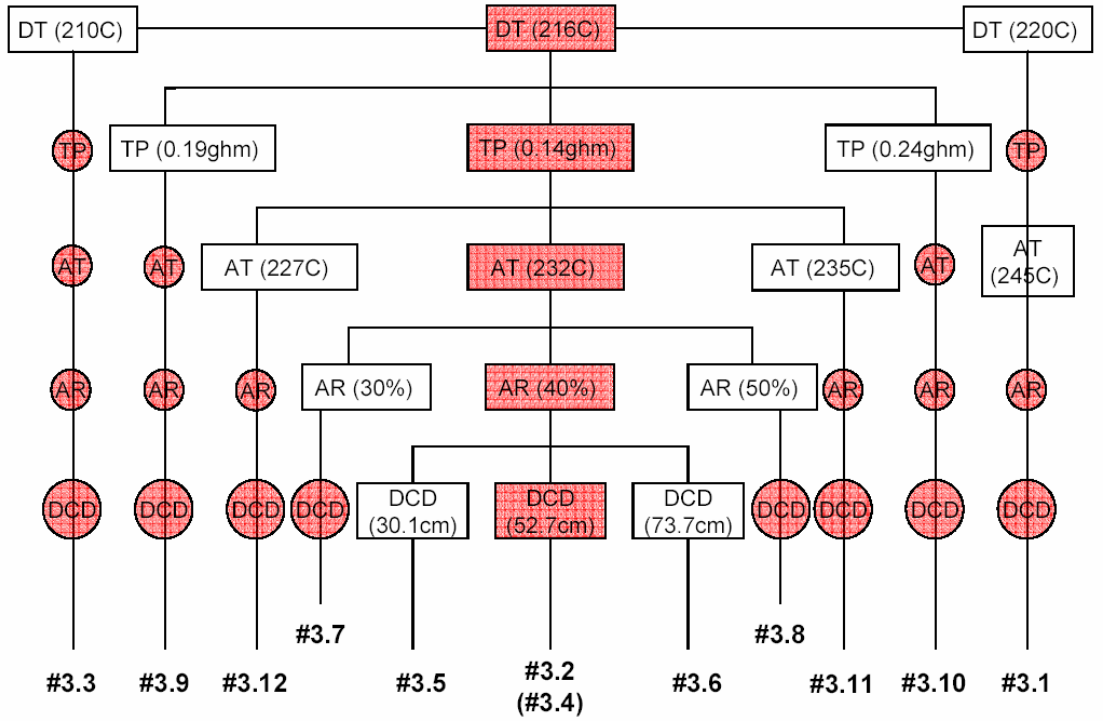


Figure 3-5. The experimental design for TPU_{280} (Phase 4).

3.5 Polymer Materials

The MB processing of TPUs was studied with different classes of ESTANE® polymers. Noveon ESTANE® 58277 was used for the preliminary study on the 6-inch line, and then TPU_{237}, TPU_{238}, TPU_{245} and TPU_{280} were processed on the 6-inch line and 20-inch line in the next phases of this research. However, commercially acceptable MB TPU fibers and webs were only obtained from TPU_{237}, TPU_{245} and TPU_{280}. Therefore, more specific information about those polymers was provided by Noveon [2002].

ESTANE® 58237 (TPU_{237}) is a polyether-based TPU produced by Noveon Inc. It has a high moisture vapor transmission and is designed for film/sheet extrusion and fabric coating in competition with Gore-Tex® membranes. It was dried for 6-12 hours at 105°C in a Conair Franklin Compu-Dry CD 60 hopper dryer for dehumidifying to an acceptable moisture volume of less than 200 ppm. Melt index (MI) = 14/10 g/min at 190/8700 °C/g, Heat of Fusion (ΔH_f) = 8 J/g, glass transitions (Tg) = 88°C and density (ρ) = 1.22 g/cm^3 [Noveon, 2002].

ESTANE® 58245 (TPU_{245}) is a polyether-based TPU obtained from Noveon Inc. It has a high moisture vapor transmission, is highly breathable and moderately elastic, and is designed for film/sheet extrusion and fabric coating for competing with Gore-Tex® membranes. It was dried for 6-12 hours at 105°C for dehumidifying. MI = 54/10 g/min at 190/8700 °C/g, ΔH_f = 11 J/g, Tg = 68°C and ρ = 1.21 g/cm^3 [Noveon, 2002].

ESTANE® 58280 (TPU_{280}, ESTAGRIPTM ST 80A), polyether-based TPU was also obtained from Noveon Inc. It is moderately breathable and highly elastic and is designed to provide good adhesion for a mold on substrate. It is also designed to provide a surface which resists abrasion and scratching, oil and grease resistance, toughness, dynamic flexibility, vibration damping. TPU_{280} was designated to compete with Lycra® fiber. A minimum time of 5 hours at 104°C was required for drying, ΔH_f = 9.2 J/g, Tg = 66°C and ρ = 1.06 g/cm^3 [Noveon, 2002].

3.6 Characterizations of Polymer Resins

3.6.1 Viscoelastic Properties

The apparent viscosity of the TPU polymers were measured and provided by Noveon at a temperatures range between 180°C and 220°C. Each polymer was measured with a 10°C interval. The apparent viscosities of TPU_{237} and TPU_{245} were measured at 180, 190 and 200°C, and TPU_{280} was measured at 200, 210 and 220°C. All measurements were conducted in the shear rate range of 3s^{-1} to 3,000s^{-1}.

Advanced Rheometric Expansion System (ARES) at The University of Tennessee was also used for characterization of TPUs. ARES is a controlled strain rheometer for evaluating viscoelastic properties such as shear modulus, complex viscosity, storage modulus, loss modulus and damping. Controlled strain rheometers employ an actuator to apply a deforming strain to the sample and a separate transducer to measure the resultant stress developed within the sample. ARES

performs steady, transient, and dynamic shear measurements using parallel plate, cone plate, Couette, torsion rectangular and etc. The lower plate of the ARES rheometer is attached to a motor that is able to rotate in different modes and speeds, and the upper plate is attached to a torque transducer and force transducers. The rheometer plates are enclosed in an oven with the ability to vent gases for cooling and heating [Morrison, 2001]. The Couette rheometer has a concentric-cylinder geometry testing chamber, and the fluid is tested in the narrow space between the two cylinders. The gap must be small enough (approximately 1mm) for a linear velocity profile assumption [Li, 2003]. The Couette geometry is limited to modest rotational speeds because of the instabilities that lead to three-dimensional flows. The instabilities are due to the high shear rate, inertia and the elasticity characteristics of the materials [Morrison, 2001]. In this experiment, ARES-LS model number 0012005, which is produced by Rheometric Scientific®, was used under the conditions of dynamic frequency, sweep test (strain-controlled) with the 1.000mm gap by parallel plate geometry. Three specimens for each polymer was achieved directly from melt index instrument for circular shape, then the average of the storage modulus, loss modulus, tangent delta and complex viscosity was calculated.

3.6.2 Differential Scanning Calorimetry

A Mettler Toledo DSC 821e system was utilized, a set of DSC scans was performed for single polymer samples to construct a curve reflecting the relationship

between heat of fusion (ΔH_f).

Each sample was prepared with the approximate weight of 5mg, N_2 gas was used with the rate of 200 ml/min, and scans consisting of four segments, i.e. heating from -65°C to 250°C with a rate of 10 °C/min, staying at 250°C for 2 min, cooling from 250°C to -65°C with a rate of -10 °C/min, and re-heating from -65°C to 250°C with a same rate of 10 °C/min. These DSC analyses were performed for each of the polymer pellets and MB TPU webs, which was prepared on the melt index tester and taken from right to left side in cross direction (CD) at uniformly scattered positions of MB TPU webs, respectively.

3.7 Characterizations of Fiber and Web

3.7.1 Fiber Diameter

All microstructures from MB TPU webs were examined by optical microscopy (YS1-T Nikon) and scanning electron microscopy (SEM, Hitachi S-3500). The image analysis process can be mainly divided into;

Image capture – Segmentation – Object detection – Measuring – Analysis

Ten fiber width measurements were made from three web specimens (1 x 2 inch dimensions) taken diagonally from the two edges (2-3 inches from actual edge of web) and from the middle of the web for a total of 30 diameter measurements per

each sample.

An image analysis program from the Scion Company was used. Fiber diameters were converted from pixels to micrometers using the factor, 3.99/1 pixels/μm. Then imaging techniques such as thresholding, edge finding and region growing were employed. Finally software was used for automatically detecting optimal fiber images using macro-function steps [Wadsworth et al, 2002].

3.7.2 Fiber Bundle Size and Orientation

The fiber bundle size and orientation of MB TPU webs with different DCDs was studied by image analysis technique using WebPro Vedrsion 2.1. The specimen was prepared on the slide glass as a size of 70 x 80mm. MB TPU webs were carefully detached from the Kraft paper to prevent deformation of MB webs and avoid fiber breakage. The optical microscopy having 10x objective lens and CCD camera having 640 pixel (843.7μm)* 480 pixel (641.4μm) resolutions were used for this study.

As a first procedure, the specimen was measured as normal MD and CD positions with the CCD camera; then a second measurement was performed by rotating the CCD camera 45^{o} in the counter clockwise direction from the initial setting points. As a third step, two data sets were combined in that the data sets from first and second groups were carefully collected and controlled to prevent over counting the number of fibers from each data group. About 100 images were taken from each angle; therefore, about 200 images were taken from each specimen.

Average fiber bundle diameter, fiber bundle diameter distribution, mean of fiber bundle orientation and MD/CD ratio was determined for each specimen.

3.7.3 Basis Weight and Thickness

Ten specimens were cut carefully in the CD direction for both basis weight and thickness measurements. The average values of basis weight were reported according to the INDA Standard Test Methods: IST 130.1-92 and IST 120.1 (ASTM Standard D 5729-97). Thickness of fabrics was obtained and reported by a TMI 49-70-00 micrometer according to ASTM Standard D 1777-64.

3.7.4 Air Permeability

According to the ASTM Standard D 737-96, the air permeability of the MB webs was determined by a TexTest FX 3300 machine at a pressure drop of 125Pa. Specimens are clamped into place, and the machine increases the flow rate of air through the sample until the pressure drop reaches 125Pa. A digital readout provides the flow rate, volume per unit area per unit time, in a variety of units. This procedure and results were reported according to ASTM-D 737-96.

3.7.5 Tensile Strength and Elongation

According to the ASTM Standard D 3822-91, tensile strength and elongation were measured on a tensile tester with a loading cell of 10 pound capacity and a

gauge length of 5 inches. Five strips of 8"x1" in MD and CD were randomly taken across the web along the MD and CD direction [Choi, et.al., 1988].

3.7.6 Abrasion Resistance

According to the ASTM Standard D 3884-92, the abrasion resistance of samples was measured by a Model 505 Dual Abrasion tester produced by Teledyne Taber, which has a rotary platform and a double-head. A load of 250g per wheel was applied, and 50, 100, 200 revolutions were run.

Five specimens of 15cm^2 (6 inches^2) were randomly taken across the CD direction of the MB web. Residual breaking load and percent loss in breaking load were reported by ASTM Standard D 3884-92.

$$\text{Loss in breaking load, \%} = 100(A-B)/A$$

A: breaking load before abrasion,

B: breaking load after abrasion

3.7.7 Fourier Transform Infrared Spectroscopy

Bio-Rad FTS-6000e Fourier Transform Infrared Spectrometer (Cambridge, MA) equipped with an UMA-500 FTIR microscope was used for investigation of the molecular composition and Bio-Rad Win-IR Pro 3.0 was used as analysis software.

The wavelength range was set from 500-4000cm^{-1}, number of scans was set

as 500 times for each specimen, and resolution was a $4cm^{-1}$. Three specimens for each sample were taken from right side, center and left side on CD direction at uniformly spaced positions.

CHAPTER 4

RESULTS AND DISCUSSION

4.1 Phase 1

4.1.1 Preliminary Research

Preliminary MB studies of thermoplastic polyurethane (Noveon ESTANE® 58277) were performed on the 6-inch MB line. MB TPU webs were produced with light, medium and heavy average basis weights of 23.9, 75.4 and 164.9 g/m^2, three different air flow rates and at die-to-collector distances of 25, 30, 36, 46 and 61cm. All fabrics were tested for basis weight, thickness, air permeability, and tear/tensile strength. It was found that medium weight, 75.4 g/m^2, MB nonwoven fabrics of ESTANE® thermoplastic elastomer exhibited the best balance of weight and strength, as well as acceptable air and moisture vapor transport properties. It also appeared from this study that heavy weight (164.9 g/m^2) nonwovens could be processed to maximize strength while minimizing resistance to air flow and moisture vapor diffusion.

4.1.2 The 6-inch and 20-inch MB Lines

Continuous web could only be produced in Trial #1.3 on the 6-inch MB line with TPU_{237}. The fabric weight was 150 g/m^2, thickness was 0.616mm and the air permeability was 61.9 m^3/m^2/min. However, the average fiber diameter as determined

by optical microscopy was low as 6.91μm. The information gained from the 6-inch MB line trials was helpful in the MB trials on the 20-inch Accurate Products MB line at TANDEC.

As shown in Table 3-1 (Page 37), continuous MB webs were produced with TPU_{280} in Trials #2.2 and #2.3 resulting in basis weights of 71.25 and 100 g/m^2, and with TPU_{245} resulted in a basis weight of 17.5 g/m^2.

In efforts to obtain finer fibers and softer, more uniform webs, the die temperature was increased from 193^{o}C to 199^{o}C and the primary air temperature was increased from 212^{o}C to 214^{o}C for TPU_{280}. The die temperature of TPU_{245} was also increased from 193^{o}C to 199^{o}C and the primary air temperature was increased from 206^{o}C to 214^{o}C.

However, both webs produced with TPU_{280} were rather coarse as was verified by the large fiber diameters, which were on the order of 19-20μm, as determined by optical microscopy. Nevertheless, an average optically determined fiber diameter of TPU_{245} was 5.42μm and the web was quite uniform in the appearance and had a much softer hand on the 20-inch MB line.

4.2 Phase 2

The results of Phase 1 trials on the 6-inch and 20-inch MB line provided MB TPU processing information for the next series of 20-inch MB TPUs trials in Phase 2. To produce continuous and uniform webs from 20-inch MB line, TPU_{237}, TPU_{245} and

TPU_{280} were used. The MB TPU fibers and webs obtained from Phase 2 were smaller fiber diameter and better appearance than Phase 1. The MB TPU web properties obtained in the Phase 2 are given in Table 4-1.

The basis weights of MB TPU_{245} webs were varied from 79 g/m^2 to 136 g/m^2, even at the low polymer throughput rate of 0.13 g/hole/min in Trials #1.1 through #1.6. The MB TPU webs in this series were uniform in appearance and had a soft and dense structure.

Even though it is difficult to produce small fiber diameters in MB elastomeric polymers, average fiber diameters of less than 6μm were obtained with Trials #1.4, #1.5 and #1.6. In the next series of runs with TPU_{245} in Trials #2.4 and #2.5, average optical fiber diameters of 7.89μm and 5.24μm were respectively obtained.

As shown in Table 3-2, the air flow rates were increased as much as possible without causing excessive fiber breakage. It is remarkable that small fiber diameters were produced with the TPU_{245} in Trials #2.4 and #2.5 without loss of basis weight. Furthermore, it was demonstrated that heavy weight MB TPUs can be made with TPU_{245} in that web weights of 145 g/m^2 and 273 g/m^2 were obtained in Trials #2.5 and #2.4, respectively.

Although both webs were uniform in appearance and had good elasticity, these two webs had a firmer hand and were more dense, apparently due to less quenching at the very high polymer throughput rates employed.

Table 4-1. Melt blown web properties of the 20-inch line in Phase 2.

Description		Weight (g/m^2)	Thickness (mm)	Tear Strength (gf)	Air Permeability ($m^3/m^2/min$)	Optical fiber diameter (um)	Touch and structure of surface	Tensile strength	
Resin	Sample No.							Peak force (kgf)	Peak Elong. (%)
58245	1.1	79	0.261	103.3	47.58	5.68	S, D	0.97	331.0
	1.2	131	0.538	280.7	42.18	10.67	S, D	2.21	443.5
	1.3	124	0.422	226.3	52.06	6.92	S, D	2.34	442.8
	1.4	136	0.561	287.8	34.07	5.98	S, D	1.33	233.4
	1.5	97	0.333	194.7	39.31	5.71	S, D	1.44	418.8
	1.6	120	0.430	145.0	32.54	5.97	S, D	1.31	266.6
58280	1.7	110	0.759	222.3	260.23	23.85	H, R	0.56	218.4
58237	2.1	68	0.353	64.5	177.54	15.91	H, R	0.49	43.2
	2.2	NA							
	2.3	118	0.650	135.9	120.23	16.15	H, R	0.92	78.5
58245	2.4	273	0.900	137.2	29.28	7.89	H, D	1.96	208.4
	2.5	145	0.498	83.7	52.70	5.24	H, D	0.96	154.8

H: Harsh surface S: Soft surface
R: Rough structure D: Dense structure

In contrast to the MB TPU webs from TPU_{245}, the MB webs of TPU_{237} and TPU_{280} resulted in coarser webs with a harder hand, although they were all highly elastic. Given the progress that was made in the melt blowing of TPU_{245}, it was believed that better quality of MB webs could be produced with the TPU_{237} and TPU_{280} polymers with further optimization of processing conditions.

Although three different ESTANE® TPUs were used in Phase 2, the emphasis was on determining the relationships between MB processing conditions and fiber diameters and web properties for TPU_{245}.

The volumetric flow rate and velocity of air was determined according to the Khan's procedure [Khan, 1993]. The air flow rate can be calculated to standard cubic feet per minute (SCFM) using standard density at pressure (Ps = 14.7 PSI) and temperature at T = 20°C (68°F).

The volumetric flow rate of air, Q, in SCFM is given by,

$$Q = W_h / 60Y_s \tag{4-1}$$

Where standard density of air (Y_s) at 20°C (68°F) is 1.20395 kg/m^3, (0.07516 lb/ft^3) and air flow rate (W_h) is the air mass flow rate in lb/hour and can be calculated from following equation,

$$W_h = 359 \cdot C \cdot F \cdot d^2 \cdot \sqrt{Y \cdot h_w} \tag{4-2}$$

Where, C is the discharge coefficient (C = 0.61), F is the velocity approach factor (F = 1.023), d is the diameter of the orifice in inches (d = 1.335), Y ($Y = P/RT$), P is the absolute pressure in lb/ft^2, T is the absolute temperature in ^{o}R, R = 0.286 J/g/^{o}K (53.34 ft-lb/lb/^{o}R) is the gas constant of air is the specific weight of air in lb/ft^3 entering the orifice and h_w is the differential pressure in inches of water.

The actual air flow rate (ACFM) is essential to calculate the air velocity at the air knife exit, since air expends when heated. Assuming the hot air passing through the air knives at the die to follow the ideal gas law equation, the actual flow rate of air at the air knife exit (Q_a) in ACFM is given by equation (4-3),

$$Q_a = Q\frac{(T_a/T_s)}{(P_s/P_a)} \tag{4-3}$$

Q is the standard air flow rate in SCFM at 14.7 PSI and 20^{o}C from (4-1). T_s = 530^{o}R is the standard air temperature, T_a is the actual air temperature at the die in ^{o}R, P_s = 14.7 PSI is the standard air pressure, and P_a = 14.5 + stagnation pressure, which is the actual air pressure at the die in PSI. For ACFM calculations,

primary air temperature at the die and stagnation pressure in the air manifold was used.

The actual air velocity, V in ft/sec, at the air knife exit is given by,

$$V = Q_a / \text{air knife exit slot area (ft}^2\text{)} \qquad (4\text{-}4)$$

The momentum of the air at the air knife exit is the product of the actual air velocity in ft/sec and the mass of air passing through the die per second [Khan, 1993].

Based on the Khan's study, the air flow rate of MB TPU process was calculated in Phase 2, the fiber diameters of MB webs decided by melt temperature, throughput etc, however, air flow rate mostly determined fiber diameters, and other factors were marginal for MB TPUs. Figure 4-1 shows that fiber diameters of MB TPU_{245} webs appeared to slightly decrease with the increase of air flow rate. However, the fiber diameters showed a large difference even for the same air flow rates at 121 scfm (3.46 m^3/min) and 152 scfm (4.34 m^3/min).

Trial #1.1, #1.2 and #1.3 were produced at the same volumetric air flow rate of 121 scfm (3.46 m^3/min) on the 6-inch line; however, the basis weights of those trials were different. The basis weights of TPU_{245} were increased in the order of Trial #1.1 (79 g/m^2), #1.3 (124 g/m^2) and #1.2 (131 g/m^2), and the average optical fiber diameters of TPU_{245} increased in the order of Trial #1.1 (5.68μm), #1.3 (6.92μm) and #1.2 (10.67μm).

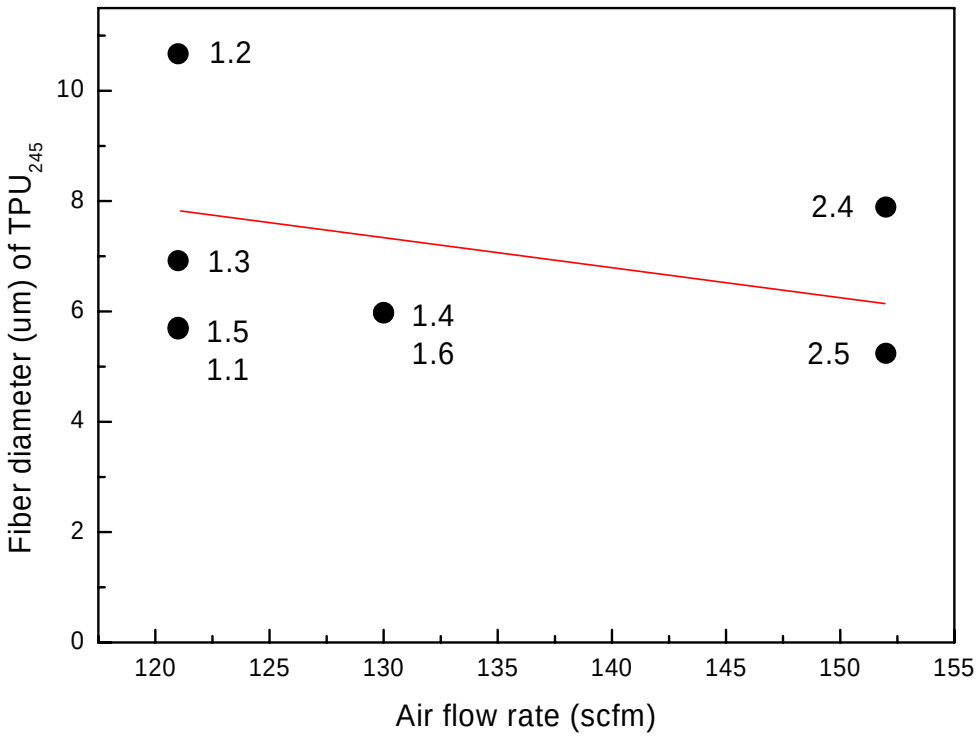


Figure 4-1. Optical fiber diameters of MB TPU_{245} webs depending on the volumetric air flow rate (Phase 2).

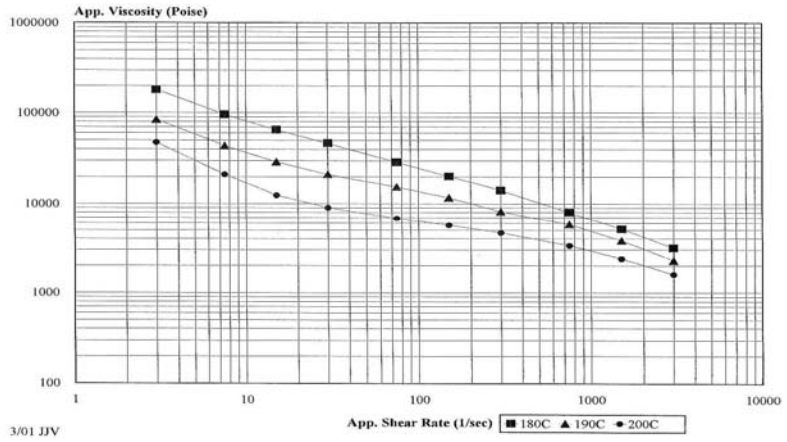
So, eventually, the fiber diameter increased with basis weight. This relationship also supported by Trial #2.4 and #2.5 on the 20-inch line. The heavier basis weight of Trial #2.4 (273 g/m^2) had larger fiber diameter of 7.89μm than lighter basis weight of Trial #2.5 (145 g/m^2), which had smaller fiber diameter of 5.24μm.

Furthermore, web thickness of MB TPU_{245} was continuously increased and air permeability was roughly decreased with an increase of basis weight. This phenomenon is due to the fact that the increase of basis weight resulted in a thicker/denser structure based on the heavier web, and these structures provide better barrier properties. On the other hand, tear and tensile strength of MB TPU_{245} webs did not show clear trends. These results contrast to the general trends that mechanical strength increases with basis weight; however, the variances of basis weight of MB TPU_{245} webs were large across the cross direction on the MB webs, which indicated that the MB TPU webs were not uniform in Phase 2.

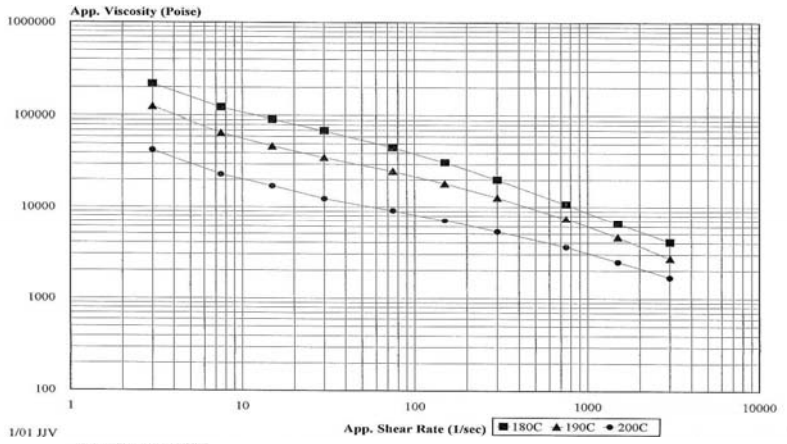
4.3 Phase 3

4.3.1 Rheological Properties of Polymers

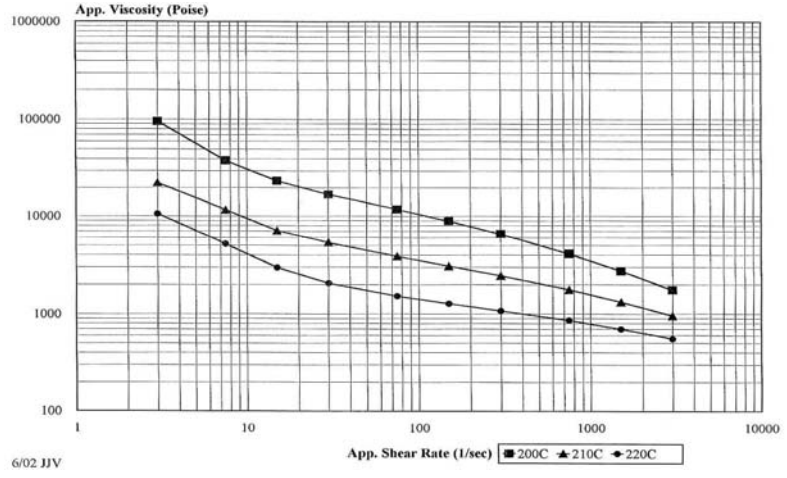
For the investigation of rheological properties of TPUs, the apparent viscosities of the TPU_{237}, TPU_{245} and TPU_{280} polymers were measured and provided by Noveon at temperature ranges between 180°C and 220°C on Figure 4-2. The apparent viscosities of TPU_{237} and TPU_{245} were measured at 180, 190 and 200°C with the shear rate range of $3s^{-1}$ to $3{,}000s^{-1}$.



(a) TPU_{237}



(b) TPU_{245}



(c) TPU_{280}

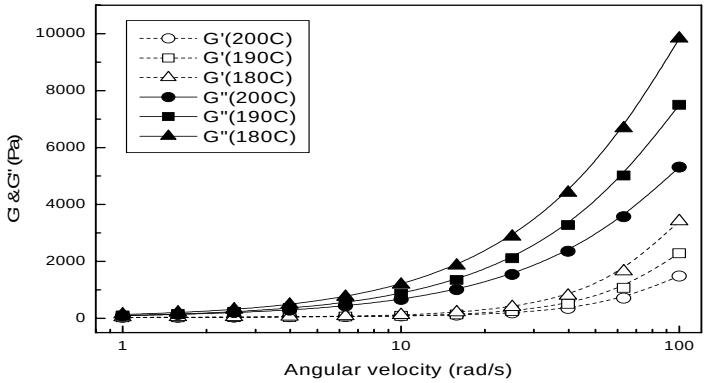
Figure 4-2. Apparent viscosity of TPU resins depending on the apparent shear rates [Noveon, 2003] (Phase 3).

Apparent viscosity gradually decreased with the increase of shear rate and temperature for TPU_{237} and TPU_{245}. On the other hand, the apparent viscosity of TPU_{280} was measured at 200, 210 and 220^{o}C in the shear rate range of 3s^{-1} to 3,000s^{-1}, and the apparent viscosity appeared lower than TPU_{237} and TPU_{245}, even though TPU_{280} has fiber grade viscosity instead of film grade (TPU_{237} and TPU_{245}). This was attributed to the higher testing temperature of TPU_{280}.

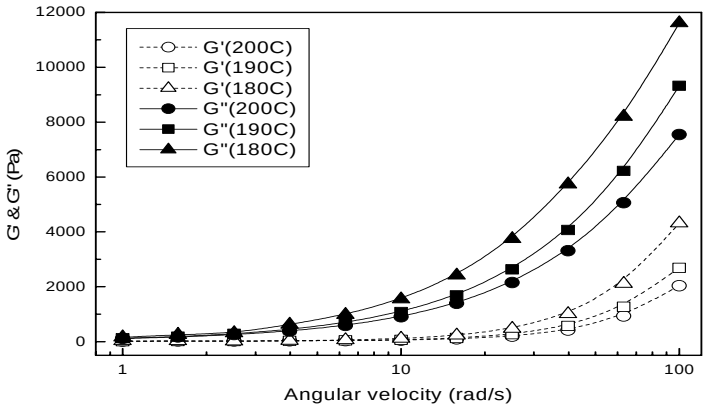
Viscoelastic properties of TPUs were more specifically evaluated using the Advanced Rheometric Expansion System (ARES). The storage modulus (the amplitude of the in-phase stress component/strain, G') and loss modulus (the amplitude of the out-of-phase component/strain amplitude, G") of TPUs are shown in Figure 4-3.

The storage and loss modulus of TPUs exponentially increased with frequencies in the range of 0 to 100 rad/s and decreased with temperatures for all TPU resins (the range of 180^{o}C to 200^{o}C for TPU_{237} and TPU_{245}, and the range of 200 to 220^{o}C for TPU_{280}).

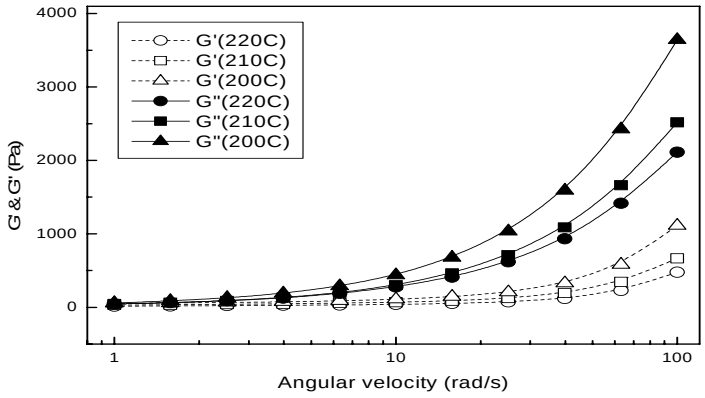
In the experimental conditions, storage modulus and loss modulus of TPU_{237} were varied from 0 to 3,500Pa and 0 to 10,000Pa at 180^{o}C, respectively. On the other hand, storage modulus and loss modulus were decreased with increase of temperature. The differences between 180^{o}C and 200^{o}C were smaller at lower angular velocity, and exponentially increased with frequencies, and then reached maximum at 100 rad/s as 1100Pa.



(a) TPU_{237}



(b) TPU_{245}



(c) TPU_{280}

Figure 4-3. Storage and loss modulus (G' and G") depending on angular velocity of TPU resins (Phase 3).

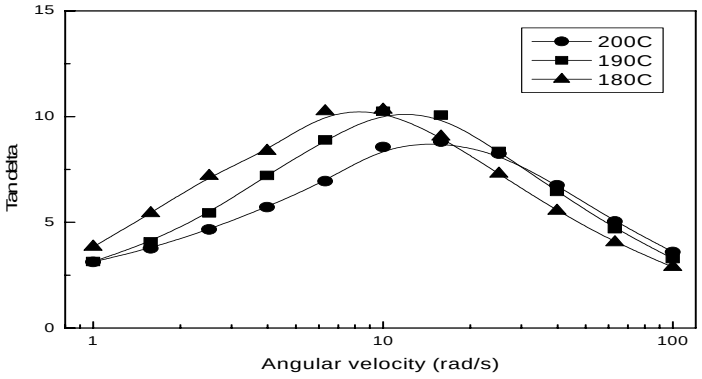
For TPU_{245}, storage modulus was diverse from 0 to 4,100Pa, and the loss modulus was varied from 0 to 11,500Pa at 180°C. However, the storage modulus decreased to 1,700Pa and the loss modulus also decreased to 7,500Pa at 200°C.

In the case of TPU_{280}, the storage and loss modulus were relatively much lower than TPU_{237} and TPU_{245} resins, because of the high testing temperature. Storage modulus was from 0 to 1,000Pa, and the loss modulus distributed from 0 to 3,700Pa at 200°C. On the other hand, the storage modulus varied from 0 to 500Pa, and the loss modulus was 0 to 2,000Pa at 220°C.

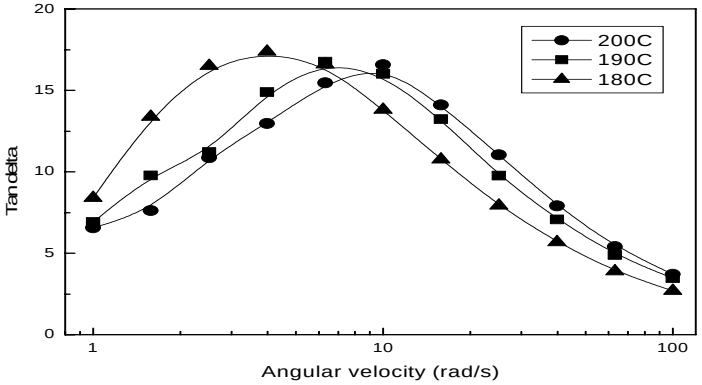
These results imply the properties of TPUs such as elongational properties and flexibility could be critically affected by change of temperature, therefore, the extrusion process of MB process should be carefully controlled in a narrow processing temperature range to improve the web uniformity.

Tangent delta ($\tan\delta$) of TPUs are given on Figure 4-4. The increase of the tangent delta represents the materials in a more viscous state and the decrease of the tangent delta represents the materials properties being more like metal-spring materials.

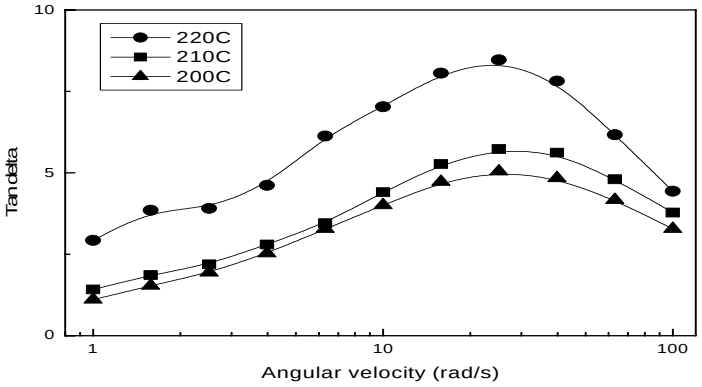
For TPU_{237}, tangent delta increased with angular velocity at below 10 rad/s, the tangent delta of lower temperature showed a higher value than that of higher temperature in the lower angular velocity. However, tangent delta decreased in the temperature ranges from 10 to 100 rad/s, and the tangent delta of higher temperature showed higher value than tangent delta of lower temperature.



(a) TPU_{237}



(b) TPU_{245}



(c) TPU_{280}

Figure 4-4. Tangent delta ($\tan\delta$) depending on angular velocity of TPU resins (Phase 3).

Furthermore, the maximum tangent delta of 200^{o}C appeared lower than that of 180^{o}C and 190^{o}C. These results imply the elastic properties of TPUs can be improved by higher processing temperature at below the polymer degradation temperature.

The tangent delta of TPU_{245} also showed the same tendency as TPU_{237}. The lower tested temperature reached the maximum tangent delta at lower angular frequency than that of higher tested temperature.

However, the maximum value of tangent delta appeared before 10 rad/s, so roughly the graphs showed left-mountain structure. Therefore, the state of TPU_{245} was more viscous state at lower angular velocity than TPU_{237}, and TPU_{245} rapidly changed to metal-spring material state than TPU_{237} with the increase of angular velocity; however, there was no significant change on the maximum value of tangent delta.

On the other hand, TPU_{280} showed right-mountain structure, the maximum tangent delta appeared in the relatively higher angular velocity.

The value of tangent delta rapidly increased with an increase of temperature, but the change of the temperature did not show any effect on the change of peak positions of tangent delta.

These results indicate that the elasticity of TPU_{280} was probably highly affected by processing temperature and the change of processing temperature caused the huge change of elastic properties of the TPU fibers.

The complex viscosities of the TPUs are shown on Figure 4-5. Complex viscosity is an angular velocity-dependent viscosity function determined with forced harmonic oscillation of shear stress.

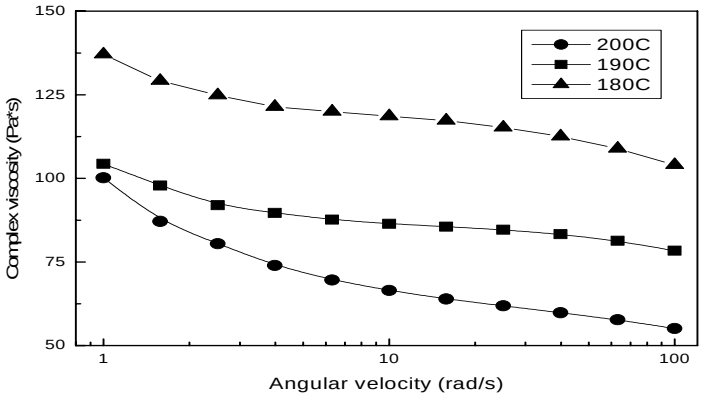
The complex viscosity is related to the complex shear modulus and represents the angle between the viscous stress and the shear stress. The complex viscosity function is equal to the difference between the dynamic viscosity and the out-of-phase viscosity or imaginary part of the complex viscosity.

The value of complex viscosity of TPU_{280}, which is fiber grade, had lower viscosity than TPU_{237} and TPU_{245}, which are film grades. It should be noted that the experimental temperature of polymer viscosity was different for each grade of TPUs depending on their melting points.

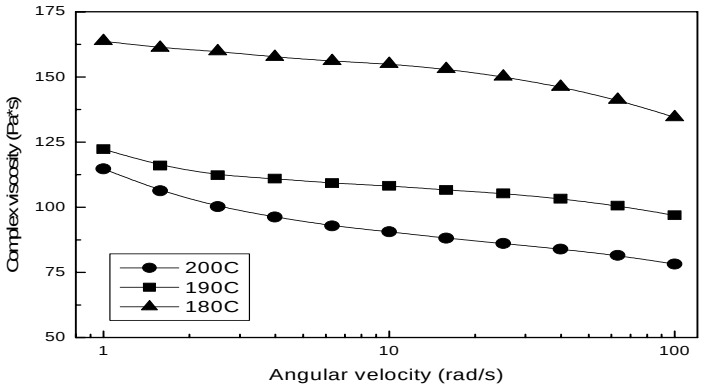
The properties of viscosity are critically affected by temperature, and especially for TPUs, which have very narrow temperature range between the melting point and thermal degradation.

Therefore, the same experimental temperature for different TPUs is theoretically impracticable and undesirable, and the higher analysis temperature for the TPU_{280} caused lower viscosity than TPU_{237} and TPU_{245}, even though TPU_{280} has higher viscosity than other TPUs at the same temperature.

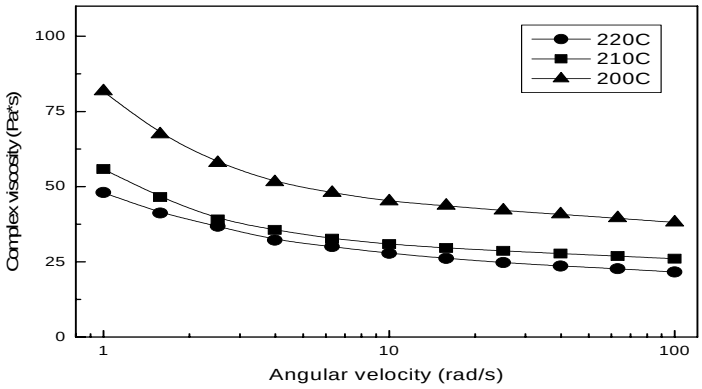
The complex viscosity of TPU_{237} decreased with an increase of angular velocity, complex viscosity decreased rapidly until 20 rad/s, but the decrease ratio was moderate after 20 rad/s.



(a) TPU_{237}



(b) TPU_{245}



(c) TPU_{280}

Figure 4-5. Complex viscosity depending on angular velocity of TPU resins (Phase 3).

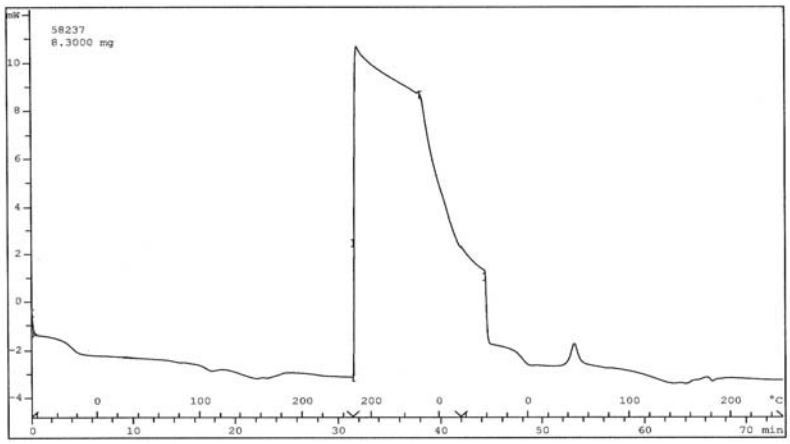
The complex viscosity was higher at lower temperature and decreased with increasing temperature. The complex viscosity was varied from 140 to 110 Pa*s at 180^{o}C, 107 to 80 Pa*s at 190^{o}C, and 100 to 55 Pa*s at 200^{o}C. The complex viscosity of TPU_{245} also decreased with increase of angular velocity, but the decrease ratio was moderate. The complex viscosity of TPU_{245} was varied from 163 to 138 Pa*s at 180^{o}C, 123 to 96 Pa*s at 190^{o}C, and 114 to 76 Pa*s at 200^{o}C.

The trends of TPU_{280} decreased exponentially with the increase of angular velocity, viscosity decreased rapidly until 7 rad/s, but after that the decrease ratio was moderate. The complex viscosity ranged from 83 to 42 Pa*s at 200^{o}C, 58 to 27 Pa*s at 210^{o}C, and 49 to 24 Pa*s at 220^{o}C.

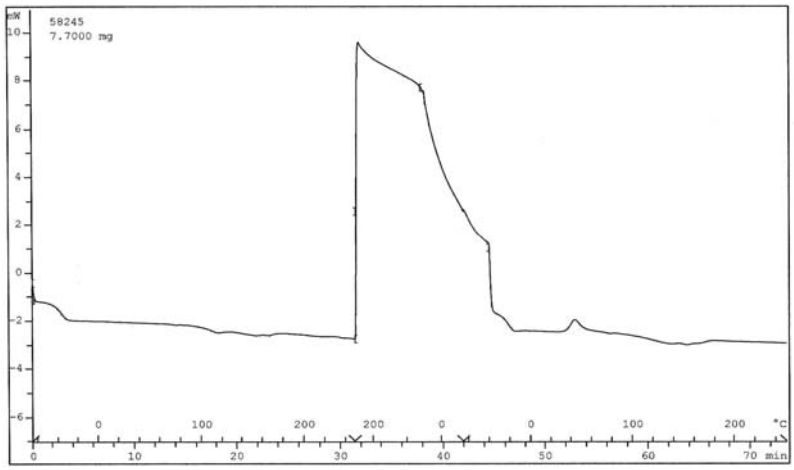
4.3.2 Thermal Properties of Polymers and MB Webs

The thermal properties of TPUs pellets were determined with a Mettler Toledo DSC (Differential Scanning Calorimetry) 821e system and depicted in Figure 4-6. Each TPU resin was prepared as a form of filament, and then dried for 4 hours at 105^{o}C in the oven to remove excessive moisture.

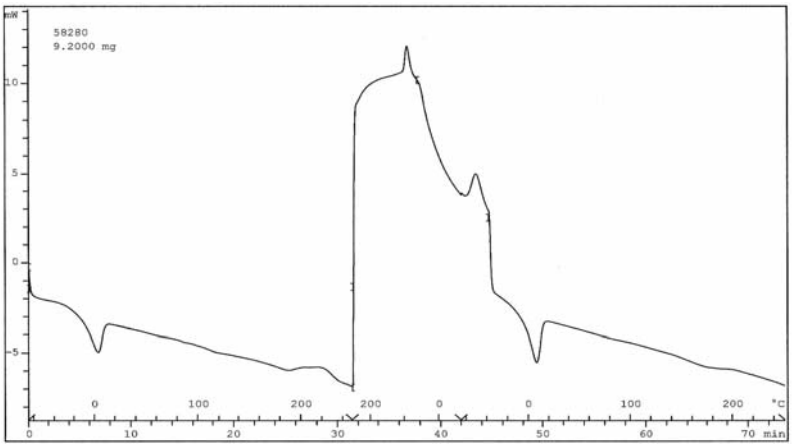
Specimens of each TPU was prepared to the approximate weight of 5-10mg and four segments for each test were conducted. All three TPUs showed unstable base lines in the first segment, which was heating from -65^{o}C to 250^{o}C with a rate of 10 ^{o}C/min, because of the moisture contents, even though those were pre-dried before the experiment.



(a) TPU_{237}



(b) TPU_{245}



(c) TPU_{280}

Figure 4-6. DSC curves of TPU pellets (Phase 3).

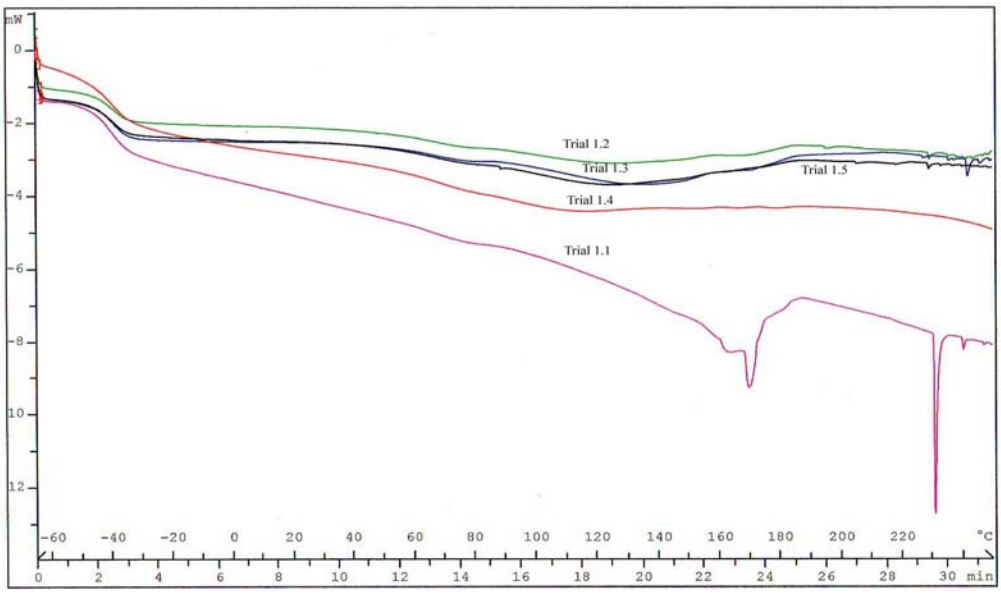
There were only shallow peaks of heat of fusion (ΔH_f) for TPU_{237} and TPU_{245}, and deeper endotherm peak was observed around 0°C for TPU_{280}. This endotherm peak of TPU_{280} pellets may came from dissociation of the urethane soft segment hydrogen bonds.

During the re-heating from -65°C to 250°C with a same rate of 10 °C/min, there was exotherm peak, which was considered from degradation of the soft segment (polyether) around 50°C for TPU_{237} and TPU_{245}, but there was no clear difference between heating and re-heating for TPU_{280}.

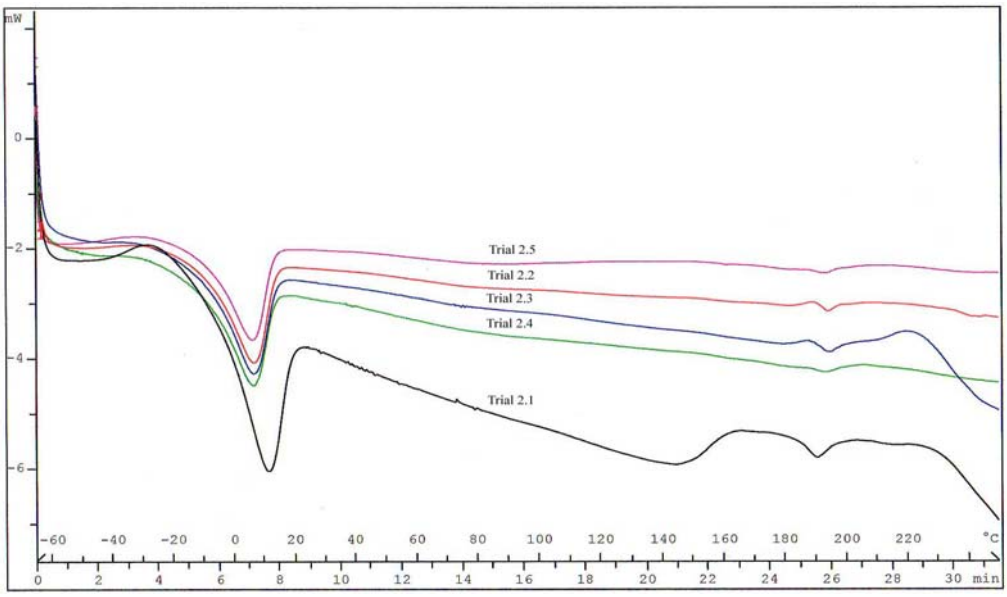
These results show that TPU_{280} was not affected by thermal degradation or oxidation in the testing temperature range. The degradation of TPU_{237} and TPU_{245} also imply these polymers probably need to be processed at lower temperature than TPU_{280}.

The DSC curves of MB TPU_{245} and TPU_{280} webs obtained from Phase 3 shown in Figure 4-7.

For TPU_{245}, Trial #1.1 showed two clear endotherm peaks at 170°C and 230°C, but other trials did not show clear difference from TPU pellets. Those two endotherm peaks of #1.1 are considered to come from breakup of inter-urethane hydrogen bond and thermal degradation during the MB process, respectively. Nevertheless, considering the other DSC curves of TPU_{245} webs, these results also could be caused by excessive tension from collector to the winding device or other experimental conditions.



(a) TPU_{245}



(b) TPU_{280}

Figure 4-7. DSC curves of MB TPU webs (Phase 3).

For TPU_{280}, Trial #2.1 showed clear endotherm peaks at 15°C and 190°C, and other trials also showed two endotherm peaks at 5°C and 190°C, the endotherm peak at lower temperature came from dissociation of hydrogen bonds in soft segment and the endotherm peak at higher temperature came from breakup of hydrogen bonds in hard segments. However, the percent crystallinity reported in this study, which is based on the heat of fusion (ΔH_f = 9.2 J/g), was as low as 1-5%.

4.3.3 Molecular Compositions of MB TPU Webs

The modifications of molecular composition during MB processing were investigated by FTIR spectroscopy. The major absorbance peaks of MB TPU webs roughly appeared in the same wavenumber positions with intensity.

Figure 4-8 shows the FTIR spectra, which were achieved from the middle of the MB TPU_{245} webs.

The intensity and width of the peaks were approximately the same for all samples, because basically MB TPU web compositions originated from TPU polymer compositions, so only minor changes of compositions were caused by the heating and cooling process during the resin drying and extrusion process.

The spectra of MB TPU_{245} webs showed clear peaks of 1100cm^{-1} (C-O-C stretching), 1530cm^{-1} (NH bending + CN stretching), 1600cm^{-1} (C=O stretching in urea group), 1700cm^{-1} (C=O stretching in urethane group), 2870cm^{-1} (C-H) and 3300cm^{-1} (N-H stretching).

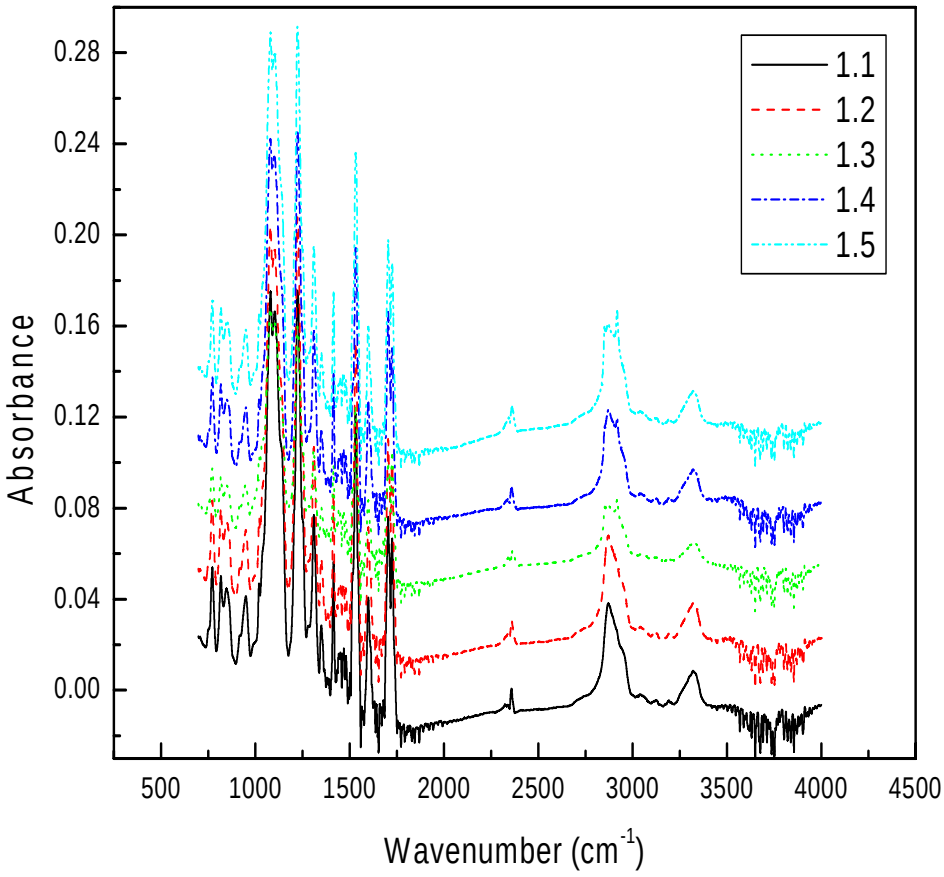


Figure 4-8. FTIR spectra from the middle of the MB TPU_{245} web (Phase 3).

For the MB TPU_{245} webs in which polyether is used as a soft segment, C-H (2800 to 3000cm^{-1}) and C-O-C stretching peaks (~1100cm^{-1}) are mainly due to the soft segments. However, carbonyl peaks in the urethane group (~1700cm^{-1}) and urea group (~1640cm^{-1}) are due to the hard segments [Lee, 1997].

There was notable difference at 2800cm^{-1} between MB TPU_{245} webs having different processing conditions. Basically, the first group; Trial #1.1 and #1.2 showed almost identical absorbance curve, and other groups as #1.3, #1.4 and #1.5 showed roughly the same absorbance trends.

Trial #1.1 and #1.2 have one sharp and medium height peak, but other groups of #1.3, #1.4 and #1.5 have two broad and separated peaks at 2800cm^{-1}. These differences of spectra between two groups of MB TPU_{245} webs showed heat sensitivity of TPU polymers, during the MB process. Because this result probably caused by the change of molecular structure during the MB process when die temperature changed from 207^{o}C to 210^{o}C, and also could be caused by the large change of basis weight of MB TPU webs from around 50 to 85 g/m^2.

Phase 2 also showed that the MB TPU web properties such as fiber diameter can be changed depending on the change of MB TPU basis weight, even for the same MB processing conditions. These results also suggest the molecular structure could be changed at the collector; in other words, there could be notable change in the molecular structure at heavier MB TPU basis weight and minor change could occur at lighter MB TPU basis weight.

Figure 4-9 is the spectra of TPU_{245} from the edge of the MB webs. The peak intensity of TPU_{245} achieved from the middle and edge of the web showed some difference in width and sharpness. Especially, as a major peak positions, the peak intensity and shape of Trial #1.2 and #1.3 were changed from middle of the MB TPU webs at the $2800cm^{-1}$. It should be noted that the peak intensity and position of the spectra was different even for the same MB TPU_{245} webs depending on the processing parameters and basis weight.

This was probably caused by the heat content of the fiber, which the extruded fiber from the spinneret contained and held, even after the MB TPU fibers arrived on the collector. So the contained heat on the edge and the middle of the MB TPU webs were totally different from each other because of the web thickness and uniformity, and MB TPU web was cooled more on the edge.

Figure 4-10 and Figure 4-11 show the IR spectrum of MB TPU_{280} web. Two figures from the middle and edge of the TPU_{280} web showed about the same shape and widths of the peak.

In the Figure 4-10, spectrum, which was achieved from the middle of the MB TPU_{280} web, showed almost same peak positions and shapes for different processing conditions, but intensity was distinguished as two groups, one group of Trial #2.1 and #2.2 and the other group of #2.3, #2.4, and #2.5. Former group (#2.1 and #2.2) showed relatively weak intensity of peak, and other group (#2.3, #2.4 and #2.5) showed sharper intensity at $\sim 2870cm^{-1}$.

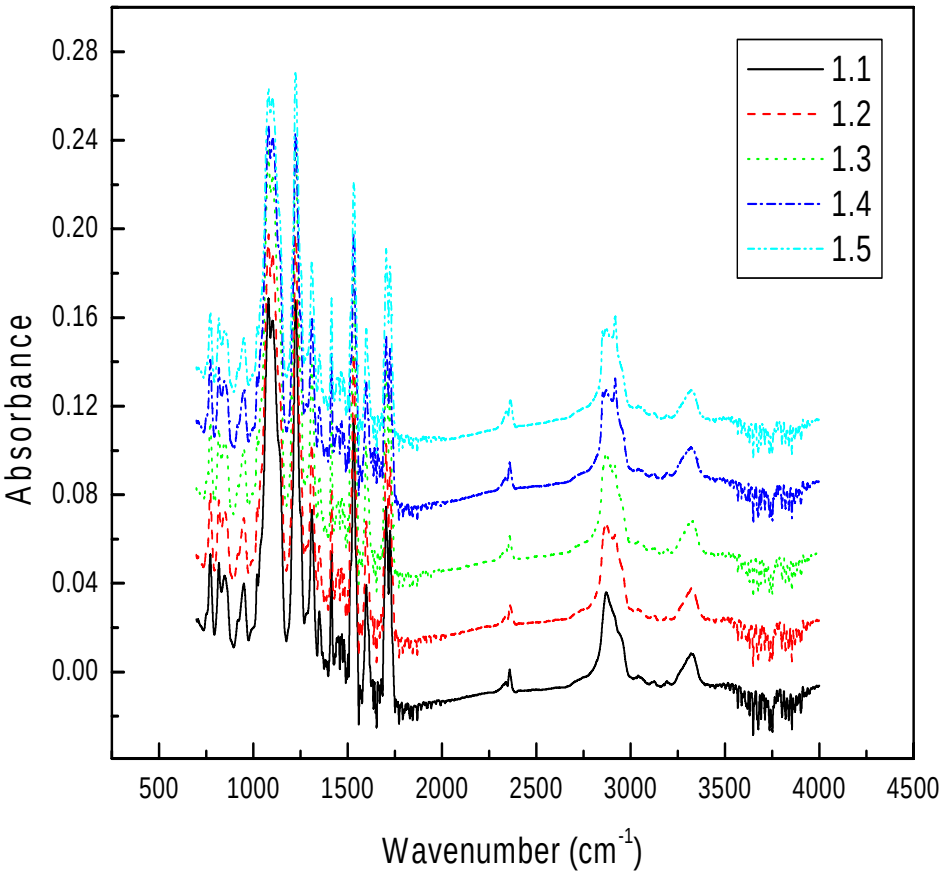


Figure 4-9. FTIR spectra from the edge of the MB TPU_{245} web (Phase 3).

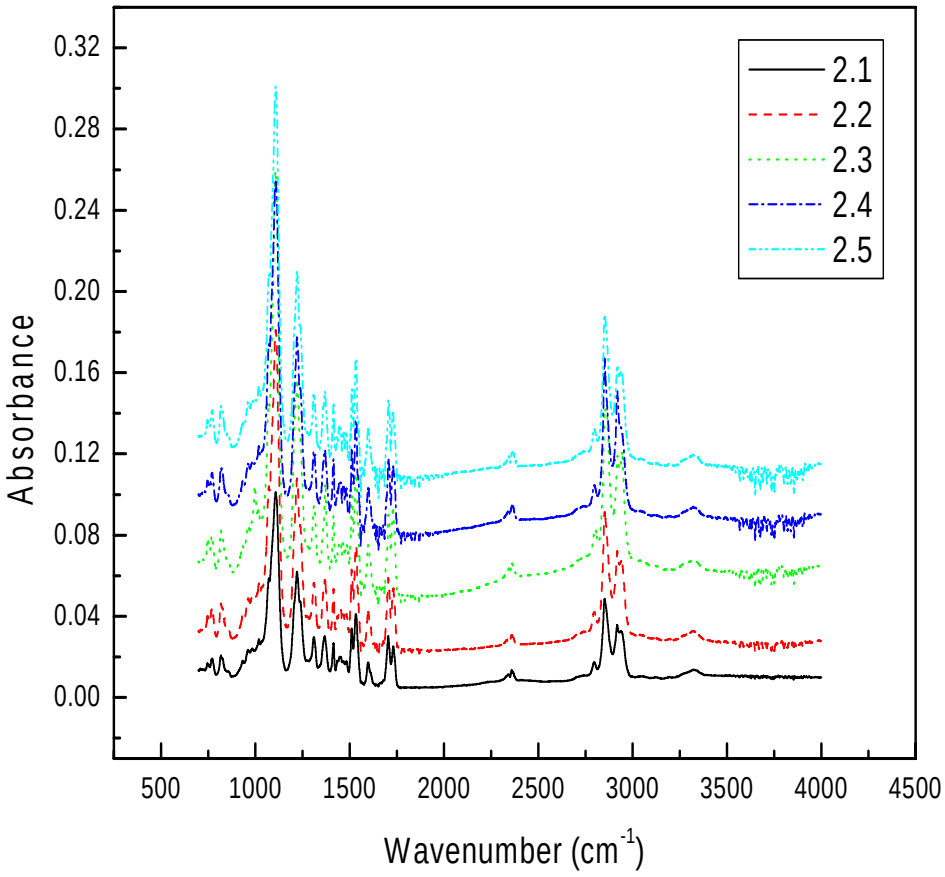


Figure 4-10. FTIR spectra from the middle of the MB TPU_{280} web (Phase 3).

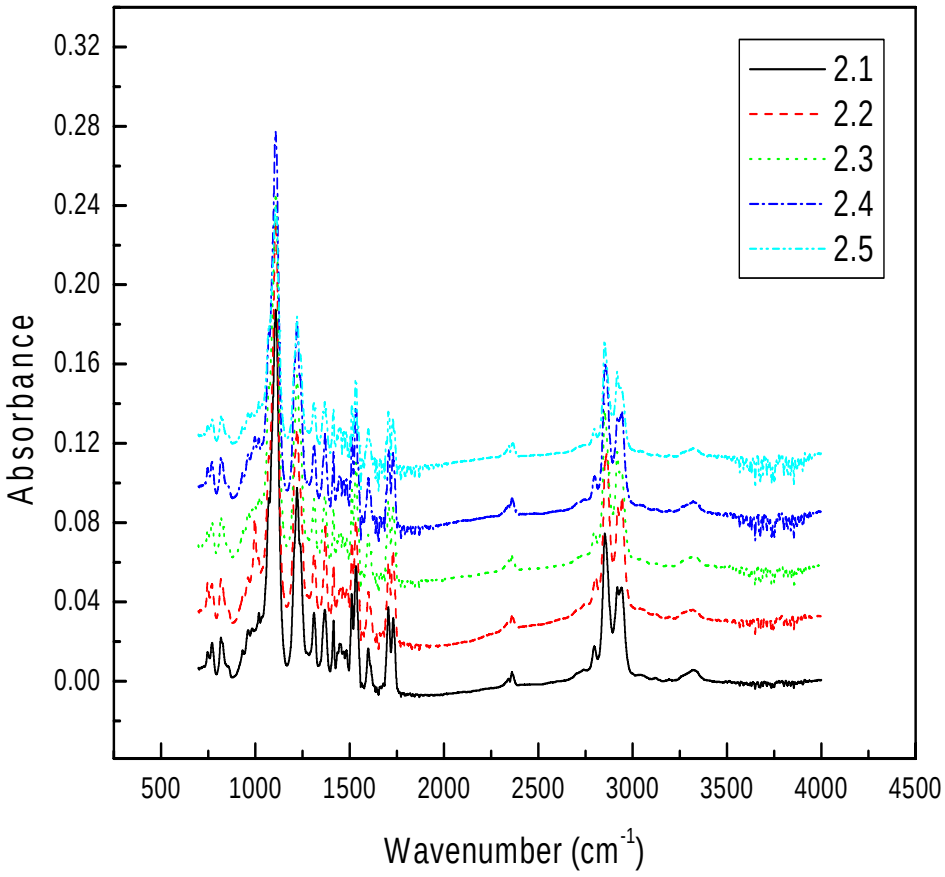


Figure 4-11. FTIR spectra from the edge of the MB TPU_{280} web (Phase 3).

However, the peak intensity of the MB TPU web, one was taken from the edge and the other was taken from the middle of the web was different at ~2870cm^{-1} for Trial #2.1 and Ttrial #2.2. The peak intensity of those trials were as sharp as other group (Trial #2.3, Trial #2.4, and Trial #2.5) in the edge of the web, it is shown on Figure 4-11.

This could be explained by the heat content of the middle of the web being higher than edge of the web, because the edge of the web is closer to room temperature.

Trials #2.1, Trial #2.2 and Trail #2.3 were produced with the same processing conditions except basis weight, however, the peak intensity at ~2870cm^{-1} was increased with decrease of the basis weight, which also can explain the molecular structure could be changed depending on the basis weight of the MB TPU webs.

4.3.4 Mechanical Properties of MB TPU Fibers and Webs

The uniform and continuous MB webs were produced from all TPU trials with TPU_{245} and TPU_{280} polymers. TPU_{245} in Trials #1.1 through #1.5 result in basis weight of 45 to 88 g/m^2 with 5.0 to 13.0µm fiber diameters, and TPU_{280} in Trials #2.1 through Trail #2.5 resulted in basis weight of 52 to 615 g/m^2 with 5.3 to 14.5µm of fiber diameters.

The mechanical properties of MB TPU fibers and webs in Phase 3 are given on Table 4-2.

Table 4-2. Melt blown web properties of the 20-inch line in Phase 3.

Description			Weight (g/m^2)	Thickness (mm)	Tear Strength (gf)	Air Permeability (cfm, $m^3/m^2/min$)	Fiber Diameter (um)	Tensile	
Resin	Sample No.							Peak Force (Kgf)	Peak Elong. (%)
TPU_{245}	20"	**1.1**	45	0.15	65	335 (102)	5.4	0.88	243
		1.2	52	0.18	76	259 (79)	5.2	1.40	342
		1.3	82	0.40	145	463 (141)	13.0	1.32	209
		1.4	88	0.47	71	699 (213)	7.0	0.75	96
		1.5	76	0.48	58	814 (248)	5.0	0.60	81
TPU_{280}	20"	**2.1**	615	1.77	966	61 (19)	14.5	19.26	607
		2.2	139	0.70	418	330 (101)	11.6	2.73	348
		2.3	52	0.43	119	1079 (329)	11.2	0.89	197
		2.4	161	0.74	192	205 (63)	7.8	2.79	350
		2.5	79	0.37	59	370 (113)	5.3	1.11	244

Figure 4-12 shows the relationship between MB processing time passage and pressure after pump for TPU_{245} and TPU_{280}. These TPUs showed completely different processing trends of the pressure after pump depending on time. These results represent that during the extrusion process, the flows of melted TPU fluid or high viscosity materials needs to be explained differently from general polyolefin families such as PP and PE, which normally show stable pressure after the metering pump with time. The pressure after pump of TPU_{245} increased continuously with time, even though the die/air temperature and extrusion rate were kept almost in the same range. On the other hand, the melt pressure after pump of TPU_{280} continuously decreased with time. This also represents the difficulty of the extrusion process of MB TPUs. The processing conditions of TPUs could be completely changed depending on the TPU rheological properties. TPUs have very high viscosity compared to PP and PE, and are easy to degrade by excessive die and air temperature. So, TPUs have a very narrow die/air temperature processing range, the unsuitable die temperature easily results in carbonization and degradation of TPUs and these probably interrupt the flow of melted TPU fluid.

On the other hand, Figure 4-13 shows the relationship between the volumetric air flow rate and fiber diameter of TPU_{245} (#1.3, #1.4 and #1.5) and TPU_{280} (#2.2, #2.4 and #2.5). The fiber diameters of MB webs are normally decided by die/air temperature, throughput and etc, however air flow rate mostly determined fiber sizes of MB TPU webs, and other factors were marginal in Phase 3.

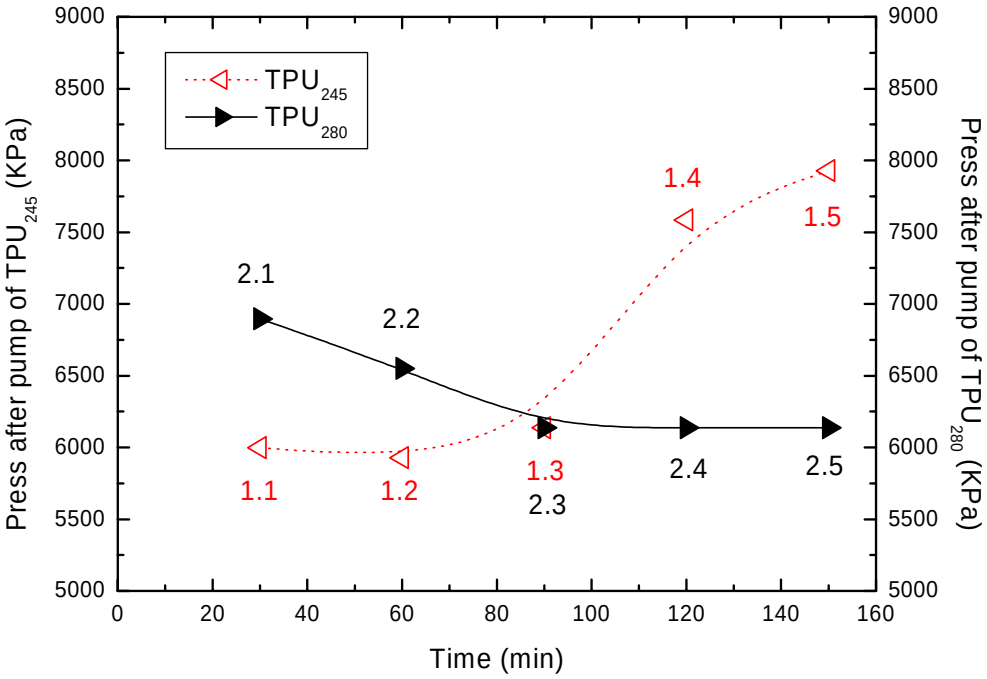


Figure 4-12. Relationship between time and pressure after pump for TPU_{245} and TPU_{280} (Phase 3).

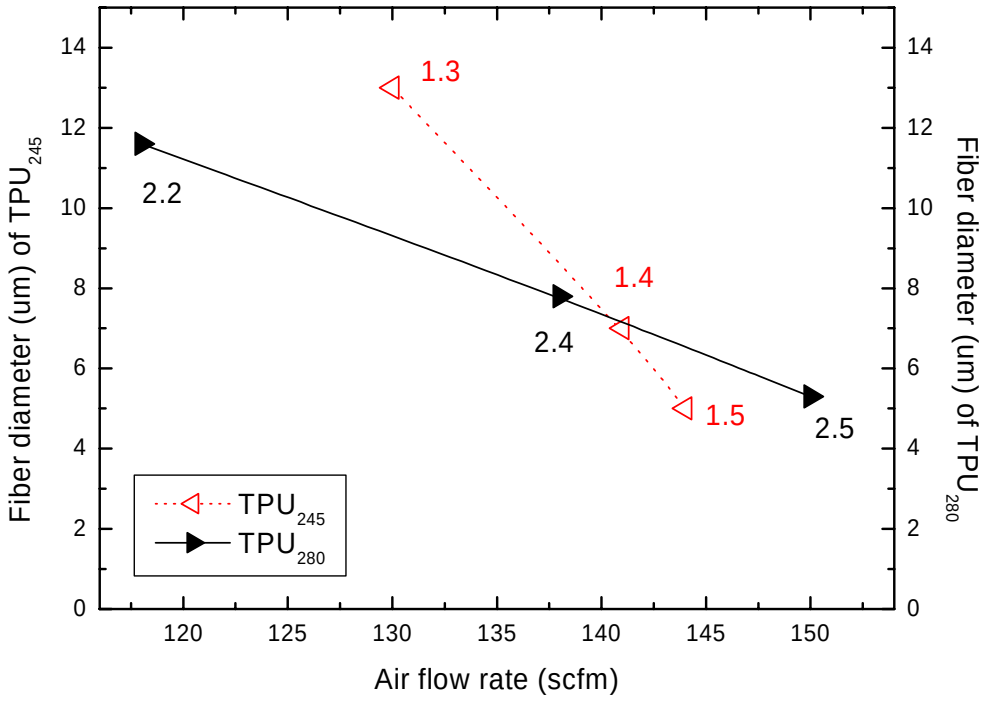


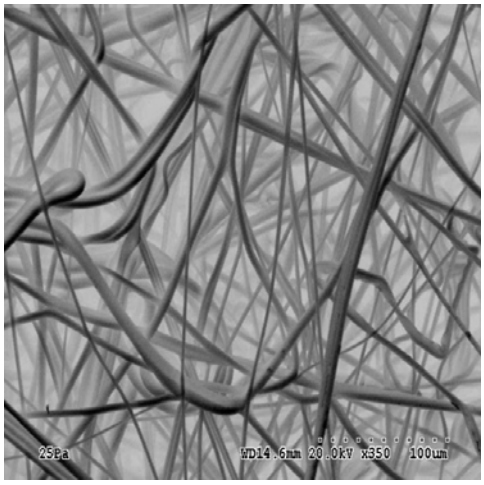
Figure 4-13. Relationship between the volumetric air flow rate and fiber diameter of TPU_{245} and TPU_{280} (Phase 3).

The fiber diameters of MB TPUs decreased with the increase of air flow rate in the same processing conditions for each polymer for the same DCD, collector speed, metering pump speed, extrusion rate and almost same die and air temperature. The difference of the fiber diameters between two TPU polymers is considered to come from different polymer processing temperatures. That could be the reason that the fiber diameters of TPU_{280} are smaller than film grade TPU_{245} below 140 scfm (4.00 m^3/min), although TPU_{280} has fiber grade rheological properties, but the fiber diameters of TPU_{245} rapidly decreased more than TPU_{280} with the increase of air flow rate.

Figure 4-14 shows the morphological features obtained from optical microscopy (YS1-T Nikon) and scanning electron microscopy (SEM, Hitachi S-3500) of the TPU_{245} and TPU_{280}, respectively. Some of MB TPU fibers from Trial #1.5 (TPU_{245}) and Trial #2.5 (TPU_{280}) were as small as ~2μm with volumetric air flow rate of 144 scfm (4.11 m^3/min) and 150 scfm (4.29 m^3/min), respectively. The standard deviation of fiber diameter was less than 2μm, so most of fiber diameters from both polymers were in the range of conventional MB PP fiber diameters.

Figure 4-15 shows that the basis weight increased with the increase of air flow rate, and then basis weight decreased with increase of air flow rate after 140 scfm (4.00 m^3/min). When the TPU filaments from the spinneret arrive to the collector, the filaments loose their heat and begin to shrink. So, if the air flow rate is low enough, the fibers contain more heat than fibers produced from high air flow rate.

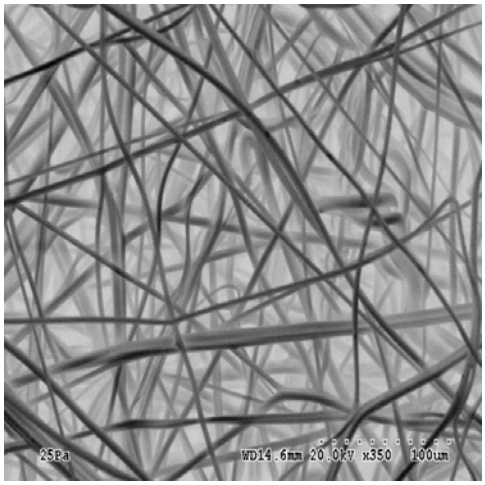




Optical microscopy (x500) SEM (x350)

(a) TPU_{245} (Trial #1.5)





Optical microscopy (x500) SEM (x350)

(b) TPU_{280} (Trial #2.5)

Figure 4-14. The morphological features of TPUs (Phase 3).

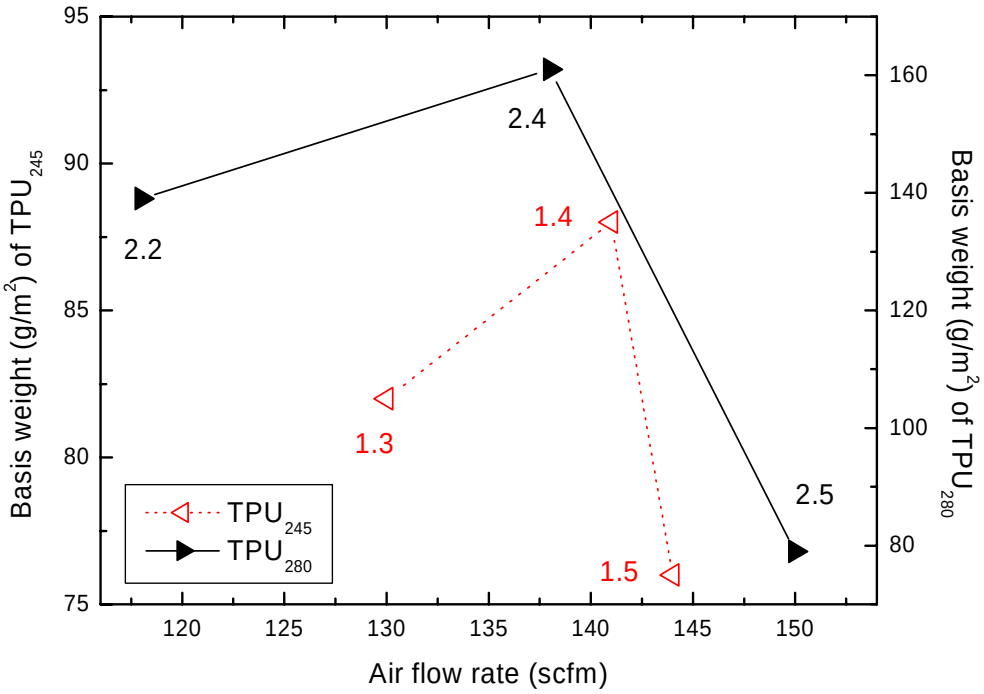
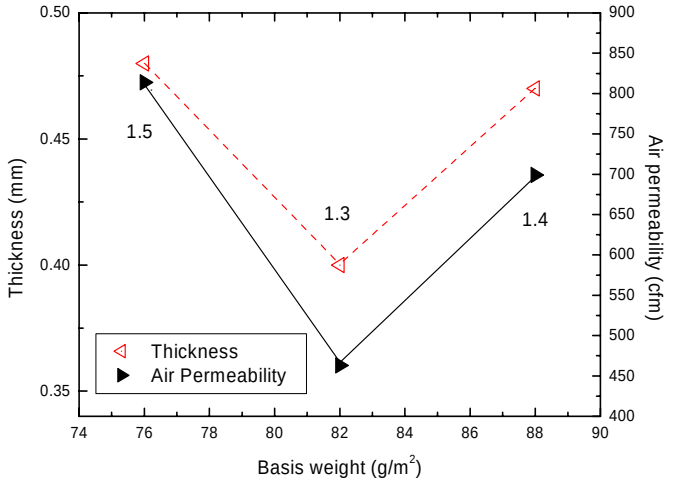


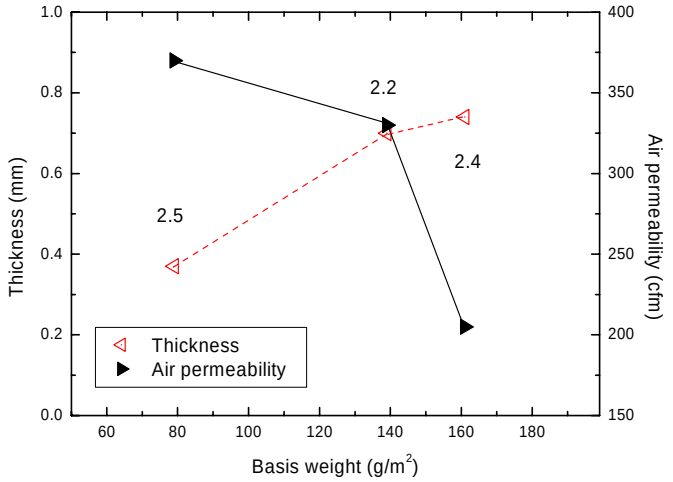
Figure 4-15. Relationship between the volumetric air flow rate and basis weight of TPU_{245} and TPU_{280} (Phase 3).

Therefore, the width of MB TPU webs produced from lower air flow rate shrink more than that of higher air flow rate. Higher air flow rate should also spread the web out more and draw in more quench air. The decrease of basis weight also can explained by the width of MB TPU webs, the width of MB TPU webs below 140 scfm (4.00 m^3/min) did not show much difference, but the width of the MB TPU rapidly increased after 140 scfm (4.00 m^3/min).

Figure 4-16(a) shows the web thickness and air permeability depending on the basis weight of MB TPU_{245} web. Thickness and air permeability of Trial #1.3 (82 g/m^2), #1.4 (88 g/m^2) and #1.5 (76 g/m^2) showed the same trends for each basis weight. Thickness and air permeability of MB TPU_{245} webs were initially decreased, but afterwards increased with basis weight. These results contrast to the normal trends of MB webs as web thickness increase and air permeability decrease with increase of basis weight. This trend can be explained by MB TPU fiber and web properties were highly dependent on air flow rate. The increase of air flow rate resulted in a decrease of fiber diameter, which contributed to a decrease of air permeability. However, it results in a rough MB web structure, bigger pore size and expansion of MB web width, which contributed to the increase of air permeability. The thickness of the MB TPU webs also did not completely depend on the basis weight, in that the high air flow rate and tension from the collector to take-up device highly contributed to final web properties because of the MB TPU web structure had not fully stabilized in morphology on the collector.



(a) TPU_{245}



(b) TPU_{280}

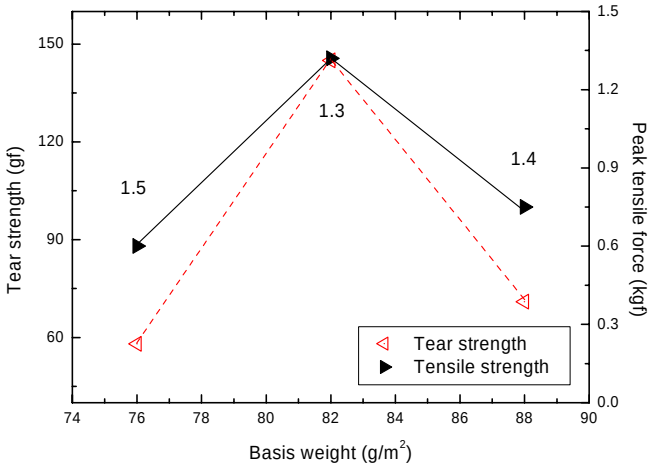
Figure 4-16. Relationship between basis weight and thickness and air permeability of TPUs (Phase 3).

On the other hand, Figure 4-16(b) shows that the web thickness and air permeability completely depended on the basis weight of MB TPU_{280} web. In the same processing conditions (#2.2, #2.4 and #2.5), web thickness was increased and air permeability was decreased with an increase of basis weight. This phenomenon is based on the increase of basis weight caused to thicker/denser structure based on heavier web and these structures provide better barrier properties.

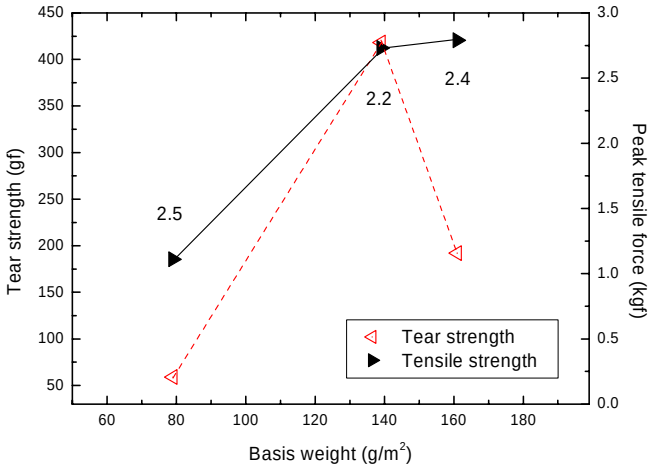
Two different results about thickness and air permeability of MB TPU webs depending on basis weight from TPU_{245} and TPU_{280} imply the rheological properties of TPUs are closely related to MB web properties. Especially, air flow rate could be a critical factor for decreasing fiber diameter of MB TPU_{245} webs which have lower melt viscosity.

The web strength of TPU_{245} was given in Figure 4-17(a), tear and tensile strength increased first, and then decreased with basis weight. These results also contrast to the general trends as mechanical strength increased with basis weight, however, the peak elongation MB TPU_{245} web was proportional to the tensile peak force.

Figure 4-17(b) shows the web strength of TPU_{280}; tear strength shows the same tendency as TPU_{245}, but tensile strength increased with increasing basis weight. The peak elongation of TPU_{280} web was almost three times higher than elongation of TPU_{245} web and the peak tensile force of MB TPU_{280} web almost twice of TPU_{245} web.



(a) TPU_{245}



(b) TPU_{280}

Figure 4-17. Relationship between basis weight and tear strength and tensile strength of TPUs.

It should be noted that the tensile strength of the MB webs is largely decided by tensile strength of the fiber and also affected by fiber entanglements and bonding in the MB webs; however, the tear strength of MB web is mainly decided by fiber entanglements and bonding. Therefore, the migration and cumulating of the fiber at tearing points in the MB webs followed by tear force direction decided the tear strength.

The large decrease of tear strength for Trial #2.4 compared to #2.2, in spite of the increase of basis weight, could be explained by fiber orientation and entanglements. Air flow rate of Trail #2.4 was increased from 118 scfm (3.37 m^3/min) to 138 scfm (3.94 m^3/min).

The increase of air flow rate resulted in more machine direction (MD) oriented fiber arrangement in the MB webs, so the migration of fiber should be easier than randomly oriented fiber structure on the MB web. The lowest tear strength of #2.5 also mainly attributed to the difference of basis weight from other two trials. Also, it should be highly affected by higher air flow rate of 150 scfm (4.29 m^3/min) than #2.2 and #2.4.

The abrasion resistance of MB TPU fabrics was measured by a rotary platform table abrasion tester, which had two heads. 50, 100 and 200 revolutions of the rotating head were applied with 250g per wheel of load for each specimen.

Then, those specimens were compared to non-cycled samples and to a 40 g/m^2 MB PP web.

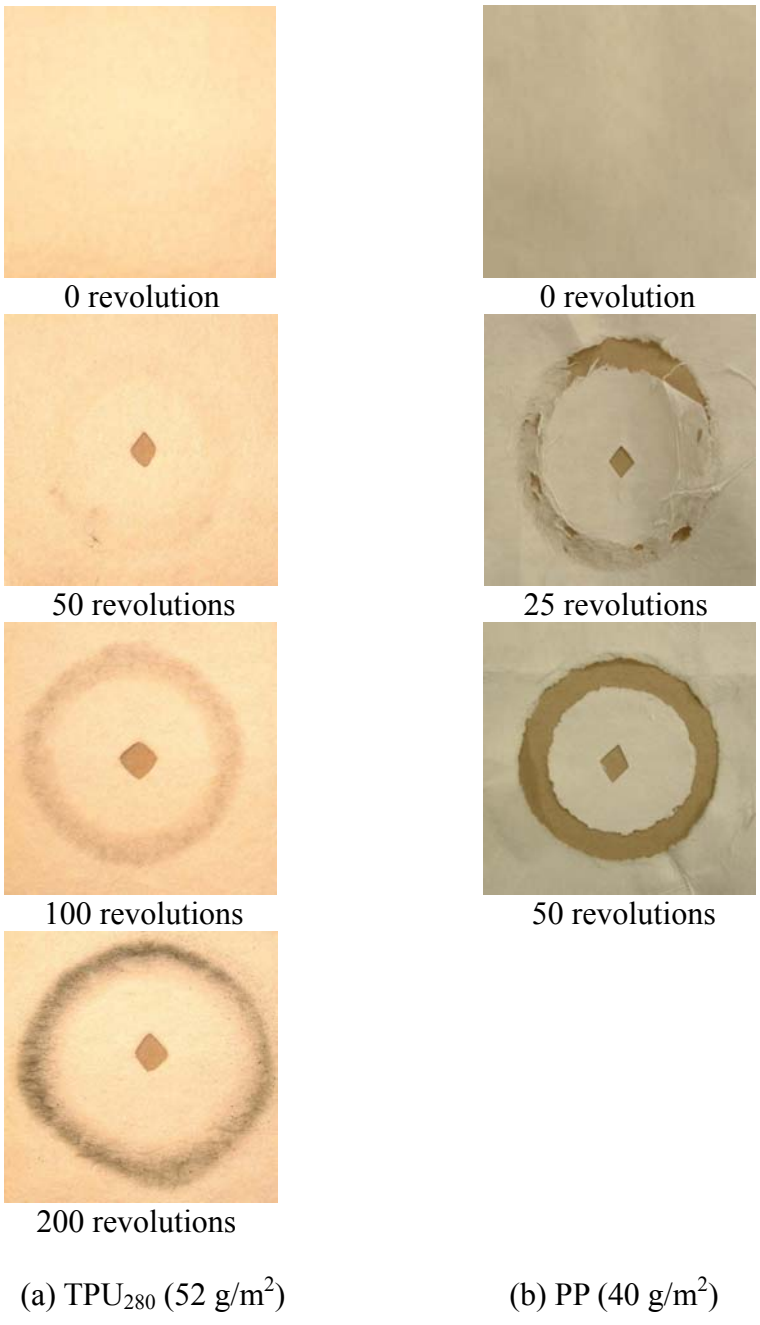
Figure 4-18 shows that the MB TPU_{280} Trial #2.3 (52 g/m^2) and 40 g/m^2 of MB PP webs after applied revolutions of wheel, respectively. Apparently, the increase of revolutions caused a clear green circle mark and fragments to MB TPU_{280} webs, but there was no development of TPU web breakage. Overall, MB TPU_{280} webs exhibited substantially more abrasion resistance than similar PP MB webs.

The light weight webs of TPU_{245} such as Trial #1.1 and #1.2 showed some fiber breakages at a higher number of revolutions around 200. However, the MB PP web start lost mechanical strength after 10 revolutions and MB PP web totally lost mechanical strength after 50 revolutions.

Table 4-3 shows the tensile properties of the MB TPU web after abrasion, peak force and peak elongation decreased with increase of revolution of the wheels for all TPUs, but the rate of loss in breaking load was different depending on the types of TPUs.

Figure 4-19 represents the rate of tensile strength loss of MB TPUs webs after abrasion. The tensile strength of MB TPU_{245} webs decreased with increase of revolutions. MB TPU_{245} webs lost notable tensile strength from 50 revolutions, but after that, the ratio of tensile strength loss was more moderate than MB TPU_{280} webs of light weight.

The tensile strength of fiber-grade MB TPU_{280} webs showed lower strength loss even after the high revolutions. Strength loss was higher for the light weight web and lower for heavy weight web.



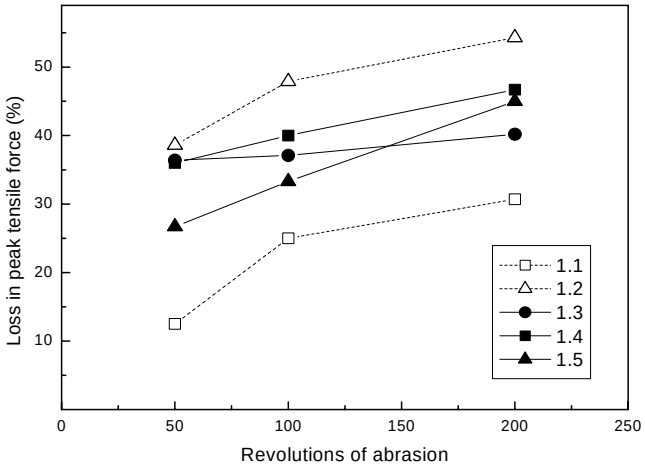
(a) TPU_{280} (52 g/m^2) (b) PP (40 g/m^2)

Figure 4-18. MB TPU_{280} and MB PP specimens after abrasion (Phase 3).

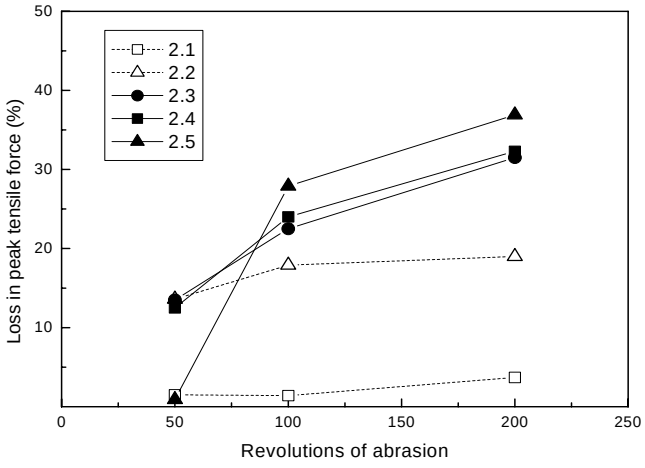
Table 4-3. Abrasion resistance of MB TPU webs.

Description				Tensile Properties							
Resin	Sample No.		Rev.	0		50		100		200	
			Weight (g/m^2)	Peak Force (Kgf)	Peak Elong. (%)	Peak Force (Kgf)	Peak Elong. (%)	Peak Force (Kgf)	Peak Elong. (%)	Peak Force (Kgf)	Peak Elong. (%)
TPU_{245}		1.1	45	0.88	243	0.77	190	0.66	152	0.61	143
		1.2	52	1.40	342	0.86	165	0.73	162	0.64	148
		1.3	82	1.32	209	0.84	146	0.83	133	0.79	131
		1.4	88	0.75	96	0.48	69	0.45	72	0.40	65
		1.5	76	0.60	81	0.44	61	0.40	60	0.33	51
TPU_{280}		2.1	615	19.26	607	18.98	580	18.99	599	18.55	572
		2.2	139	2.73	348	2.36	273	2.24	277	2.21	271
		2.3	52	0.89	197	0.77	170	0.69	142	0.61	140
		2.4	161	2.79	350	2.44	241	2.12	220	1.89	191
		2.5	79	1.11	244	1.10	145	0.80	128	0.70	123
PP		3.1	40	0.32	35	NA*					

NA*: Specimen is not available due to failure of abrasion resistance.



(a) TPU_{245}



(b) TPU_{280}

Figure 4-19. Loss in peak tensile force of MB TPU webs after abrasion (Phase 3).

The loss of peak tensile force for the Trial #2.1 was less than 4% even after 200 revolutions.

However, the other trials of MB TPU_{280} webs showed relatively higher tensile strength loss than Trial #2.1, but those webs still contained more than 60% of tensile strength compared to the peak force before abrasion.

For #2.2 (139 g/m^2) and #2.4 (161 g/m^2), the rate of tensile peak force loss showed quite different tendency. Trial #2.2, which has lower basis weight, showed less rate of peak tensile force loss than #2.4, which have higher basis weight.

This probably caused by orientation of fiber bundle on the MB TPU_{280} webs. MB TPU_{280} webs having randomly oriented fiber bundles, because of less air flow rate (3.37 m^3/min), showed more abrasion resistance than MB TPU webs having uni-directional fiber bundle orientation because of higher air flow rate (3.94 m^3/min).

Furthermore, the rate of peak tensile strength loss was also in the order of Trial #1.3 (3.71 m^3/min), Trail #1.4 (4.03 m^3/min) and Trail 1.5 (4.11 m^3/min) as increase of air flow rate order, although MB TPU_{245} webs have about same basis weight.

On the other hand, for the purpose of measuring the cycling load and relaxation, eight segments of cycling tensile tests were performed.

The gage was set at 3 inches and MB TPU webs were extended to 150% of the original gage, and then relaxed to initial gage, and released for 60 sec, and then this routine was repeated two more times. Except Trial #1.4 and Trial #1.5, all

specimens did not break during cycling test. MB webs of TPU_{245} and TPU_{280} showed clear difference for first tensile loading from each other.

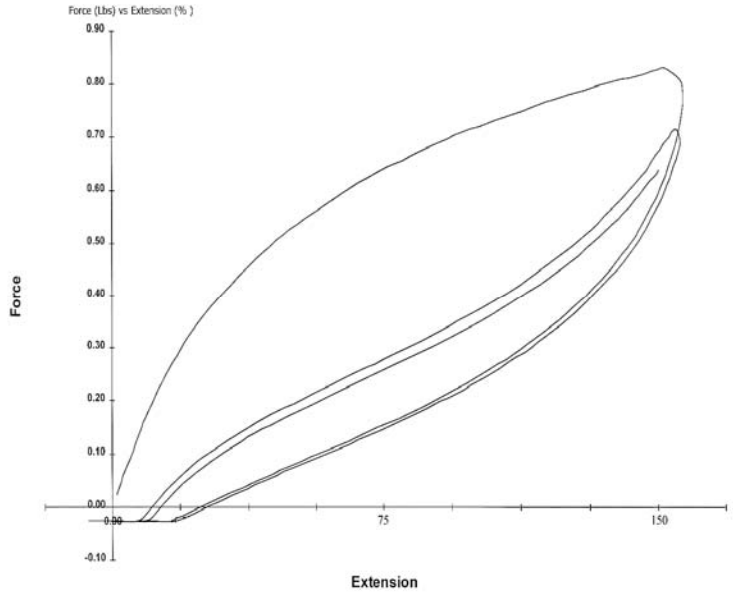
The representative specimen of TPU_{245} and TPU_{280} was presented in Figure 4-20. For the Trial #1.2 of TPU_{245} and Trial #2.3 of TPU_{280}, those samples did not reach the maximum tensile strength, but for the same extension below 150%, TPU_{245} received more tensile load than TPU_{280}.

For Trials #1.2, the peak tensile force reached 0.37kgf at the first loading and then peak force decreased to 0.32kgf at second loading for 150% extension; however, #2.3 reached 0.33kgf at the first loading and decreased to 0.30kgf with the second loading for 150% extension. Therefore, loss of tensile strength by cycling load was 13.41% for #1.2 and 9.72% for #2.3, but after the second loading, the loss of tensile strength for third loading, #1.2 was 9.86% and #2.3 was 7.69%. More specific tensile cycling load test results are presented in Appendix I.

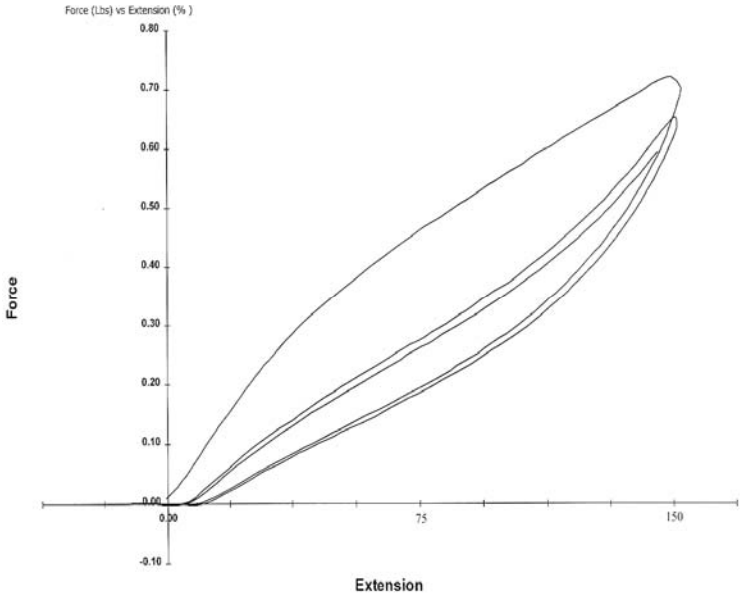
4.4 Phase 4

4.4.1 Fiber and Web Formation Studies

The fiber/web formation during MB TPU processing and advanced statistical analyses using different processing conditions of TPU_{237}, TPU_{245} and TPU_{280} were studied in Phase 4. Air temperature, air velocity, fiber temperature, fiber velocity, fiber diameter and orientation of the fiber on the webs were investigated following with different distance from the die.



(a) Trial #1.2 (TPU_{245})



(b) Trial #2.3 (TPU_{280})

Figure 4-20. Cycling test of extension and relaxation (Phase 3).

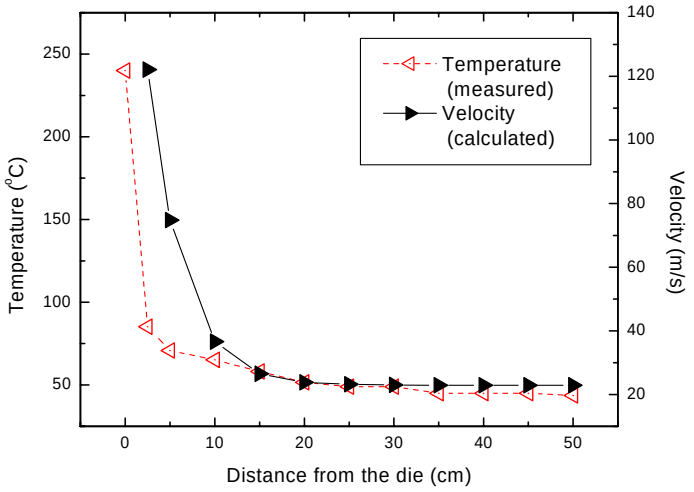
Even though the die temperature was set at 220^{o}C, the distribution of the measured die temperature at the front surface of the air knife detected by infrared thermometer MX2^{TM} Rasytek$^{®}$ was different across the die width as shown below:

(Left) 162^{o}C -188^{o}C -218^{o}C -203^{o}C -192^{o}C (Right)

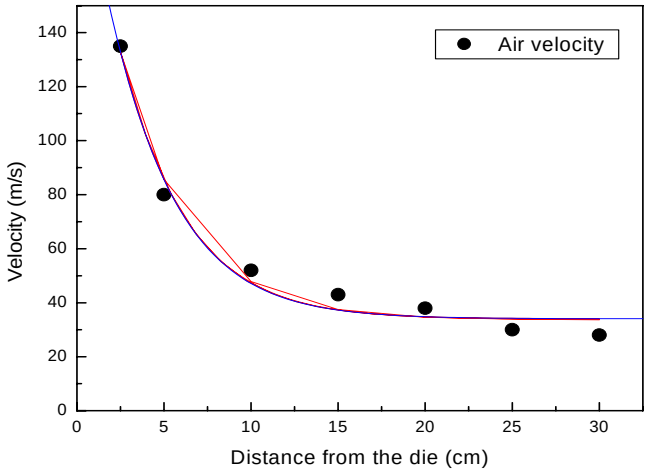
Temperature was measured about 30cm from the die on recommend by the manufacturer without polymer extrusion. The infrared beam was focused on the gap between air knife at the die exit and average temperature was recoded.

However, measured air temperature by Series 471 Digital Thermo-anometer produced by Dwyer$^{®}$ without polymer extrusion did not show any major difference across the die, but air temperature dramatically decreased with the increase of distance from the die.

Although the air temperature was set on 240^{o}C in the air manifold, the air temperature rapidly decreased to below 100^{o}C very near the die exit. Air temperature and velocity profiles are shown Figure 4-21(a). The air temperature was decreased from 240^{o}C to 71^{o}C during the first 6cm from the die, and the air temperature from 6cm to 20cm was moderately decreased from 71^{o}C to 51^{o}C. After 51cm, the decrease of air temperature was minimal. On the other hand, the air velocity was measured at 50cm from the die without polymer extrusion with 60% of air valve opening, and based on the experimental study of the PP.



(a) Air temperature and velocity profiles



(b) Air velocity profiles of PP study [Bresee, 2002].

Figure 4-21. Air temperature and velocity profiles at various DCDs (Phase 4).

Air velocity was calculated using mathematical models. For the fiber and web formation study of MB TPU process, the logged data fit using Boltzmann function was used on PP experimental data sets to produce a sigmoidal curve based on the findings by Bresee [2002].

Figure 4-21(b) is the air velocity profiles of PP, The equation (4-5) using Boltzmann fitting model had 98.8% accuracy and was the interpretation as best fitting model for PP.

$$y = \frac{A_1 - A_2}{1 + e^{(x - x_o)/dx}} + A_2 \qquad (4\text{-}5)$$

Where A_1: 1622.44, A_2: 33.83, x_o: -7.47, and d_x: 3.68. The air velocity of MB TPU study was measured from 30cm from the die and compared to the PP data set. After that based on equation (4-5), the velocity near the die was assumed.

On the other hand, the relationship between air velocity and fiber velocity was introduced as a 2nd degree of polynomial regression based on the experimental PP study and presented an equation (4-6),

$$y = A + B1x + B2x^2 \qquad (4\text{-}6)$$

Where A: -10.66, $B1$: 1.64 and $B2$: -0.01. This regression model fitted

with 99.9% of accuracy with experimental PP data sets.

During the MB process, fiber velocity is decided by air velocity, and the air speed continuously decreased from die. However, fiber velocity starts from nearly zero at the die exit, and then the fiber velocity abruptly increased because of the difference of higher speed of air and lower speed of the fiber. Since air and fiber velocity are identical after 4-6cm from the die, the fiber velocity also continuously decreased with air velocity.

Using the equation (4-6), the air velocity and the fiber velocity of MB TPU process was introduced. Figure 4-22 shows the calculated MB TPU air/fiber velocity at 60% of air valve opening and experimental PP air/fiber velocity. Based on the PP experimental spin-line study, the MB TPU fiber could reach the maximum speed of 55m/s at 3cm from the die, after that decreased with air speed, and after 4cm from the die, the velocity of TPU fibers are identically matched with air velocity.

Figure 4-23 shows the MB TPU_{280} fibers captured on the Kraft paper at the high speed (100mpm) of collector with different distances from the die. The TPU_{280} fibers were captured at 15cm, 23cm, 30cm, 38cm, 46cm, 56cm, 64cm and 74cm from the die. Generally, the air velocity near the die is much higher than collector speed, and caused fly fiber and make unstable web structure. However, the fiber entanglements increased with an increase of DCD in certain levels and decreased again. The fiber orientation of the MB TPU webs shows minor differences depending on the DCD.

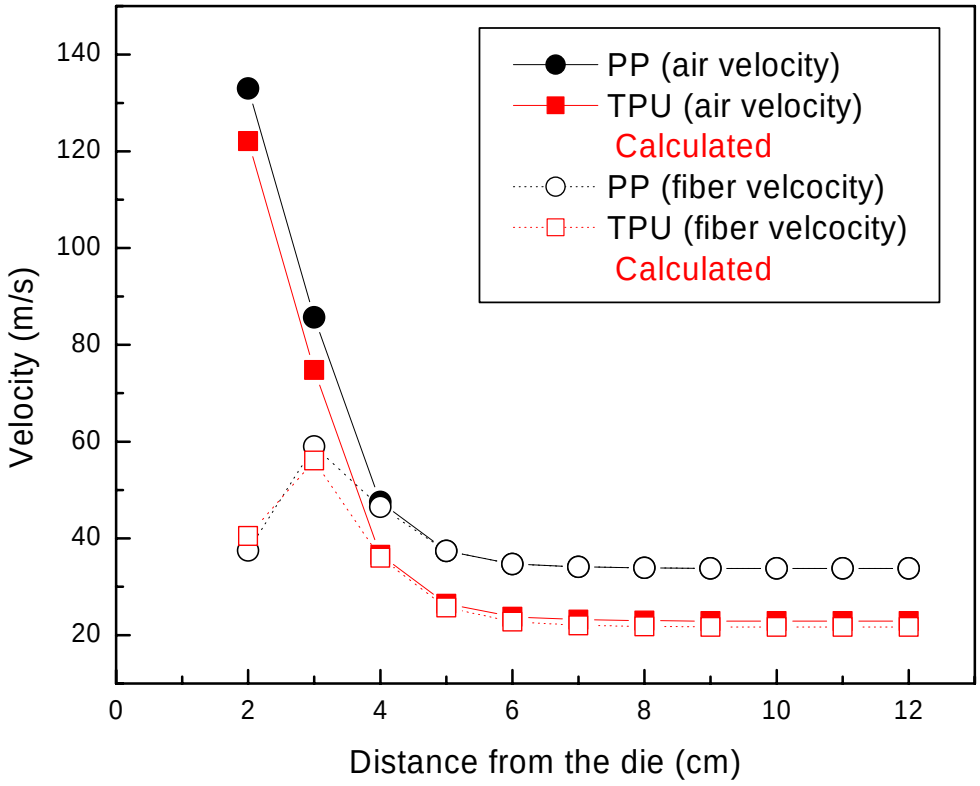


Figure 4-22. The air/fiber velocity of MB PP and TPU process at various DCDs (Phase 4).

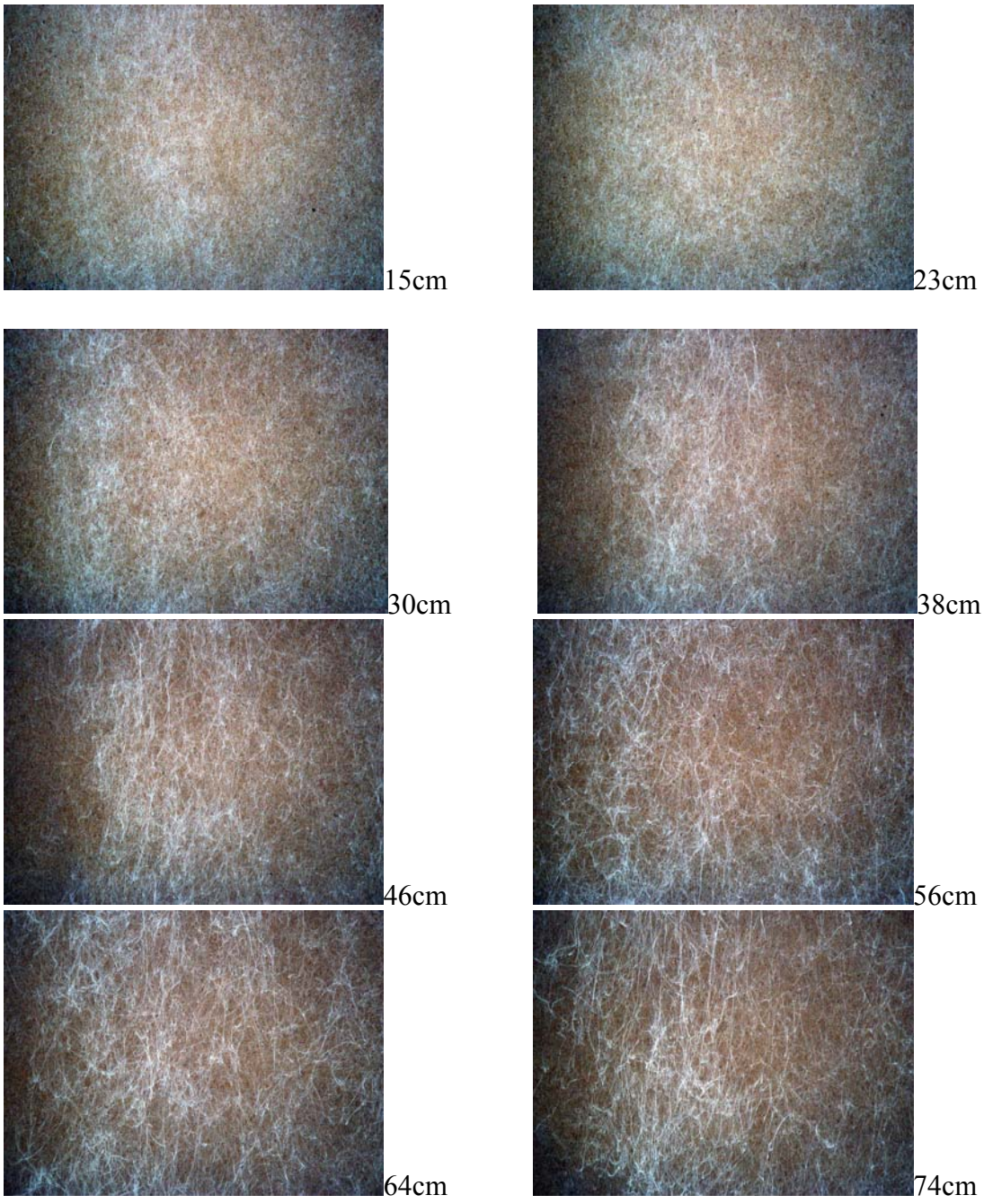


Figure 4-23. The MB TPU fibers collected at various DCDs with maximum speed (100mpm) of collector (Phase 4).

Figure 4-24 showed the change of fiber diameters with increase of DCD. Unlike the PP experimental study of Bresee [2002], the fiber diameters of MB TPU webs continuously increased with increase DCD, instead of decreasing. Thus, TPUs exhibit fundamentally different fiber diameter attenuation during MB process. This may be due to difference in thermal and elastic relaxation of TPU_{280} compared to PP.

Figure 4-23 also showed the fiber entanglements were smaller at lower DCD than higher DCD.

However, the fiber entanglements very close to the die were not determined in this study due to excessive air turbulence and sticking of the fiber to the Kraft paper, but the profiles of MB TPU fiber diameter imply smaller fiber diameters can be achieved near the die and these fiber diameters can increase with DCD, although fiber bundle size could be different from single fiber diameters size because of the increase of fiber entanglements with the increase of DCD.

Figure 4-25 shows the morphological change of fiber bundle on the MB TPU_{280} webs with the increase of the DCD, the smaller fiber diameters and curled TPU fibers achieved at the smaller DCD, and then the fiber bundle size and orientation increased with the DCD.

Figure 4-26 shows the distribution of mean fiber bundle diameters with various DCDs. The MB TPU_{280} webs collected at smaller DCD have a greater portion of small fiber diameter distribution and the ratio of distribution of smaller fiber diameters decreased with the increase of DCD.

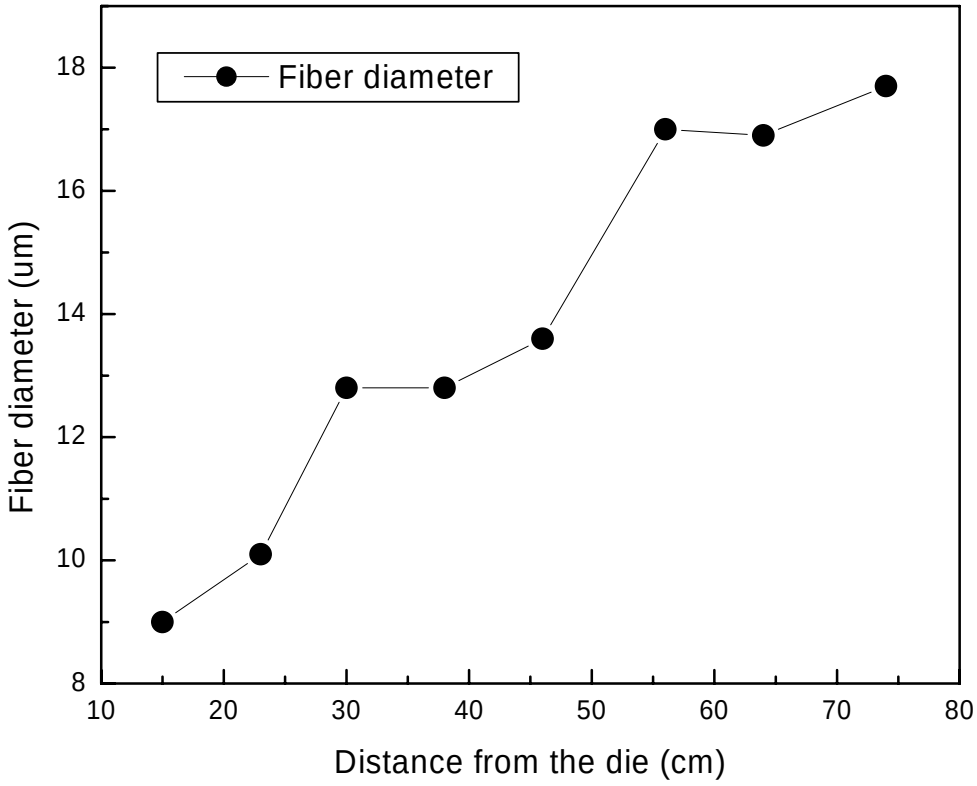
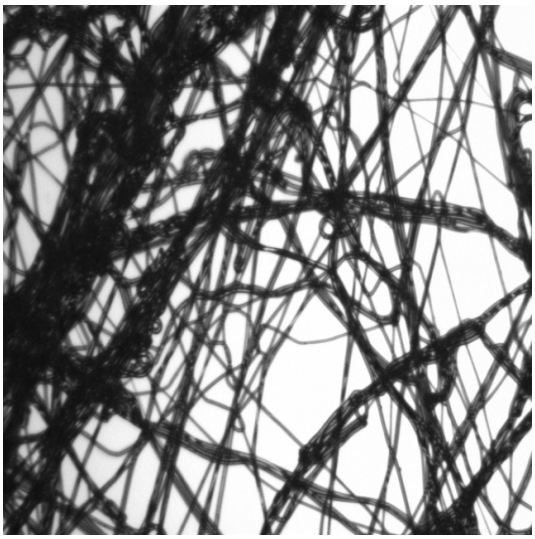


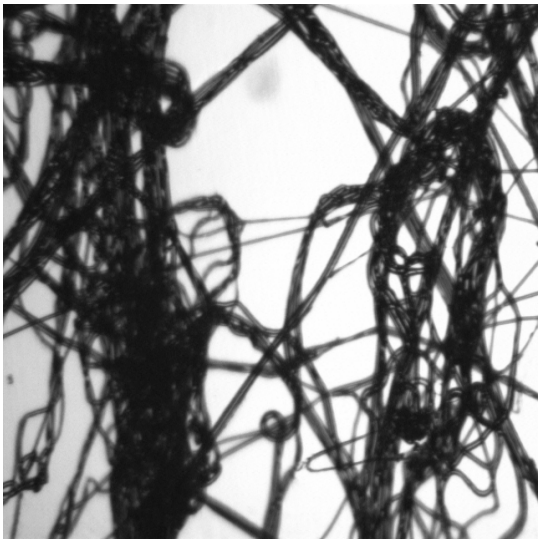
Figure 4-24. The fiber diameters of MB TPU_{280} webs collected at various DCDs (Phase 4).



(a) 23cm



(b) 38cm



(a) 56cm



(b) 74cm

Figure 4-25. The optical microscopy of MB TPU_{280} fiber bundle collected at different DCDs (Phase 4).

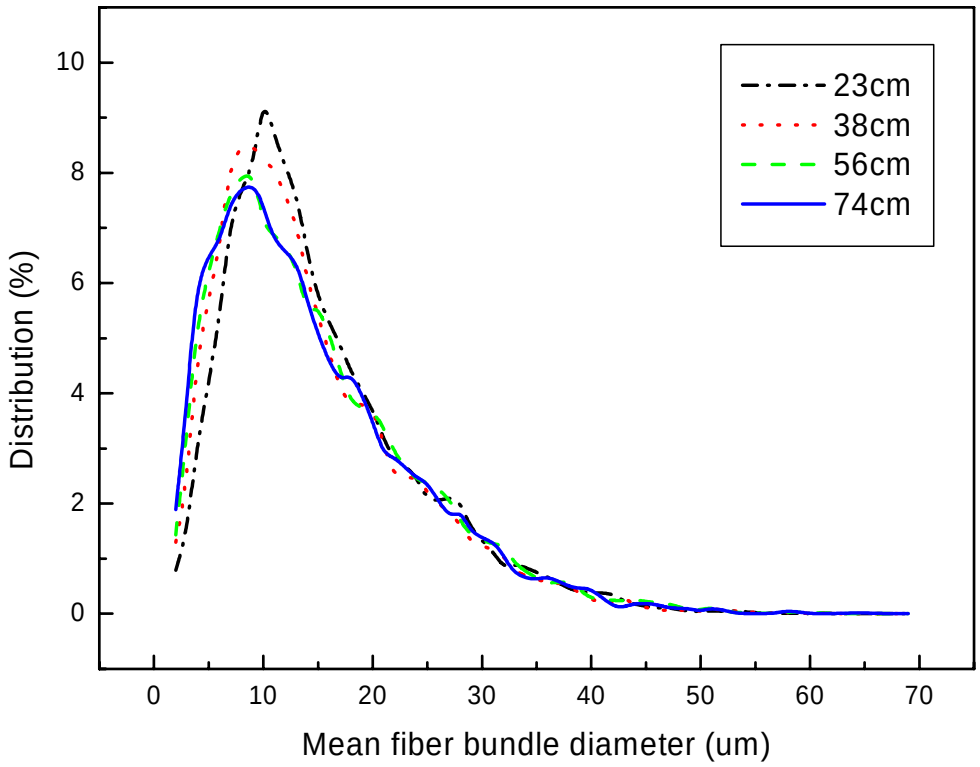


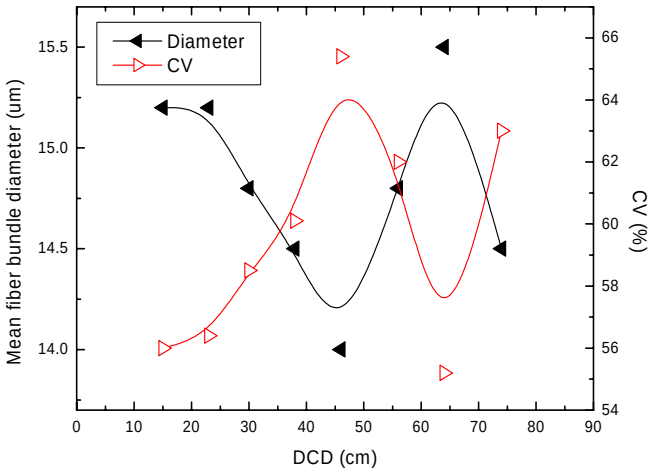
Figure 4-26. The mean fiber bundle diameter of MB TPU_{280} collected at various DCDs (Phase 4).

Figure 4-27 shows minimum, mean and maximum fiber bundle diameter, and coefficient of variation with various DCDs. Minimum and mean fiber bundle diameters initially decreased with the increase of DCD; however, the coefficient of variation was showed the opposite tendency from fiber bundle diameter. On the other hand, maximum fiber bundle diameter initially decreased, and increased later. These results imply that the web uniformity of MB TPU_{280} may have decreased with the increase of the DCD until 45cm. The MB TPU_{280} webs having smaller DCD have larger fiber bundle diameter but also have smaller coefficient of variation. After 45cm DCD, the increase of DCD increased the coefficient of variation because of a wide distribution from single fiber to big fiber bundle in the same web.

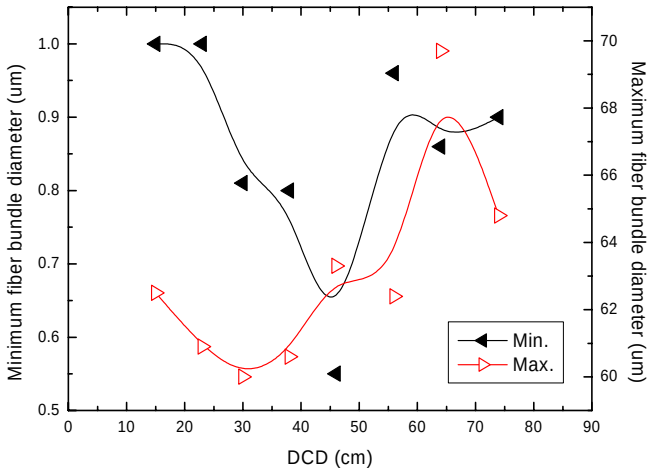
Figure 4-28 and Figure 4-29 show the orientation distribution of fiber bundles with different DCDs, and mean degree and MD/CD ratio of fiber bundles, respectively. The fiber bundles of the MB TPU_{280} web are generally more uni-directional in MD rather than iso-directional orientation with increasing DCD, and the orientation of the webs were more randomly distributed near the die. The general MD/CD ratio initially showed moderate decrease with increase of DCD but increased rapidly after 30cm of DCD.

4.4.2 Mechanical Properties of MB TPU Fibers and Webs

The mechanical properties of MB TPU fibers and webs in Phase 4 are given on Table 4-4, Table 4-5 and Table 4-6 for TPU_{237}, TPU_{245} and TPU_{280}, respectively.



(a) Mean fiber bundle diameter and coefficient of variation



(b) Minimum and maximum fiber diameter

Figure 4-27. Fiber diameter and coefficient of variation of MB TPU_{280} collected at various DCDs (Phase 4).

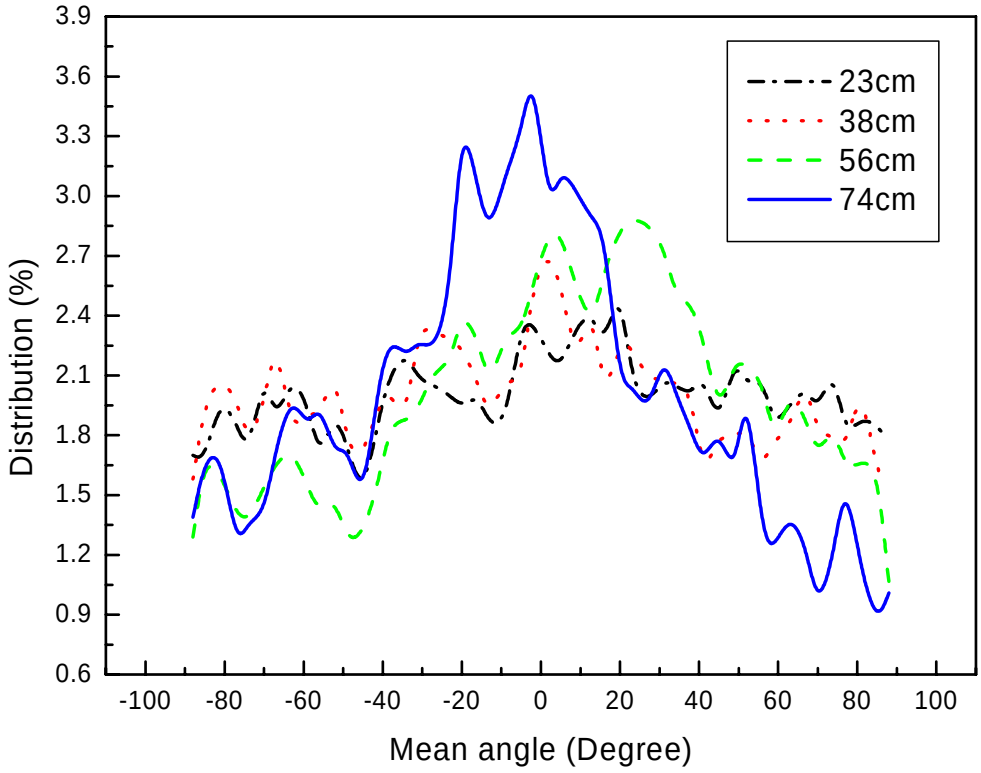


Figure 4-28. The mean fiber bundle angle of MB TPU_{280} collected at various DCDs (Phase 4).

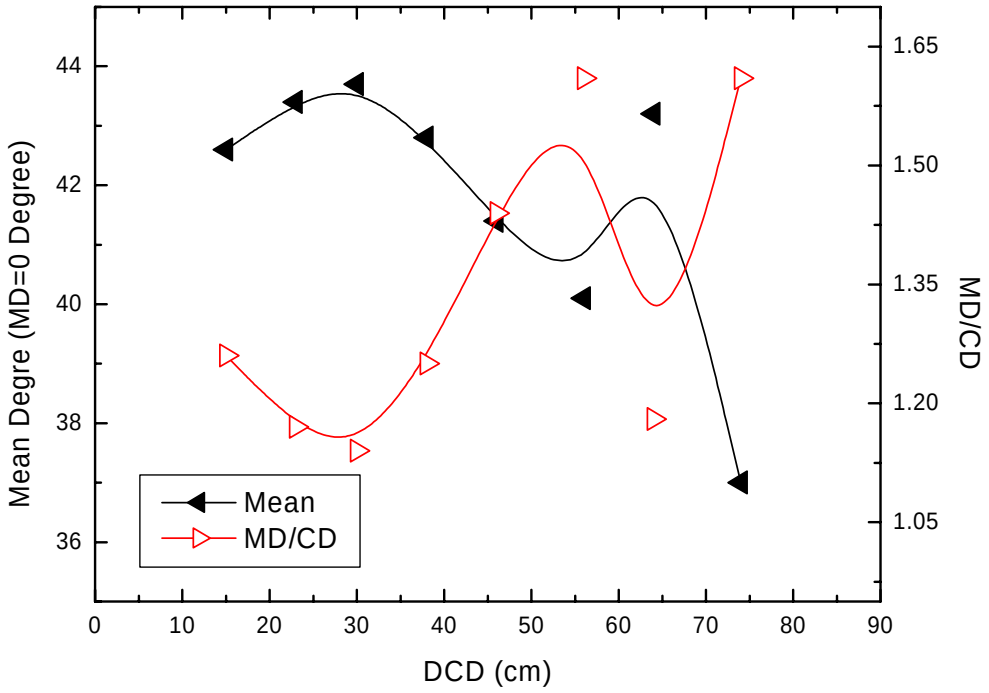


Figure 4-29. The mean fiber bundle degree and MD/CD ratio of MB TPU_{280} collected at various DCDs (Phase 4).

Table 4-4. Melt blown web properties of TPU_{237} on the 20-inch line in Phase 4.

Sample ID.	Weight (g/m^2)	Width (cm)	Thickness (mm)	Tear Strength (gf)		Air Permeability ($m^3/m^2/min$)	Fiber Diameter (um)	Peak Force (Kgf)		Peak Elong. (%)	
				MD	CD			MD	CD	MD	CD
1.1	105	33	0.489	281	428	73.4	6.88	1.22	0.50	186	407
1.2	155	34	0.717	549	816	84.5	15.20	1.88	0.86	243	360
1.3	151	33	0.680	539	959	72.2	11.74	1.73	0.64	238	307
1.4	117	32	0.574	213	545	92.1	6.42	1.07	0.38	148	138
1.5	99	30	0.530	153	321	100.4	4.80	0.76	0.35	146	135
1.6	82	32	0.389	95	234	75.0	6.17	0.98	0.40	160	192
1.7	99	32	0.580	220	428	106.1	6.31	0.99	0.41	127	183
1.8	82	33	0.455	199	461	136.0	6.85	0.86	0.29	141	199
1.9	93	32	0.463	98	200	91.6	5.16	0.80	0.31	81	132
1.10	72	30	0.432	39	132	118.7	3.82	0.59	0.15	58	133
1.11	66	34	0.394	49	118	141.2	5.50	0.43	0.22	54	152
1.12	77	29	0.425	78	165	110.7	5.65	0.68	0.26	73	155
1.13	172	30	0.769	236	485	56.2	7.36	1.57	0.71	155	185
1.14	143	37	0.684	249	582	67.1	6.94	1.25	0.63	158	254
1.15	265	36	1.079	817	1694	39.7	9.76	3.12	2.04	299	389

Table 4-5. Melt blown web properties of TPU_{245} on the 20-inch line in Phase 4.

Sample ID.	Weight (g/m^2)	Width (cm)	Thickness (mm)	Tear Strength (gf)		Air Permeability ($m^3/m^2/min$)	Fiber Diameter (um)	Peak Force (Kgf)		Peak Elong. (%)	
				MD	CD			MD	CD	MD	CD
2.1	111	33	0.438	79	131	86.0	5.18	0.45	0.16	59	177
2.2	149	33	0.575	60	156	69.8	5.35	0.32	0.16	50	121
2.3	146	30	0.540	160	276	41.1	6.91	1.35	0.57	178	357
2.4	81	36	0.394	16	59	66.7	4.30	0.48	0.20	43	115
2.6	224	36	0.790	176	363	17.9	9.83	2.34	0.96	132	309
2.7	77	33	0.279	32	101	22.6	4.78	0.67	0.35	75	279
2.8	59	29	0.266	46	96	37.4	4.25	0.83	0.28	85	216
2.9	52	34	0.279	30	116	65.0	4.17	0.58	0.24	61	216
2.10	54	27	0.209	41	110	48.0	4.48	1.00	0.25	51	296
2.11	117	28	0.390	53	127	20.7	5.40	1.42	0.52	106	309
2.12	137	29	0.477	133	286	32.5	6.65	1.72	0.65	173	398
2.13	124	28	0.438	82	191	23.7	5.87	1.68	0.65	169	424
2.14	160	30	0.583	223	329	45.7	7.11	2.05	0.67	215	301
2.15	88	33	0.412	29	77	57.1	6.89	0.47	0.19	58	99

Table 4-6. Melt blown web properties of TPU_{280} on the 20-inch line in Phase 4.

Sample ID.		Weight (g/m^2)	Width (cm)	Thickness (mm)	Tear Strength (gf)		Air Permeability ($m^3/m^2/min$)	Fiber Diameter (um)	Peak Force (Kgf)		Peak Elong. (%)	
					MD	CD			MD	CD	MD	CD
3.1		351	51	1.520	208	451	29.2	11.03	3.46	2.08	502	396
3.2		300	51	1.335	225	421	38.5	15.99	2.40	1.86	485	397
3.3		146	43	0.772	107	198	70.1	17.17	0.88	0.80	334	394
3.4	**D**	212	50	0.925	172	281	46.9	15.84	1.74	1.14	480	405
	W	197	50	0.952	160	302	49.3	16.51	1.48	1.00	369	368
3.5	**D**	265	46	0.937	215	440	23.9	14.75	2.98	3.06	598	576
	W	236	46	0.908	201	400	27.0	15.59	2.70	2.41	618	562
3.6	**D**	204	47	0.971	189	324	50.3	16.14	1.30	0.94	324	318
	W	245	47	1.342	214	350	42.9	15.30	1.34	1.30	342	409
3.7		272	50	1.323	652	718	39.8	15.22	3.79	2.76	668	690
3.8		174	46	0.848	100	169	44.0	15.22	1.18	1.03	341	396
3.9		206	48	1.003	142	259	32.9	12.55	1.66	1.19	483	385
3.10		211	51	1.023	179	286	30.5	12.18	2.02	1.68	493	474
3.11		133	43	0.632	79	124	43.9	9.45	1.22	0.67	405	405
3.12		133	51	0.701	107	174	53.3	13.96	1.22	0.73	440	378

Uniform and continuous MB webs were produced from all TPU trials and rolled up with Kraft paper for TPU_{237} and TPU_{245} to prevent from the sticking together.

The TPU_{237} resulted in basis weight from 66 to 265 g/m^2 with 3.82 to 15.20μm average fiber diameter, peak tensile force varied from 0.43 to 3.12kgf in machine direction (MD) and 0.15 to 2.04kgf in cross direction (CD), peak elongation varied from 54 to 299% in MD, and 132 to 407% in CD.

On the other hand, MB TPU_{245} webs resulted in basis weight from 52 to 224 g/m^2 with 4.17 to 9.83μm of average fiber diameter. Peak tensile force varied from 0.32 to 2.34kgf in MD and 0.16 to 0.96kgf in CD; peak elongation varied from 43 to 215% in MD; and 99 to 424% in CD.

On the other hand, TPU_{280} resulted in a basis weight of 133 to 351 g/m^2 with 9.45 to 17.17μm average fiber diameters. In efforts to obtain finer fibers, the die temperature was held at 210ºC and 220ºC, but fiber diameter was much larger than fiber diameter of Phase 3.

Peak tensile force of MD and CD varied from 0.88 to 3.79kgf and 0.67 to 3.06kgf, respectively. Peak elongation varied from 324 to 668% in MD, and 318 to 690% in CD, and the tendency of tear strength showed the same tendency with other TPU fibers and webs.

However, MB TPU_{280} webs showed different relationships of peak tensile force and peak elongation from other TPUs.

The TPU_{237}, TPU_{245} and TPU_{280} showed that peak tensile force increased with increase of peak elongation, and tensile strength of MD showed stronger than that of CD. MB TPU_{237} and TPU_{245} webs have more peak elongation in CD than MD, but MB TPU_{280} webs showed almost the same peak elongation for both directions.

More specifically, the effect of each processing parameter on MB TPU webs was studied for TPU_{237}, TPU_{245} and TPU_{280} polymers. Figure 4-30 shows the effect of the die temperature on fiber diameter and air permeability of the MB TPU_{237} webs. The results of air permeability, which probably come from elastic properties of the MB web, contrasts to the general polyolefin webs in that air permeability generally decreased with increase of basis weight and web thickness when fiber diameter remained the same.

The fiber diameters of TPU_{237} webs also continuously increased with increasing die temperature and this result also contrasts to the properties of normal polyolefin MB web.

These results could be explained by the different crystallization and extension processes of MB TPU fibers at the spin-line compared to PP and other polyolefin fibers. The molecular structure of TPU fibers continues to shrink with heat and expand in fiber diameter even after the fibers arrive on the collector. The results of DSC in Phase 3 showed very low percent crystallinity for TPU_{245} and TPU_{280}, although MB TPU webs had much higher mechanical strength compared to general polyolefin MB webs.

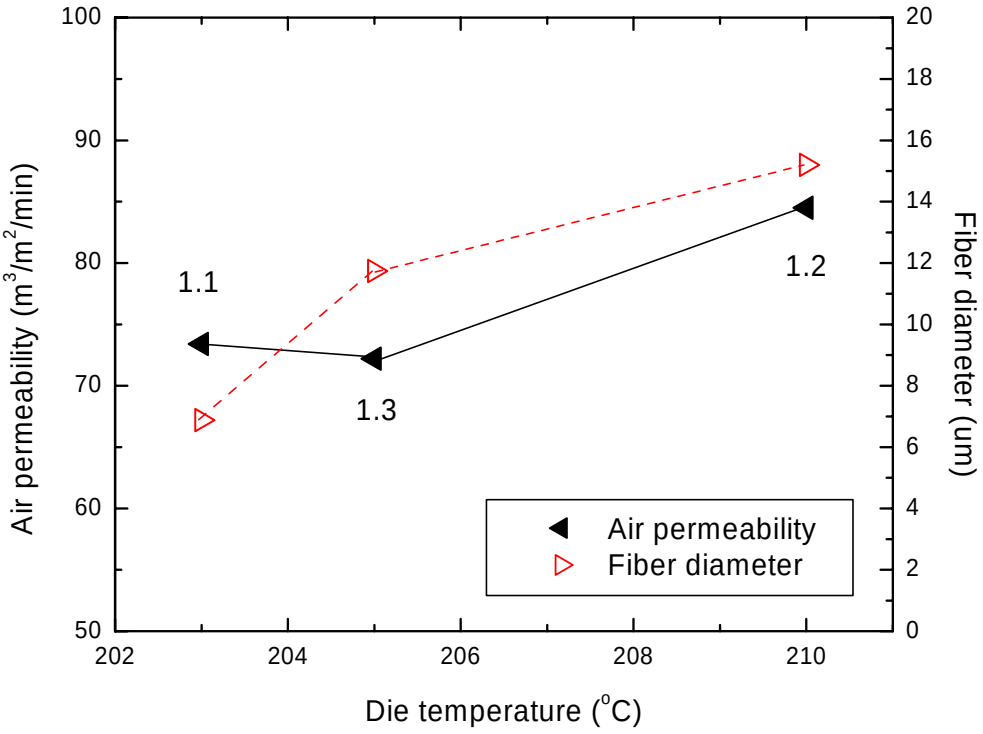


Figure 4-30. The fiber diameter and air permeability of MB TPU_{237} webs produced by various die temperatures (Phase 4).

The mechanical strength of MB TPU_{237} webs having different die temperature is presented in Figure 4-31.

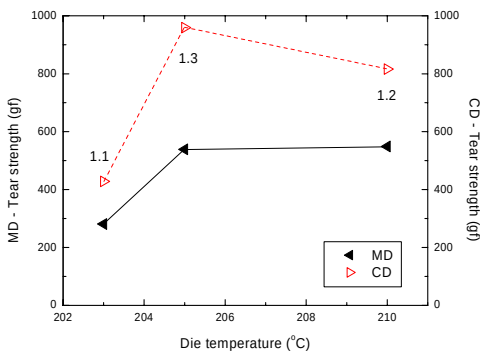
Both tear and tensile strength increased with die temperature. This increase of web strength may be caused by the increase of basis weight and web thickness. The CD tear strength was higher than that of MD, but tensile strength of MD much higher than that of CD.

Considering the trends of tear and tensile strength of the MB TPU_{237} webs, the TPU fibers may have more uni-directional fiber orientation rather than iso-directional fiber orientation.

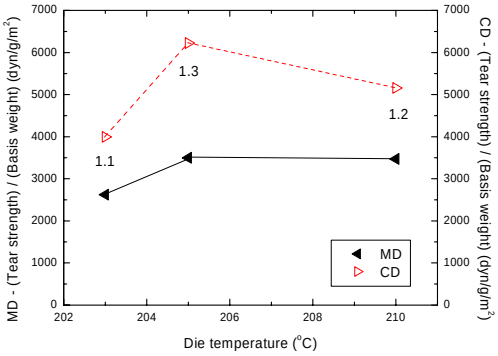
Furthermore, the normalized mechanical strength, which is peak force and tear strength divided by basis weight, also show about the same tendency with non-normalized strength profiles, although the difference of normalized tensile strength between different die temperatures was smaller than that of non-normalized strength.

These results imply the increase of basis weight contributed to the mechanical strength by not only increasing of quantitative weight but also increasing of fiber entanglement, thermal bonding and development of fiber structure by TPUs sensitive thermal properties.

Previous results from FTIR and DSC analysis in Phase 3 also showed the fiber molecular structure and crystallization could be changed by basis weight. The molecular structure of TPUs showed clear differences depending on web positions and web thickness, even for the same processing conditions.

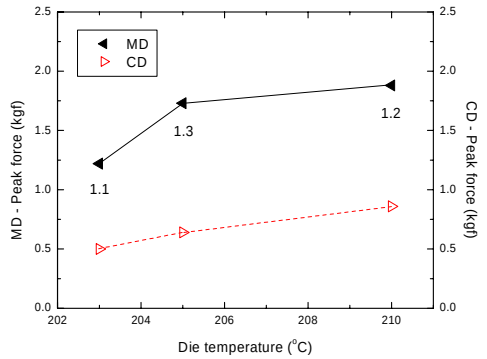


Original

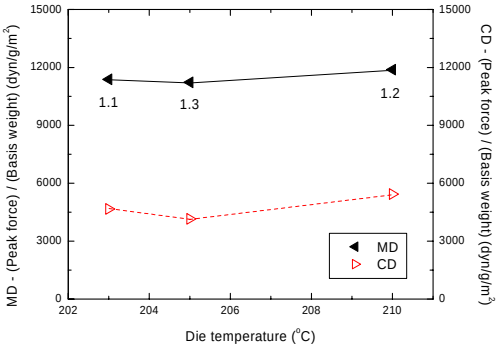


Normalized

(a) Tear strength



Original



Normalized

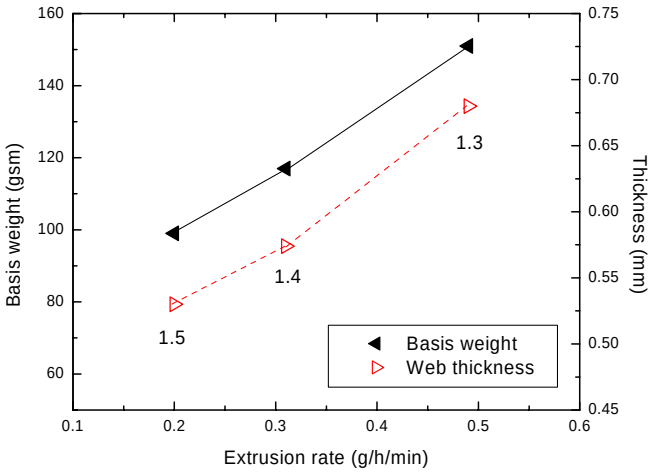
(b) Tensile strength

Figure 4-31. The tear and tensile strength of MB TPU_{237} webs produced by various die temperatures (Phase 4).

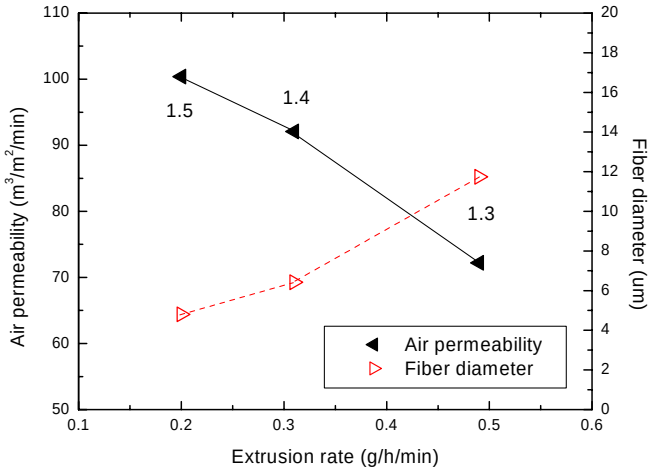
Figure 4-32 shows the effect of extrusion rate on the fiber and web properties, basis weight, thickness, and fiber diameter increased with extrusion rate, but air permeability decreased with extrusion rate. These results correlated with general trends of MB webs, however, the results of air permeability depending on extrusion rate, contrast to the previous results of the change of die temperature. The air permeability increased with increase of basis weight for the change of die temperature; however, air permeability decreased with increasing basis weight for the change of extrusion rate.

Figure 4-33 shows the tear and tensile strength depending on the change of extrusion rate. Both tear and tensile strength increased with increase of extrusion rate caused by increase of basis weight and thickness, and the normalized strength showed the same tendency. The difference of strength between MD and CD was smaller at lower extrusion rate, and then increased with increasing extrusion rate. This indicates that the increase of polymer throughput contributed on the increase of web strength by the number of fibers for unit area. However fiber diameter and the number of fiber did not increase as much in the CD with increasing throughput.

Figure 4-34 and Figure 4-35 show the effect of air temperature on fiber and web properties. The basis weight and web thickness tended to go through a minimum at 216^{o}C, but did not notably differ over the temperature range of 210-221^{o}C, and air permeability did not show any clear trends against the change of air temperature; however, the fiber diameter increased with air temperature.

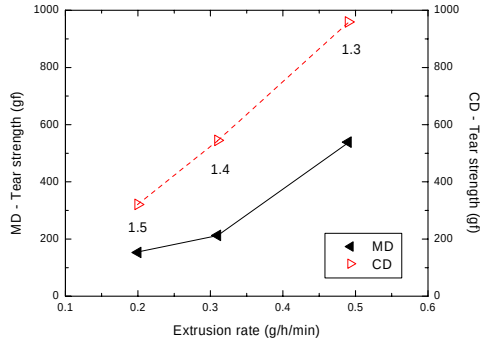


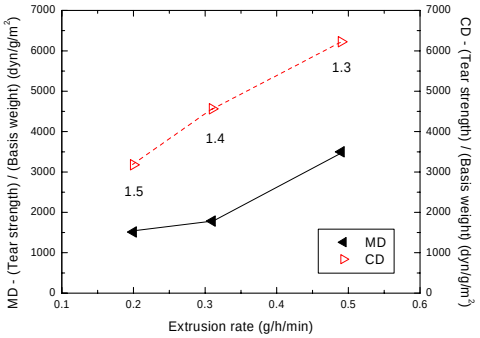
(a) Basis weight and thickness



(b) Air permeability and fiber diameter

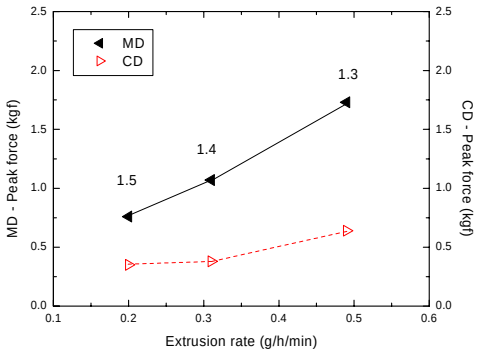
Figure 4-32. The fiber and web properties of MB TPU_{237} webs produced with various extrusion rates (Phase 4).

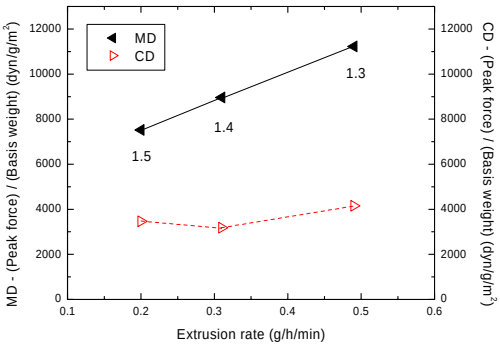




Original Normalized

(a) Tear strength

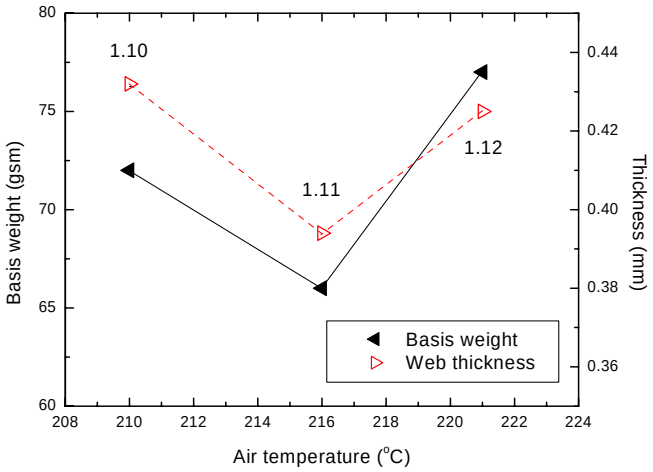




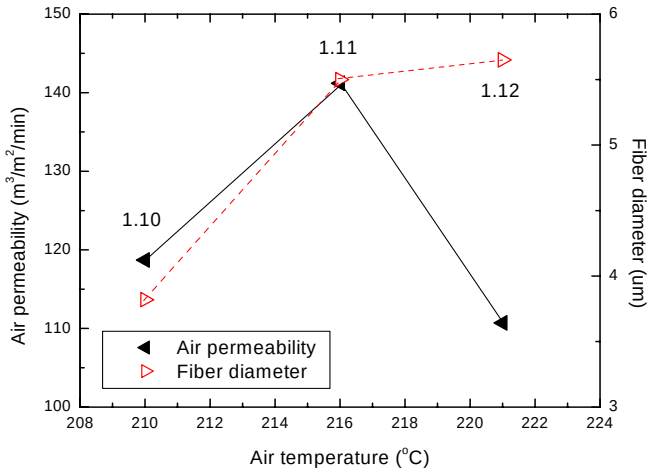
Original Normalized

(b) Tensile strength

Figure 4-33. The tear and tensile strength of MB TPU_{237} webs produced with various extrusion rates (Phase 4).

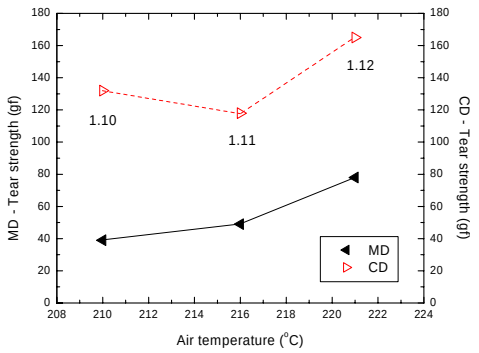


(a) Basis weight and thickness

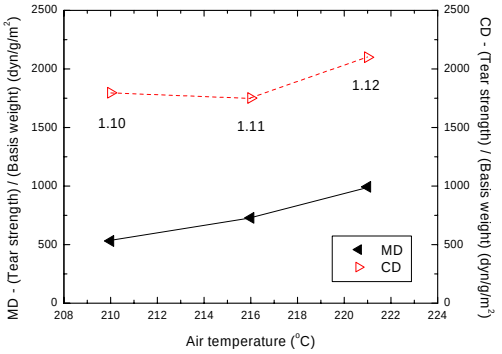


(b) Air permeability and fiber diameter

Figure 4-34. The fiber and web properties of MB TPU_{237} webs produced at various air temperatures (Phase 4).

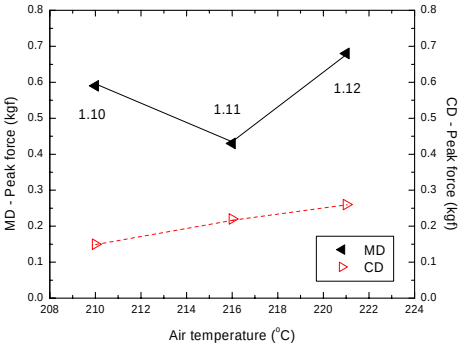


Original

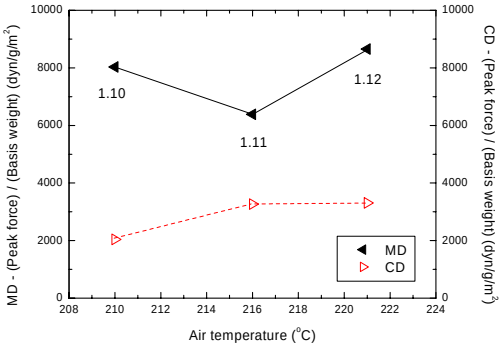


Normalized

(a) Tear strength



Original



Normalized

(b) Tensile strength

Figure 4-35. The tear and tensile strength of MB TPU_{237} webs produced at various air temperatures (Phase 4).

The tear and tensile strengths of MB TPU_{237} webs were also showed a slight increase for both MD and CD. This indicates that the increase of air temperature is related to the increase of die temperature; however, the change of the web strength was small compared to the effects of other processing variables on the web strength.

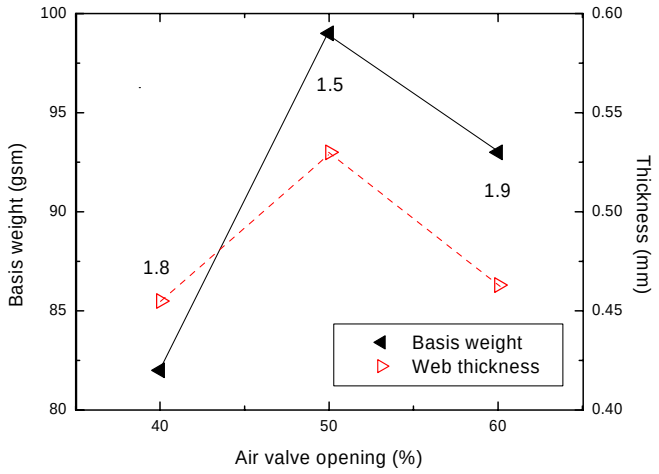
Figure 4-36(a) shows the effect of air valve opening, which is directly related to the air velocity on basis weight and web thickness.

The air valve opening decides the amount and speed of the air, the more air valve opening result in higher speed of air. In Phase 3, the 30%, 40% and 50% of air valve opening referred to 3.37 m^3/min (118scfm), 3.94 m^3/min (138scfm) and 4.29 m^3/min (150scfm) for TPU_{280}.

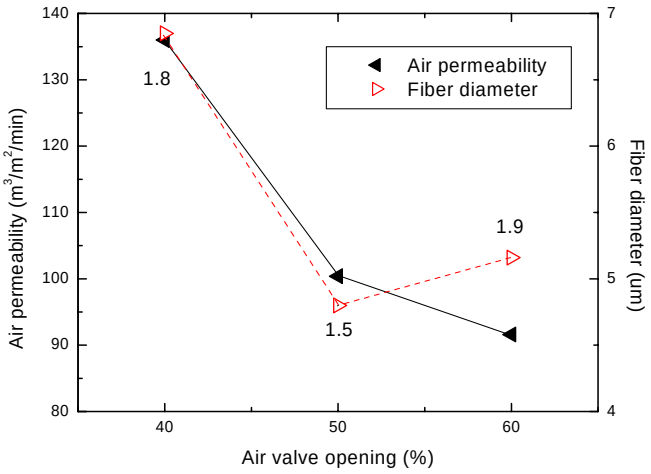
For TPU_{237}, the basis weight and web thickness initially increased with air valve opening; however, air acceleration and turbulence caused fiber breakage and fly formation, which likely resulted in reduced basis weight and thickness of the MB TPU_{237} webs.

Therefore those values were decreased in the webs with excessive air valve opening. Figure 4-36(b) represents that the fiber diameter and air permeability of the webs rapidly decreased with increase of air velocity.

Figure 4-37 shows that tear strength in the CD and MD notably decreased with increase of air velocity, the tear strength of CD decreased from 461 to 200gf, and 199 to 98gf in MD. However, there was only a minor change in MD and CD tensile strength with air flow rate.

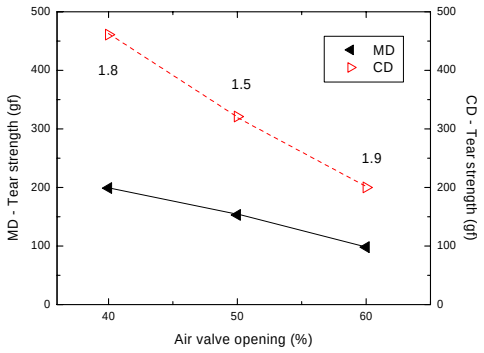


(a) Basis weight and thickness

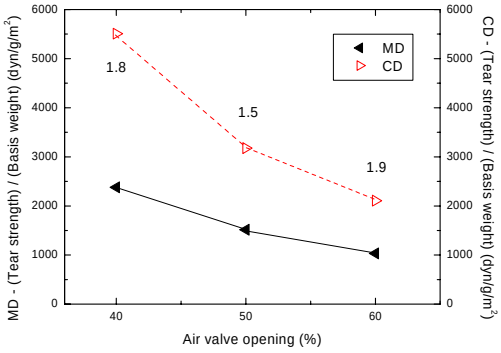


(b) Air permeability and fiber diameter

Figure 4-36. The fiber and web properties of MB TPU_{237} webs produced with various air velocities (Phase 4).

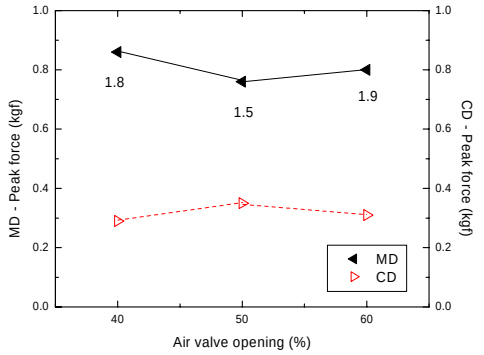


Original

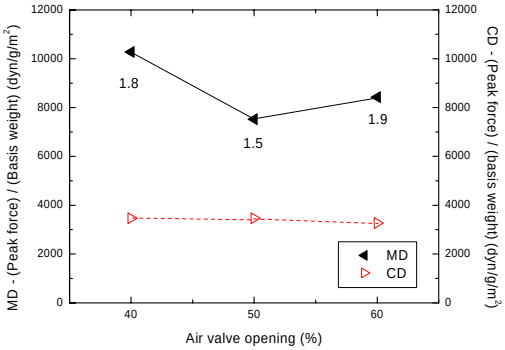


Normalized

(a) Tear strength



Original



Normalized

(b) Tensile strength

Figure 4-37. The tear and tensile strength of MB TPU_{237} webs produced with various air velocities (Phase 4).

The peak elongation of MD showed a big difference depending on air velocity; however, the change of peak elongation in CD was relatively smaller than the MD. Considering peak elongation and decrease of tear strength, the orientation of fibers on the MB webs were highly related to air velocity.

On the other hand, the basis weight and web thickness increased with increase of DCD. During the MB TPU process, TPU fibers have more heat content near the die than at the collector, and the increase of DCD translates to increase of spin-line stress and decrease of heat contents in the fiber.

For lower DCD, MB TPU_{237} fibers stick more to the collector and unstabilized fiber and web structures were probably easily affected by heat and air turbulence. Figure 4-38 shows the effect of DCD on fiber diameter and air permeability of TPU_{237} webs.

Although basis weight increased with DCD, air permeability also increased with increase of DCD, probably, because the web was less uniform as a result of fiber entanglements. The larger DCD did not make the web structure as dense as much closer DCD. These results also corresponded to the results of fiber and web formation study in Figure 4-25 and Figure 4-26. However, single fiber diameter was not highly related with DCD and did not show any clear tendency.

Figure 4-39 shows the web strength of TPU_{237} depending on DCD. Tear strength increased with DCD, but tensile strength had only a minor effect from changing the DCD.

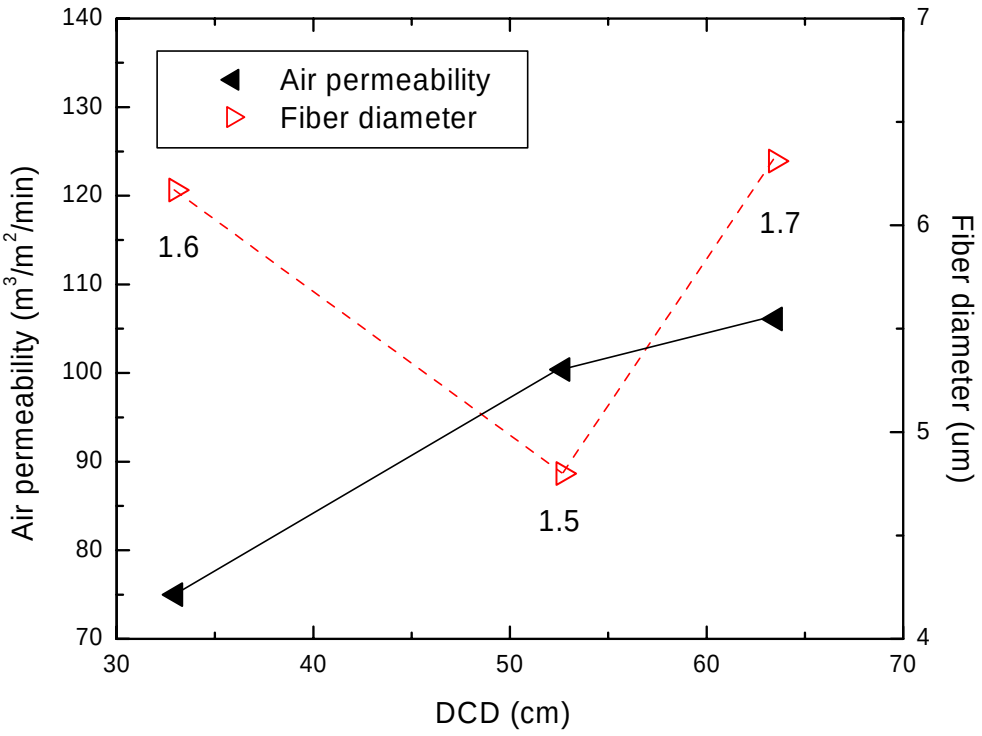
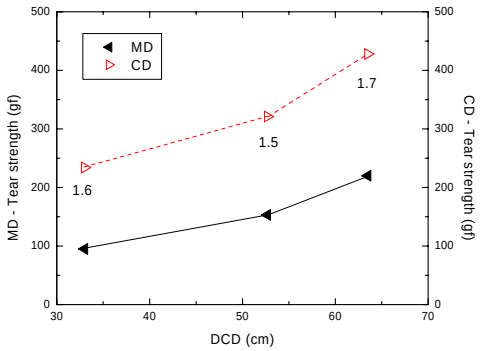
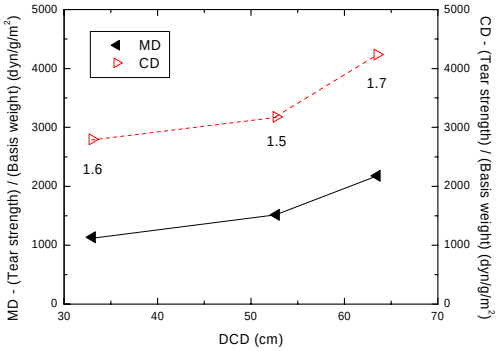


Figure 4-38. The fiber diameter and air permeability of MB TPU_{237} webs collected at various DCDs (Phase 4).

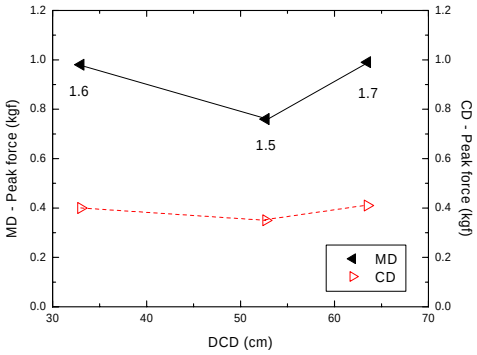


Original

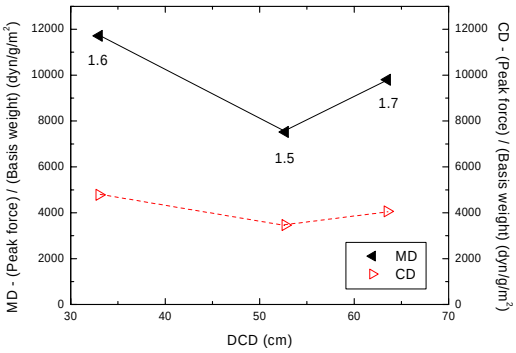


Normalized

(a) Tear strength



Original



Normalized

(b) Tensile strength

Figure 4-39. The tear and tensile strength of MB TPU_{237} webs collected at various DCDs (Phase 4).

These results may be caused by the increase of DCD resulting in a decrease of web density by increasing fiber entanglement and fiber bundle size. This could affect the tear strength much more than tensile strength.

Figure 4-40 shows the effect of die temperature on fiber diameter and air permeability on MB TPU_{245} webs. The fiber diameters of MB TPU_{245} webs increased first, then decreased with increasing die temperature, and the air permeability was decreased first and then increased with die temperature.

It should be noted that normally air permeability should increase with increase of fiber diameter and decrease with decrease of fiber diameter; therefore, the structural features or properties of MB TPU_{245} webs were probably related to this air permeability change.

Fiber diameters of MB TPU_{245} webs were varied from 7 to 5μm, but air permeability of the webs showed relatively large change from 41.1 to 86 $m^3/m^2/min$. Furthermore, the optimum tensile and tear strength were obtained at the mid-range die temperature of 205^oC. However, the peak elongation of TPU_{245} was only one-fourth of TPU_{237} in MD and about half of TPU_{237} in CD.

Figure 4-41 shows the effect of extrusion rate on the fiber and web properties. Basis weight, thickness, fiber diameter and air permeability increased with extrusion rate. The increase of air permeability with the increase of basis weight of MB TPU_{245} webs are contrast to the general trend of MB PP webs.

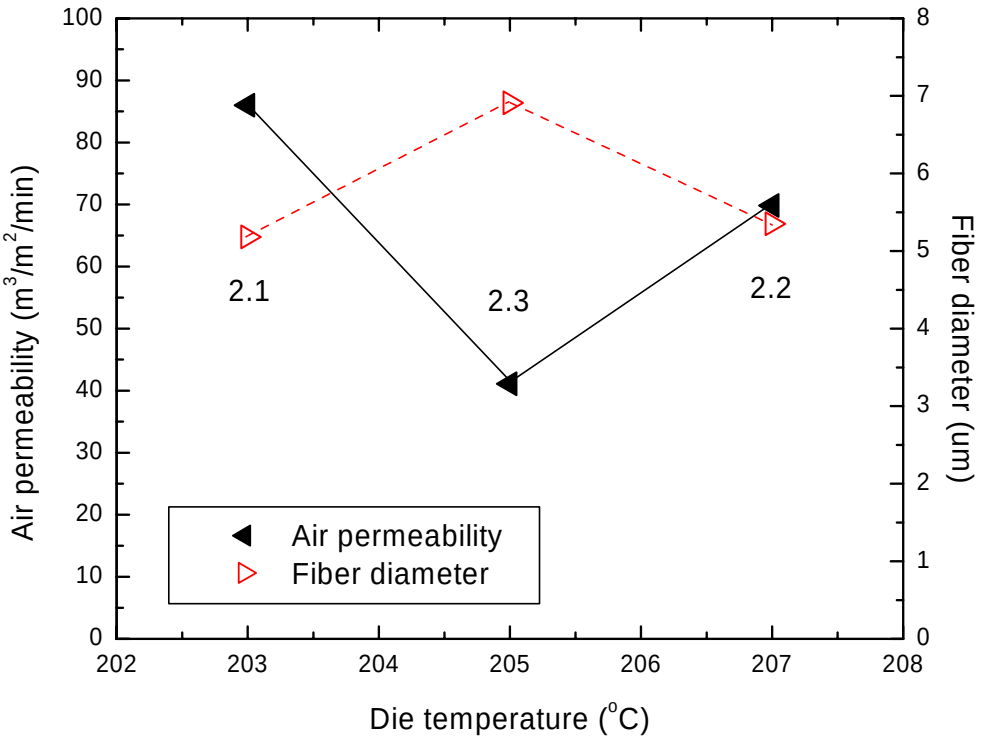
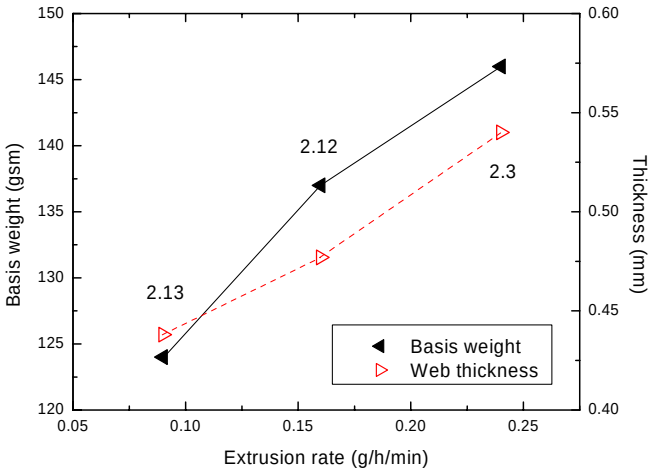
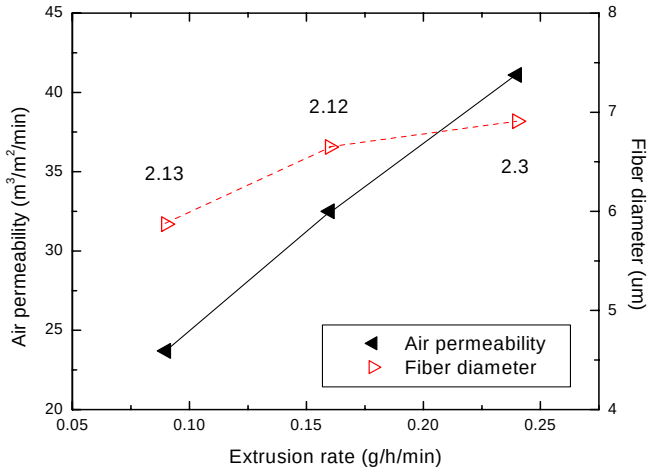


Figure 4-40. The fiber diameter and air permeability of MB TPU_{245} webs produced by the die temperatures (Phase 4).



(a) Basis weight and thickness



(b) Air permeability and fiber diameter

Figure 4-41. The fiber and web properties of MB TPU_{245} webs produced with various extrusion rates (Phase 4).

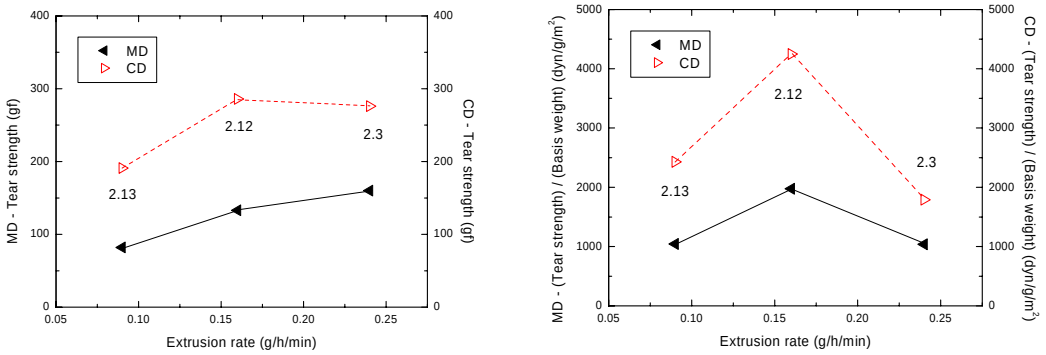
The increase of air permeability for #2.3, #2.12 and #2.13 may caused by the increase of fiber diameter, however, the air permeability was probably more affected by structural features of MB TPU_{245} webs such as fiber entanglements rather than fiber diameter.

Figure 4-42 shows the effect of extrusion rate on tear and tensile strength of the MB TPU_{245} webs. Tear strength increased with increase of extrusion rate caused by increase of basis weight and thickness, but tensile strength slightly decreased in MD and did not show clear trends for CD.

The standard deviations of the basis weight (15g), thickness (0.05mm), fiber diameter (3μm) and air permeability (6 $m^3/m^2/min$) from MB TPU_{245} webs were much lower than MB TPU webs from other TPU resins (all standard deviations were roughly twice or three times higher than MB TPU_{245} webs), so, it provides the possibility of web structure and uniformity of the MB TPU_{245} webs better than MB webs from TPU_{237}.

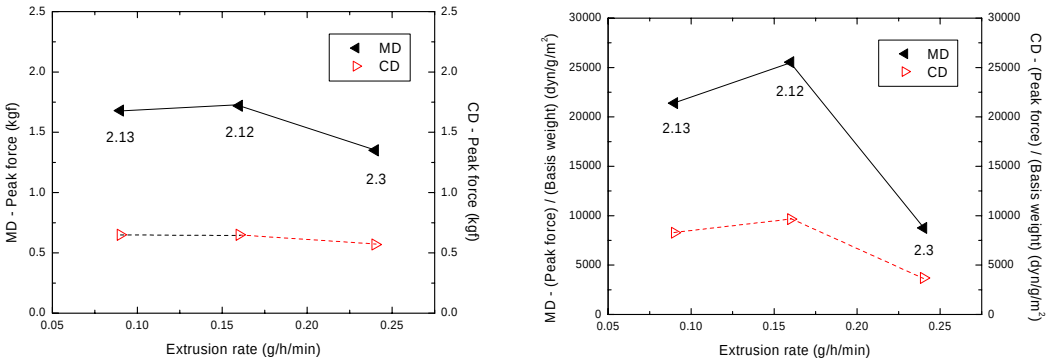
The normalized mechanical strength implies the web strength of TPU_{245} was not highly decided by the basis weight. Both normalized tear and tensile strength were lower at higher basis weight.

Figure 4-43 shows the effect of air temperature on fiber and web properties. The basis weight and web thickness rapidly decreased with an increase of air temperature and fiber diameter slightly decreased with increase of air temperature, but air permeability appeared to first decrease and then increase with air temperature.



Original Normalized

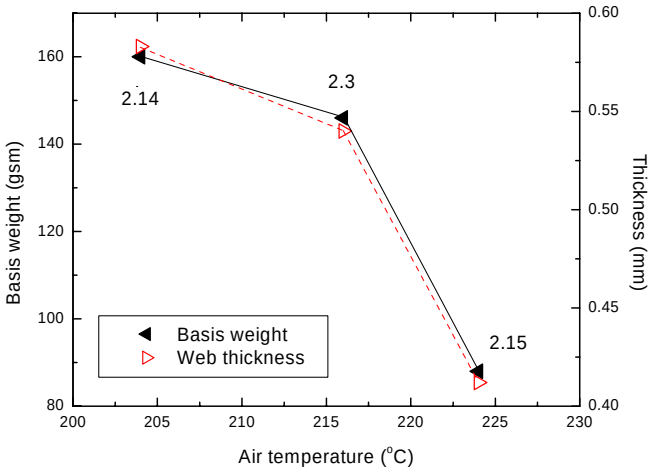
(a) Tear strength



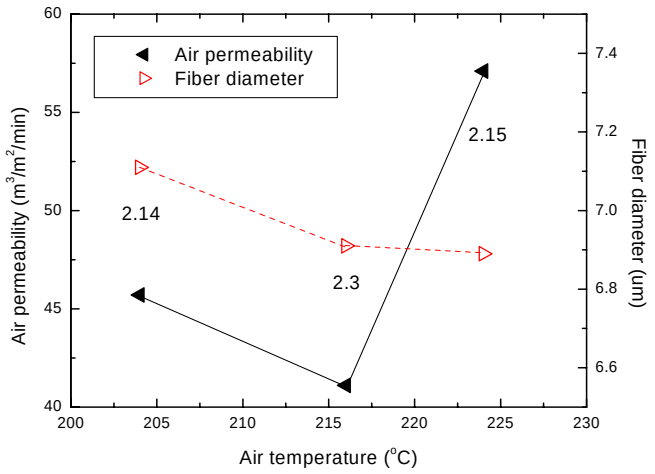
Original Normalized

(b) Tensile strength

Figure 4-42. The tear and tensile strength of MB TPU_{245} webs produced with various extrusion rates (Phase 4).



(a) Basis weight and thickness



(b) Air permeability and fiber diameter

Figure 4-43. The fiber and web properties of MB TPU_{245} webs produced at various air temperatures (Phase 4).

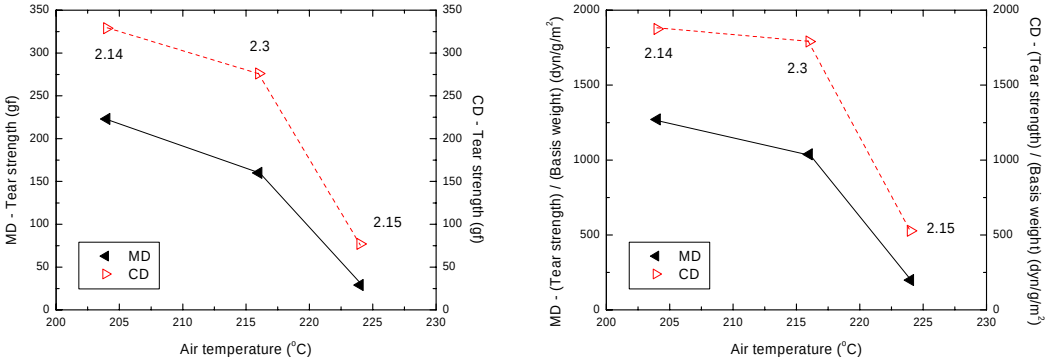
Figure 4-44 shows the mechanical strengths of MB TPU_{245} webs with the change of air temperature. Both tear and tensile strengths showed rapid decrease with increase of air temperature.

Apparently, the increase of air temperature was related to the decrease of basis weight and thickness of the webs, which resulted in rapid decrease of web strength. The difference of web strength between MD and CD was larger in low temperature range, but the difference was smaller at high temperature.

Figure 4-45(a) shows the effect of air flow rate on basis weight and web thickness. For TPU_{245}, the basis weight and web thickness basically showed the same trends as TPU_{237}. Those were initially increased with air valve opening, and then decreased with excessive air valve opening. The air permeability of the TPU_{245} webs was rapidly decreased with the increase of air velocity, but fiber diameters did not show a clear trend with air velocity (Figure 4-45(b)).

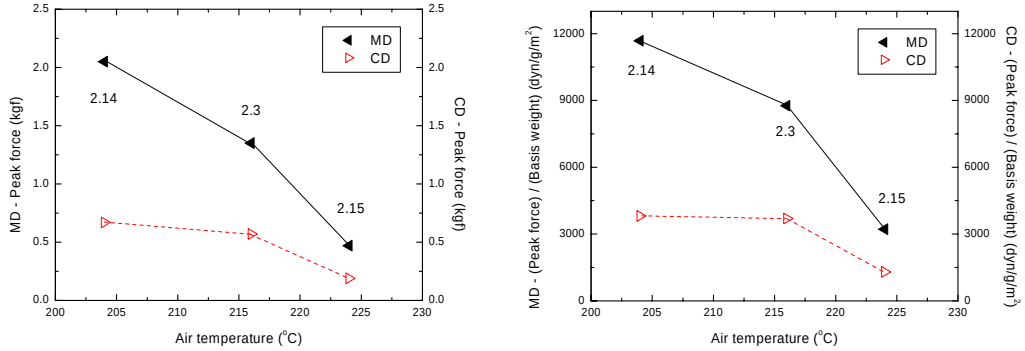
Figure 4-46 shows the mechanical strength of MB TPU_{245} depending on the air velocity. Tear strength of MB TPU_{245} webs did not show clear trends with air velocity. The tear strength in the MD and CD initially increased with increase of air velocity, and then decreased.

These results agreed well with the basis weight and thickness results. On the other hand, tensile strength increased with the increase of air velocity. Peak tensile force increased from 1.00 to 1.42kgf in MD and 0.25 to 0.57kgf in CD with the increase of air valve opening from 40 to 60%.



Original Normalized

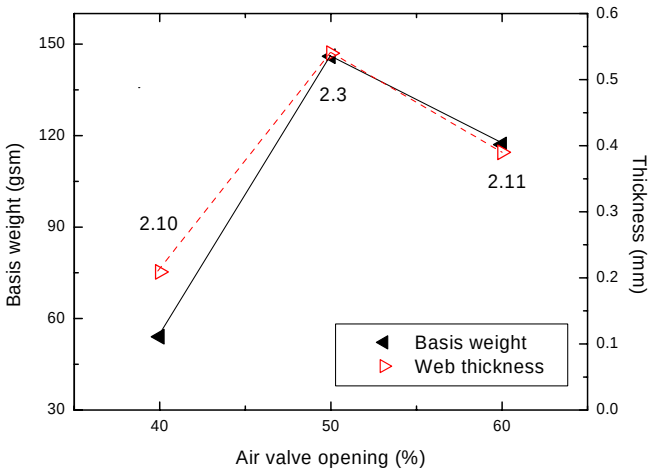
(a) Tear strength



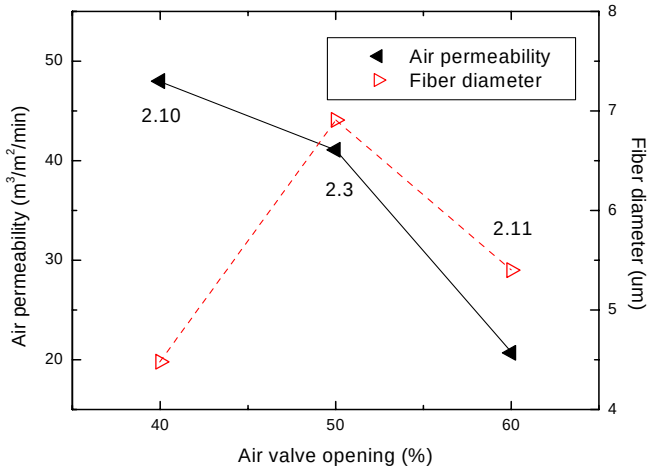
Original Normalized

(b) Tensile strength

Figure 4-44. The tear and tensile strength of MB TPU_{245} webs produced at various air temperatures (Phase 4).

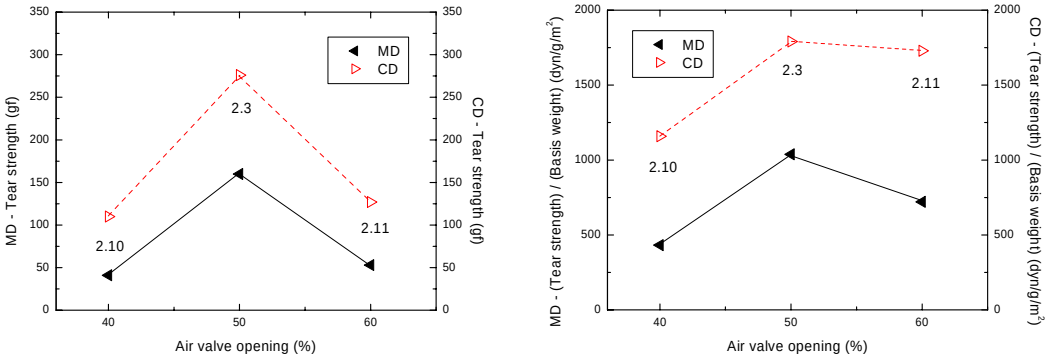


(a) Basis weight and thickness



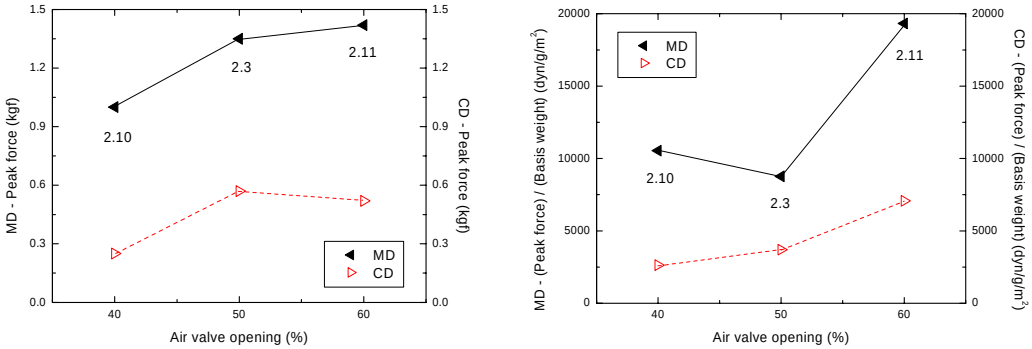
(b) Air permeability and fiber diameter

Figure 4-45. The fiber and web properties of MB TPU_{245} webs produced with various air velocities (Phase 4).



Original Normalized

(a) Tear strength



Original Normalized

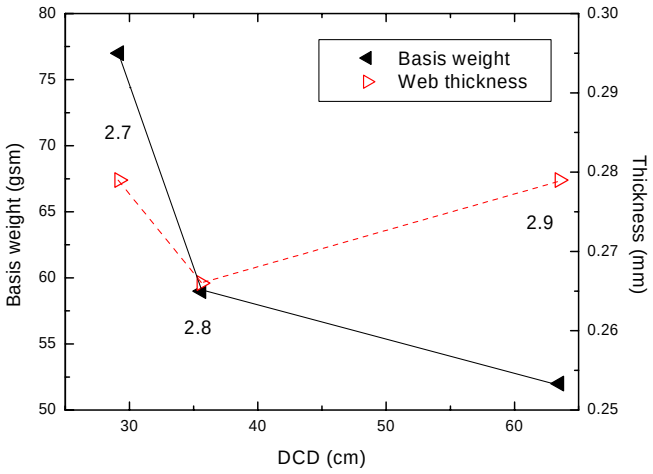
(b) Tensile strength

Figure 4-46. The tear and tensile strength of MB TPU_{245} webs produced with various air velocities (Phase 4).

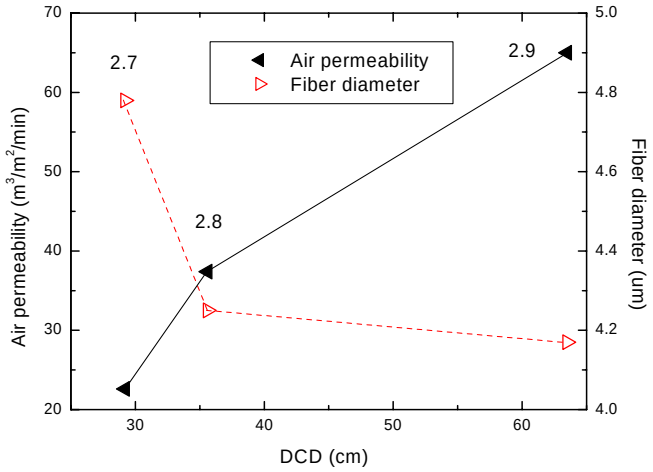
The effect of DCD on basis weight and web thickness of TPU_{245} is presented in Figure 4-47(a), The basis weight decreased with increasing DCD, but web thickness was slightly changed. Considering the basis weight, the air permeability was increased because of the loss of basis weight. However, the fiber diameters appeared to slightly decrease with DCD (Figure 4-47(b)). For these processing conditions, the increase of DCD provides more cooling time of MB TPU fibers before lay down on the collector. Therefore, the web shrinkage of MB TPU_{245} webs decreased and the shrinkage of MB TPU fibers was also decreased after lay down on the collector, so MB TPU_{245} fiber diameters decreased with increase of DCD.

Figure 4-48 shows the web strength of TPU_{245} depending on DCD. Tear strength and tensile strength only has minor effects from the change of DCD, although the loss of basis weight was about 25 g/m^2.

The effect of MB processing parameters on MB TPU_{280} webs were also studied in Phase 4. The TPU_{237} and TPU_{245} polymers are primarily designed to compete with Gore-Tex® membranes, so these have film grade melt viscosities. However, TPU_{280} is primarily designed to compete with Lycra® fiber, so TPU_{280} has fiber grade melt viscosity. Figure 4-49 shows the effect of die temperature to MB TPU_{280} fiber diameter and air permeability. Basis weight and web thickness increased with die temperature, but fiber diameter and air permeability decreased with increasing die temperature. Compared to the MB TPU_{280} produced from Phase 3, larger average fiber diameters of more than 10μm were produced in Phase 4.

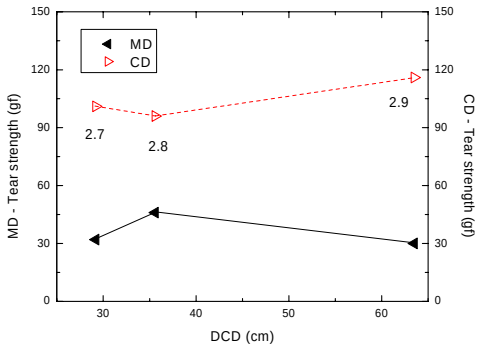


(a) Basis weight and thickness

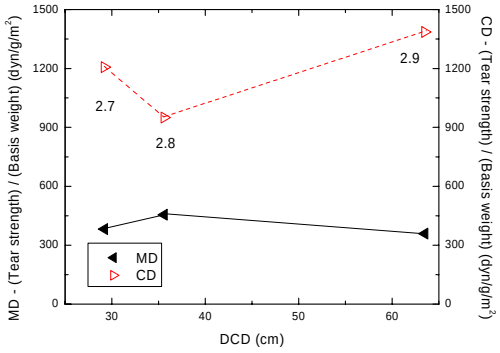


(b) Air permeability and fiber diameter

Figure 4-47. The fiber and web properties of MB TPU_{245} collected at various DCDs (Phase 4).

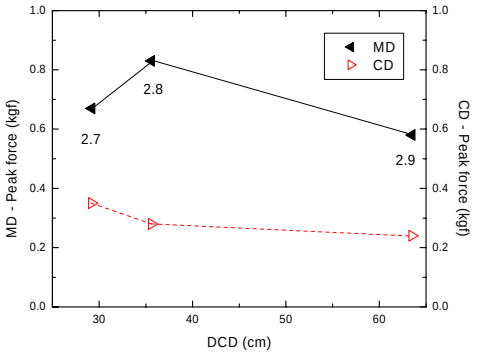


Original

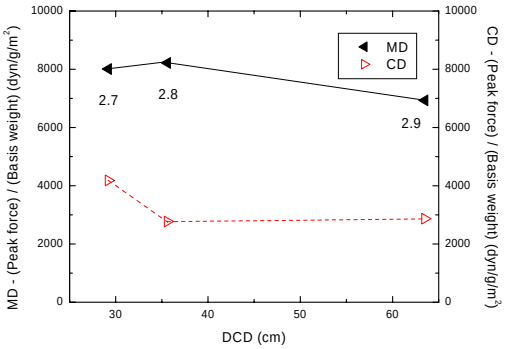


Normalized

(a) Tear strength



Original



Normalized

(b) Tensile strength

Figure 4-48. The tear and tensile strength of MB TPU_{245} webs collected at various DCDs (Phase 4).

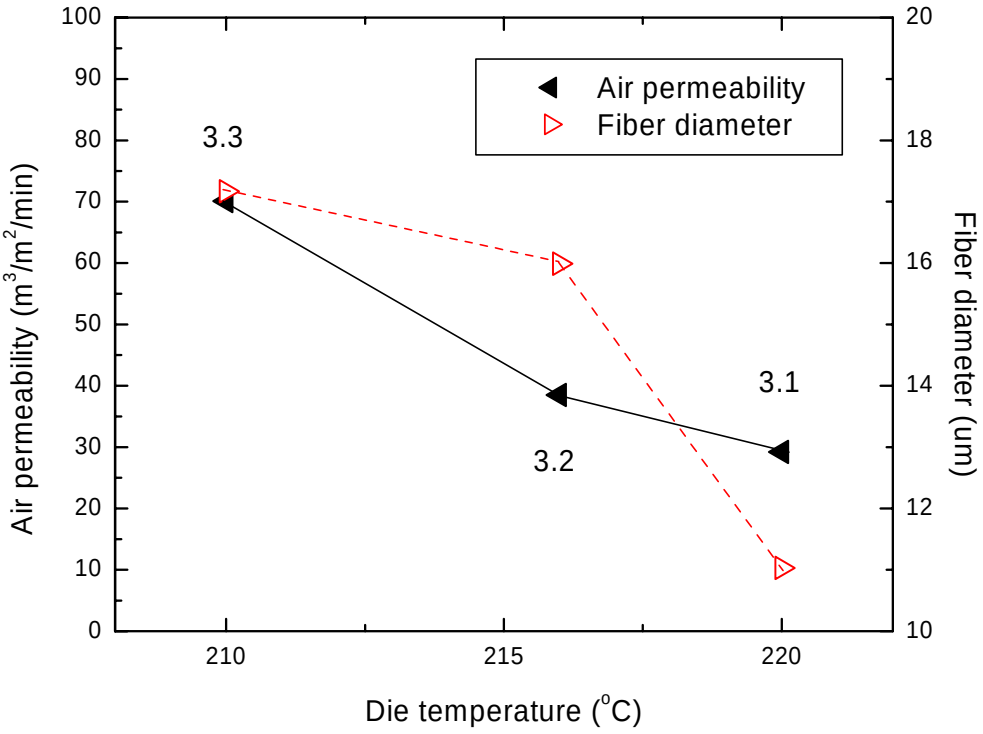
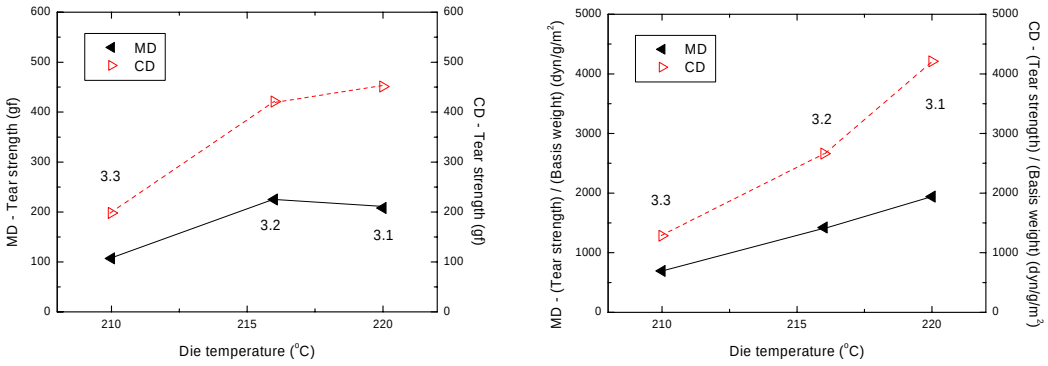


Figure 4-49. The fiber diameter and air permeability of MB TPU_{280} webs produced by various die temperatures (Phase 4).

The mechanical strengths of MB TPU_{280} webs collected with different die temperature are shown in Figure 4-50. The tear and tensile strength of MB TPU_{280} webs increased with increase of die temperature, which was probably caused by the increase of basis weight and web thickness. The difference of MB TPU_{280} web strength between MD and CD was smaller at lower die temperature, but the rate of difference increased with increaseing die temperature. However, comparing the MB webs from other TPUs, the peak elongation of MB TPU_{280} webs in MD was more than twice of other TPUs peak elongation. The MB webs from TPU_{237} and TPU_{245} have much higher peak elongation in CD than MD, but the difference of peak elongation between MD and CD was small for the MB TPU_{280} webs.

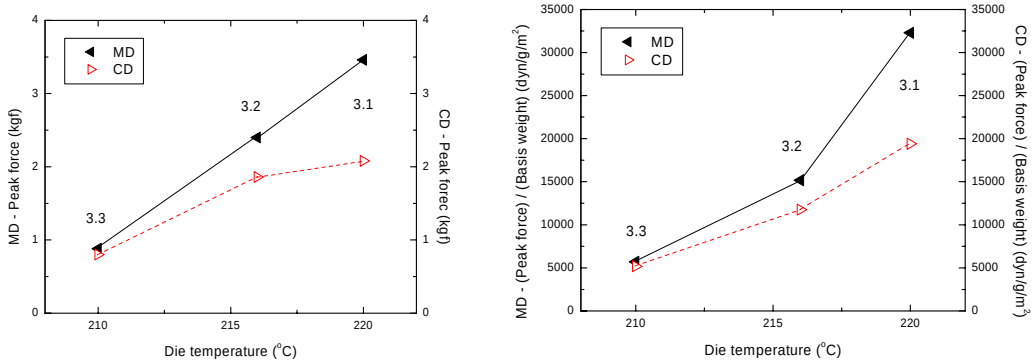
Figure 4-51 shows the effect of extrusion rate on MB TPU_{280} fiber and web properties. Basis weight and web thickness slightly changed with the extrusion rate. The air permeability decreased slightly with increase of extrusion rate based on small changes of MB web basis weight, and the fiber diameters of the MB TPU_{280} webs also decreased from 16 to 12μm with increasing extrusion rate.

Figure 4-52 shows the tear and tensile strength depending on the change of extrusion rate, Tear strength and tensile strength did not show clear trends in MD and CD with the change of extrusion rate. However, the mechanical strength of the MB TPU_{280} webs was stronger than other MB webs from TPU_{237} and TPU_{245} because of heavier basis weight. The difference of web strength between MD and CD was almost same for all extrusion rates.



Original Normalized

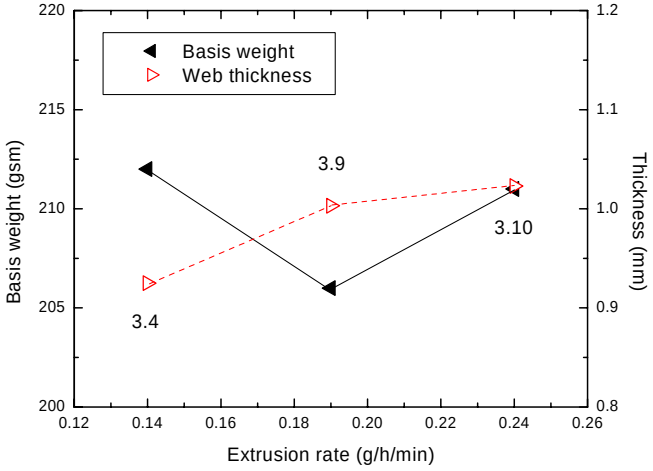
(a) Tear strength



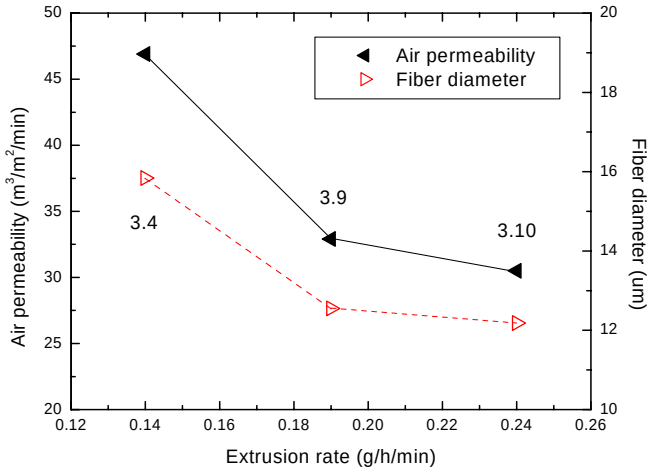
Original Normalized

(b) Tensile strength

Figure 4-50. The tear and tensile strength of MB TPU_{280} webs produced by various die temperatures (Phase 4).

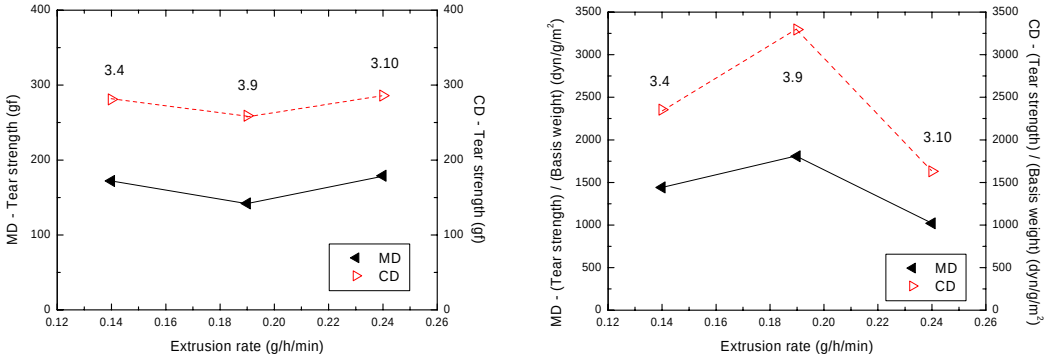


(a) Basis weight and thickness



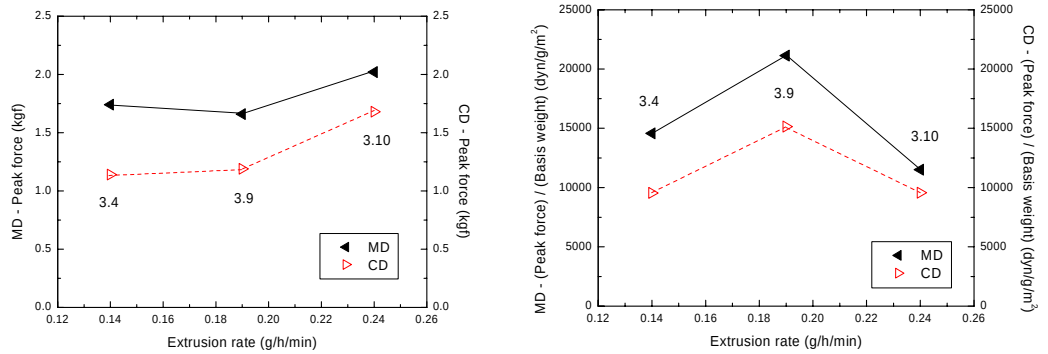
(b) Air permeability and fiber diameter

Figure 4-51. The fiber and web properties of MB TPU_{280} webs produced with various extrusion rates (Phase 4).



Original Normalized

(a) Tear strength



Original Normalized

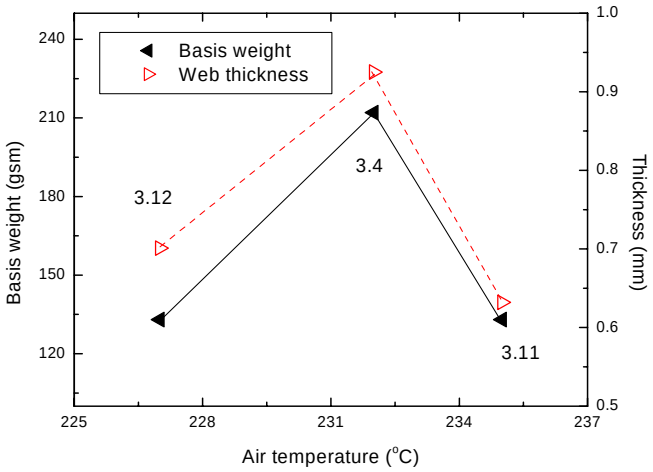
(b) Tensile strength

Figure 4-52. The tear and tensile strength of MB TPU_{280} webs produced with various extrusion rates (Phase 4).

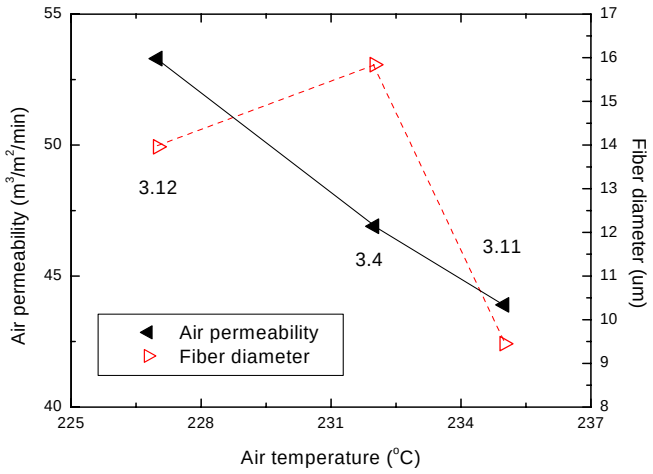
Figure 4-53 shows the fiber and web properties of MB TPU_{280} webs compared to the change of air temperature. MB TPU_{280} webs showed a relatively large change in mechanical properties with the change of air temperature compared to other TPU polymers. Basis weight and web thickness of TPU_{280} was optimum at the mid temperature of 232°C. However, air permeability of the TPU_{280} webs continuously decreased with increase of air temperature and fiber diameters were also decreased with increase of air temperature. The effect of air temperature on mechanical strength of MB TPU_{280} webs are presented in Figure 4-54. The change of tear and tensile strength were related to the change of basis weight in that both strength properties initially increased with basis weight and then decreased.

Figure 4-55 shows the effect of air valve opening, which is related increasing air flow rate, on MB TPU_{280} fiber and web properties. Basis weight and web thickness decreased with the increase of air velocity because of the loss of the edge of the web and fly formation caused by difference between air speed and fiber speed on the collector. However, the fiber diameters showed only minor change with the change of air velocity. In Phase 3, the fiber diameters of MB TPU_{280} webs dramatically decreased with the increase of air velocity.

This difference between Phase 3 and Phase 4 probably came from lower die and air processing temperature of Phase 4 than that of Phase 3. This implies fiber diameters could be decreased by increase of air velocity, however, appropriate processing temperature of TPUs should be provided.

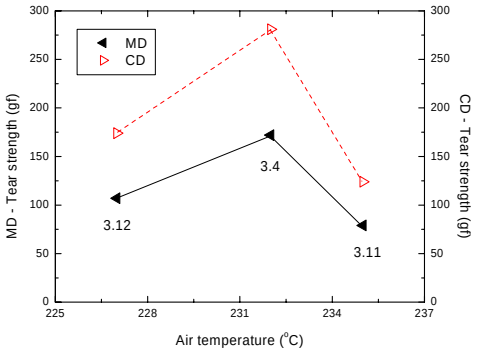


(a) Basis weight and thickness

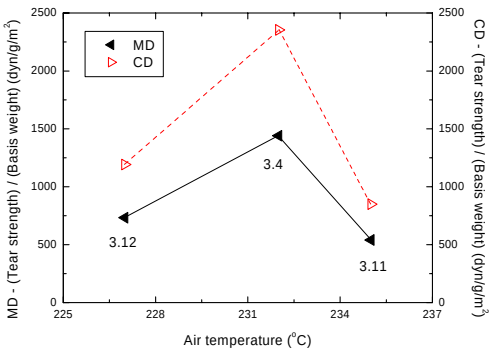


(b) Air permeability and fiber diameter

Figure 4-53. The fiber and web properties of MB TPU_{280} webs produced at various air temperatures (Phase 4).

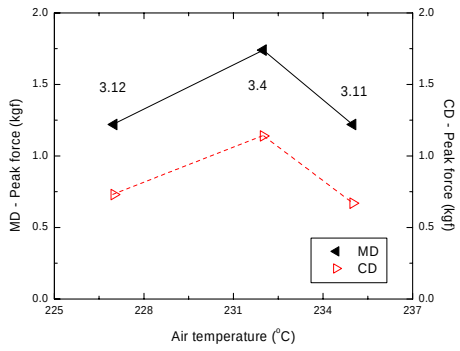


Original

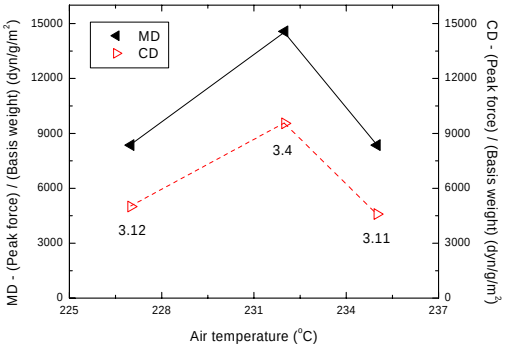


Normalized

(a) Tear strength



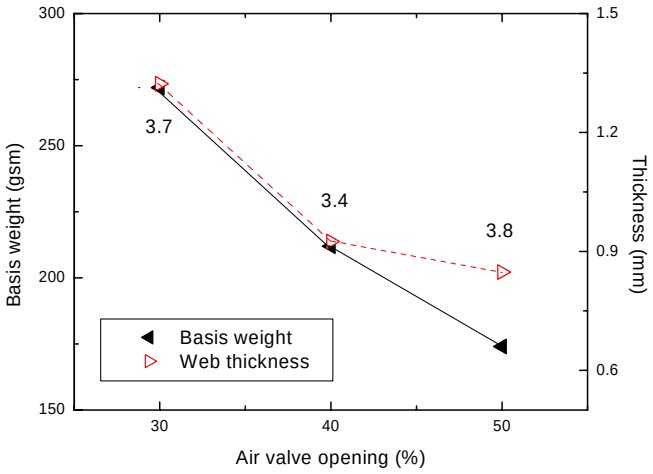
Original



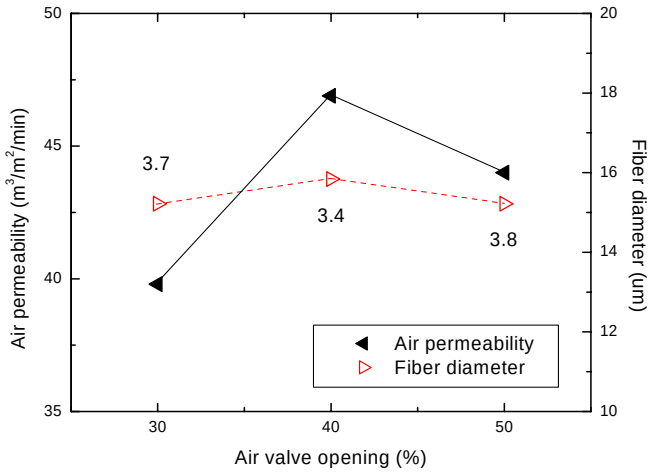
Normalized

(b) Tensile strength

Figure 4-54. The tear and tensile strength of MB TPU_{280} webs produced at various air temperatures (Phase 4).



(a) Basis weight and thickness

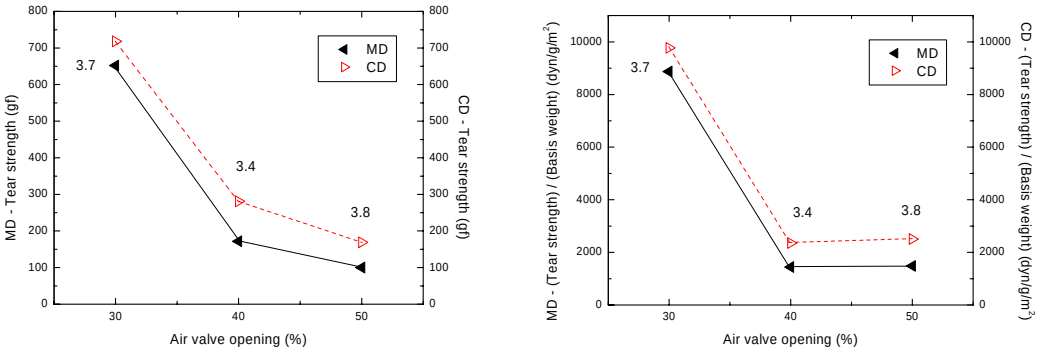


(b) Air permeability and fiber diameter

Figure 4-55. The fiber and web properties of MB TPU_{280} webs produced with various air velocities (Phase 4).

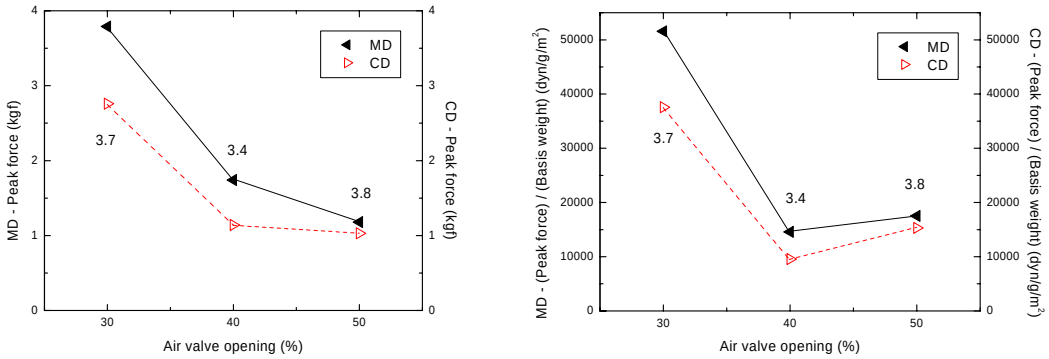
Figure 4-56 shows the effect of air velocity on tear and tensile strength. Both tear and tensile strength decreased with increasing air velocity, apparently because of loss of basis weight in high air velocity by fly formation and fiber breakage. On the other hand, the effect of DCD on MB TPU_{280} fiber and webs were also studied in Phase 4. The basis weight of MB TPU_{280} webs decreased, but web thickness increased with increasing DCD. The properties of fiber diameter and air permeability depending on DCD are presented in Figure 4-57. The rough structure of MB TPU_{280} resulted in increase of web thickness, even basis weight was decreased. The air permeability increased because of the loss of basis weight and the fiber diameters also appeared to increase slightly with DCD. Figure 4-58 shows the web strength of TPU_{280} for different DCDs. Tear strength and tensile strength decreased with increase of DCD because of the decrease of basis weight.

Furthermore, there was an effort to the find the heat effect on MB TPU_{280} webs. All TPUs produced by the MB process showed large difference in fiber and web properties by MB web positions and different basis weights from earlier studies. The fibers placed on the edge of the MB webs normally had small fiber diameters than the fibers placed on the center of the MB webs, and the heavier webs have larger fiber diameter than lighter basis weight of MB TPU webs. For the investigation of heat properties of MB TPU webs, cooling water was sprayed during MB process for MB webs of #3.4, #3.5 and #3.6, which have same processing parameters except DCD.



Original Normalized

(a) Tear strength



Original Normalized

(b) Tensile strength

Figure 4-56. The tear and tensile strength of MB TPU_{280} webs produced with various air velocities (Phase 4).

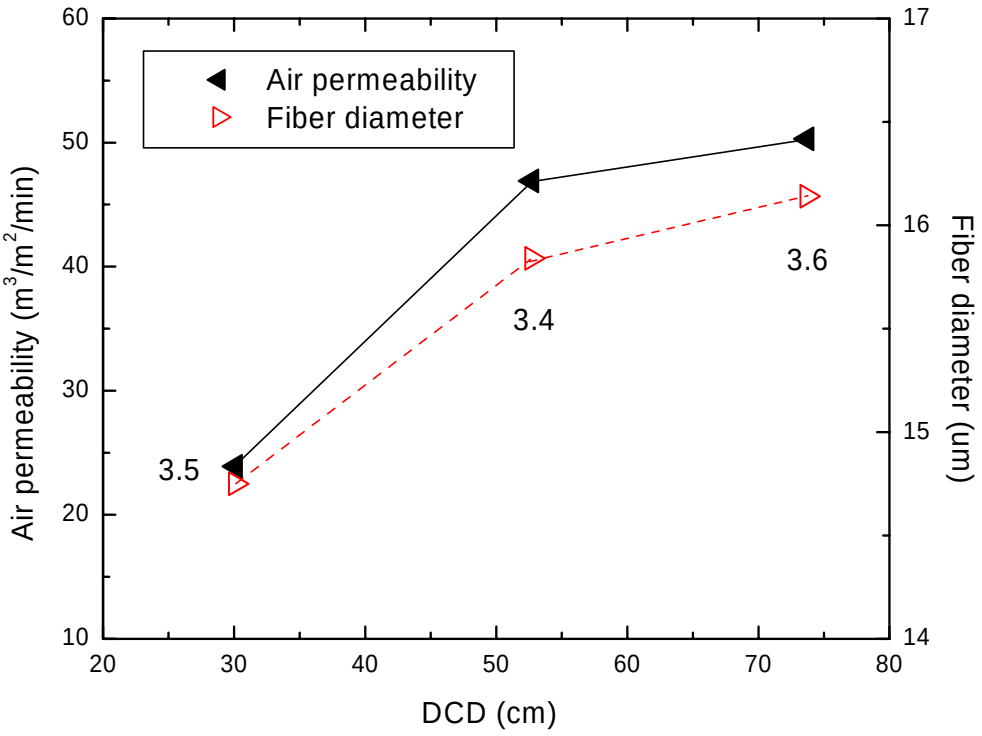
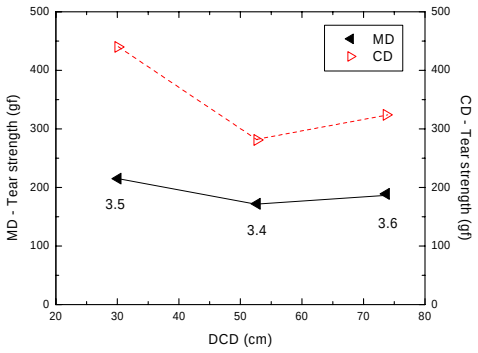
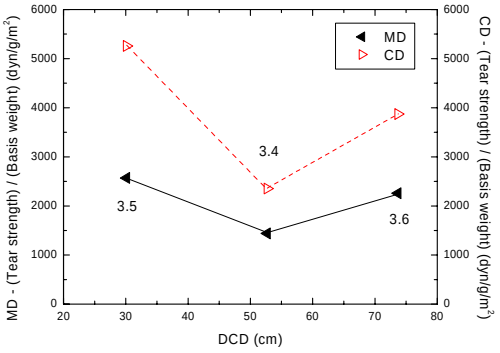


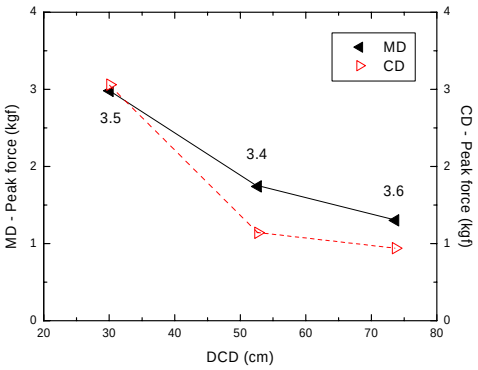
Figure 4-57. The fiber diameter and air permeability of MB TPU_{280} webs collected at various DCDs (Phase 4).

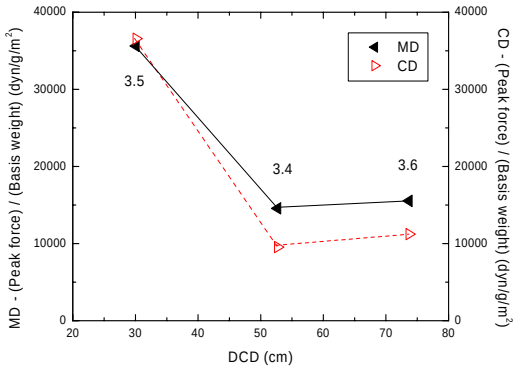




Original Normalized

(a) Tear strength





Original Normalized

(b) Tensile strength

Figure 4-58. The tear and tensile strength of MB TPU_{280} webs collected at various DCDs (Phase 4).

In this experiment, the fiber diameters increased with DCD. However, the wet webs appeared not to depend as much as dry webs on the DCD. Fiber diameters increased from 14.75, 15.84 and 16.14μm with increase of DCD for dry webs, but fiber diameters of wet webs were less different at 15.59, 16.51 and 15.30μm with increase of DCD from 30.1cm, 52.7cm and 73.7cm, respectively. However, differences are too small to make any conclusions concerning the effect of water quenching and further study should be performed for confirm possible effect.

4.4.3 Milti Liner Regression Models

Statistical analysis was performed for the MB TPU processing and MB web properties in Phase 4. The variance inflation factor (VIF), which represented the index of multicollinearity (a case of multiple regression in which the predictor variables are themselves highly correlated) was introduced to increase accuracy of statistical analysis. VIF can be expressed as,

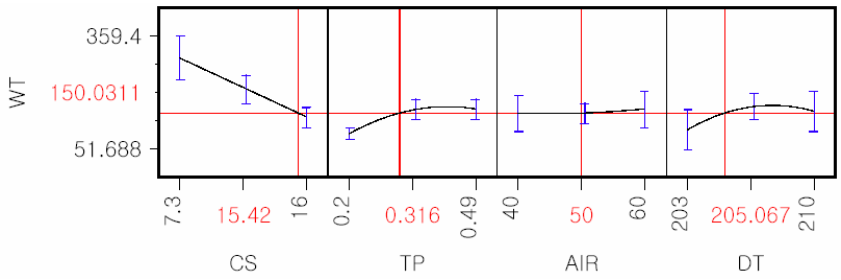
$$VIF_j = \frac{1}{1 - r_j^2}, \qquad j = 1, 2, \cdots, \ k$$

Where r_j^2 is the coefficient, If, VIF_j >10, corresponding to r_j^2 >.9, are regarded as unacceptable for large populations. However, the limited trials of MB TPU process trials caused to VIF >10 because of the few numbers of trial, and

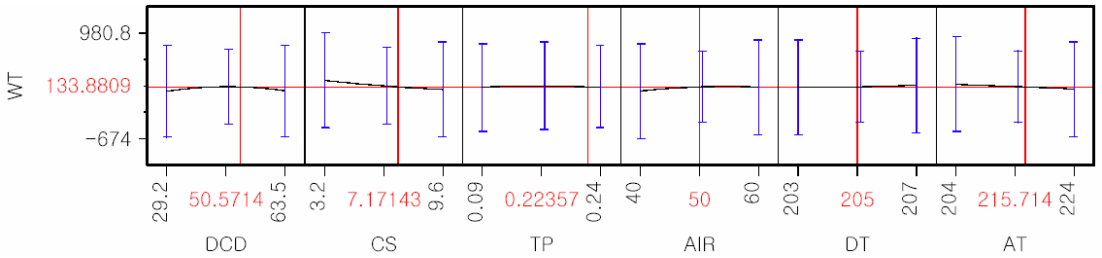
showed more than 99% correlation coefficient in Phase 3 (The prediction profiles were also proposed with a 95% confidence level, and detail, more information is provided in Appendix II).

In Phase 4, the number of trials increased from 5 to 15 for TPU_{245} and TPU_{280} with the new trial group of TPU_{237} samples and the processing parameters were also well controlled for statistical analysis. Based on the previous results of correlation coefficients and statistical analysis of Phase 3, multicollinearity predictors and responses were selected to avoid statistical problems. Basis weight and web thickness of MB TPUs showed almost the same tendencies of processing parameters. Mechanical strength such as tear and tensile strengths in MD and CD showed similar trends, although the values of the strength showed large differences in Phase 4. Therefore, basis weight, fiber diameter, air permeability, tear strength, peak tensile force and peak elongation were selected as major response variables in the Phase 4 and web thickness was also added as a reference in Appendix III.

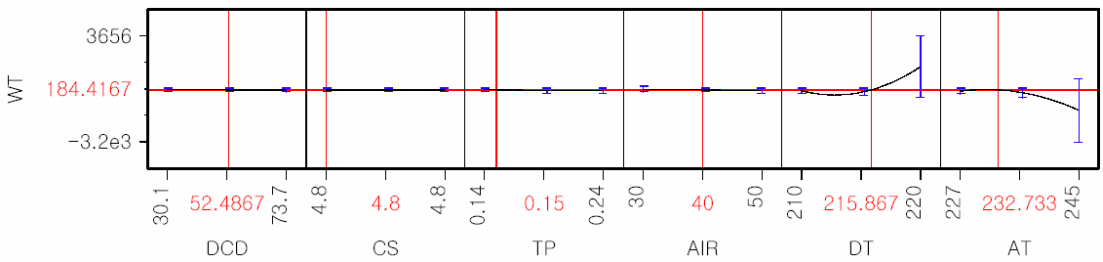
In Phase 4, collector speeds were selected as well as predictors because the basis weight of MB process is normally decided by collector speed. The basis weight of TPU_{237} mostly depended on the collector speed and throughput; furthermore, air velocity and die temperature were also related to the basis weight. The prediction profiles of basis weight depended on predictors presented in Figure 4-59. The basis weight of TPU_{245} mostly depended on collector speed (CS), polymer throughput (TP), air valve opening (AIR) and die temperature (DT).



(a) TPU_{237}



(b) TPU_{245}



(c) TPU_{280}

Figure 4-59. Prediction profiles of MB TPUs basis weight depending on the processing conditions (Phase 4).

On the other hand, the basis weight of TPU_{280} was mostly decided by die temperature (DT) and air temperature (AT) in that collector speed was kept constant, but the other predictors had a minor role for deciding basis weight of the MB TPU_{280} webs. Multiple liner regression was introduced for fitting on identical process model for response variables of each TPU polymer.

Basis weight (BW_{237}) = $-2925.556-18.391(CS)+318.013(TP)+0.55(AIR)$
$+15.757(DT)-1463.23(TP-0.316)^2+0.058(AIR-50)^2$
$-3.005(DT-205.067)^2$

Basis weight (BW_{245}) = $133.880-28.960(DCD)-64.534(CS)-26.450(TP)$
$+31.5(AIR)+19(DT)-36.816(AT)-67.911(DCD-50.571)^2$
$+14.447(CS-7.171)^2-15.361(TP-0.224)^2$
$-33.586(AIR-50)^2+10.914(DT-205)^2-2.381(AT-215.714)^2$

Basis weight (BW_{280}) = $-59588.75-0.595(DCD)+3996.398(CS)-818.667(TP)$
$-4.9(AIR)+215.404(DT)-23.881(AT)$
$+0.001(DCD-52.487)^2+7066.667(TP-0.15)^2$
$-0,133(AIR-40)^2+34.944(DT-201.867)^2$
$-6.889(AT-232.733)^2$

For the basis weight of MB TPU webs, TPUs showed about 90% or greater accuracy with less than 10 of VIFs. However, multicollinearity problem was not

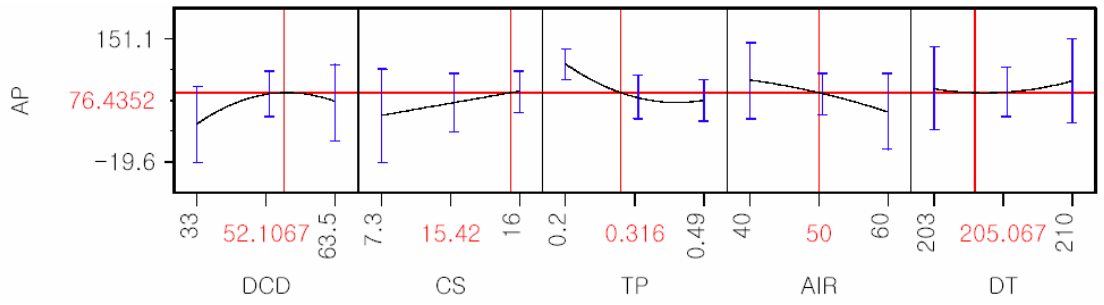
completely removed for TPU_{280} because of the notable decrease of the correlation coefficient from 0.9 to 0.8.

Figure 4-60 shows the prediction profiles of air permeability depending on processing parameters. Air permeability is normally decided by basis weight and thickness of the webs; however, DCD was also highly attributed to the air permeability of TPU_{237}, and throughput, air velocity and die temperature were also related to the air permeability. In addition, the TPU_{245} properties depended on DCD, basis weight, air speed and die temperature.

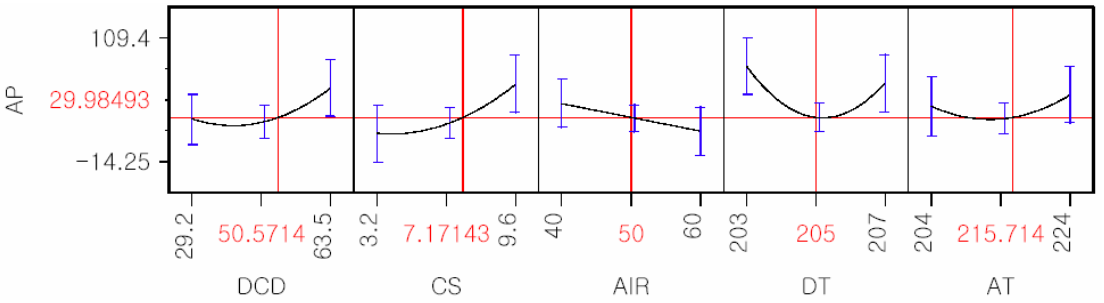
However, the air permeability of TPU_{245} was changed by air temperature instead of throughput. For the TPU_{280}, the collector speed was kept constant and then air permeability of TPU_{280} was mainly decided by die temperature.

$$\begin{aligned}\text{Air Permeability } (AP_{237}) = \; & 357.288+0.172(DCD)+3.874(CS) \\ & -229.499(TP)-2.22(AIR)-0.810(DT) \\ & -0.110(DCD-52.107)^2+969.262(TP-0.316)^2 \\ & -0.047(AIR-50)^2+0.836(DT-205.067)^2\end{aligned}$$

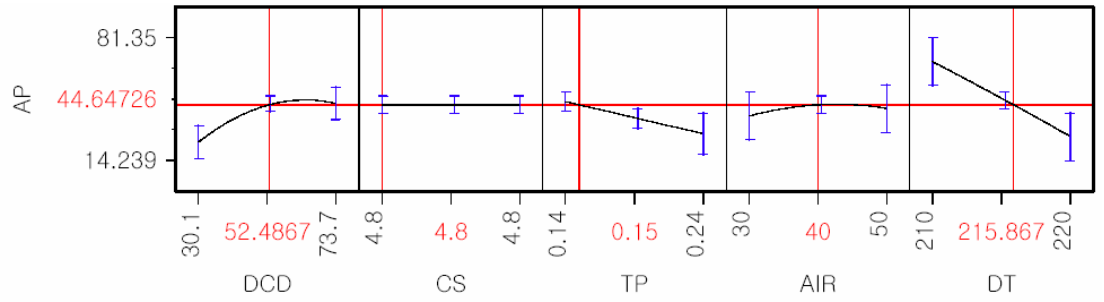
$$\begin{aligned}\text{Air Permeability } (AP_{245}) = \; & 526.045+1.448(DCD)+9.939(CS)-1.365(AIR) \\ & -4.05(DT)+1.196(AT)+0.065(DCD-50.571)^2 \\ & +1.500(CS-7.171)^2+10.720(DT-205)^2 \\ & +0.183(AT-215.714)^2\end{aligned}$$



(a) TPU_{237}



(b) TPU_{245}



(c) TPU_{280}

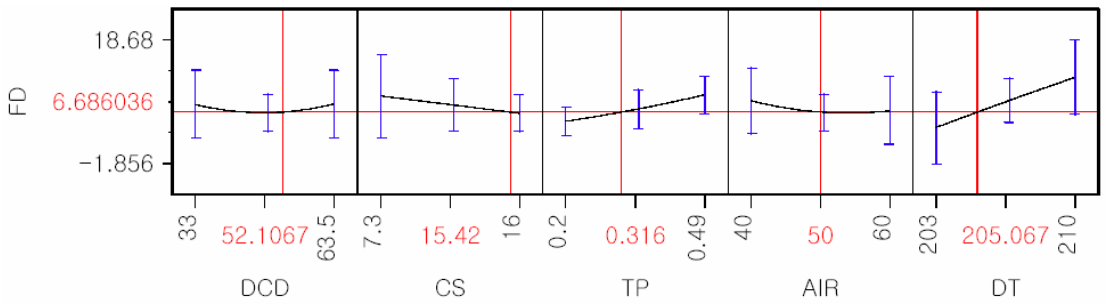
Figure 4-60. Prediction profiles of MB TPUs air permeability depending on the processing conditions (Phase 4).

Air Permeability (AP_{280}) = 1187.141+0.462(DCD)-54.105(CS)-175.846(TP)
+0.21(AIR)-4.118(DT)-0.020(DCD-52.487)^2
-0.041(AIR-40)^2-0.016(DT-215.867)^2

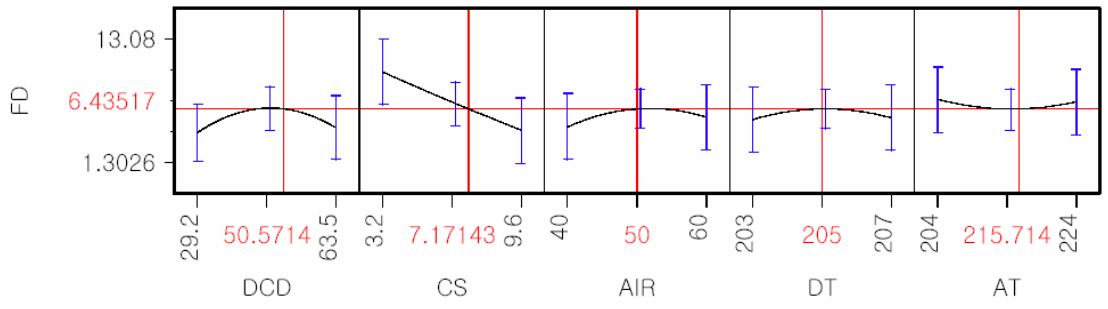
Figure 4-61 shows the effect of predictors on fiber diameters of the TPU webs. Fiber diameters of the TPUs are mostly decided by the die and air temperature, and collector speed was also highly related to the fiber diameters, however, the results of air velocity related to fiber diameters were relatively lower than previous results of Phase 3.

These prediction profiles of Phase 4 imply the prediction of fiber diameters for TPUs should be really difficult because all processing parameters were highly related to fiber diameters. In the case of TPU_{280}, the prediction profiles of fiber diameters were only decided by die and air temperature (collector speed kept constant), however, the actual fiber diameters were larger than normal MB TPU webs because of low MB die and air processing temperature.

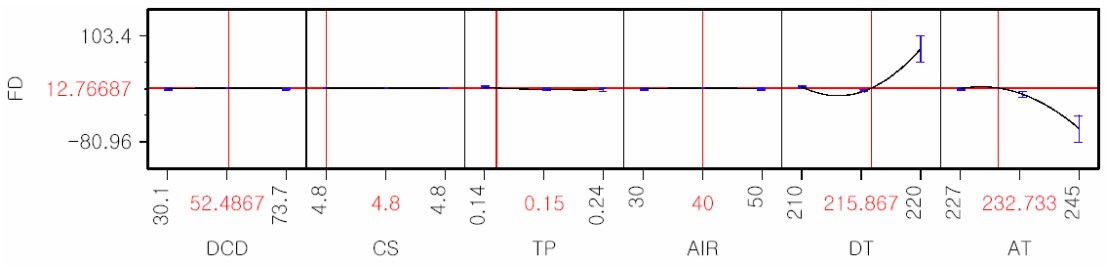
Fiber Diameter (FD_{237}) = -239.441+0.052(DCD)-0.331(CS)+14.396(TP)
-0.085(AIR)+1.210(DT)+0.006(DCD-52.107)^2
+12.599(TP-0.316)^2+0.011(AIR-50)^2
-0.008(DT-205.067)^2



(a) TPU_{237}



(b) TPU_{245}



(c) TPU_{280}

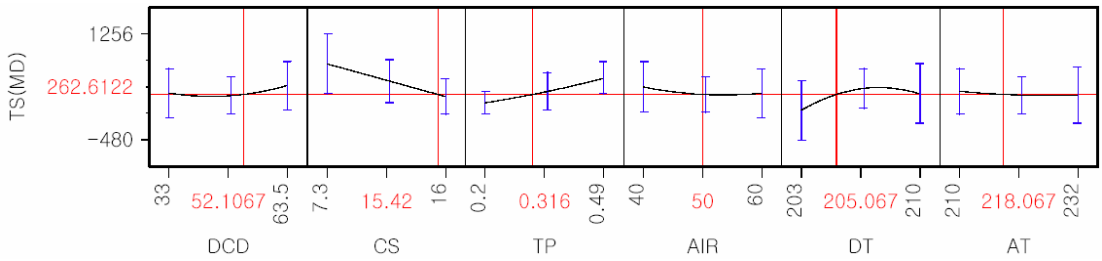
Figure 4-61. Prediction profiles of MB TPUs fiber diameters depending on the processing conditions (Phase 4).

Fiber Diameter (FD_{245}) = 0.280-0.047(DCD)-0.849(CS)+0.046(AIR)
+0.043(DT)+0.017(AT)-0.007(DCD-50.571)^2
+0.009(CS-7.171)^2-0.012(AIR-50)^2
-0.233(DT-205)^2+0.008(AT-215.714)^2

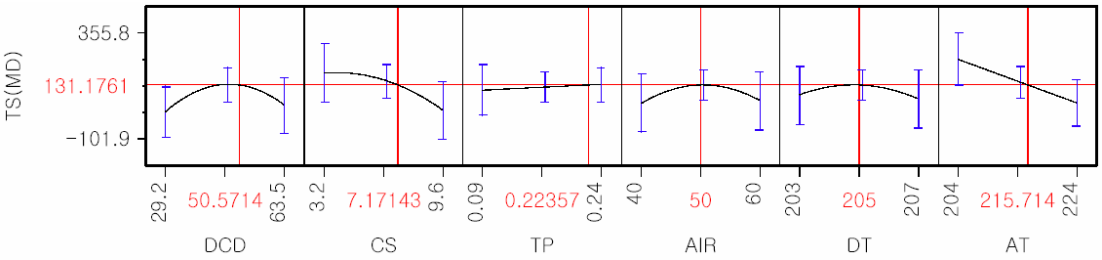
Fiber Diameter (FD_{280}) = -2646.319+0.011(DCD)+211.985(CS)-90.427(TP)
+6.29*10-14(AIR)+9.511(DT)-1.713(AT)
-0.001(DCD-52.487)^2+638.667(TP-0.15)^2
-0.009(AIR-40)^2+1.690(DT-215.867)^2
-0.331(AT-232.733)^2

Prediction profiles of tear strength of TPUs are shown in Figure 4-62. The collector speed and die/air temperature were the major predictors for tear strength. TPU_{237} and TPU_{245} showed all six predictors were related to the tear strength and these factors also showed good relationship with basis weight.

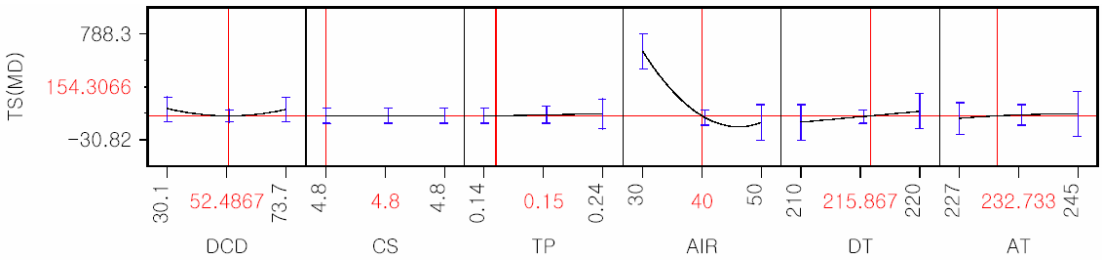
Tear strength (TS_{237}) = -16660.56+7.696(DCD)-61.609(CS)+1316.908(TP)
-5.05(AIR)+88.848(DT)-4.179(AT)
+0.466(DCD-52.107)^2+1197.785(TP-0.316)^2
-92.421(TP-0.316)(AT-218.067)+0.720(AIR-50)^2
-17.638(DT-205.07)^2+0.250(AT-218.07)^2



(a) TPU_{237}



(b) TPU_{245}



(c) TPU_{280}

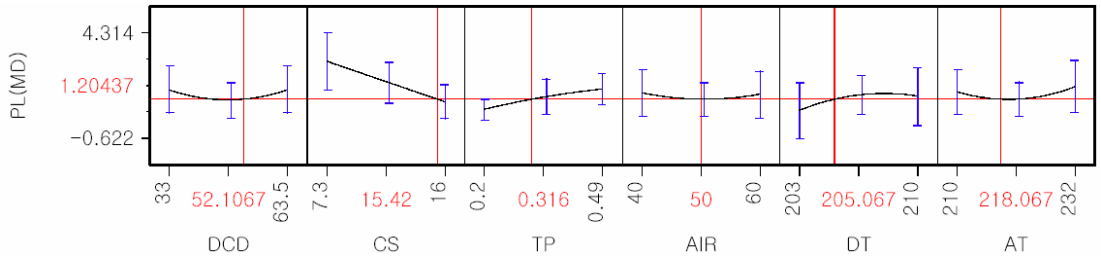
Figure 4-62. Prediction profiles of MB TPUs tear strength depending on the processing conditions (Phase 4).

Tear strength (TS_{245}) = 3415.012-2.156(DCD)-32.731(CS)+167.221(TP)
+0.6(AIR)-4.75(DT)-9.428(AT)-0.353(DCD-50.571)^2
-5.011(CS-7.171)^2-0.738(AIR-50)^2-12.813(DT-205)^2

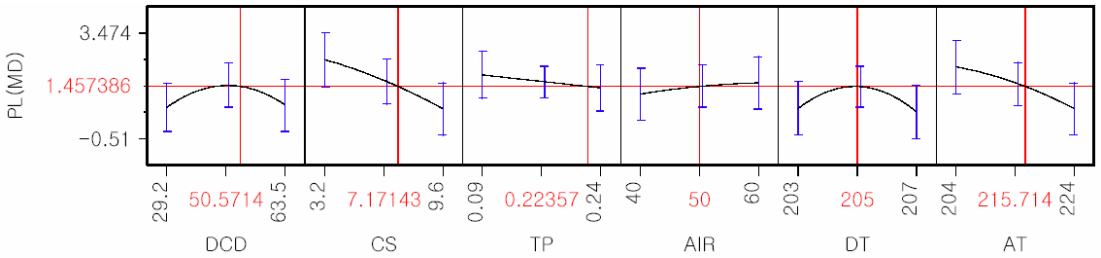
Tear strength (TS_{280}) = -1856.197-0.018(DCD)+137.427(CS)+181.378(TP)
-27.6(AIR)+8.337(DT)+2.702(AT)+0.112(DCD-52.487)^2
-0.135(AT-232.733)^2+2.244(AIR-40)^2

Figure 4-63 showed the prediction profiles of tensile strength depending on the predictors. These tensile strengths also showed higher relationship with basis weight of the web. All peak tensile forces of TPUs were highly affected by collector speed and die/air temperature. However, because of the elongation properties of TPUs, TPU_{237} and TPU_{280} showed relatively similar properties for predictors, and TPU_{245} showed relatively different tendency against to the predictors from other TPUs. For example, increase of throughput was attributed to the increase of peak force for TPU_{237} and TPU_{280}, however, peak force of TPU_{245} decreased with increase of polymer throughput.

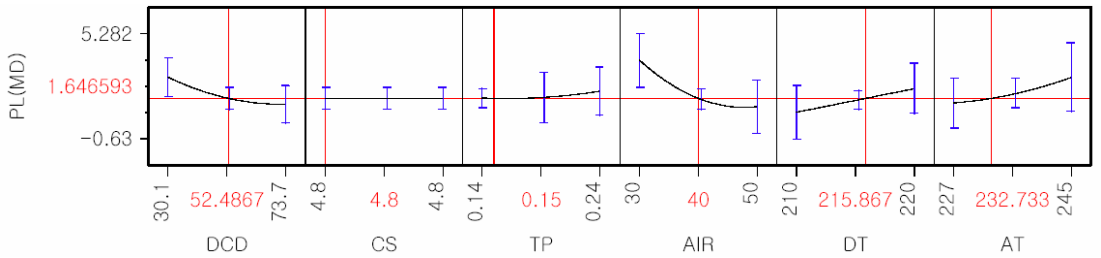
Peak force (PL_{237}) = -32.495+0.0159(DCD)-0.218(CS)+3.527(TP)-0.003(AIR)
+0.184(DT)-0.012(AT)+0.002(DCD-52.107)^2
-4.544(TP-0.316)^2-0.363(TP-0.316)(AT-218.067)
+0.003(AIR-50)^2-0.031(DT-205.067)^2+0.004(AT-218.067)^2



(a) TPU_{237}



(b) TPU_{245}



(c) TPU_{280}

Figure 4-63. Prediction profiles of MB TPUs peak tensile force depending on the processing conditions (Phase 4).

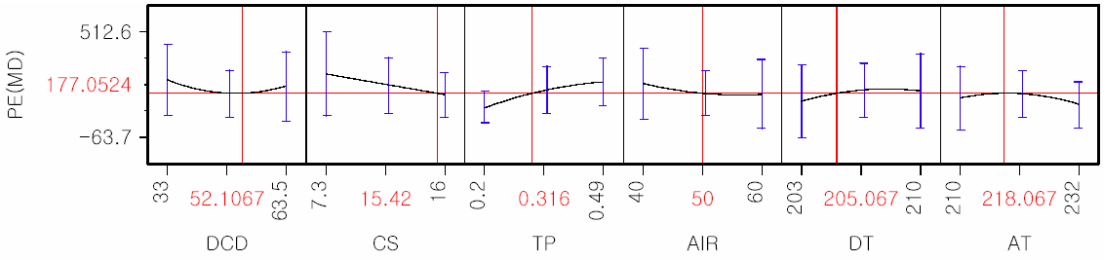
Peak force (PL_{245}) = 29.486-0.020(DCD)-0.313(CS)-3.254(TP)+0.021(AIR)
-0.033(DT)-0.086(AT)-0.003(DCD-50.571)^2
-0.014(CS-7.171)^2-0.001(AIR-50)^2-0.225(DT-205)^2
-0.002(AT-215.714)^2

Peak force (PL_{280}) = -32.791-0.034(DCD)-0.263(CS)-1.535(TP)
-0.131(AIR)+0.133(DT)+0.061(AT)+0.001(DCD-52.487)^2
+67.192(TP-0.15)^2+0.008(AIR-40)^2+0.003(AT-232.733)^2

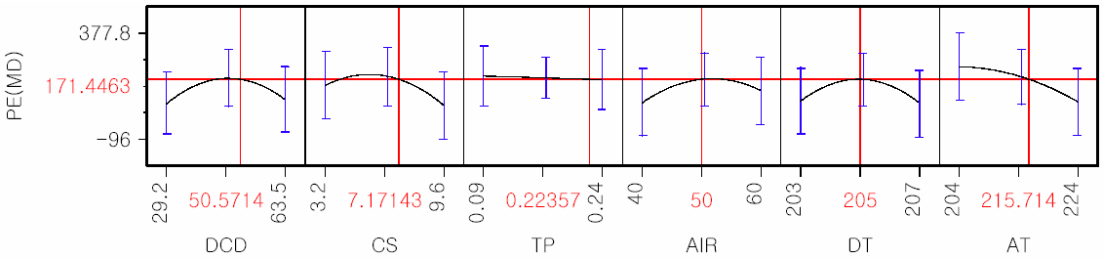
Figure 4-64 represents the prediction profiles of tensile elongation depending on the predictors. The elongation is highly related to the peak tensile force, because the tensile strength of TPUs normally increases with increase of peak elongation. The multi liner regression models of peak elongation model are presented as:

Peak elongation (PE_{237}) = -3003.618+0.775(DCD)-12.989(CS)+552.410(TP)
-3(AIR)+15.723(DT)+0.420(AT)+0.241(DCD-52.107)^2
-1125.463(TP-0.316)^2+0.235(AIR-50)^2
-2.644(DT-205.067)^2-0.340(AT-218.067)^2

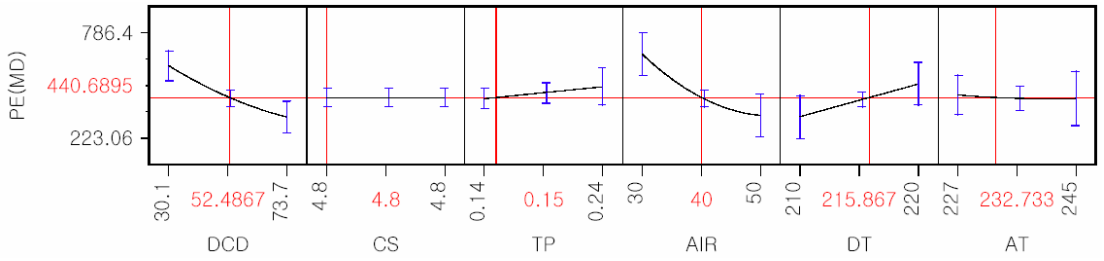
Peak elongation (PE_{245}) = 2809.117-2.491(DCD)-27.230(CS)-111.177(TP)
+2.75(AIR)-2.25(DT)-9.122(AT)
-0.0356(DCD-50.571)^2-8.636(CS-7.171)^2
-0.779(AIR-50)^2-25.480(DT-205)^2-0.371(AT-215.714)^2



(a) TPU_{237}



(b) TPU_{245}



(c) TPU_{280}

Figure 4-64. Prediction profiles of MB TPUs peak elongation depending on the processing conditions (Phase 4).

$$\text{Peak elongation } (PE_{280}) = -4200.98 - 6.236(DCD) + 453.978(CS) + 635.833(TP) - 16.35(AIR) + 17.420(DT) - 1.769(AT) + 0.061(DCD - 52.487)^2 + 0.678(AIR - 40)^2 + 0.106(AT - 232.733)^2$$

CHAPTER 5

CONCLUSIONS AND RECOMMENDATIONS

MB TPU webs having small fiber diameters were obtained from TPU_{237}, TPU_{245} and $TPU_{280,}$ and those webs were mechanically strong and durable to abrasion. Overall, the basic MB process was fundamentally valid for MB TPU process, however, the MB TPU process was more complicated than MB PP, because web structures and properties of MB TPUs are very sensitive to MB process conditions, especially for the die/air temperature and DCD. Furthermore, different TPU grades responded quite differently to MB processing and exhibited different web structure and properties.

In the Phase 1, MB webs produced from TPU_{237} were rather coarse as was verified by the large fiber diameters, which were on the order of 16μm, as determined by optical microscopy. Nevertheless, it was encouraging that for the trials on the 20-inch MB line, an average optically determined fiber diameter of 5.42μm was obtained with TPU_{245}, and the MB webs were quite uniform in appearance and had a much softer hand.

In the Phase 2, MB fabrics from TPU_{245} exhibited the best balance of weight, strength and fiber diameter as well as good MB processing performance. Strong positive correlations were obtained between fiber diameter and melt pressure after the pump, and moderate positive correlation was shown between fiber diameter and air

flow rate. Strong positive correlation was found between fiber size and air permeability; whereas, a moderate positive correlation was found between MB TPU basis weight and peak tensile force, and essentially no correlation was found between basis weight and tearing strength.

In the Phase 3, both MB TPU webs obtained from TPU_{245} and TPU_{280} showed fiber diameter and web properties, which would likely be considered on commercially acceptable. Compared to Phase 1 and Phase 2, fiber-grade TPU_{280}, which have high elasticity, was successfully produced with as low as 5μm average fiber diameter, excellent web uniformity, high peak tensile force, and extraordinary high peak elongation. For TPU_{280}, the pressure after pump and fiber diameter decreased with time. The basis weight initially increased and then decreased later with increase of air flow rate at the same processing conditions; however, the width of MB TPU webs increased with decrease of basis weight. The thickness of web increased with basis weight, and air permeability was decreased with basis weight as with conventional MB PP nonwoven. Tensile strength of TPU_{280} web increased with basis weight, but tear strength was not highly dependent on basis weight.

On the other hand, for TPU_{245}, pressure after pump increased with time, but fiber diameter decreased with air flow rate. Basis weight depending on air flow rate showed the same trends with TPU_{280}. Therefore, the thickness of MB TPU webs was not completely dependent on basis weight of the MB TPU webs, even though those were related to each other. Air permeability showed some relationship with basis

weight, but it depended more on thickness of MB TPU webs. Tear strength and tensile strength also initially increased with basis weight, but decreased later.

Statistical analysis was first applied to the data in Phase 3. Designed statistical models for each response variables using predictors showed more than 99% matches for all cases; however, the population number was relatively small. Although the lack of the populations, the high correlation of predictors and responses showed that MB TPU trials could be interpreted and optimized as a mathematical method.

The fiber and web formation studies of Phase 4 concentrated on the TPU fiber diameter formation and web orientation process during the MB process using TPU_{280}. The fiber diameters of the MB TPU fibers increased with increase of DCD and the MB TPU fibers were more entangled with increase of DCD. MB webs of TPU_{237} were produced as fiber diameters of 3.82μm.

The mechanical strength of TPU_{237} was generally proportional to the basis weight, and peak elongation was also proportional to the tensile strength. MB TPU_{245} webs showed the best balance of basis weight and mechanical strength with less than 5μm of average fiber diameters. However compared to the TPU_{237} and TPU_{280}, the peak elongation of TPU_{245} was only about half of TPU_{237} and TPU_{280}.

MB TPU_{280} webs were produced with heavier basis weight with stronger mechanical strength, much higher peak elongation and lower air permeability compared to other TPUs. However, fiber sizes of TPU_{280} were much larger than previous results from Phase 3 and other TPUs from Phase 4. These results were

probably caused by lower MB process temperature.

The statistical analyses were performed with more populations for TPU_{237}, TPU_{245} and TPU_{280} in Phase 4. All prediction profiles showed the reliable prediction levels with VIFs of less than 10 and more than 90% of correlation coefficient; however, minor multicollinearity problems were appeared for some cases of TPU_{280} prediction profiles.

REFERENCES

REFERENCES

1. Forsberg, K. & Mansdorf, S. (1993). Quick selection guide to chemical protective clothing (2nd ed.). New York: Van Nostrand Reinhold.
2. Ko, F. (2000). Strategies to protect the health of deployed U. S. Forces. Washington, DC: National Academy Press.
3. Wente, V. (1956). Superfine thermoplastic fibers. Industrial and Engineering Chemistry, 48(8), 1342-1346.
4. Zhao, R. (2001). An investigation of bicomponent polypropylene / poly(ethylene terephthalate) melt blown microfiber nonwovens (Doctoral dissertation, The University of Tennessee at Knoxville).
5. Wadsworth, L., Lee, Y., Bresee, R., Gibson, S., & Gibson, P. (2002). Melt blown thermoplastic polyurethane for elastic military protective chemical liners. International Nonwovens Technical Conferences, Atlanta, USA.
6. Zhang, D., Sun, C., Beard, J., Brown, H., Carson I., & Hwo, C. (2002). Development and Characterization of Poly(trimethylene terephthalate)-Based Bicomponent Meltblown Nonwovens, Journal of Applied Polymer Science, 83, 1280-1287.
7. Woods, G. (1990). The ICI Polyurethanes Book. New York: John Wiley and Sons, Inc.
8. Hepburn, C. (1982). Polyurethane elastomers, London: Applied Science.

9. Seymour, E., & Cooper, S. (1973). Thermal analysis of polyurethane block polymers. Macromolecules, 6(1), 48-53.

10. Oertel, G. (1993). Polyurethane handbook (2nd ed.). New York: Hanser Gardner Publications.

11. Szycher, M. (1999). Szycher's handbook of polyurethanes, FL: CRC Press.

12. Buist, J. (1978). Development in Polyurethane - 1, London: Applied Science Publishers Ltd.

13. Wilks, E. (2001). Industrial polymers handbook, Weinheim: WILEY-VCH Verlag GmbH.

14. Bhowmick, A., & Stephens, H. (2001). Handbook of elastomers (2nd ed). New York: Marcel Dekker, Inc.

15. Holden, G., Legge, N. & Quirk, R. (1996). Thermoplastic Elastomers. New York: Hanser Gardner Publications.

16. Bruins, P. (1969). Polyurethane technology, New York: Interscience Publishers.

17. Dombrow, B. (1965). Polyurethanes (2nd) New York: Reinhold Publishing Corporation.

18. Xiao, H., & Frisch, K. (1995). Advances in urethane ionomers. Pennsylvania: Technomic Publishing Company, Inc.

19. Li, Y., Gao T., Linliu, K., Desper, R., & Chu, B. (1992). Multiphase structure of a segemented polyurethane. Effects of temperature and annealing, 25(26), 7365-7372.

20. Petrovic, Z., & Ferguson, J. (1991). Polyurethane elastomers, Prog. Polym. Sci. 16, 695.

21. Koichi, M., U. S. Patent 4,410,595, October 18, 1983, Laminate of thermoplastic resinous composition.

22. Koichi, M., U. S. Patent 4,423,185, December 27, 1983, Thermoplastic resinous composition.

23. Hlavacek, R., & Wolf, H., U. S. Patent 3,929,928, December 30, 1975, Blend of thermoplastic polyurethane elastomer, chlorinated polyethylene, and additional polyethylene.

24. McKinney, L., U. S. Patent 4,525,405, June 25, 1985, Polyurethane backed carpet containing a non-chlorinated polymer.

25. McCulloch, J. G. (1999). The history of the development of melt blowing technology. International Nonwoven Journal, 8(1), 138-148.

26. Private communication with Susan Hemphill, Noveon, October 2001.

27. Shambaugh R. (1988). A Macroscopic View of the Melt Blowing Process. Ind. Eng. Chem. Res. 27, 2363-2372.

28. Morrison, F. A. (2001). Understanding Rheology, Oxford University Press.

29. Barnes, H. A., Hutton, J. F. & Walters, K. (1989). An introduction to rheology, St. Louis: Elsevier Science Publishers.

30. Mastubara, Y. (1980). Residence time distribution of polymer melt in the T-die. Polymer engineering and science, 20(3), 212-214.

31. Collier, J. R., Romanoschi, O., & Petrovan, S. (1998). Elongational rheology of polymer melts and solutions. Journal of Applied Polymer Science, 69(12), 2357-2367.

32. Petrovan, S., Collier, J. R., & Morton, G.H. (2000). Rheology of cellulosic N-methylmorpholine oxide monohydrate solutions. Journal of Applied Polymer Science, 77(6), 1369-1377.

33. Wadsworth, L., & Malkan, S. (1991). A review on melt blowing technology. Nonwoven. 2, 46-52.

34. Wadsworth, L., & Malkan, S. (1991). A review on melt blowing technology. Nonwoven. 3, 22-28.

35. Mastubara, Y. (1983). Residence time distribution of polymer melts in the linearly tapered coat-hanger die. Polymer engineering and science, 23(1), 17-19.

36. Mastubara, Y. (1980). Design of coat-hanger sheeting dies based on ratio of residence times in manifold and slot. Polymer engineering and science, 20(11), 716-719.

37. Mastubara, Y. (1979). Geometry design of a coat-hanger die with uniform flow rate and residence time across the die width. Polymer engineering and science, 19(11), 169-172.

38. Breese, R., & Qureshi, U. (2002). Fiber motion near the collector during melt blowing. Part I: General considerations. International Nonwovens Journal, 11(2), 27-34.

39. McKelvey, M. (1962). Polymer processing. New York: John Wiley and Sons, Inc.

40. Ziabicki, A. (1976). Fundamentals of fiber formation. New York: John Wiley & Sons, Inc.

41. Ziabicki, A., & Kawai, H. (1985). High-speed Fiber Spinning, Science and Engineering Aspects: New York:, John Wiley & Sons, Inc.

42. Milligan, M. W., & Haynes, B. D. (1995). Empirical Models for Melt Blowing, Journal of Applied Polymer Science, 58, 159-163.

43. Breese, R., & Qureshi, U. (2002). Fiber motion near the collector during melt blowing. Part II: Fly formation. International Nonwovens Journal, 11(3), 21-27.

44. Khan, A. Y. A. (1993). A Fundamental Investigation of the effects of Die Geometry and Process Variables on Fiber Diameter and Quality of Melt Blown Polypropylene Webs (Doctoral dissertation, The University of Tennessee at Knoxville).

45. Sun, C., Zhang, D., Wadsworth, L. C., & Zhao, R. (2000). Processing Development and Investigation of Mono- and Bi-component Fiber Meltblown Nonwovens. 10th TANDEC Conference, Knoxville, USA.

46. Zhao, R., Wadsworth, L. C. (2003). Study of Polypropylene/ Poly(ethylene terephalate) bicomponent melt-blowing process: The fiber temperature and elongational viscosity profiles of the spinline. Journal of Applied Polymer Science, 89(4), 1145-1150.

47. Staff report. (1989). Melt blown technology today. San Francisco: Miller Freeman Publication, Inc.

48. Zhao, R., Wadsworth, L. C., Zhang, D. & Sun, C. (2002). Polymer distribution during biocomponent melt blowing of Poly(propylene)/ Poly(ethylene terephalate) and its improvement. Journal of Applied Polymer Science, 85(14), 2885-2889.

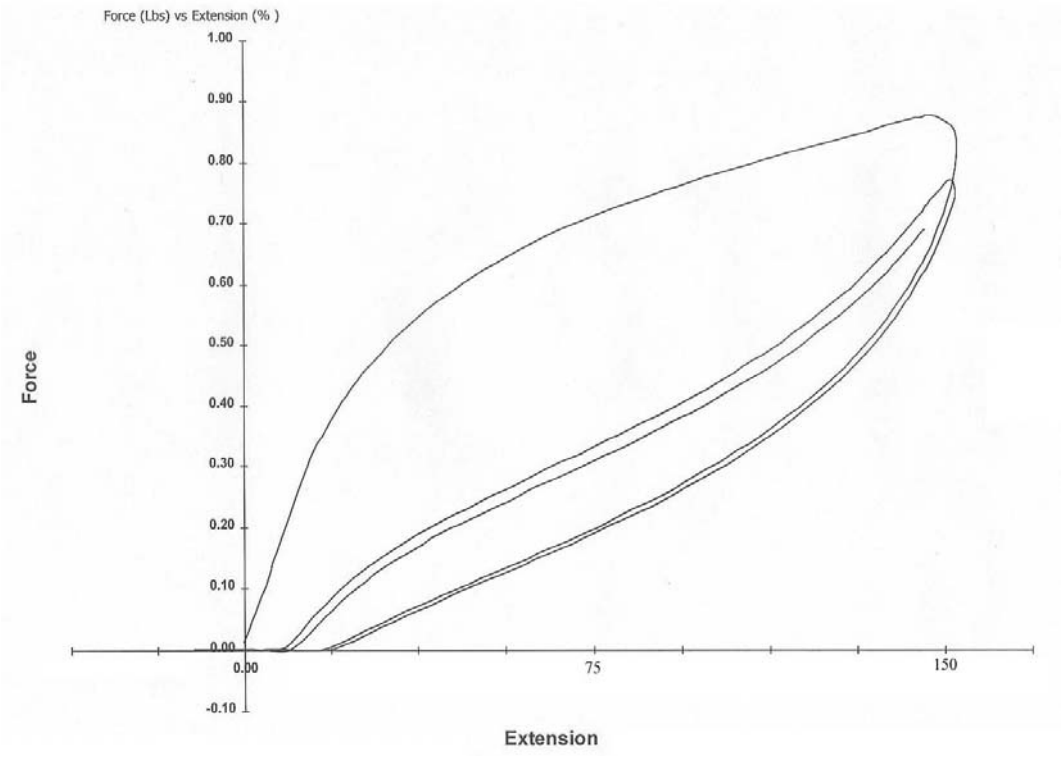
49. Zhao, R., Wadsworth, L. C., Zhang, D. & Sun, C. (2003). Properties of PP/PET bicomponent melt blown microfiber nonwovens after heat-treatment. Polymer International, 52(1), 133-137.

50. Zhao, R. (2001). An investigation of bicomponent polypropylene / poly(ethylene terephthalate) melt blown microfiber nonwovens (Doctoral dissertation, The University of Tennessee at Knoxville).

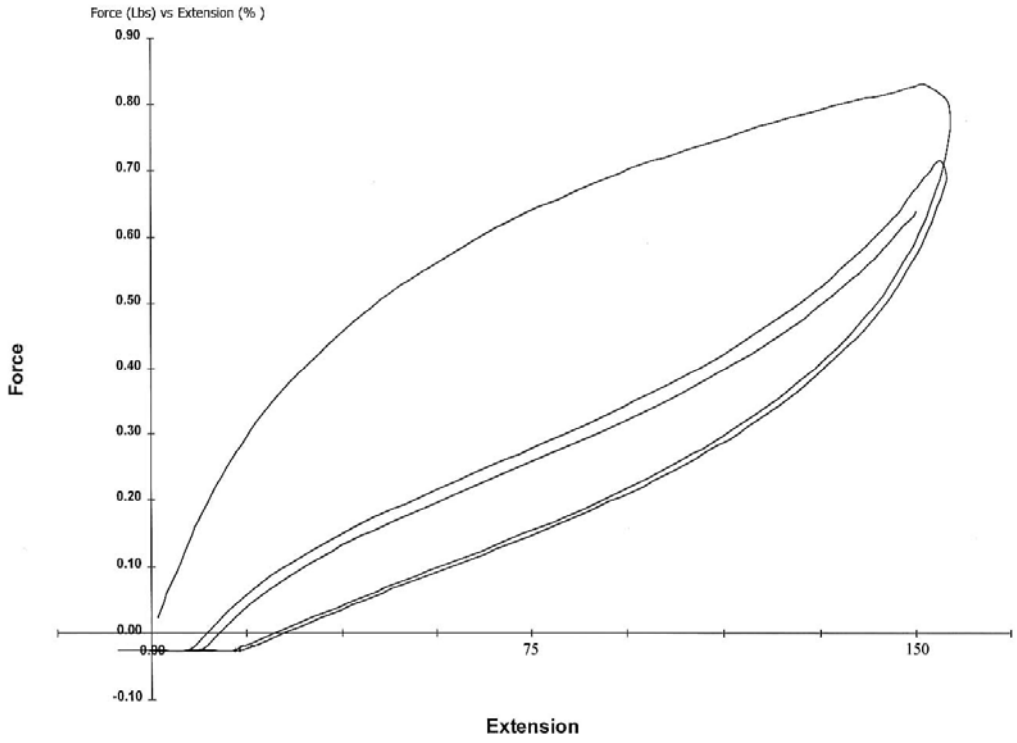
51. Li, Z. (2003). Rheology of lyocell solutions from different cellulosic sources and development of regenerated cellulosic microfibers (Doctoral dissertation, The University of Tennessee at Knoxville).

APPENDICES

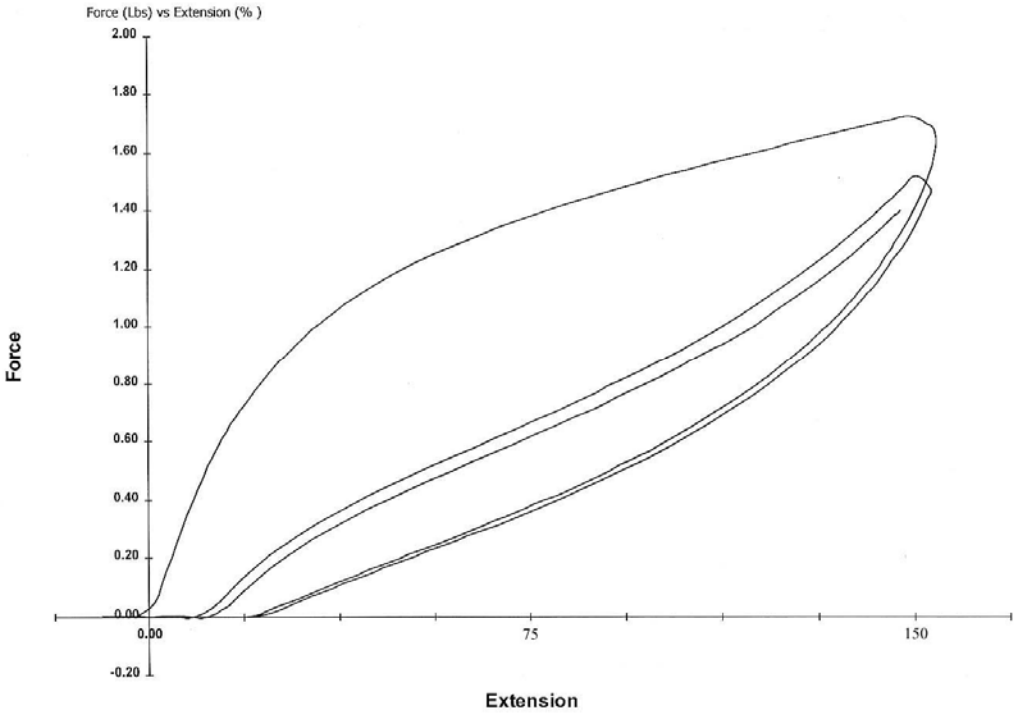
APPENDIX I



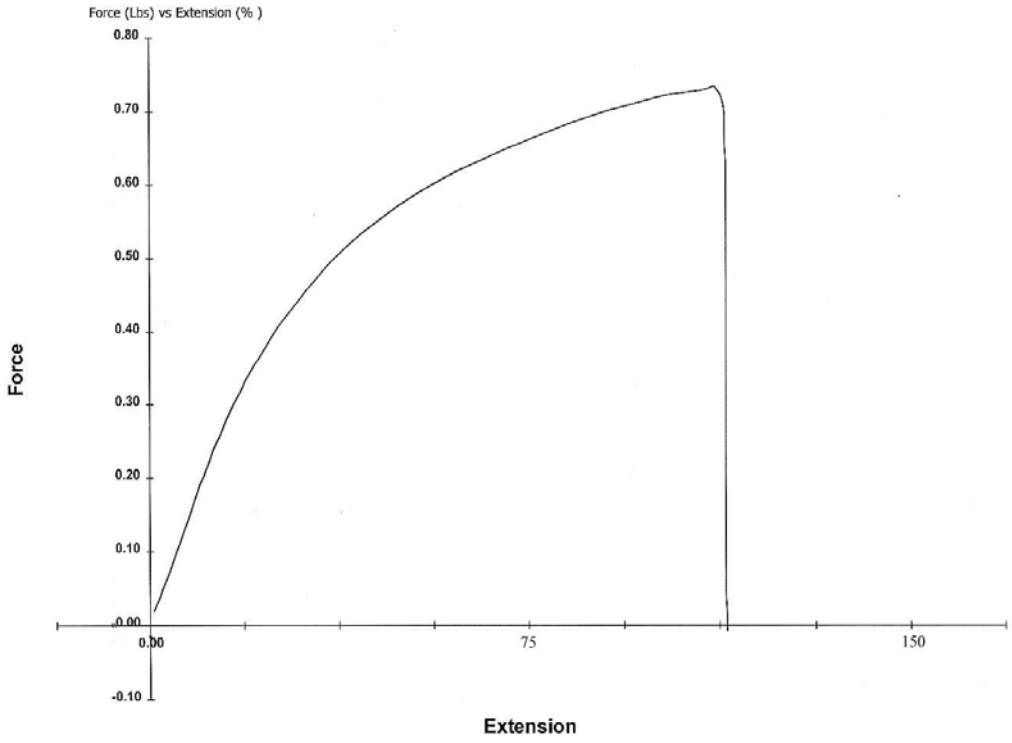
Cycling test of extension and relaxation for Trial 1.1



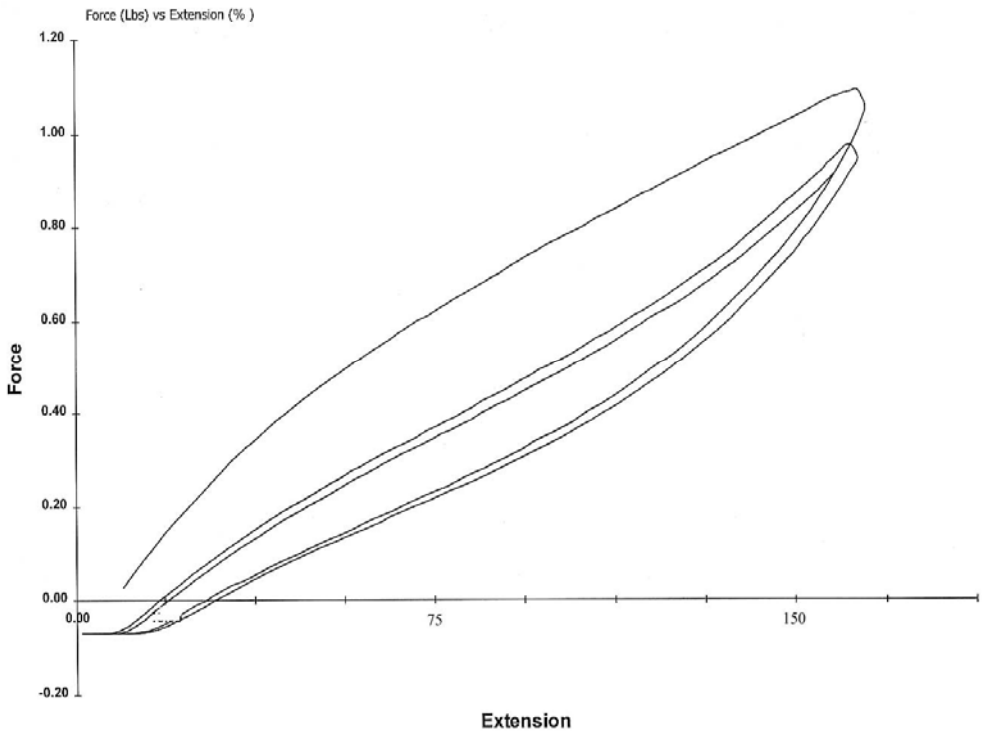
Cycling test of extension and relaxation for Trial 1.2



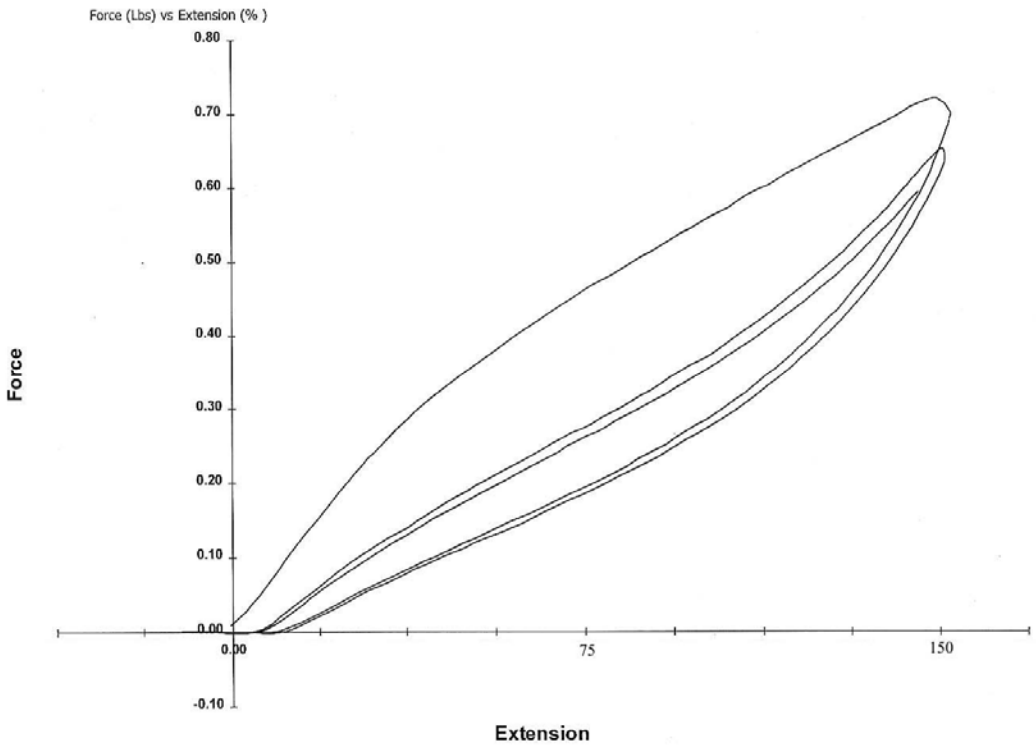
Cycling test of extension and relaxation for Trial 1.3



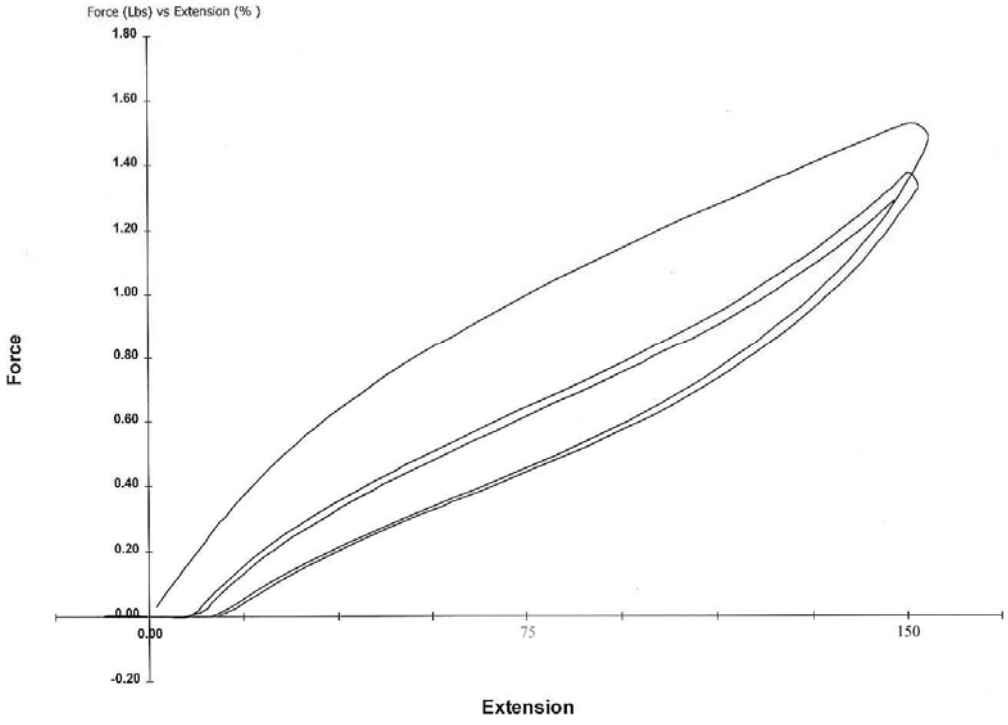
Cycling test of extension and relaxation for Trial 1.4



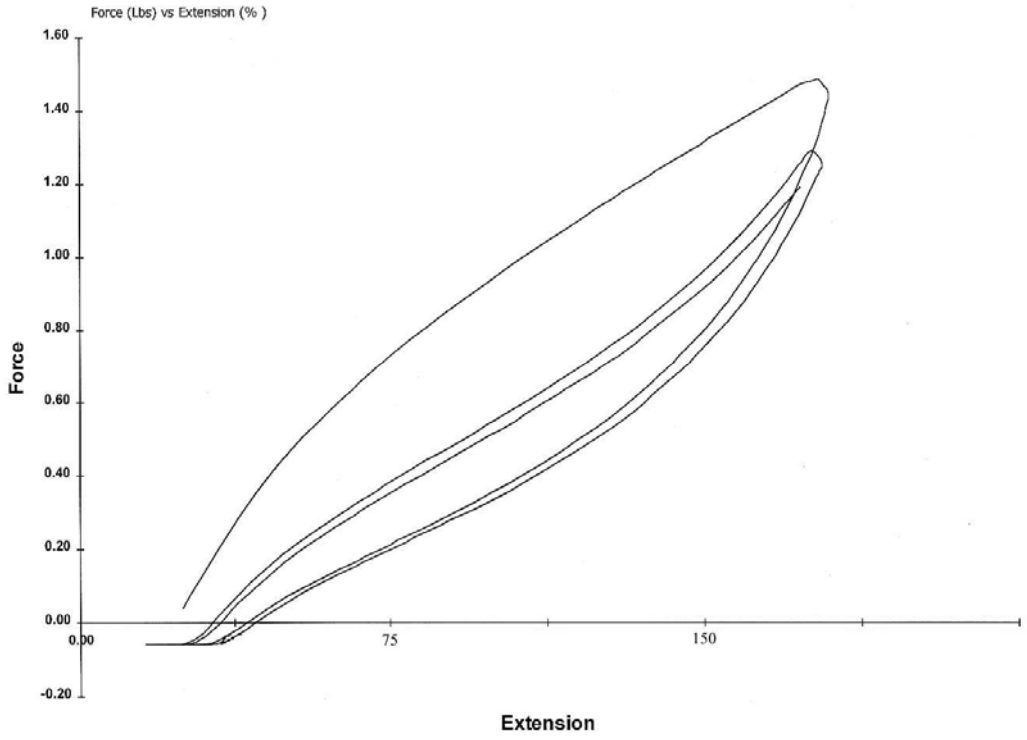
Cycling test of extension and relaxation for Trial 2.2



Cycling test of extension and relaxation for Trial 2.3



Cycling test of extension and relaxation for Trial 2.4



Cycling test of extension and relaxation for Trial 2.5

APPENDIX II

Multiple liner regression between basis weight and processing parameter for TPU_{245}

Response W

Summary of Fit

RSquare	0.999483
RSquare Adj	0.995864
Root Mean Square Error	1.30351
Mean of Response	69.55556
Observations (or Sum Wgts)	9

Analysis of Variance

Source	DF	Sum of Squares	Mean Square	F Ratio
Model	7	3284.5231	469.218	276.1504
Error	1	1.6991	1.699	Prob > F
C. Total	8	3286.2222		0.0463

Parameter Estimates

Term	Estimate	Std Error	t Ratio	Prob>|t|	Lower 95%	Upper 95%	VIF
Intercept	−2000.164	836.9867	−2.39	0.2523	−12635.09	8634.7601	.
DCD	1.1005595	2.539883	0.43	0.7397	−31.17171	33.372827	2488.904
TP	55.45217	16.14893	3.43	0.1804	−149.7394	260.64375	7.1249971
AR	−2.935624	0.438624	−6.69	0.0944	−8.508873	2.6376249	190.47584
DT	12.575792	6.248109	2.01	0.2936	−66.81396	91.96554	2527.3257
AT	−1.047528	1.530775	−0.68	0.6180	−20.49787	18.40281	212.38053
(DCD−60.2222)*(AR−135.444)	−0.281747	0.048993	−5.75	0.1096	−0.904266	0.3407726	40.080612
(TP−0.28556)*(TP−0.28556)	−30.96925	98.3407	−0.31	0.8058	−1280.506	1218.5678	2.5721747

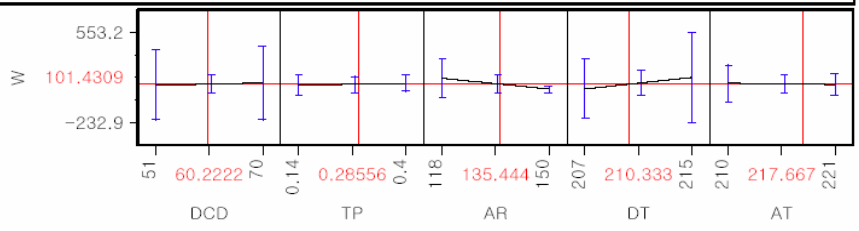
Effect Tests

Source	Nparm	DF	Sum of Squares	F Ratio	Prob > F
DCD	1	1	0.319028	0.1878	0.7397
TP	1	1	20.034491	11.7910	0.1804
AR	1	1	76.110450	44.7936	0.0944
DT	1	1	6.883386	4.0511	0.2936
AT	1	1	0.795678	0.4683	0.6180
DCD*AR	1	1	56.191701	33.0707	0.1096
TP*TP	1	1	0.168509	0.0992	0.8058

Scaled Estimates

Continuous factors centered by mean, scaled by range/2

Term	Scaled Estimate	Std Error	t Ratio	Prob>|t|
Intercept	101.43092	5.495882	18.46	0.0345
DCD	10.455315	24.12888	0.43	0.7397
TP	7.2087821	2.099361	3.43	0.1804
AR	−46.96998	7.017987	−6.69	0.0944
DT	50.303166	24.99243	2.01	0.2936
AT	−5.761404	8.419261	−0.68	0.6180
(DCD−60.2222)*(AR−135.444)	−42.82549	7.446986	−5.75	0.1096
(TP−0.28556)*(TP−0.28556)	−0.52338	1.661958	−0.31	0.8058



Prediction Profiler

Multiple liner regression between thickness and processing parameter for TPU_{245}

Response T

Summary of Fit

RSquare	0.999733
RSquare Adj	0.997867
Root Mean Square Error	0.008165
Mean of Response	0.345556
Observations (or Sum Wgts)	9

Analysis of Variance

Source	DF	Sum of Squares	Mean Square	F Ratio
Model	7	0.24995556	0.035708	535.6190
Error	1	0.00006667	0.000067	Prob > F
C. Total	8	0.25002222		0.0333

Parameter Estimates

Term	Estimate	Std Error	t Ratio	Prob>|t|	VIF
Intercept	9.9594821	6.682602	1.49	0.3762	.
DCD	0.0400773	0.020741	1.93	0.3040	4230.3496
TP	0.182846	0.113798	1.61	0.3544	9.0174499
AR	0.0016987	0.002755	0.62	0.6482	191.45833
DT	−0.061348	0.050548	−1.21	0.4387	4215.845
AT	0.0025	0.012583	0.20	0.8751	365.75
(DCD−60.2222)*(TP−0.28556)	0.0017544	0.011812	0.15	0.9061	4.7749415
(DCD−60.2222)*(AR−135.444)	0.0004327	0.000311	1.39	0.3970	41.241681

Effect Tests

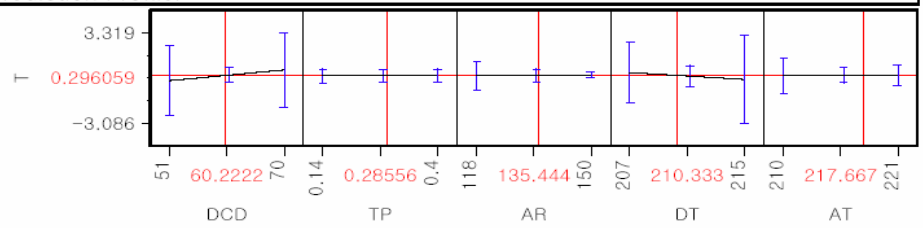
Source	Nparm	DF	Sum of Squares	F Ratio	Prob > F
DCD	1	1	0.00024890	3.7335	0.3040
TP	1	1	0.00017211	2.5817	0.3544
AR	1	1	0.00002535	0.3803	0.6482
DT	1	1	0.00009820	1.4730	0.4387
AT	1	1	0.00000263	0.0395	0.8751
DCD*TP	1	1	0.00000147	0.0221	0.9061
DCD*AR	1	1	0.00012880	1.9320	0.3970

Scaled Estimates

Continuous factors centered by mean, scaled by range/2

Term	Scaled Estimate	Std Error	t Ratio	Prob>|t|
Intercept	0.296059	0.034463	8.59	0.0738
DCD	0.3807343	0.197043	1.93	0.3040
TP	0.02377	0.014794	1.61	0.3544
AR	0.0271795	0.044073	0.62	0.6482
DT	−0.24539	0.20219	−1.21	0.4387
AT	0.01375	0.069207	0.20	0.8751
(DCD−60.2222)*(TP−0.28556)	0.0021667	0.014588	0.15	0.9061
(DCD−60.2222)*(AR−135.444)	0.0657692	0.047317	1.39	0.3970

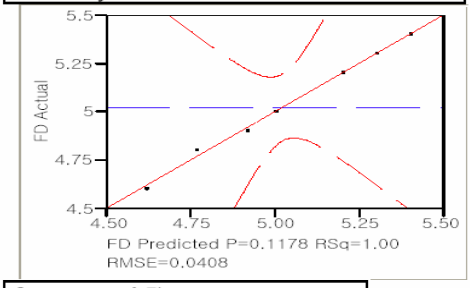
Prediction Profiler



Multiple liner regression between fiber diameter and processing parameter for TPU_{245}

Response FD

Actual by Predicted Plot



Summary of Fit

RSquare	0.996637
RSquare Adj	0.973094
Root Mean Square Error	0.040825
Mean of Response	5.022222
Observations (or Sum Wgts)	9

Analysis of Variance

Source	DF	Sum of Squares	Mean Square	F Ratio
Model	7	0.49388889	0.070556	42.3333
Error	1	0.00166667	0.001667	Prob > F
C. Total	8	0.49555556		0.1178

Parameter Estimates

Term	Estimate	Std Error	t Ratio	Prob>|t|	Lower 95%	Upper 95%	VIF
Intercept	20.932615	4.698209	4.46	0.1406	−38.76379	80.629021	.
DCD	0.0144121	0.029726	0.48	0.7126	−0.363296	0.3921206	347.57025
TP	−7.888889	2.373551	−3.32	0.1861	−38.04772	22.269937	156.91857
AR	−0.020031	0.01481	−1.35	0.4053	−0.208215	0.1681529	221.39539
AT	−0.053612	0.024005	−2.23	0.2680	−0.358621	0.2513976	53.243411
(DCD−60.2222)*(AR−135.444)	−0.00143	0.002314	−0.62	0.6476	−0.030831	0.0279709	91.145041
(TP−0.28556)*(AT−217.667)	4.6666667	1.122167	4.16	0.1502	−9.59182	18.925153	128.64966
(AR−135.444)*(AT−217.667)	−0.003317	0.002226	−1.49	0.3762	−0.031601	0.0249663	37.169186

Effect Tests

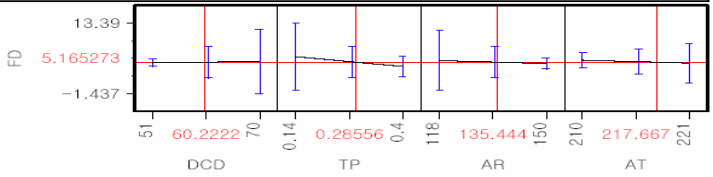
Source	Nparm	DF	Sum of Squares	F Ratio	Prob > F
DCD	1	1	0.00039176	0.2351	0.7126
TP	1	1	0.01841125	11.0467	0.1861
AR	1	1	0.00304878	1.8293	0.4053
AT	1	1	0.00831326	4.9880	0.2680
DCD*AR	1	1	0.00063661	0.3820	0.6476
TP*AT	1	1	0.02882353	17.2941	0.1502
AR*AT	1	1	0.00370178	2.2211	0.3762

Scaled Estimates

Continuous factors centered by mean, scaled by range/2

Term	Scaled Estimate	Std Error	t Ratio	Prob>|t|
Intercept	5.1652734	0.243892	21.18	0.0300
DCD	0.1369146	0.2824	0.48	0.7126
TP	−1.025556	0.308562	−3.32	0.1861
AR	−0.320498	0.236967	−1.35	0.4053
AT	−0.294863	0.132026	−2.23	0.2680
(DCD−60.2222)*(AR−135.444)	−0.217372	0.351714	−0.62	0.6476
(TP−0.28556)*(AT−217.667)	3.3366667	0.80235	4.16	0.1502
(AR−135.444)*(AT−217.667)	−0.291934	0.195886	−1.49	0.3762

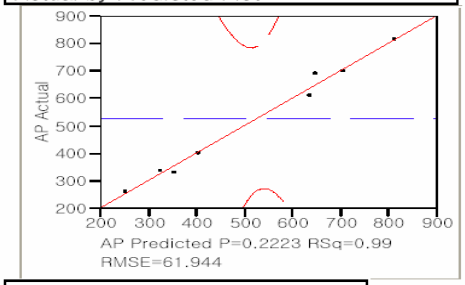
Prediction Profiler



Multiple liner regression between air perm. and processing parameter for TPU_{245}

Response AP

Actual by Predicted Plot



Summary of Fit

RSquare	0.987854
RSquare Adj	0.902836
Root Mean Square Error	61.94409
Mean of Response	527.4444
Observations (or Sum Wgts)	9

Analysis of Variance

Source	DF	Sum of Squares	Mean Square	F Ratio
Model	7	312087.15	44583.9	11.6192
Error	1	3837.07	3837.1	Prob > F
C. Total	8	315924.22		0.2223

Parameter Estimates

Term	Estimate	Std Error	t Ratio	Prob>|t|	Lower 95%	Upper 95%	VIF
Intercept	6986.9374	4282.512	1.63	0.3501	−47427.53	61401.409	.
DCD	−27.35028	32.5163	−0.84	0.5548	−440.509	385.80847	180.63916
TP	−24.19033	591.5059	−0.04	0.9740	−7539.985	7491.6048	4.232961
AR	27.822113	20.2183	1.38	0.4001	−229.0757	284.71992	179.2143
AT	−40.44926	24.11755	−1.68	0.3423	−346.8917	265.99323	23.344639
(DCD−60.2222)*(TP−0.28556)	62.254832	194.5285	0.32	0.8028	−2409.465	2533.9743	22.499646
(DCD−60.2222)*(AR−135.444)	2.0119203	2.44612	0.82	0.5618	−29.06898	33.09282	44.243019
(TP−0.28556)*(TP−0.28556)	−4627.804	13101.9	−0.35	0.7838	−171103.3	161847.67	20.21769

Effect Tests

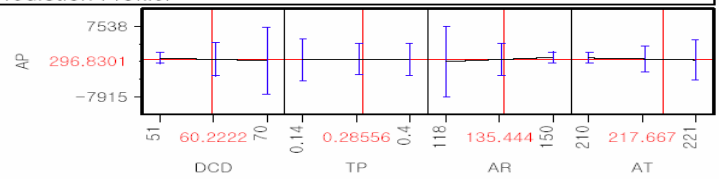
Source	Nparm	DF	Sum of Squares	F Ratio	Prob > F
DCD	1	1	2714.696	0.7075	0.5548
TP	1	1	6.417	0.0017	0.9740
AR	1	1	7265.926	1.8936	0.4001
AT	1	1	10793.311	2.8129	0.3423
DCD*TP	1	1	392.988	0.1024	0.8028
DCD*AR	1	1	2595.768	0.6765	0.5618
TP*TP	1	1	478.719	0.1248	0.7838

Scaled Estimates

Continuous factors centered by mean, scaled by range/2

Term	Scaled Estimate	Std Error	t Ratio	Prob>|t|
Intercept	296.83013	264.3511	1.12	0.4632
DCD	−259.8277	308.9048	−0.84	0.5548
TP	−3.144743	76.89577	−0.04	0.9740
AR	445.15382	323.4927	1.38	0.4001
AT	−222.4709	132.6465	−1.68	0.3423
(DCD−60.2222)*(TP−0.28556)	76.884718	240.2427	0.32	0.8028
(DCD−60.2222)*(AR−135.444)	305.81189	371.8102	0.82	0.5618
(TP−0.28556)*(TP−0.28556)	−78.20988	221.4222	−0.35	0.7838

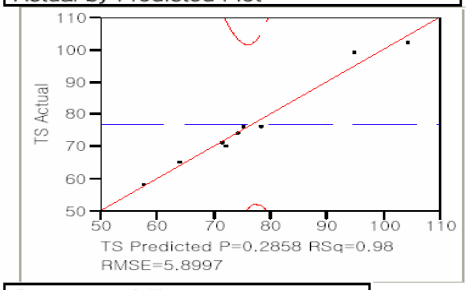
Prediction Profiler



Multiple liner regression between tear strength and processing parameter for TPU_{245}

Response TS

Actual by Predicted Plot



Summary of Fit

RSquare	0.97964
RSquare Adj	0.837119
Root Mean Square Error	5.89972
Mean of Response	76.77778
Observations (or Sum Wgts)	9

Analysis of Variance

Source	DF	Sum of Squares	Mean Square	F Ratio
Model	7	1674.7489	239.250	6.8737
Error	1	34.8067	34.807	Prob > F
C. Total	8	1709.5556		0.2858

Parameter Estimates

Term	Estimate	Std Error	t Ratio	Prob>|t|	Lower 95%	Upper 95%	VIF
Intercept	−850.1243	407.8778	−2.08	0.2848	−6032.703	4332.4546	.
DCD	5.0381495	3.096939	1.63	0.3509	−34.31219	44.388488	180.63916
TP	117.1828	56.33659	2.08	0.2853	−598.6415	833.0071	4.232961
AR	−3.177146	1.925644	−1.65	0.3469	−27.64478	21.290484	179.2143
AT	4.8490453	2.297019	2.11	0.2816	−24.33735	34.035442	23.344639
(DCD−60.2222)*(TP−0.28556)	32.852177	18.52742	1.77	0.3269	−202.561	268.26531	22.499646
(DCD−60.2222)*(AR−135.444)	−0.37943	0.232975	−1.63	0.3506	−3.339658	2.5807972	44.243019
(TP−0.28556)*(TP−0.28556)	−1392.999	1247.86	−1.12	0.4650	−17248.57	14462.567	20.21769

Effect Tests

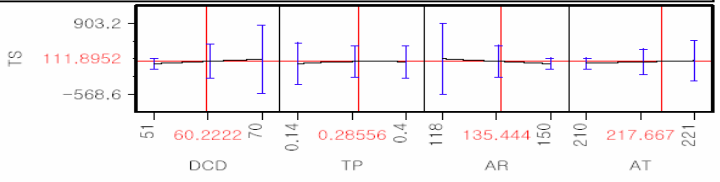
Source	Nparm	DF	Sum of Squares	F Ratio	Prob > F
DCD	1	1	92.11698	2.6465	0.3509
TP	1	1	150.59460	4.3266	0.2853
AR	1	1	94.75129	2.7222	0.3469
AT	1	1	155.11223	4.4564	0.2816
DCD*TP	1	1	109.43631	3.1441	0.3269
DCD*AR	1	1	92.32268	2.6524	0.3506
TP*TP	1	1	43.37433	1.2461	0.4650

Scaled Estimates

Continuous factors centered by mean, scaled by range/2

Term	Scaled Estimate	Std Error	t Ratio	Prob>|t|
Intercept	111.89515	25.1775	4.44	0.1409
DCD	47.86242	29.42092	1.63	0.3509
TP	15.233764	7.323757	2.08	0.2853
AR	−50.83434	30.81031	−1.65	0.3469
AT	26.669749	12.63361	2.11	0.2816
(DCD−60.2222)*(TP−0.28556)	40.572438	22.88136	1.77	0.3269
(DCD−60.2222)*(AR−135.444)	−57.67341	35.41219	−1.63	0.3506
(TP−0.28556)*(TP−0.28556)	−23.54169	21.08884	−1.12	0.4650

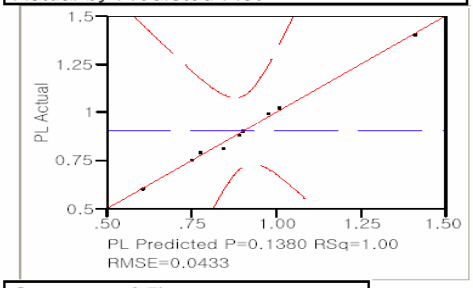
Prediction Profiler



Multiple liner regression between peak force and processing parameter for TPU_{245}

Response PL

Actual by Predicted Plot



Summary of Fit

RSquare	0.995379
RSquare Adj	0.963032
Root Mean Square Error	0.043283
Mean of Response	0.904444
Observations (or Sum Wgts)	9

Analysis of Variance

Source	DF	Sum of Squares	Mean Square	F Ratio
Model	7	0.40354877	0.057650	30.7720
Error	1	0.00187345	0.001873	Prob > F
C. Total	8	0.40542222		0.1380

Parameter Estimates

Term	Estimate	Std Error	t Ratio	Prob>|t|	Lower 95%	Upper 95%	VIF
Intercept	−1.950413	2.992403	−0.65	0.6323	−39.9725	36.071676	.
DCD	0.0451635	0.022721	1.99	0.2967	−0.243531	0.333858	180.63916
TP	2.7019258	0.413315	6.54	0.0966	−2.549733	7.9535845	4.232961
AR	−0.045686	0.014128	−3.23	0.1909	−0.225193	0.1338211	179.2143
AT	0.0260085	0.016852	1.54	0.3660	−0.188118	0.2401351	23.344639
(DCD−60.2222)*(TP−0.28556)	−0.240633	0.135927	−1.77	0.3273	−1.967746	1.4864804	22.499646
(DCD−60.2222)*(AR−135.444)	−0.000604	0.001709	−0.35	0.7839	−0.022321	0.0211142	44.243019
(TP−0.28556)*(TP−0.28556)	12.873689	9.15495	1.41	0.3935	−103.451	129.19836	20.21769

Effect Tests

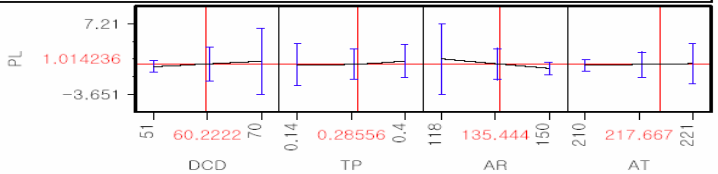
Source	Nparm	DF	Sum of Squares	F Ratio	Prob > F
DCD	1	1	0.00740241	3.9512	0.2967
TP	1	1	0.08006238	42.7352	0.0966
AR	1	1	0.01959204	10.4577	0.1909
AT	1	1	0.00446236	2.3819	0.3660
DCD*TP	1	1	0.00587141	3.1340	0.3273
DCD*AR	1	1	0.00023359	0.1247	0.7839
TP*TP	1	1	0.00370456	1.9774	0.3935

Scaled Estimates

Continuous factors centered by mean, scaled by range/2

Term	Scaled Estimate	Std Error	t Ratio	Prob>|t|
Intercept	1.0142362	0.184715	5.49	0.1147
DCD	0.4290534	0.215847	1.99	0.2967
TP	0.3512504	0.053731	6.54	0.0966
AR	−0.730978	0.22604	−3.23	0.1909
AT	0.1430468	0.092687	1.54	0.3660
(DCD−60.2222)*(TP−0.28556)	−0.297181	0.16787	−1.77	0.3273
(DCD−60.2222)*(AR−135.444)	−0.091739	0.259802	−0.35	0.7839
(TP−0.28556)*(TP−0.28556)	0.2175654	0.154719	1.41	0.3935

Prediction Profiler



Multiple liner regression between peak elong. and processing parameter for TPU_{245}

Response PE

Summary of Fit

RSquare	0.999717
RSquare Adj	0.997734
Root Mean Square Error	5.307228
Mean of Response	181.8889
Observations (or Sum Wgts)	9

Analysis of Variance

Source	DF	Sum of Squares	Mean Square	F Ratio
Model	7	99426.722	14203.8	504.2775
Error	1	28.167	28.2	Prob > F
C. Total	8	99454.889		0.0343

Parameter Estimates

Term	Estimate	Std Error	t Ratio	Prob>|t|	Lower 95%	Upper 95%	VIF
Intercept	−15628.94	4343.691	−3.60	0.1726	−70820.77	39562.897	.
DCD	−54.97956	13.4819	−4.08	0.1531	−226.2833	116.32422	4230.3496
TP	581.11111	73.96847	7.86	0.0806	−358.7474	1520.9696	9.0174499
AR	−5.090812	1.790454	−2.84	0.2153	−27.84069	17.659064	191.45833
DT	115.98227	32.85593	3.53	0.1757	−301.4918	533.45639	4215.845
AT	−21.75	8.178987	−2.66	0.2290	−125.6739	82.173888	365.75
(DCD−60.2222)*(TP−0.28556)	−40	7.677986	−5.21	0.1207	−137.5581	57.558066	4.7749415
(DCD−60.2222)*(AR−135.444)	0.0240385	0.202344	0.12	0.9247	−2.546992	2.5950688	41.241681

Effect Tests

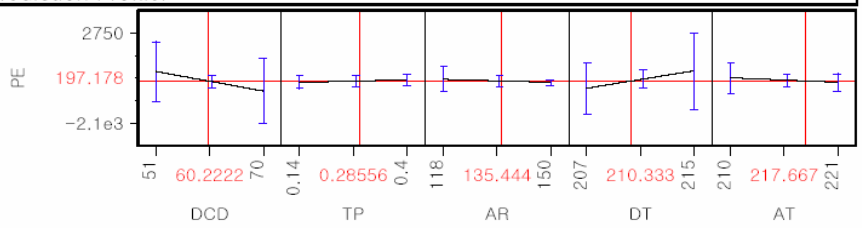
Source	Nparm	DF	Sum of Squares	F Ratio	Prob > F
DCD	1	1	468.4204	16.6303	0.1531
TP	1	1	1738.4434	61.7199	0.0806
AR	1	1	227.7106	8.0844	0.2153
DT	1	1	350.9872	12.4611	0.1757
AT	1	1	199.1842	7.0716	0.2290
DCD*TP	1	1	764.4706	27.1410	0.1207
DCD*AR	1	1	0.3975	0.0141	0.9247

Scaled Estimates

Continuous factors centered by mean, scaled by range/2

Term	Scaled Estimate	Std Error	t Ratio	Prob>|t|
Intercept	197.17799	22.40071	8.80	0.0720
DCD	−522.3058	128.0781	−4.08	0.1531
TP	75.544444	9.615901	7.86	0.0806
AR	−81.45299	28.64726	−2.84	0.2153
DT	463.92908	131.4237	3.53	0.1757
AT	−119.625	44.98443	−2.66	0.2290
(DCD−60.2222)*(TP−0.28556)	−49.4	9.482313	−5.21	0.1207
(DCD−60.2222)*(AR−135.444)	3.6538462	30.75636	0.12	0.9247

Prediction Profiler



Multiple liner regression between basis weight and processing parameter for TPU_{280}

Response W

Summary of Fit

RSquare	1
RSquare Adj	.
Root Mean Square Error	.
Mean of Response	117.875
Observations (or Sum Wgts)	8

Analysis of Variance

Source	DF	Sum of Squares	Mean Square	F Ratio
Model	7	8652.8750	1236.13	.
Error	0	0.0000	.	Prob > F
C. Total	7	8652.8750		.

Parameter Estimates

Term	Estimate	Std Error	t Ratio	Prob>|t|
Intercept	14612.244	.	.	.
TP	5091.3542	.	.	.
AR	2.175651	.	.	.
DT	19.758073	.	.	.
AT	−87	.	.	.
(TP−0.35625)*(AR−133)	363.4375	.	.	.
(AR−133)*(DT−236)	−1.335417	.	.	.
(AR−133)*(AR−133)	−0.383854	.	.	.

Effect Tests

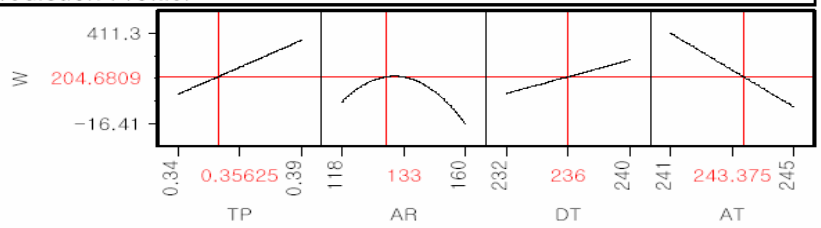
Source	Nparm	DF	Sum of Squares	F Ratio	Prob > F
TP	1	1	4076.8229	.	.
AR	1	1	4117.2494	.	.
DT	1	1	1087.3027	.	.
AT	1	1	3784.5000	.	.
TP*AR	1	1	3349.7856	.	.
AR*DT	1	1	2833.6621	.	.
AR*AR	1	1	5542.5408	.	.

Scaled Estimates

Continuous factors centered by mean, scaled by range/2

Term	Scaled Estimate	Std Error	t Ratio	Prob>|t|
Intercept	204.68086	.	0.00	.
TP	127.28385	.	0.00	.
AR	45.688672	.	0.00	.
DT	79.032292	.	0.00	.
AT	−174	.	0.00	.
(TP−0.35625)*(AR−133)	190.80469	.	0.00	.
(AR−133)*(DT−236)	−112.175	.	0.00	.
(AR−133)*(AR−133)	−169.2797	.	0.00	.

Prediction Profiler



Multiple liner regression between thickness and processing parameter for TPU_{280}

Response T

Summary of Fit

RSquare	1
RSquare Adj	.
Root Mean Square Error	.
Mean of Response	0.555
Observations (or Sum Wgts)	8

Analysis of Variance

Source	DF	Sum of Squares	Mean Square	F Ratio
Model	7	0.16420000	0.023457	.
Error	0	0.00000000	.	Prob > F
C. Total	7	0.16420000		.

Parameter Estimates

Term	Estimate	Std Error	t Ratio	Prob>|t|
Intercept	54.696799	.	.	.
TP	28.210417	.	.	.
AR	0.0049922	.	.	.
DT	0.0049948	.	.	.
AT	−0.27	.	.	.
(TP−0.35625)*(AR−133)	1.4520833	.	.	.
(AR−133)*(DT−236)	−0.004906	.	.	.
(AR−133)*(AR−133)	−0.001448	.	.	.

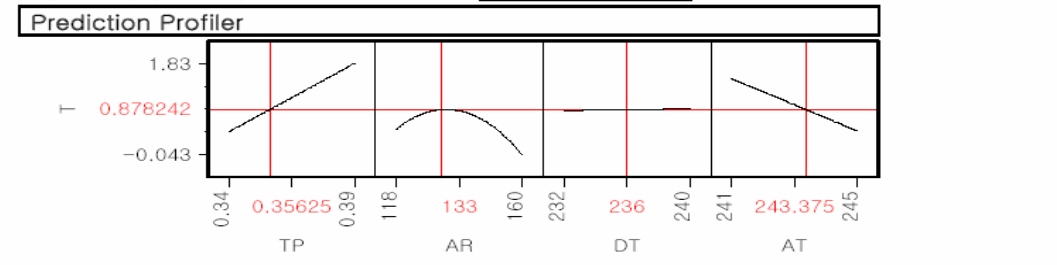
Effect Tests

Source	Nparm	DF	Sum of Squares	F Ratio	Prob > F
TP	1	1	0.12516250	.	.
AR	1	1	0.02167756	.	.
DT	1	1	0.00006949	.	.
AT	1	1	0.03645000	.	.
TP*AR	1	1	0.05347375	.	.
AR*DT	1	1	0.03824845	.	.
AR*AR	1	1	0.07886122	.	.

Scaled Estimates

Continuous factors centered by mean, scaled by range/2

Term	Scaled Estimate	Std Error	t Ratio	Prob>|t|
Intercept	0.8782422	.	0.00	.
TP	0.7052604	.	0.00	.
AR	0.1048359	.	0.00	.
DT	0.0199792	.	0.00	.
AT	−0.54	.	0.00	.
(TP−0.35625)*(AR−133)	0.7623438	.	0.00	.
(AR−133)*(DT−236)	−0.412125	.	0.00	.
(AR−133)*(AR−133)	−0.638531	.	0.00	.



Prediction Profiler

Multiple liner regression between fiber diameter and processing parameter for TPU_{280}

Response FD

Summary of Fit

RSquare	1
RSquare Adj	.
Root Mean Square Error	.
Mean of Response	9.4
Observations (or Sum Wgts)	8

Analysis of Variance

Source	DF	Sum of Squares	Mean Square	F Ratio
Model	7	59.900000	8.55714	.
Error	0	0.000000	.	Prob > F
C. Total	7	59.900000		.

Parameter Estimates

Term	Estimate	Std Error	t Ratio	Prob>|t|
Intercept	1.3123047	.	.	.
TP	−63.67708	.	.	.
AR	−0.137826	.	.	.
DT	0.6215885	.	.	.
AT	−0.4	.	.	.
(TP−0.35625)*(AR−133)	−7.71875	.	.	.
(AR−133)*(DT−236)	0.0423958	.	.	.
(AR−133)*(AR−133)	−0.001198	.	.	.

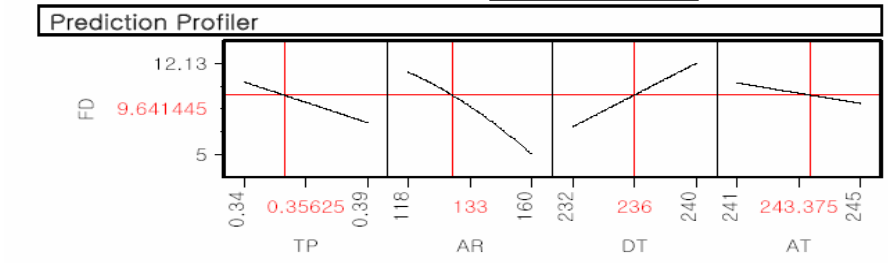
Effect Tests

Source	Nparm	DF	Sum of Squares	F Ratio	Prob > F
TP	1	1	0.637708	.	.
AR	1	1	16.522965	.	.
DT	1	1	1.076136	.	.
AT	1	1	0.080000	.	.
TP*AR	1	1	1.510955	.	.
AR*DT	1	1	2.856017	.	.
AR*AR	1	1	0.053980	.	.

Scaled Estimates

Continuous factors centered by mean, scaled by range/2

Term	Scaled Estimate	Std Error	t Ratio	Prob>|t|
Intercept	9.6414453	.	0.00	.
TP	−1.591927	.	0.00	.
AR	−2.894336	.	0.00	.
DT	2.4863542	.	0.00	.
AT	−0.8	.	0.00	.
(TP−0.35625)*(AR−133)	−4.052344	.	0.00	.
(AR−133)*(DT−236)	3.56125	.	0.00	.
(AR−133)*(AR−133)	−0.528281	.	0.00	.



Prediction Profiler

Multiple liner regression between air perm. and processing parameter for TPU_{280}

Response AP

Summary of Fit

RSquare	1
RSquare Adj	.
Root Mean Square Error	.
Mean of Response	402
Observations (or Sum Wgts)	8

Analysis of Variance

Source	DF	Sum of Squares	Mean Square	F Ratio
Model	7	542538.00	77505.4	.
Error	0	0.00	.	Prob > F
C. Total	7	542538.00		.

Parameter Estimates

Term	Estimate	Std Error	t Ratio	Prob>|t|
Intercept	−115282.2	.	.	.
TP	−24329.06	.	.	.
AR	−19.51237	.	.	.
DT	−236.293	.	.	.
AT	749	.	.	.
(TP−0.35625)*(AR−133)	−1691.979	.	.	.
(AR−133)*(DT−236)	8.4322917	.	.	.
(AR−133)*(AR−133)	1.7953125	.	.	.

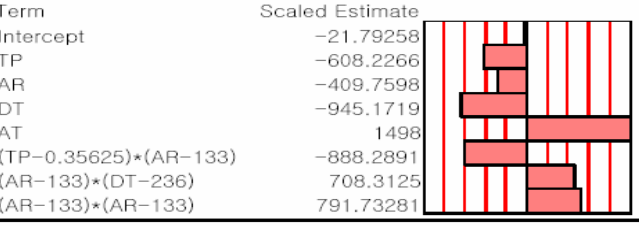
Effect Tests

Source	Nparm	DF	Sum of Squares	F Ratio	Prob > F
TP	1	1	93090.63	.	.
AR	1	1	331168.28	.	.
DT	1	1	155511.63	.	.
AT	1	1	280500.50	.	.
TP*AR	1	1	72601.83	.	.
AR*DT	1	1	112981.08	.	.
AR*AR	1	1	121242.95	.	.

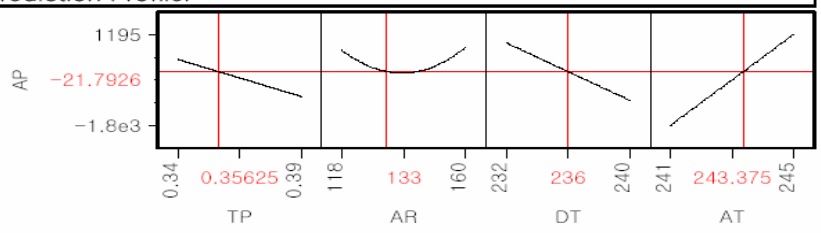
Scaled Estimates

Continuous factors centered by mean, scaled by range/2

Term	Scaled Estimate	Std Error	t Ratio	Prob>|t|
Intercept	−21.79258	.	0.00	.
TP	−608.2266	.	0.00	.
AR	−409.7598	.	0.00	.
DT	−945.1719	.	0.00	.
AT	1498	.	0.00	.
(TP−0.35625)*(AR−133)	−888.2891	.	0.00	.
(AR−133)*(DT−236)	708.3125	.	0.00	.
(AR−133)*(AR−133)	791.73281	.	0.00	.



Prediction Profiler



Multiple liner regression between tear strength and processing parameter for TPU_{280}

Response TS

Summary of Fit

RSquare	1
RSquare Adj	.
Root Mean Square Error	.
Mean of Response	240.5
Observations (or Sum Wgts)	8

Analysis of Variance

Source	DF	Sum of Squares	Mean Square	F Ratio
Model	7	109534.00	15647.7	.
Error	0	0.00	.	Prob > F
C. Total	7	109534.00		.

Parameter Estimates

Term	Estimate	Std Error	t Ratio	Prob>|t|
Intercept	46373.847	.	.	.
TP	9364.1667	.	.	.
AR	1.8135417	.	.	.
DT	98.135417	.	.	.
AT	−299	.	.	.
(TP−0.35625)*(AR−133)	207.5	.	.	.
(AR−133)*(DT−236)	−0.151042	.	.	.
(AR−133)*(AR−133)	−0.460417	.	.	.

Effect Tests

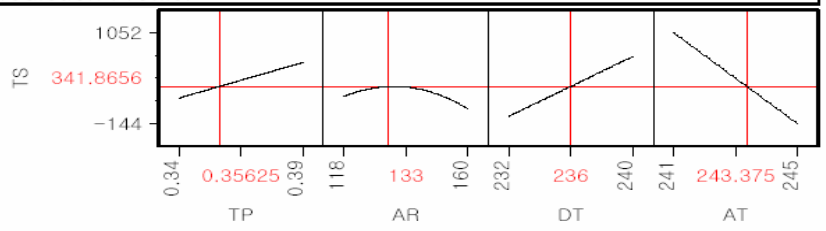
Source	Nparm	DF	Sum of Squares	F Ratio	Prob > F
TP	1	1	13790.928	.	.
AR	1	1	2860.775	.	.
DT	1	1	26823.338	.	.
AT	1	1	44700.500	.	.
TP*AR	1	1	1091.927	.	.
AR*DT	1	1	36.250	.	.
AR*AR	1	1	7974.041	.	.

Scaled Estimates

Continuous factors centered by mean, scaled by range/2

Term	Scaled Estimate	Std Error	t Ratio	Prob>|t|
Intercept	341.86563	.	0.00	.
TP	234.10417	.	0.00	.
AR	38.084375	.	0.00	.
DT	392.54167	.	0.00	.
AT	−598	.	0.00	.
(TP−0.35625)*(AR−133)	108.9375	.	0.00	.
(AR−133)*(DT−236)	−12.6875	.	0.00	.
(AR−133)*(AR−133)	−203.0438	.	0.00	.

Prediction Profiler



Multiple liner regression between peak force and processing parameter for TPU_{280}

Response PL

Summary of Fit

RSquare	1
RSquare Adj	.
Root Mean Square Error	.
Mean of Response	2.2275
Observations (or Sum Wgts)	8

Analysis of Variance

Source	DF	Sum of Squares	Mean Square	F Ratio
Model	7	4.8363500	0.690907	.
Error	0	0.0000000	.	Prob > F
C. Total	7	4.8363500		.

Parameter Estimates

Term	Estimate	Std Error	t Ratio	Prob>|t|
Intercept	301.97676	.	.	.
TP	107.79375	.	.	.
AR	0.0438047	.	.	.
DT	0.4469531	.	.	.
AT	−1.84	.	.	.
(TP−0.35625)*(AR−133)	5.36875	.	.	.
(AR−133)*(DT−236)	−0.01625	.	.	.
(AR−133)*(AR−133)	−0.007344	.	.	.

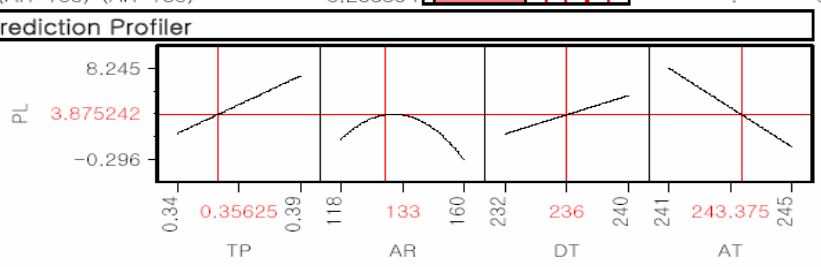
Effect Tests

Source	Nparm	DF	Sum of Squares	F Ratio	Prob > F
TP	1	1	1.8274369	.	.
AR	1	1	1.6690520	.	.
DT	1	1	0.5563976	.	.
AT	1	1	1.6928000	.	.
TP*AR	1	1	0.7309773	.	.
AR*DT	1	1	0.4195862	.	.
AR*AR	1	1	2.0286735	.	.

Scaled Estimates

Continuous factors centered by mean, scaled by range/2

Term	Scaled Estimate	Std Error	t Ratio	Prob>|t|
Intercept	3.8752422	.	0.00	.
TP	2.6948438	.	0.00	.
AR	0.9198984	.	0.00	.
DT	1.7878125	.	0.00	.
AT	−3.68	.	0.00	.
(TP−0.35625)*(AR−133)	2.8185938	.	0.00	.
(AR−133)*(DT−236)	−1.365	.	0.00	.
(AR−133)*(AR−133)	−3.238594	.	0.00	.



Prediction Profiler

Multiple liner regression between peak elong. and processing parameter for TPU_{280}

Response PE

Summary of Fit

RSquare	1
RSquare Adj	.
Root Mean Square Error	.
Mean of Response	309.125
Observations (or Sum Wgts)	8

Analysis of Variance

Source	DF	Sum of Squares	Mean Square	F Ratio
Model	7	29496.875	4213.84	.
Error	0	0.000	.	Prob > F
C. Total	7	29496.875		.

Parameter Estimates

Term	Estimate	Std Error	t Ratio	Prob>|t|	VIF
Intercept	25692.243	.	.	.	.
TP	9383.8542	.	.	.	17.723915
AR	3.4079427	.	.	.	2.1613702
DT	32.570573	.	.	.	45.956684
AT	−151	.	.	.	43.75
(TP−0.35625)*(AR−133)	452.60417	.	.	.	31.407129
(AR−133)*(DT−236)	−1.611458	.	.	.	18.608333
(AR−133)*(AR−133)	−0.515104	.	.	.	8.8940104

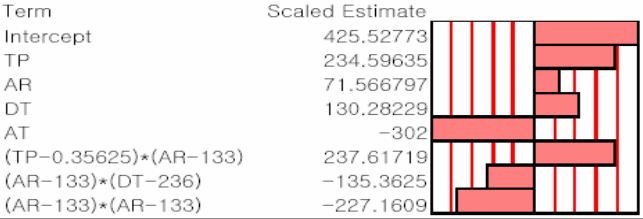
Effect Tests

Source	Nparm	DF	Sum of Squares	F Ratio	Prob > F
TP	1	1	13848.978	.	.
AR	1	1	10102.137	.	.
DT	1	1	2954.691	.	.
AT	1	1	11400.500	.	.
TP*AR	1	1	5195.109	.	.
AR*DT	1	1	4126.222	.	.
AR*AR	1	1	9980.827	.	.

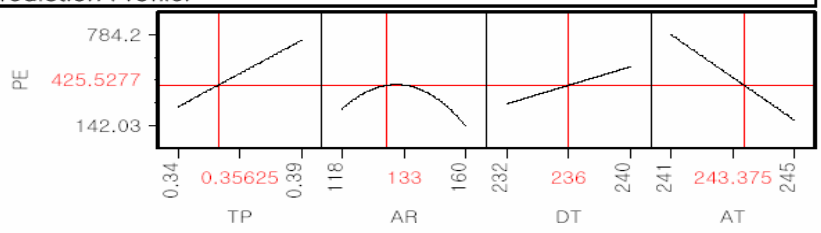
Scaled Estimates

Continuous factors centered by mean, scaled by range/2

Term	Scaled Estimate	Std Error	t Ratio	Prob>|t|
Intercept	425.52773	.	0.00	.
TP	234.59635	.	0.00	.
AR	71.566797	.	0.00	.
DT	130.28229	.	0.00	.
AT	−302	.	0.00	.
(TP−0.35625)*(AR−133)	237.61719	.	0.00	.
(AR−133)*(DT−236)	−135.3625	.	0.00	.
(AR−133)*(AR−133)	−227.1609	.	0.00	.



Prediction Profiler

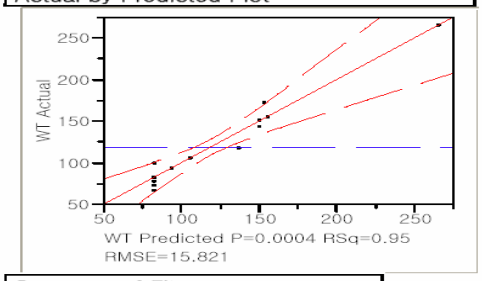


APPENDIX III

Basis weight of TPU_{237}

Response WT

Actual by Predicted Plot



Summary of Fit

RSquare	0.95415
RSquare Adj	0.9083
Root Mean Square Error	15.82084
Mean of Response	118.5333
Observations (or Sum Wgts)	15

Analysis of Variance

Source	DF	Sum of Squares	Mean Square	F Ratio
Model	7	36461.641	5208.81	20.8103
Error	7	1752.093	250.30	Prob > F
C. Total	14	38213.733		0.0004

Lack Of Fit

Source	DF	Sum of Squares	Mean Square	F Ratio
Lack Of Fit	1	762.5927	762.593	4.6241
Pure Error	6	989.5000	164.917	Prob > F
Total Error	7	1752.0927		0.0751
				Max RSq
				0.9741

Parameter Estimates

Term	Estimate	Std Error	t Ratio	Prob>|t|	Lower 95%	Upper 95%	VIF
Intercept	−2925.556	1298.512	−2.25	0.0589	−5996.05	144.93771	.
CS	−18.3908	2.571729	−7.15	0.0002	−24.47198	−12.30963	1.8666667
TP	318.01276	50.49522	6.30	0.0004	198.61055	437.41497	2.6807808
AIR	0.55	1.118702	0.49	0.6380	−2.095311	3.1953105	1
DT	15.756735	6.427545	2.45	0.0440	0.5580056	30.955465	5.4358438
(TP−0.316)*(TP−0.316)	−1463.23	652.0186	−2.24	0.0597	−3005.009	78.548811	2.4315329
(AIR−50)*(AIR−50)	0.0577804	0.1291	0.45	0.6680	−0.247492	0.3630527	1.1541796
(DT−205.067)*(DT−205.067)	−3.004841	1.647718	−1.82	0.1110	−6.901075	0.8913922	6.0363732

Effect Tests

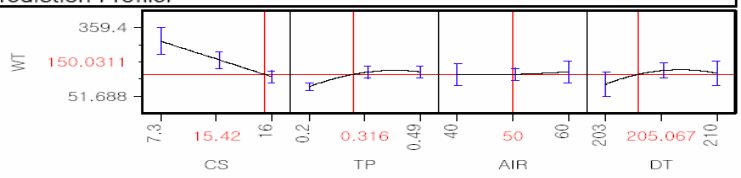
Source	Nparm	DF	Sum of Squares	F Ratio	Prob > F
CS	1	1	12800.000	51.1388	0.0002
TP	1	1	9927.678	39.6633	0.0004
AIR	1	1	60.500	0.2417	0.6380
DT	1	1	1504.185	6.0096	0.0440
TP*TP	1	1	1260.562	5.0362	0.0597
AIR*AIR	1	1	50.138	0.2003	0.6680
DT*DT	1	1	832.408	3.3257	0.1110

Scaled Estimates

Continuous factors centered by mean, scaled by range/2

Term	Scaled Estimate	Std Error	t Ratio	Prob>|t|
Intercept	150.03113	11.59883	12.94	<.0001
CS	−80	11.18702	−7.15	0.0002
TP	46.111851	7.321806	6.30	0.0004
AIR	5.5	11.18702	0.49	0.6380
DT	55.148574	22.49641	2.45	0.0440
(TP−0.316)*(TP−0.316)	−30.76441	13.70869	−2.24	0.0597
(AIR−50)*(AIR−50)	5.7780424	12.90997	0.45	0.6680
(DT−205.067)*(DT−205.067)	−36.80931	20.18454	−1.82	0.1110

Prediction Profiler

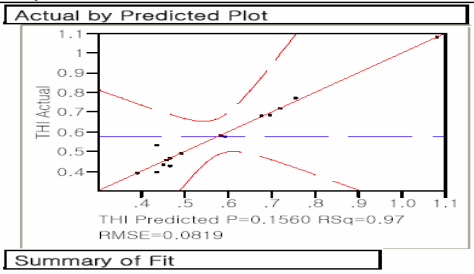


Thickness of TPU_{237}

58237-MD- Fit Least Squares

Response THI

Actual by Predicted Plot



Summary of Fit

RSquare	0.972123
RSquare Adj	0.804863
Root Mean Square Error	0.081909
Mean of Response	0.577333
Observations (or Sum Wgts)	15

Analysis of Variance

Source	DF	Sum of Squares	Mean Square	F Ratio
Model	12	0.46791922	0.038993	5.8120
Error	2	0.01341812	0.006709	Prob > F
C. Total	14	0.48133733		0.1560

Lack Of Fit

Source	DF	Sum of Squares	Mean Square	F Ratio
Lack Of Fit	1	0.00417012	0.004170	0.4509
Pure Error	1	0.00924800	0.009248	Prob > F
Total Error	2	0.01341812		0.6235
				Max RSq
				0.9808

Parameter Estimates

Term	Estimate	Std Error	t Ratio	Prob>|t|	Lower 95%	Upper 95%	VIF
Intercept	−12.83516	7.420952	−1.73	0.2258	−44.76494	19.094625	.
DCD	0.0091581	0.005141	1.78	0.2168	−0.012962	0.0312782	1.9675859
CS	−0.067816	0.013315	−5.09	0.0365	−0.125104	−0.010528	1.8666667
TP	0.9263789	0.383724	2.41	0.1371	−0.72465	2.5774082	5.7755754
AIR	0.0004	0.005792	0.07	0.9512	−0.02452	0.0253202	1
DT	0.0669069	0.037176	1.80	0.2137	−0.09305	0.2268641	6.784364
AT	0.0000079	0.007832	0.00	0.9993	−0.033691	0.0337066	4.6532229
(DCD−52.1067)*(DCD−52.1067)	0.0003754	0.000352	1.07	0.3974	−0.001137	0.0018879	2.45883
(TP−0.316)*(TP−0.316)	−3.331715	4.166209	−0.80	0.5078	−21.25746	14.594035	3.7037335
(TP−0.316)*(AT−218.067)	−0.048079	0.079411	−0.61	0.6064	−0.389759	0.2936003	7.0496102
(AIR−50)*(AIR−50)	0.0002651	0.000729	0.36	0.7508	−0.00287	0.0033999	1.3714068
(DT−205.067)*(DT−205.067)	−0.011977	0.010305	−1.16	0.3651	−0.056318	0.0323632	8.8092898
(AT−218.067)*(AT−218.067)	0.0008098	0.001203	0.67	0.5703	−0.004368	0.0059879	13.517934

Effect Tests

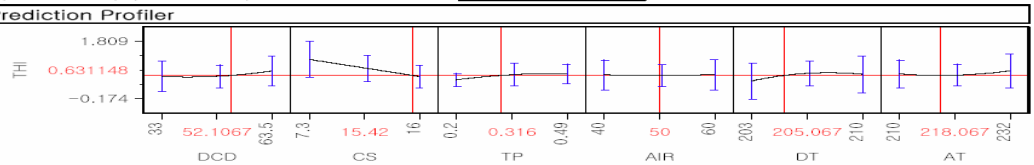
Source	Nparm	DF	Sum of Squares	F Ratio	Prob > F
DCD	1	1	0.02128953	3.1733	0.2168
CS	1	1	0.17405000	25.9425	0.0365
TP	1	1	0.03910227	5.8283	0.1371
AIR	1	1	0.00003200	0.0048	0.9512
DT	1	1	0.02173043	3.2390	0.2137
AT	1	1	0.00000001	0.0000	0.9993
DCD*DCD	1	1	0.00765209	1.1406	0.3974
TP*TP	1	1	0.00429057	0.6395	0.5078
TP*AT	1	1	0.00245930	0.3666	0.6064
AIR*AIR	1	1	0.00088813	0.1324	0.7508
DT*DT	1	1	0.00906275	1.3508	0.3651
AT*AT	1	1	0.00303810	0.4528	0.5703

Scaled Estimates

Continuous factors centered by mean, scaled by range/2

Term	Scaled Estimate	Std Error	t Ratio	Prob>|t|
Intercept	0.631148	0.087245	7.23	0.0186
DCD	0.1396606	0.078401	1.78	0.2168
CS	−0.295	0.057918	−5.09	0.0365
TP	0.1343249	0.05564	2.41	0.1371
AIR	0.004	0.057918	0.07	0.9512
DT	0.2341741	0.130117	1.80	0.2137
AT	0.0000869	0.086153	0.00	0.9993
(DCD−52.1067)*(DCD−52.1067)	0.0873098	0.081753	1.07	0.3974
(TP−0.316)*(TP−0.316)	−0.070049	0.087595	−0.80	0.5078
(TP−0.316)*(AT−218.067)	−0.076686	0.126661	−0.61	0.6064
(AIR−50)*(AIR−50)	0.0265082	0.072857	0.36	0.7508
(DT−205.067)*(DT−205.067)	−0.146724	0.126242	−1.16	0.3651
(AT−218.067)*(AT−218.067)	0.0979905	0.145617	0.67	0.5703

Prediction Profiler

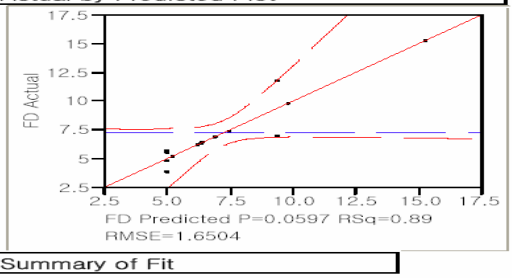


Fiber diameter of TPU_{237}

58237-MD- Fit Least Squares

Response FD

Actual by Predicted Plot



Summary of Fit

RSquare	0.887039
RSquare Adj	0.683708
Root Mean Square Error	1.650387
Mean of Response	7.237333
Observations (or Sum Wgts)	15

Analysis of Variance

Source	DF	Sum of Squares	Mean Square	F Ratio
Model	9	106.94340	11.8826	4.3625
Error	5	13.61889	2.7238	Prob > F
C. Total	14	120.56229		0.0597

Lack Of Fit

Source	DF	Sum of Squares	Mean Square	F Ratio
Lack Of Fit	1	0.007219	0.00722	0.0021
Pure Error	4	13.611675	3.40292	Prob > F
Total Error	5	13.618894		0.9655
				Max RSq
				0.8871

Parameter Estimates

Term	Estimate	Std Error	t Ratio	Prob>|t|	VIF
Intercept	−239.4411	135.5738	−1.77	0.1376	.
DCD	0.0522398	0.102842	0.51	0.6331	1.9393733
CS	−0.331034	0.268276	−1.23	0.2721	1.8666667
TP	14.395959	5.753077	2.50	0.0543	3.197779
AIR	−0.0845	0.1167	−0.72	0.5015	1
DT	1.2102675	0.670507	1.81	0.1309	5.4358897
(DCD−52.1067)*(DCD−52.1067)	0.0061776	0.006898	0.90	0.4115	2.3320856
(TP−0.316)*(TP−0.316)	12.598825	69.09018	0.18	0.8625	2.5088809
(AIR−50)*(AIR−50)	0.0105891	0.014276	0.74	0.4916	1.2969115
(DT−205.067)*(DT−205.067)	−0.007568	0.171887	−0.04	0.9666	6.0364676

Effect Tests

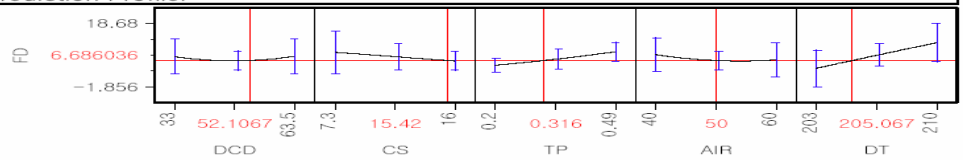
Source	Nparm	DF	Sum of Squares	F Ratio	Prob > F
DCD	1	1	0.702803	0.2580	0.6331
CS	1	1	4.147200	1.5226	0.2721
TP	1	1	17.055036	6.2615	0.0543
AIR	1	1	1.428050	0.5243	0.5015
DT	1	1	8.874171	3.2580	0.1309
DCD*DCD	1	1	2.184503	0.8020	0.4115
TP*TP	1	1	0.090573	0.0333	0.8625
AIR*AIR	1	1	1.498624	0.5502	0.4916
DT*DT	1	1	0.005281	0.0019	0.9666

Scaled Estimates

Continuous factors centered by mean, scaled by range/2

Term	Scaled Estimate	Std Error	t Ratio	Prob>|t|
Intercept	6.6860358	1.213466	5.51	0.0027
DCD	0.7966572	1.568342	0.51	0.6331
CS	−1.44	1.167	−1.23	0.2721
TP	2.0874141	0.834196	2.50	0.0543
AIR	−0.845	1.167	−0.72	0.5015
DT	4.2359363	2.346775	1.81	0.1309
(DCD−52.1067)*(DCD−52.1067)	1.436671	1.604231	0.90	0.4115
(TP−0.316)*(TP−0.316)	0.2648903	1.452621	0.18	0.8625
(AIR−50)*(AIR−50)	1.0589135	1.427579	0.74	0.4916
(DT−205.067)*(DT−205.067)	−0.092713	2.105614	−0.04	0.9666

Prediction Profiler

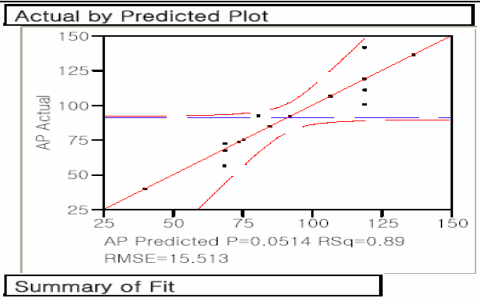


Air permeability of TPU_{237}

58237-MD- Fit Least Squares

Response AP

Actual by Predicted Plot



Summary of Fit

RSquare	0.894396
RSquare Adj	0.70431
Root Mean Square Error	15.51271
Mean of Response	90.99333
Observations (or Sum Wgts)	15

Analysis of Variance

Source	DF	Sum of Squares	Mean Square	F Ratio
Model	9	10190.528	1132.28	4.7052
Error	5	1203.221	240.64	Prob > F
C. Total	14	11393.749		0.0514

Lack Of Fit

Source	DF	Sum of Squares	Mean Square	F Ratio
Lack Of Fit	1	288.6862	288.686	1.2627
Pure Error	4	914.5350	228.634	Prob > F
Total Error	5	1203.2212		0.3240
				Max RSq
				0.9197

Parameter Estimates

Term	Estimate	Std Error	t Ratio	Prob>|t|	Lower 95%	Upper 95%	VIF
Intercept	357.28787	1274.317	0.28	0.7904	-2918.449	3633.0247	.
DCD	0.1720731	0.966658	0.18	0.8657	-2.3128	2.6569459	1.9393733
CS	3.8735632	2.521642	1.54	0.1851	-2.608525	10.355651	1.8666667
TP	-229.4987	54.07568	-4.24	0.0081	-368.5046	-90.49271	3.197779
AIR	-2.22	1.096914	-2.02	0.0989	-5.039708	0.5997082	1
DT	-0.809627	6.302389	-0.13	0.9028	-17.01043	15.391179	5.4358897
(DCD-52.1067)*(DCD-52.1067)	-0.109888	0.064838	-1.69	0.1509	-0.276559	0.0567837	2.3320856
(TP-0.316)*(TP-0.316)	969.26244	649.4088	1.49	0.1958	-700.0959	2638.6208	2.5088809
(AIR-50)*(AIR-50)	-0.046672	0.134184	-0.35	0.7421	-0.391604	0.2982598	1.2969115
(DT-205.067)*(DT-205.067)	0.8355843	1.615639	0.52	0.6271	-3.317549	4.9887177	6.0364676

Effect Tests

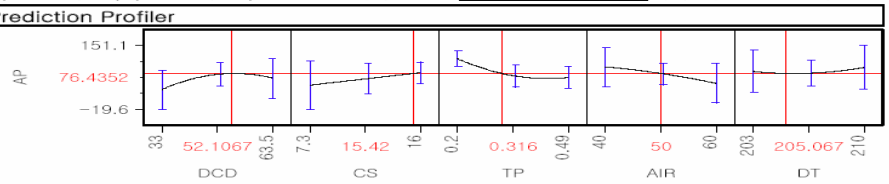
Source	Nparm	DF	Sum of Squares	F Ratio	Prob > F
DCD	1	1	7.6253	0.0317	0.8657
CS	1	1	567.8450	2.3597	0.1851
TP	1	1	4334.4281	18.0118	0.0081
AIR	1	1	985.6800	4.0960	0.0989
DT	1	1	3.9713	0.0165	0.9028
DCD*DCD	1	1	691.2162	2.8724	0.1509
TP*TP	1	1	536.0705	2.2276	0.1958
AIR*AIR	1	1	29.1129	0.1210	0.7421
DT*DT	1	1	64.3676	0.2675	0.6271

Scaled Estimates

Continuous factors centered by mean, scaled by range/2

Term	Scaled Estimate	Std Error	t Ratio	Prob>|t|
Intercept	76.435198	11.4059	6.70	0.0011
DCD	2.6241155	14.74153	0.18	0.8657
CS	16.85	10.96914	1.54	0.1851
TP	-33.27731	7.840974	-4.24	0.0081
AIR	-22.2	10.96914	-2.02	0.0989
DT	-2.833696	22.05836	-0.13	0.9028
(DCD-52.1067)*(DCD-52.1067)	-25.55571	15.07887	-1.69	0.1509
(TP-0.316)*(TP-0.316)	20.378743	13.65382	1.49	0.1958
(AIR-50)*(AIR-50)	-4.667207	13.41843	-0.35	0.7421
(DT-205.067)*(DT-205.067)	10.235908	19.79158	0.52	0.6271

Prediction Profiler

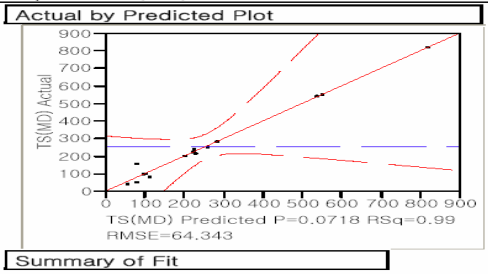


Tear strength of TPU_{237}

58237-MD- Fit Least Squares

Response TS(MD)

Actual by Predicted Plot



Summary of Fit

RSquare	0.987664
RSquare Adj	0.913647
Root Mean Square Error	64.34296
Mean of Response	254.3333
Observations (or Sum Wgts)	15

Analysis of Variance

Source	DF	Sum of Squares	Mean Square	F Ratio
Model	12	662921.30	55243.4	13.3438
Error	2	8280.03	4140.0	Prob > F
C. Total	14	671201.33		0.0718

Lack Of Fit

Source	DF	Sum of Squares	Mean Square	F Ratio
Lack Of Fit	1	2872.0338	2872.03	0.5311
Pure Error	1	5408.0000	5408.00	Prob > F
Total Error	2	8280.0338		0.5991
				Max RSq
				0.9919

Parameter Estimates

Term	Estimate	Std Error	t Ratio	Prob>|t|
Intercept	-16660.56	5829.481	-2.86	0.1037
DCD	7.6956795	4.03852	1.91	0.1970
CS	-61.6092	10.45916	-5.89	0.0276
TP	1316.9076	301.4316	4.37	0.0486
AIR	-5.05	4.549735	-1.11	0.3826
DT	88.848254	29.20369	3.04	0.0932
AT	-4.178855	6.152442	-0.68	0.5671
(DCD-52.1067)*(DCD-52.1067)	0.4663767	0.276143	1.69	0.2333
(TP-0.316)*(TP-0.316)	1197.7848	3272.739	0.37	0.7495
(TP-0.316)*(AT-218.067)	-92.4211	62.3811	-1.48	0.2766
(AIR-50)*(AIR-50)	0.719886	0.572326	1.26	0.3354
(DT-205.067)*(DT-205.067)	-17.6381	8.095372	-2.18	0.1612
(AT-218.067)*(AT-218.067)	0.2500143	0.945363	0.26	0.8162

Effect Tests

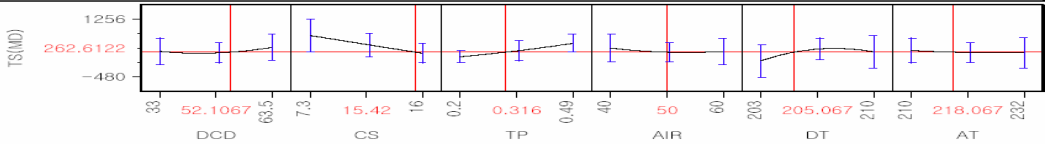
Source	Nparm	DF	Sum of Squares	F Ratio	Prob > F
DCD	1	1	15033.21	3.6312	0.1970
CS	1	1	143648.00	34.6974	0.0276
TP	1	1	79019.67	19.0868	0.0486
AIR	1	1	5100.50	1.2320	0.3826
DT	1	1	38319.90	9.2560	0.0932
AT	1	1	1909.95	0.4613	0.5671
DCD*DCD	1	1	11808.83	2.8524	0.2333
TP*TP	1	1	554.55	0.1339	0.7495
TP*AT	1	1	9087.37	2.1950	0.2766
AIR*AIR	1	1	6550.03	1.5821	0.3354
DT*DT	1	1	19653.14	4.7471	0.1612
AT*AT	1	1	289.56	0.0699	0.8162

Scaled Estimates

Continuous factors centered by mean, scaled by range/2

Term	Scaled Estimate	Std Error	t Ratio	Prob>|t|
Intercept	262.61222	68.53492	3.83	0.0619
DCD	117.35911	61.58742	1.91	0.1970
CS	-268	45.49735	-5.89	0.0276
TP	190.9516	43.70758	4.37	0.0486
AIR	-50.5	45.49735	-1.11	0.3826
DT	310.96889	102.2129	3.04	0.0932
AT	-45.96741	67.67686	-0.68	0.5671
(DCD-52.1067)*(DCD-52.1067)	108.46173	64.22056	1.69	0.2333
(TP-0.316)*(TP-0.316)	25.183425	68.80933	0.37	0.7495
(TP-0.316)*(AT-218.067)	-147.4117	99.49785	-1.48	0.2766
(AIR-50)*(AIR-50)	71.988598	57.23256	1.26	0.3354
(DT-205.067)*(DT-205.067)	-216.0667	99.1683	-2.18	0.1612
(AT-218.067)*(AT-218.067)	30.251732	114.3889	0.26	0.8162

Prediction Profiler

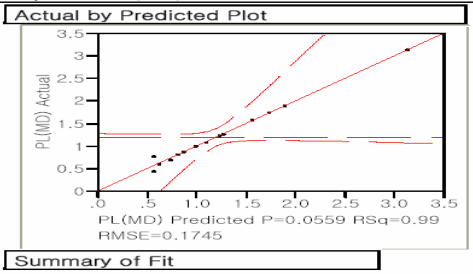


Peak force of TPU_{237}

58237-MD- Fit Least Squares

Response PL(MD)

Actual by Predicted Plot



Summary of Fit

RSquare	0.990464
RSquare Adj	0.933248
Root Mean Square Error	0.174456
Mean of Response	1.195333
Observations (or Sum Wgts)	15

Analysis of Variance

Source	DF	Sum of Squares	Mean Square	F Ratio
Model	12	6.3223034	0.526859	17.3110
Error	2	0.0608700	0.030435	Prob > F
C. Total	14	6.3831733		0.0559

Lack Of Fit

Source	DF	Sum of Squares	Mean Square	F Ratio
Lack Of Fit	1	0.00641997	0.006420	0.1179
Pure Error	1	0.05445000	0.054450	Prob > F
Total Error	2	0.06086997		0.7894
				Max RSq
				0.9915

Parameter Estimates

Term	Estimate	Std Error	t Ratio	Prob>|t|	Lower 95%	Upper 95%	VIF
Intercept	−32.4945	15.80576	−2.06	0.1761	−100.5012	35.512199	.
DCD	0.0158471	0.01095	1.45	0.2848	−0.031266	0.0629604	1.9675859
CS	−0.218391	0.028358	−7.70	0.0164	−0.340407	−0.096374	1.8666667
TP	3.5268309	0.817286	4.32	0.0497	0.0103315	7.0433303	5.7755754
AIR	−0.003	0.012336	−0.24	0.8305	−0.056077	0.0500772	1
DT	0.1842652	0.079181	2.33	0.1454	−0.156425	0.5249553	6.784364
AT	−0.011512	0.016681	−0.69	0.5614	−0.083286	0.0602623	4.6532229
(DCD−52.1067)*(DCD−52.1067)	0.002012	0.000749	2.69	0.1151	−0.001209	0.0052335	2.45883
(TP−0.316)*(TP−0.316)	−4.543765	8.873538	−0.51	0.6596	−42.72352	33.635988	3.7037335
(TP−0.316)*(AT−218.067)	−0.363256	0.169137	−2.15	0.1648	−1.090994	0.3644815	7.0496102
(AIR−50)*(AIR−50)	0.0027161	0.001552	1.75	0.2222	−0.003961	0.0093929	1.3714068
(DT−205.067)*(DT−205.067)	−0.031388	0.021949	−1.43	0.2890	−0.125829	0.0630524	8.8092898
(AT−218.067)*(AT−218.067)	0.0038732	0.002563	1.51	0.2699	−0.007155	0.0149018	13.517934

Effect Tests

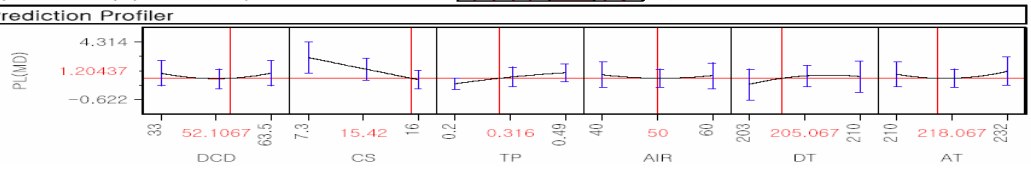
Source	Nparm	DF	Sum of Squares	F Ratio	Prob > F
DCD	1	1	0.0637463	2.0945	0.2848
CS	1	1	1.8050000	59.3067	0.0164
TP	1	1	0.5667531	18.6218	0.0497
AIR	1	1	0.0018000	0.0591	0.8305
DT	1	1	0.1648212	5.4155	0.1454
AT	1	1	0.0144949	0.4763	0.5614
DCD*DCD	1	1	0.2197794	7.2213	0.1151
TP*TP	1	1	0.0079802	0.2622	0.6596
TP*AT	1	1	0.1403854	4.6126	0.1648
AIR*AIR	1	1	0.0932432	3.0637	0.2222
DT*DT	1	1	0.0622388	2.0450	0.2890
AT*AT	1	1	0.0694941	2.2834	0.2699

Scaled Estimates

Continuous factors centered by mean, scaled by range/2

Term	Scaled Estimate	Std Error	t Ratio	Prob>|t|
Intercept	1.2043699	0.185822	6.48	0.0230
DCD	0.2416676	0.166985	1.45	0.2848
CS	−0.95	0.123359	−7.70	0.0164
TP	0.5113905	0.118507	4.32	0.0497
AIR	−0.03	0.123359	−0.24	0.8305
DT	0.6449281	0.277135	2.33	0.1454
AT	−0.126633	0.183496	−0.69	0.5614
(DCD−52.1067)*(DCD−52.1067)	0.4679146	0.174124	2.69	0.1151
(TP−0.316)*(TP−0.316)	−0.095533	0.186566	−0.51	0.6596
(TP−0.316)*(AT−218.067)	−0.579393	0.269773	−2.15	0.1648
(AIR−50)*(AIR−50)	0.271613	0.155177	1.75	0.2222
(DT−205.067)*(DT−205.067)	−0.384505	0.26888	−1.43	0.2890
(AT−218.067)*(AT−218.067)	0.4686589	0.310148	1.51	0.2699

Prediction Profiler

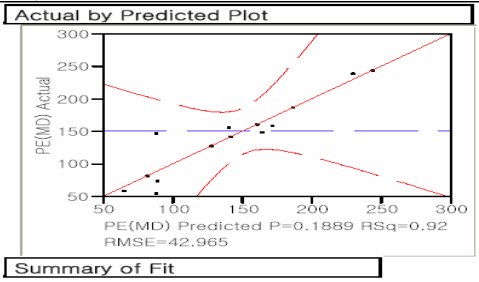


Peak elongation of TPU_{237}

58237-MD- Fit Least Squares

Response PE(MD)

Actual by Predicted Plot



Summary of Fit

RSquare	0.91981
RSquare Adj	0.625778
Root Mean Square Error	42.96484
Mean of Response	151.1333
Observations (or Sum Wgts)	15

Analysis of Variance

Source	DF	Sum of Squares	Mean Square	F Ratio
Model	11	63521.801	5774.71	3.1283
Error	3	5537.932	1845.98	Prob > F
C. Total	14	69059.733		0.1889

Lack Of Fit

Source	DF	Sum of Squares	Mean Square	F Ratio
Lack Of Fit	2	1305.9324	652.97	0.1543
Pure Error	1	4232.0000	4232.00	Prob > F
Total Error	3	5537.9324		0.8742
				Max RSq
				0.9387

Parameter Estimates

Term	Estimate	Std Error	t Ratio	Prob>|t|	Lower 95%	Upper 95%	VIF
Intercept	-3003.618	3828.254	-0.78	0.4899	-15186.83	9179.5937	.
DCD	0.7751203	2.686268	0.29	0.7917	-7.773784	9.3240249	1.9523776
CS	-12.98851	6.984076	-1.86	0.1599	-35.21495	9.2379404	1.8666667
TP	552.40951	188.6686	2.93	0.0611	-48.01828	1152.8373	5.0744955
AIR	-3	3.038073	-0.99	0.3962	-12.6685	6.6685041	1
DT	15.723243	18.87247	0.83	0.4659	-44.33738	75.783866	6.3542864
(DCD-52.1067)*(DCD-52.1067)	0.2407633	0.181814	1.32	0.2773	-0.33785	0.8193766	2.390507
(TP-0.316)*(TP-0.316)	-1125.463	1869.377	-0.60	0.5896	-7074.654	4823.7283	2.7101072
(AIR-50)*(AIR-50)	0.2353955	0.376532	0.63	0.5762	-0.962897	1.4336883	1.3312493
(DT-205.067)*(DT-205.067)	-2.644321	5.127154	-0.52	0.6416	-18.96121	13.672571	7.9249357
AT	0.4204647	3.842361	0.11	0.9198	-11.80764	12.648572	4.0703415
(AT-218.067)*(AT-218.067)	-0.339634	0.346748	-0.98	0.3996	-1.443141	0.7638731	4.0786558

Effect Tests

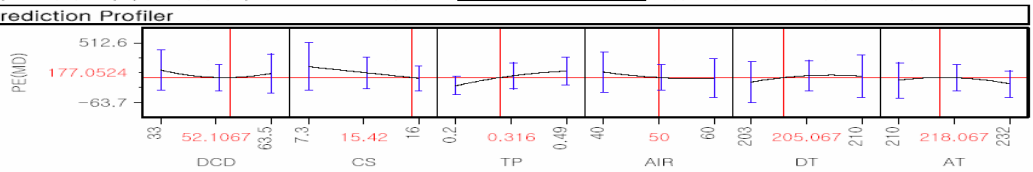
Source	Nparm	DF	Sum of Squares	F Ratio	Prob > F
DCD	1	1	153.697	0.0833	0.7917
CS	1	1	6384.500	3.4586	0.1599
TP	1	1	15825.203	8.5728	0.0611
AIR	1	1	1800.000	0.9751	0.3962
DT	1	1	1281.307	0.6941	0.4659
DCD*DCD	1	1	3237.071	1.7536	0.2773
TP*TP	1	1	669.106	0.3625	0.5896
AIR*AIR	1	1	721.471	0.3908	0.5762
DT*DT	1	1	491.023	0.2660	0.6416
AT	1	1	22.105	0.0120	0.9198
AT*AT	1	1	1771.007	0.9594	0.3996

Scaled Estimates

Continuous factors centered by mean, scaled by range/2

Term	Scaled Estimate	Std Error	t Ratio	Prob>|t|
Intercept	177.05239	38.33591	4.62	0.0191
DCD	11.820585	40.96559	0.29	0.7917
CS	-56.5	30.38073	-1.86	0.1599
TP	80.099379	27.35695	2.93	0.0611
AIR	-30	30.38073	-0.99	0.3962
DT	55.031352	66.05365	0.83	0.4659
(DCD-52.1067)*(DCD-52.1067)	55.992513	42.28312	1.32	0.2773
(TP-0.316)*(TP-0.316)	-23.66285	39.30365	-0.60	0.5896
(AIR-50)*(AIR-50)	23.539552	37.6532	0.63	0.5762
(DT-205.067)*(DT-205.067)	-32.39293	62.80763	-0.52	0.6416
AT	4.6251122	42.26597	0.11	0.9198
(AT-218.067)*(AT-218.067)	-41.09568	41.95651	-0.98	0.3996

Prediction Profiler

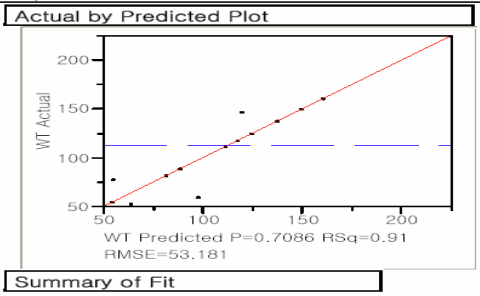


Basis weight of TPU_{245}

58245-MD- Fit Least Squares

Response WT

Actual by Predicted Plot



Summary of Fit

RSquare	0.90786
RSquare Adj	−0.19782
Root Mean Square Error	53.1807
Mean of Response	112.7857
Observations (or Sum Wgts)	14

Analysis of Variance

Source	DF	Sum of Squares	Mean Square	F Ratio
Model	12	27866.170	2322.18	0.8211
Error	1	2828.187	2828.19	Prob > F
C. Total	13	30694.357		0.7086

Parameter Estimates

Term	Estimate	Std Error	t Ratio	Prob>|t|	Lower 95%	Upper 95%	VIF
Intercept	−868.0665	3993.241	−0.22	0.8637	−51607.01	49870.872	.
DCD	−1.688635	2.849168	−0.59	0.6594	−37.89074	34.513472	2.5771554
CS	−20.16697	16.61111	−1.21	0.4386	−231.2311	190.89713	2.1335818
TP	−352.6676	1364.692	−0.26	0.8390	−17692.72	16987.382	16.542653
AIR	3.15	3.760444	0.84	0.5561	−44.63097	50.930967	1
DT	9.5	18.80222	0.51	0.7022	−229.4048	248.40483	1
AT	−3.681645	4.551962	−0.81	0.5670	−61.51981	54.156522	1.5155131
(DCD−50.5714)*(DCD−50.5714)	−0.230893	0.238966	−0.97	0.5109	−3.267245	2.8054589	4.6325059
(CS−7.17143)*(CS−7.17143)	1.4108754	6.388933	0.22	0.8616	−79.76822	82.58997	3.5994268
(TP−0.22357)*(TP−0.22357)	−2730.923	11421.34	−0.24	0.8506	−147852.8	142390.93	13.396301
(AIR−50)*(AIR−50)	0.335861	0.593121	0.57	0.6720	7.872173	7.2004519	2.1323631
(DT−205)*(DT−205)	2.7284826	14.82802	0.18	0.8842	−185.6793	191.1363	2.1323631
(AT−215.714)*(AT−215.714)	−0.023813	0.622781	−0.04	0.9757	−7.936999	7.8893724	2.8096424

Effect Tests

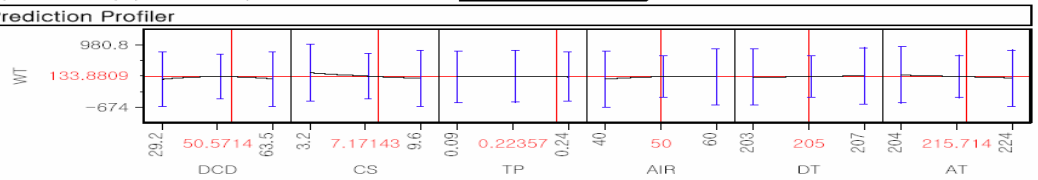
Source	Nparm	DF	Sum of Squares	F Ratio	Prob > F
DCD	1	1	993.4445	0.3513	0.6594
CS	1	1	4168.6213	1.4740	0.4386
TP	1	1	188.8732	0.0668	0.8390
AIR	1	1	1984.5000	0.7017	0.5561
DT	1	1	722.0000	0.2553	0.7022
AT	1	1	1850.0979	0.6542	0.5670
DCD*DCD	1	1	2640.3212	0.9336	0.5109
CS*CS	1	1	137.9205	0.0488	0.8616
TP*TP	1	1	161.6937	0.0572	0.8506
AIR*AIR	1	1	906.8604	0.3207	0.6720
DT*DT	1	1	95.7601	0.0339	0.8842
AT*AT	1	1	4.1350	0.0015	0.9757

Scaled Estimates

Continuous factors centered by mean, scaled by range/2

Term	Scaled Estimate	Std Error	t Ratio	Prob>|t|
Intercept	133.88089	43.15104	3.10	0.1985
DCD	−28.96009	48.86322	−0.59	0.6594
CS	−64.53431	53.15554	−1.21	0.4386
TP	−26.45007	102.3519	−0.26	0.8390
AIR	31.5	37.60444	0.84	0.5561
DT	19	37.60444	0.51	0.7022
AT	−36.81645	45.51962	−0.81	0.5670
(DCD−50.5714)*(DCD−50.5714)	−67.91079	70.2853	−0.97	0.5109
(CS−7.17143)*(CS−7.17143)	14.447364	65.42268	0.22	0.8616
(TP−0.22357)*(TP−0.22357)	−15.36144	64.24502	−0.24	0.8506
(AIR−50)*(AIR−50)	−33.58607	59.31207	−0.57	0.6720
(DT−205)*(DT−205)	10.91393	59.31207	0.18	0.8842
(AT−215.714)*(AT−215.714)	−2.381323	62.27812	−0.04	0.9757

Prediction Profiler

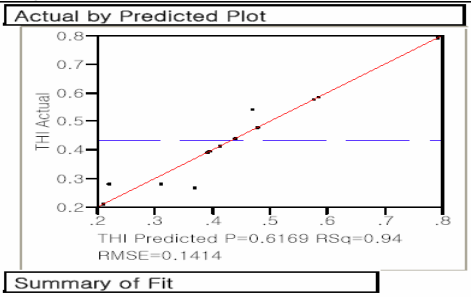


Thickness of TPU_{245}

58245-MD- Fit Least Squares

Response THI

Actual by Predicted Plot



Summary of Fit

RSquare	0.936056
RSquare Adj	0.168723
Root Mean Square Error	0.141439
Mean of Response	0.433571
Observations (or Sum Wgts)	14

Analysis of Variance

Source	DF	Sum of Squares	Mean Square	F Ratio
Model	12	0.29284633	0.024404	1.2199
Error	1	0.02000510	0.020005	Prob > F
C. Total	13	0.31285143		0.6169

Parameter Estimates

Term	Estimate	Std Error	t Ratio	Prob>|t|	Lower 95%	Upper 95%	VIF
Intercept	−4.609572	10.62042	−0.43	0.7393	−139.5549	130.33571	.
DCD	−0.003615	0.007578	−0.48	0.7166	−0.099898	0.0926682	2.5771554
CS	−0.050767	0.044179	−1.15	0.4559	−0.612113	0.5105791	2.1335818
TP	−0.316064	3.629533	−0.09	0.9447	−46.43366	45.801531	16.542653
AIR	0.00905	0.010001	0.90	0.5318	−0.118028	0.1361283	1
DT	0.03425	0.050006	0.68	0.6177	−0.601141	0.6696413	1
AT	−0.008122	0.012106	−0.67	0.6238	−0.161949	0.1457043	1.5155131
(DCD−50.5714)*(DCD−50.5714)	−0.00074	0.000636	−1.16	0.4518	−0.008815	0.0073356	4.6325059
(CS−7.17143)*(CS−7.17143)	0.0071997	0.016992	0.42	0.7449	−0.208704	0.2231036	3.5994268
(TP−0.22357)*(TP−0.22357)	−4.42931	30.37619	−0.15	0.9078	−390.3954	381.53676	13.396301
(AIR−50)*(AIR−50)	−0.001689	0.001577	−1.07	0.4782	−0.021733	0.0183544	2.1323631
(DT−205)*(DT−205)	0.0095201	0.039437	0.24	0.8492	−0.491569	0.5106095	2.1323631
(AT−215.714)*(AT−215.714)	0.0001248	0.001656	0.08	0.9521	−0.020921	0.0211707	2.8096424

Effect Tests

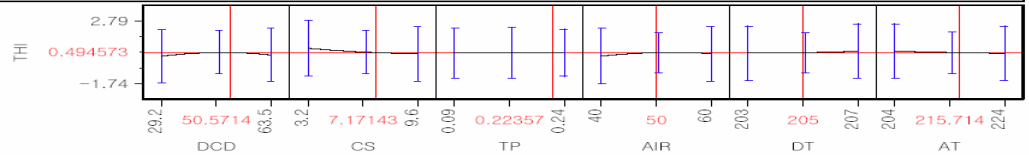
Source	Nparm	DF	Sum of Squares	F Ratio	Prob > F
DCD	1	1	0.00455264	0.2276	0.7166
CS	1	1	0.02641638	1.3205	0.4559
TP	1	1	0.00015170	0.0076	0.9447
AIR	1	1	0.01638050	0.8188	0.5318
DT	1	1	0.00938450	0.4691	0.6177
AT	1	1	0.00900432	0.4501	0.6238
DCD*DCD	1	1	0.02711349	1.3553	0.4518
CS*CS	1	1	0.00359150	0.1795	0.7449
TP*TP	1	1	0.00042535	0.0213	0.9078
AIR*AIR	1	1	0.02293944	1.1467	0.4782
DT*DT	1	1	0.00116580	0.0583	0.8492
AT*AT	1	1	0.00011356	0.0057	0.9521

Scaled Estimates

Continuous factors centered by mean, scaled by range/2

Term	Scaled Estimate	Std Error	t Ratio	Prob>|t|
Intercept	0.4945732	0.114765	4.31	0.1452
DCD	−0.061995	0.129957	−0.48	0.7166
CS	−0.162454	0.141372	−1.15	0.4559
TP	−0.023705	0.272215	−0.09	0.9447
AIR	0.0905	0.100013	0.90	0.5318
DT	0.0685	0.100013	0.68	0.6177
AT	−0.081221	0.121064	−0.67	0.6238
(DCD−50.5714)*(DCD−50.5714)	−0.217622	0.186931	−1.16	0.4518
(CS−7.17143)*(CS−7.17143)	0.0737245	0.173998	0.42	0.7449
(TP−0.22357)*(TP−0.22357)	−0.024915	0.170866	−0.15	0.9078
(AIR−50)*(AIR−50)	−0.16892	0.157746	−1.07	0.4782
(DT−205)*(DT−205)	0.0380803	0.157746	0.24	0.8492
(AT−215.714)*(AT−215.714)	0.0124795	0.165635	0.08	0.9521

Prediction Profiler

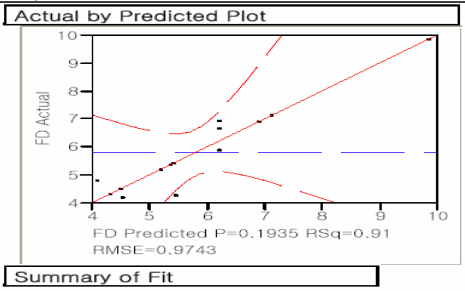


Fiber diameter of TPU_{245}

58245-MD- Fit Least Squares

Response FD

Actual by Predicted Plot



Summary of Fit

RSquare	0.910852
RSquare Adj	0.613693
Root Mean Square Error	0.974287
Mean of Response	5.797857
Observations (or Sum Wgts)	14

Analysis of Variance

Source	DF	Sum of Squares	Mean Square	F Ratio
Model	10	29.095933	2.90959	3.0652
Error	3	2.847703	0.94923	Prob > F
C. Total	13	31.943636		0.1935

Lack Of Fit

Source	DF	Sum of Squares	Mean Square	F Ratio
Lack Of Fit	1	2.2618363	2.26184	7.7213
Pure Error	2	0.5858667	0.29293	Prob > F
Total Error	3	2.8477030		0.1088
				Max RSq
				0.9817

Parameter Estimates

Term	Estimate	Std Error	t Ratio	Prob>|t|	Lower 95%	Upper 95%	VIF
Intercept	0.2804143	72.97848	0.00	0.9972	−231.9697	232.5305	.
DCD	−0.047493	0.050496	−0.94	0.4163	−0.208193	0.1132066	2.4118325
CS	−0.849455	0.285144	−2.98	0.0586	−1.75691	0.0580004	1.8731617
AIR	0.046	0.068892	0.67	0.5521	−0.173247	0.2652466	1
DT	0.0425	0.344462	0.12	0.9096	−1.053733	1.1387328	1
AT	0.0168549	0.080099	0.21	0.8468	−0.238055	0.2717652	1.3981368
(DCD−50.5714)*(DCD−50.5714)	−0.007159	0.003566	−2.01	0.1383	−0.018506	0.0041883	3.0727815
(CS−7.17143)*(CS−7.17143)	0.0094679	0.094611	0.10	0.9266	−0.291628	0.3105638	2.3517921
(AIR−50)*(AIR−50)	−0.012581	0.008709	−1.44	0.2443	−0.040296	0.0151351	1.3697413
(DT−205)*(DT−205)	−0.233265	0.217723	−1.07	0.3625	−0.926157	0.4596265	1.3697413
(AT−215.714)*(AT−215.714)	0.0081244	0.009185	0.88	0.4415	−0.021105	0.0373539	1.8206982

Effect Tests

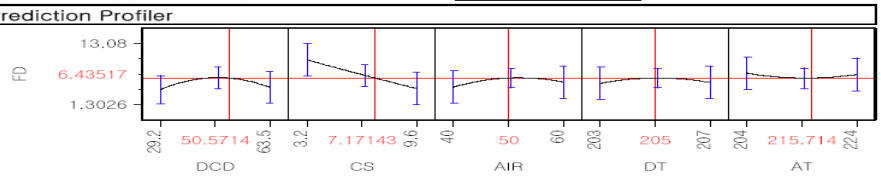
Source	Nparm	DF	Sum of Squares	F Ratio	Prob > F
DCD	1	1	0.8397030	0.8846	0.4163
CS	1	1	8.4241441	8.8747	0.0586
AIR	1	1	0.4232000	0.4458	0.5521
DT	1	1	0.0144500	0.0152	0.9096
AT	1	1	0.0420316	0.0443	0.8468
DCD*DCD	1	1	3.8266089	4.0313	0.1383
CS*CS	1	1	0.0095059	0.0100	0.9266
AIR*AIR	1	1	1.9808358	2.0868	0.2443
DT*DT	1	1	1.0895955	1.1479	0.3625
AT*AT	1	1	0.7427256	0.7824	0.4415

Scaled Estimates

Continuous factors centered by mean, scaled by range/2

Term	Scaled Estimate	Std Error	t Ratio	Prob>|t|
Intercept	6.4351699	0.596102	10.80	0.0017
DCD	−0.814506	0.866	−0.94	0.4163
CS	−2.718256	0.912461	−2.98	0.0586
AIR	0.46	0.688925	0.67	0.5521
DT	0.085	0.688925	0.12	0.9096
AT	0.1685494	0.800989	0.21	0.8468
(DCD−50.5714)*(DCD−50.5714)	−2.105597	1.048709	−2.01	0.1383
(CS−7.17143)*(CS−7.17143)	0.0969512	0.968821	0.10	0.9266
(AIR−50)*(AIR−50)	−1.258062	0.870892	−1.44	0.2443
(DT−205)*(DT−205)	−0.933062	0.870892	−1.07	0.3625
(AT−215.714)*(AT−215.714)	0.8124358	0.918463	0.88	0.4415

Prediction Profiler

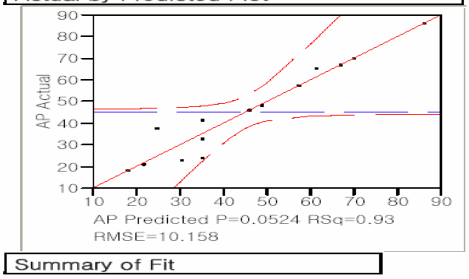


Air permeability of TPU_{245}

58245-MD- Fit Least Squares

Response AP

Actual by Predicted Plot



Summary of Fit

RSquare	0.929224
RSquare Adj	0.769979
Root Mean Square Error	10.15755
Mean of Response	45.3
Observations (or Sum Wgts)	14

Analysis of Variance

Source	DF	Sum of Squares	Mean Square	F Ratio
Model	9	5418.4364	602.048	5.8352
Error	4	412.7036	103.176	Prob > F
C. Total	13	5831.1400		0.0524

Lack Of Fit

Source	DF	Sum of Squares	Mean Square	F Ratio
Lack Of Fit	2	261.31696	130.658	1.7262
Pure Error	2	151.38667	75.693	Prob > F
Total Error	4	412.70362		0.3668
				Max RSq
				0.9740

Parameter Estimates

Term	Estimate	Std Error	t Ratio	Prob>|t|	Lower 95%	Upper 95%	VIF
Intercept	526.04531	759.928	0.69	0.5269	-1583.853	2635.9437	.
DCD	1.4479677	0.521891	2.77	0.0501	-0.001033	2.8969686	2.3702472
CS	9.9389731	2.920363	3.40	0.0272	1.8307463	18.0472	1.8076557
AIR	-1.365	0.718248	-1.90	0.1302	-3.359175	0.6291749	1
DT	-4.05	3.591238	-1.13	0.3225	-14.02087	5.9208743	1
AT	1.1957353	0.826217	1.45	0.2214	-1.09821	3.4896811	1.368612
(DCD-50.5714)*(DCD-50.5714)	0.0647073	0.034719	1.86	0.1358	-0.031688	0.1611026	2.6804487
(CS-7.17143)*(CS-7.17143)	1.4997974	0.918216	1.63	0.1777	-1.049579	4.0491735	2.0379623
(DT-205)*(DT-205)	10.720147	2.10496	5.09	0.0070	4.875841	16.564454	1.1779115
(AT-215.714)*(AT-215.714)	0.1825061	0.088974	2.05	0.1095	-0.064525	0.4295375	1.5719394

Effect Tests

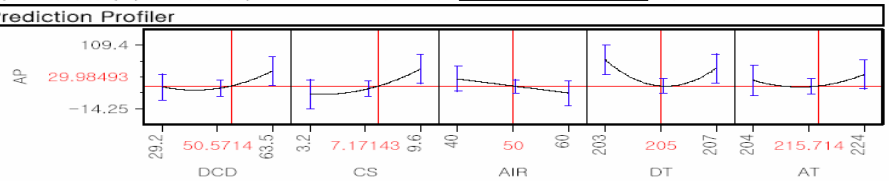
Source	Nparm	DF	Sum of Squares	F Ratio	Prob > F
DCD	1	1	794.2128	7.6977	0.0501
CS	1	1	1195.0545	11.5827	0.0272
AIR	1	1	372.6450	3.6117	0.1302
DT	1	1	131.2200	1.2718	0.3225
AT	1	1	216.1028	2.0945	0.2214
DCD*DCD	1	1	358.3854	3.4735	0.1358
CS*CS	1	1	275.2668	2.6679	0.1777
DT*DT	1	1	2676.0365	25.9366	0.0070
AT*AT	1	1	434.1175	4.2075	0.1095

Scaled Estimates

Continuous factors centered by mean, scaled by range/2

Term	Scaled Estimate	Std Error	t Ratio	Prob>|t|
Intercept	29.984934	4.978281	6.02	0.0038
DCD	24.832646	8.950426	2.77	0.0501
CS	31.804714	9.345161	3.40	0.0272
AIR	-13.65	7.182475	-1.90	0.1302
DT	-8.1	7.182475	-1.13	0.3225
AT	11.957353	8.262169	1.45	0.2214
(DCD-50.5714)*(DCD-50.5714)	19.031865	10.21164	1.86	0.1358
(CS-7.17143)*(CS-7.17143)	15.357925	9.402531	1.63	0.1777
(DT-205)*(DT-205)	42.880589	8.419841	5.09	0.0070
(AT-215.714)*(AT-215.714)	18.250614	8.897397	2.05	0.1095

Prediction Profiler

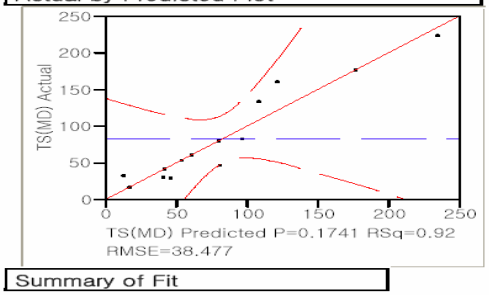


Tear strength of TPU_{245}

58245-MD- Fit Least Squares

Response TS(MD)

Actual by Predicted Plot



Summary of Fit

RSquare	0.917861
RSquare Adj	0.644065
Root Mean Square Error	38.47677
Mean of Response	82.85714
Observations (or Sum Wgts)	14

Analysis of Variance

Source	DF	Sum of Squares	Mean Square	F Ratio
Model	10	49630.329	4963.03	3.3524
Error	3	4441.385	1480.46	Prob > F
C. Total	13	54071.714		0.1741

Parameter Estimates

Term	Estimate	Std Error	t Ratio	Prob>|t|	VIF
Intercept	3415.0122	2854.936	1.20	0.3175	.
DCD	−2.155755	1.992948	−1.08	0.3586	2.4088377
CS	−32.73079	11.24679	−2.91	0.0620	1.8684443
TP	167.2213	280.1958	0.60	0.5927	1.3322027
AIR	0.6	2.720718	0.22	0.8396	1
DT	−4.75	13.60359	−0.35	0.7500	1
(DCD−50.5714)*(DCD−50.5714)	−0.352931	0.140163	−2.52	0.0863	3.0445273
(CS−7.17143)*(CS−7.17143)	−5.010695	3.718423	−1.35	0.2705	2.3291914
(AIR−50)*(AIR−50)	−0.737509	0.342196	−2.16	0.1201	1.3559265
(DT−205)*(DT−205)	−12.81271	8.554903	−1.50	0.2311	1.3559265
AT	−9.427868	2.697574	−3.49	0.0396	1.0167638

Effect Tests

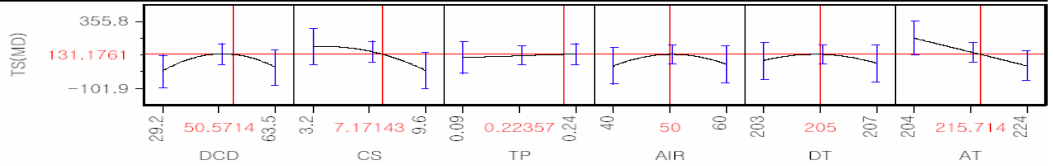
Source	Nparm	DF	Sum of Squares	F Ratio	Prob > F
DCD	1	1	1732.225	1.1701	0.3586
CS	1	1	12538.718	8.4695	0.0620
TP	1	1	527.299	0.3562	0.5927
AIR	1	1	72.000	0.0486	0.8396
DT	1	1	180.500	0.1219	0.7500
DCD*DCD	1	1	9386.677	6.3404	0.0863
CS*CS	1	1	2688.286	1.8158	0.2705
AIR*AIR	1	1	6876.717	4.6450	0.1201
DT*DT	1	1	3320.850	2.2431	0.2311
AT	1	1	18083.290	12.2146	0.0396

Scaled Estimates

Continuous factors centered by mean, scaled by range/2

Term	Scaled Estimate	Std Error	t Ratio	Prob>|t|
Intercept	131.17614	20.58945	6.37	0.0078
DCD	−36.9712	34.17906	−1.08	0.3586
CS	−104.7385	35.98972	−2.91	0.0620
TP	12.541598	21.01468	0.60	0.5927
AIR	6	27.20718	0.22	0.8396
DT	−9.5	27.20718	−0.35	0.7500
(DCD−50.5714)*(DCD−50.5714)	−103.805	41.22503	−2.52	0.0863
(CS−7.17143)*(CS−7.17143)	−51.30951	38.07665	−1.35	0.2705
(AIR−50)*(AIR−50)	−73.75085	34.21961	−2.16	0.1201
(DT−205)*(DT−205)	−51.25085	34.21961	−1.50	0.2311
AT	−94.27868	26.97574	−3.49	0.0396

Prediction Profiler

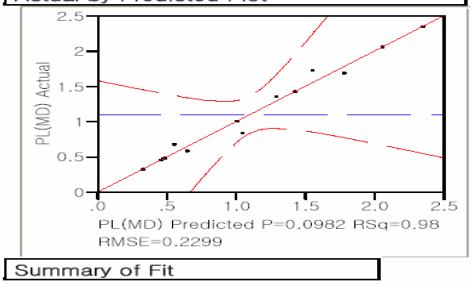


Peak force of TPU_{245}

58245-MD- Fit Least Squares

Response PL(MD)

Actual by Predicted Plot



Summary of Fit

RSquare	0.981377
RSquare Adj	0.878951
Root Mean Square Error	0.229897
Mean of Response	1.097143
Observations (or Sum Wgts)	14

Analysis of Variance

Source	DF	Sum of Squares	Mean Square	F Ratio
Model	11	5.5703805	0.506398	9.5813
Error	2	0.1057052	0.052853	Prob > F
C. Total	13	5.6760857		0.0982

Parameter Estimates

Term	Estimate	Std Error	t Ratio	Prob>|t|	Lower 95%	Upper 95%	VIF
Intercept	29.486498	17.2516	1.71	0.2295	-44.74114	103.71414	.
DCD	-0.019638	0.012243	-1.60	0.2499	-0.072313	0.0330377	2.5461939
CS	-0.312973	0.070983	-4.41	0.0478	-0.61839	-0.007557	2.0848106
TP	-3.254079	2.009995	-1.62	0.2469	-11.90239	5.3942322	1.920295
AIR	0.021	0.016256	1.29	0.3256	-0.048945	0.0909447	1
DT	-0.0325	0.081281	-0.40	0.7279	-0.382223	0.3172233	1
AT	-0.085537	0.019535	-4.38	0.0484	-0.169588	-0.001486	1.493531
(DCD-50.5714)*(DCD-50.5714)	-0.002653	0.001	-2.65	0.1175	-0.006955	0.0016493	4.3404019
(CS-7.17143)*(CS-7.17143)	-0.014485	0.026707	-0.54	0.6419	-0.129398	0.1004281	3.3657707
(AIR-50)*(AIR-50)	-0.00075	0.002477	-0.30	0.7905	-0.011407	0.0099059	1.9895398
(DT-205)*(DT-205)	-0.225008	0.061917	-3.63	0.0681	-0.491414	0.0413984	1.9895398
(AT-215.714)*(AT-215.714)	-0.001907	0.002602	-0.73	0.5400	-0.013102	0.0092889	2.6244336

Effect Tests

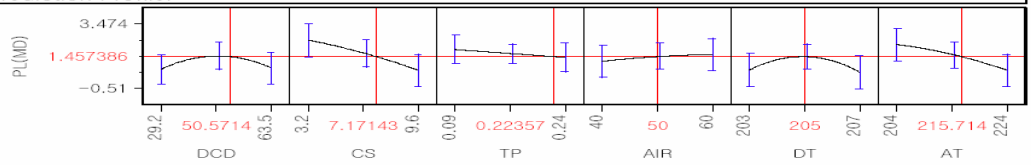
Source	Nparm	DF	Sum of Squares	F Ratio	Prob > F
DCD	1	1	0.1359907	2.5730	0.2499
CS	1	1	1.0274679	19.4402	0.0478
TP	1	1	0.1385264	2.6210	0.2469
AIR	1	1	0.0882000	1.6688	0.3256
DT	1	1	0.0084500	0.1599	0.7279
AT	1	1	1.0133570	19.1733	0.0484
DCD*DCD	1	1	0.3720691	7.0397	0.1175
CS*CS	1	1	0.0155466	0.2942	0.6419
AIR*AIR	1	1	0.0048508	0.0918	0.7905
DT*DT	1	1	0.6979839	13.2062	0.0681
AT*AT	1	1	0.0283765	0.5369	0.5400

Scaled Estimates

Continuous factors centered by mean, scaled by range/2

Term	Scaled Estimate	Std Error	t Ratio	Prob>|t|
Intercept	1.4573856	0.18381	7.93	0.0155
DCD	-0.336789	0.20996	-1.60	0.2499
CS	-1.001514	0.227147	-4.41	0.0478
TP	-0.244056	0.15075	-1.62	0.2469
AIR	0.21	0.162562	1.29	0.3256
DT	-0.065	0.162562	-0.40	0.7279
AT	-0.855368	0.195346	-4.38	0.0484
(DCD-50.5714)*(DCD-50.5714)	-0.780332	0.294104	-2.65	0.1175
(CS-7.17143)*(CS-7.17143)	-0.148326	0.273485	-0.54	0.6419
(AIR-50)*(AIR-50)	-0.075031	0.247667	-0.30	0.7905
(DT-205)*(DT-205)	-0.900031	0.247667	-3.63	0.0681
(AT-215.714)*(AT-215.714)	-0.190657	0.2602	-0.73	0.5400

Prediction Profiler

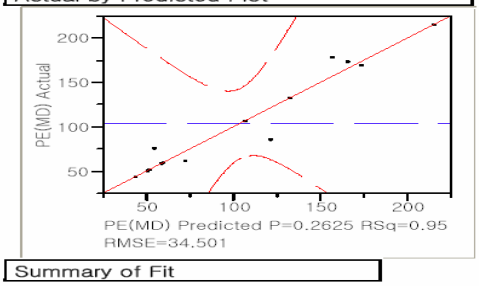


Peak elongation of TPU_{245}

58245-MD- Fit Least Squares

Response PE(MD)

Actual by Predicted Plot



Summary of Fit

RSquare	0.94615
RSquare Adj	0.649977
Root Mean Square Error	34.501
Mean of Response	103.9286
Observations (or Sum Wgts)	14

Analysis of Variance

Source	DF	Sum of Squares	Mean Square	F Ratio
Model	11	41828.290	3802.57	3.1946
Error	2	2380.638	1190.32	Prob > F
C. Total	13	44208.929		0.2625

Parameter Estimates

Term	Estimate	Std Error	t Ratio	Prob>|t|	Lower 95%	Upper 95%	VIF
Intercept	2809.1174	2588.975	1.09	0.3913	-8330.342	13948.577	.
DCD	-2.491425	1.837262	-1.36	0.3079	-10.39652	5.4136747	2.5461939
CS	-27.23034	10.65258	-2.56	0.1250	-73.06469	18.604009	2.0848106
TP	-111.1766	301.6432	-0.37	0.7478	-1409.042	1186.6892	1.920295
AIR	2.75	2.439589	1.13	0.3767	-7.746705	13.246705	1
DT	-2.25	12.19795	-0.18	0.8707	-54.73352	50.233525	1
AT	-9.122204	2.931592	-3.11	0.0896	-21.73583	3.4914187	1.493531
(DCD-50.5714)*(DCD-50.5714)	-0.356342	0.150062	-2.37	0.1408	-1.002007	0.2893224	4.3404019
(CS-7.17143)*(CS-7.17143)	-8.635985	4.008035	-2.15	0.1640	-25.88117	8.6091994	3.3657707
(AIR-50)*(AIR-50)	-0.779217	0.371678	-2.10	0.1710	-2.378417	0.8199825	1.9895398
(DT-205)*(DT-205)	-25.48043	9.29194	-2.74	0.1112	-65.46042	14.499564	1.9895398
(AT-215.714)*(AT-215.714)	-0.37106	0.390486	-0.95	0.4423	-2.051185	1.3090658	2.6244336

Effect Tests

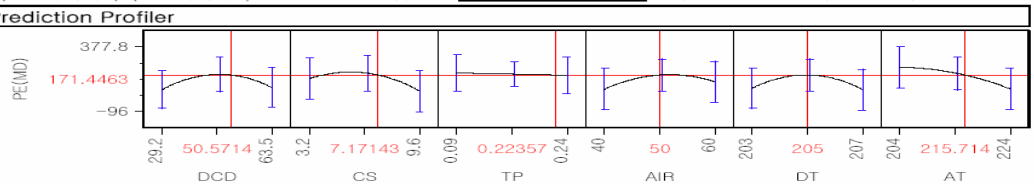
Source	Nparm	DF	Sum of Squares	F Ratio	Prob > F
DCD	1	1	2188.854	1.8389	0.3079
CS	1	1	7777.858	6.5343	0.1250
TP	1	1	161.698	0.1358	0.7478
AIR	1	1	1512.500	1.2707	0.3767
DT	1	1	40.500	0.0340	0.8707
AT	1	1	11525.396	9.6826	0.0896
DCD*DCD	1	1	6712.076	5.6389	0.1408
CS*CS	1	1	5526.168	4.6426	0.1640
AIR*AIR	1	1	5231.757	4.3953	0.1710
DT*DT	1	1	8950.845	7.5197	0.1112
AT*AT	1	1	1074.830	0.9030	0.4423

Scaled Estimates

Continuous factors centered by mean, scaled by range/2

Term	Scaled Estimate	Std Error	t Ratio	Prob>|t|
Intercept	171.44632	27.58462	6.22	0.0249
DCD	-42.72793	31.50904	-1.36	0.3079
CS	-87.13709	34.08825	-2.56	0.1250
TP	-8.338249	22.62324	-0.37	0.7478
AIR	27.5	24.39589	1.13	0.3767
DT	-4.5	24.39589	-0.18	0.8707
AT	-91.22204	29.31592	-3.11	0.0896
(DCD-50.5714)*(DCD-50.5714)	-104.8083	44.13662	-2.37	0.1408
(CS-7.17143)*(CS-7.17143)	-88.43249	41.04228	-2.15	0.1640
(AIR-50)*(AIR-50)	-77.92172	37.16776	-2.10	0.1710
(DT-205)*(DT-205)	-101.9217	37.16776	-2.74	0.1112
(AT-215.714)*(AT-215.714)	-37.10595	39.04859	-0.95	0.4423

Prediction Profiler

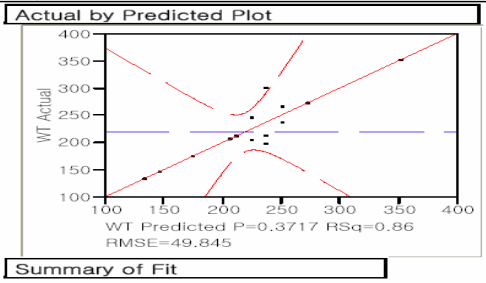


Basis weight of TPU_{280}

58280-MD- Fit Least Squares

Response WT

Actual by Predicted Plot



Summary of Fit

RSquare	0.859397
RSquare Adj	0.343851
Root Mean Square Error	49.84532
Mean of Response	219
Observations (or Sum Wgts)	15

Analysis of Variance

Source	DF	Sum of Squares	Mean Square	F Ratio
Model	11	45558.333	4141.67	1.6670
Error	3	7453.667	2484.56	Prob > F
C. Total	14	53012.000		0.3717

Lack Of Fit

Source	DF	Sum of Squares	Mean Square	F Ratio
Lack Of Fit	-1	-0.000	.	.
Pure Error	4	7453.667	1863.42	Prob > F
Total Error	3	7453.667		.
				Max RSq
				0.8594

Parameter Estimates

Term	Estimate	Std Error	t Ratio	Prob>|t|	VIF
Intercept	-59588.75	5.7938e8	-0.00	0.9999	.
DCD	-0.594625	1.149362	-0.52	0.6406	1.0117353
CS	3996.3981	1.207e+8	0.00	1.0000	0
TP	-818.6667	1787.032	-0.46	0.6780	14.138667
AIR	-4.9	3.524596	-1.39	0.2586	1
DT	215.4037	90.06661	2.39	0.0966	168.90767
AT	-23.88148	15.10847	-1.58	0.2121	17.909279
(DCD-52.4867)*(DCD-52.4867)	0.001453	0.080238	0.02	0.9867	1.7256593
(TP-0.15)*(TP-0.15)	7066.6667	23022.57	0.31	0.7790	12.849778
(AIR-40)*(AIR-40)	-0.133333	0.455023	-0.29	0.7886	1.4444444
(AT-232.733)*(AT-232.733)	-6.888889	3.089844	-2.23	0.1120	81.534687
(DT-215.867)*(DT-215.867)	34.944444	15.25606	2.29	0.1059	121.59766

Effect Tests

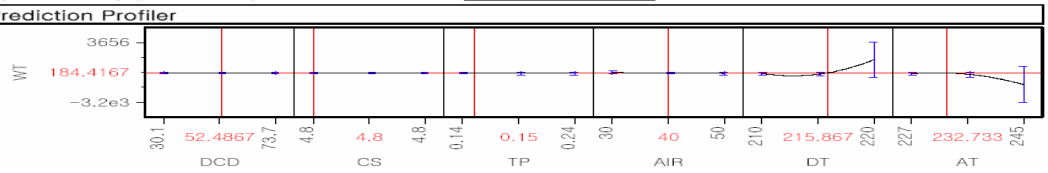
Source	Nparm	DF	Sum of Squares	F Ratio	Prob > F
DCD	1	1	665.000	0.2677	0.6406
CS	1	1	0.000	0.0000	1.0000
TP	1	1	521.433	0.2099	0.6780
AIR	1	1	4802.000	1.9327	0.2586
DT	1	1	14211.091	5.7198	0.0966
AT	1	1	6207.697	2.4985	0.2121
DCD*DCD	1	1	0.815	0.0003	0.9867
TP*TP	1	1	234.083	0.0942	0.7790
AIR*AIR	1	1	213.333	0.0859	0.7886
AT*AT	1	1	12350.201	4.9708	0.1120
DT*DT	1	1	13035.276	5.2465	0.1059

Scaled Estimates

Continuous factors centered by mean, scaled by range/2

Term	Scaled Estimate	Std Error	t Ratio	Prob>|t|
Intercept	184.41666	26.55203	6.95	0.0061
DCD	-12.96283	25.0561	-0.52	0.6406
CS	0	0	0.00	1.0000
TP	-40.93333	89.35158	-0.46	0.6780
AIR	-49	35.24596	-1.39	0.2586
DT	1077.0185	450.333	2.39	0.0966
AT	-214.9333	135.9762	-1.58	0.2121
(DCD-52.4867)*(DCD-52.4867)	0.6905324	38.13233	0.02	0.9867
(TP-0.15)*(TP-0.15)	17.666667	57.55641	0.31	0.7790
(AIR-40)*(AIR-40)	-13.33333	45.50234	-0.29	0.7886
(AT-232.733)*(AT-232.733)	-558	250.2773	-2.23	0.1120
(DT-215.867)*(DT-215.867)	873.61111	381.4015	2.29	0.1059

Prediction Profiler

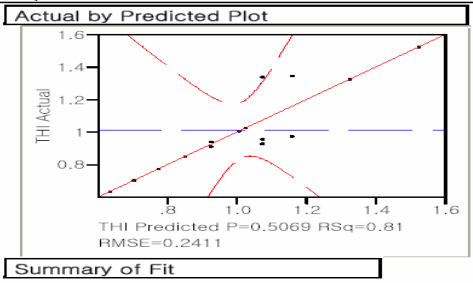


Thickness of TPU_{280}

58280−MD− Fit Least Squares

Response THI

Actual by Predicted Plot



Summary of Fit

RSquare	0.81106
RSquare Adj	0.118278
Root Mean Square Error	0.241118
Mean of Response	1.0128
Observations (or Sum Wgts)	15

Analysis of Variance

Source	DF	Sum of Squares	Mean Square	F Ratio
Model	11	0.74870073	0.068064	1.1707
Error	3	0.17441367	0.058138	Prob > F
C. Total	14	0.92311440		0.5069

Lack Of Fit

Source	DF	Sum of Squares	Mean Square	F Ratio
Lack Of Fit	−1	−0.0000000	.	.
Pure Error	4	0.1744137	0.043603	Prob > F
Total Error	3	0.1744137		.
				Max RSq
				0.8111

Parameter Estimates

Term	Estimate	Std Error	t Ratio	Prob>|t|	Lower 95%	Upper 95%	VIF
Intercept	−241.1424	2802658	−0.00	0.9999	−8.9196e6	8919068.2	.
DCD	0.0053005	0.00556	0.95	0.4107	−0.012393	0.0229944	1.0117353
CS	16.49597	583887.1	0.00	1.0000	−1858173	1858205.9	0
TP	−1.879333	8.644453	−0.22	0.8418	−29.38984	25.631174	14.138667
AIR	−0.02375	0.01705	−1.39	0.2579	−0.078009	0.0305095	1
DT	0.8708827	0.435681	2.00	0.1395	−0.51565	2.2574156	168.90767
AT	−0.104026	0.073085	−1.42	0.2498	−0.336613	0.1285619	17.909279
(DCD−52.4867)*(DCD−52.4867)	−0.000057	0.000388	−0.15	0.8933	−0.001292	0.0011786	1.7256593
(TP−0.15)*(TP−0.15)	17.533333	111.3676	0.16	0.8849	−336.8882	371.95484	12.849778
(AIR−40)*(AIR−40)	0.0001483	0.002201	0.07	0.9505	−0.006857	0.0071532	1.4444444
(DT−215.867)*(DT−215.867)	0.143216	0.073799	1.94	0.1476	−0.091644	0.3780758	121.59766
(AT−232.733)*(AT−232.733)	−0.027519	0.014947	−1.84	0.1628	−0.075086	0.0200472	81.534687

Effect Tests

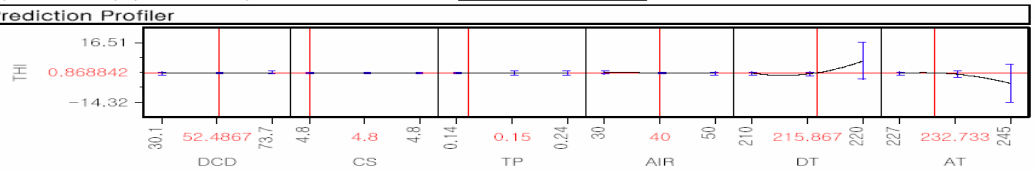
Source	Nparm	DF	Sum of Squares	F Ratio	Prob > F
DCD	1	1	0.05284139	0.9089	0.4107
CS	1	1	0.00000000	0.0000	1.0000
TP	1	1	0.00274784	0.0473	0.8418
AIR	1	1	0.11281250	1.9404	0.2579
DT	1	1	0.23229529	3.9956	0.1395
AT	1	1	0.11778490	2.0260	0.2498
DCD*DCD	1	1	0.00123728	0.0213	0.8933
TP*TP	1	1	0.00144102	0.0248	0.8849
AIR*AIR	1	1	0.00026403	0.0045	0.9505
DT*DT	1	1	0.21895097	3.7661	0.1476
AT*AT	1	1	0.19708564	3.3900	0.1628

Scaled Estimates

Continuous factors centered by mean, scaled by range/2

Term	Scaled Estimate	Std Error	t Ratio	Prob>|t|
Intercept	0.8688418	0.128441	6.76	0.0066
DCD	0.1155517	0.121205	0.95	0.4107
CS	0	0	0.00	1.0000
TP	−0.093967	0.432223	−0.22	0.8418
AIR	−0.2375	0.170496	−1.39	0.2579
DT	4.3544134	2.178407	2.00	0.1395
AT	−0.936232	0.657761	−1.42	0.2498
(DCD−52.4867)*(DCD−52.4867)	−0.026909	0.184458	−0.15	0.8933
(TP−0.15)*(TP−0.15)	0.0438333	0.278419	0.16	0.8849
(AIR−40)*(AIR−40)	0.0148333	0.22011	0.07	0.9505
(DT−215.867)*(DT−215.867)	3.5803993	1.844963	1.94	0.1476
(AT−232.733)*(AT−232.733)	−2.229075	1.210673	−1.84	0.1628

Prediction Profiler

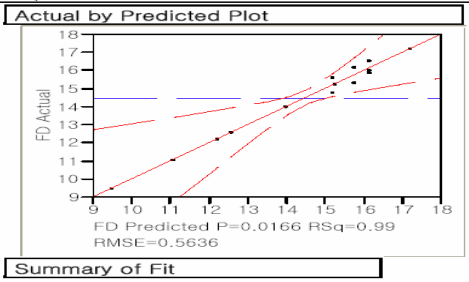


Fiber diameter of TPU_{280}

58280-MD- Fit Least Squares

Response FD

Actual by Predicted Plot



Summary of Fit

RSquare	0.985945
RSquare Adj	0.934412
Root Mean Square Error	0.56358
Mean of Response	14.46
Observations (or Sum Wgts)	15

Analysis of Variance

Source	DF	Sum of Squares	Mean Square	F Ratio
Model	11	66.844733	6.07679	19.1321
Error	3	0.952867	0.31762	Prob > F
C. Total	14	67.797600		0.0166

Lack Of Fit

Source	DF	Sum of Squares	Mean Square	F Ratio
Lack Of Fit	-1	-0.0000000	.	.
Pure Error	4	0.9528667	0.238217	Prob > F
Total Error	3	0.9528666		.
				Max RSq
				0.9859

Parameter Estimates

Term	Estimate	Std Error	t Ratio	Prob>|t|	Lower 95%	Upper 95%	VIF
Intercept	-2646.319	6550824	-0.00	0.9997	-20850293	20845000	.
DCD	0.0109873	0.012995	0.85	0.4599	-0.03037	0.0523443	1.0117353
CS	211.9849	1364755	0.00	0.9999	-4.343e+6	4343471.7	0
TP	-90.42667	20.20521	-4.48	0.0208	-154.7287	-26.12468	14.138667
AIR	6.291e-14	0.039851	0.00	1.0000	-0.126824	0.126824	1
DT	9.5113509	1.018345	9.34	0.0026	6.270523	12.752179	168.90767
AT	-1.712854	0.170825	-10.03	0.0021	-2.256495	-1.169212	17.909279
(DCD-52.4867)*(DCD-52.4867)	-0.001387	0.000907	-1.53	0.2238	-0.004274	0.0015002	1.7256593
(TP-0.15)*(TP-0.15)	638.66667	260.3064	2.45	0.0914	-189.7444	1467.0777	12.849778
(AIR-40)*(AIR-40)	-0.008933	0.005145	-1.74	0.1809	-0.025306	0.0074396	1.4444444
(DT-215.867)*(DT-215.867)	1.6896736	0.172494	9.80	0.0023	1.1407214	2.2386258	121.59766
(AT-232.733)*(AT-232.733)	-0.331472	0.034936	-9.49	0.0025	-0.442653	-0.220292	81.534687

Effect Tests

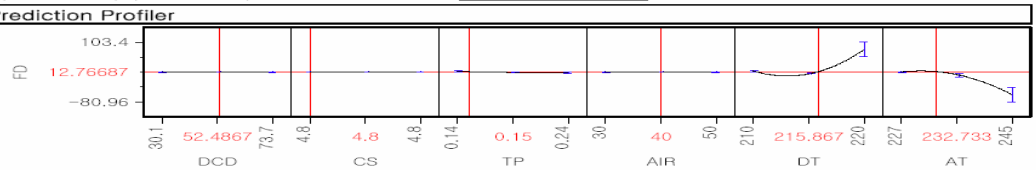
Source	Nparm	DF	Sum of Squares	F Ratio	Prob > F
DCD	1	1	0.227049	0.7148	0.4599
CS	1	1	0.000000	0.0000	0.9999
TP	1	1	6.361760	20.0293	0.0208
AIR	1	1	0.000000	0.0000	1.0000
DT	1	1	27.708021	87.2358	0.0026
AT	1	1	31.933648	100.5397	0.0021
DCD*DCD	1	1	0.742341	2.3372	0.2238
TP*TP	1	1	1.912008	6.0198	0.0914
AIR*AIR	1	1	0.957653	3.0151	0.1809
DT*DT	1	1	30.476816	95.9530	0.0023
AT*AT	1	1	28.593673	90.0242	0.0025

Scaled Estimates

Continuous factors centered by mean, scaled by range/2

Term	Scaled Estimate	Std Error	t Ratio	Prob>|t|
Intercept	12.766866	0.300212	42.53	<.0001
DCD	0.2395239	0.283299	0.85	0.4599
CS	0	0	0.00	1.0000
TP	-4.521333	1.01026	-4.48	0.0208
AIR	6.291e-13	0.398511	0.00	1.0000
DT	47.556755	5.091724	9.34	0.0026
AT	-15.41568	1.537425	-10.03	0.0021
(DCD-52.4867)*(DCD-52.4867)	-0.659129	0.431146	-1.53	0.2238
(TP-0.15)*(TP-0.15)	1.5966667	0.650766	2.45	0.0914
(AIR-40)*(AIR-40)	-0.893333	0.514476	-1.74	0.1809
(DT-215.867)*(DT-215.867)	42.24184	4.312345	9.80	0.0023
(AT-232.733)*(AT-232.733)	-26.84925	2.82978	-9.49	0.0025

Prediction Profiler

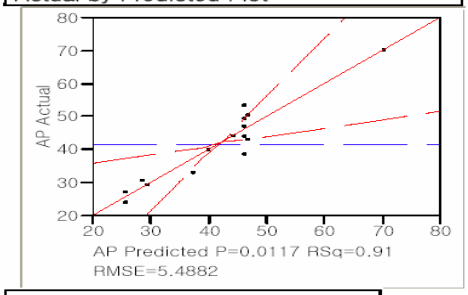


Air permeability of TPU_{280}

58280-MD- Fit Least Squares

Response AP

Actual by Predicted Plot



Summary of Fit

RSquare	0.91039
RSquare Adj	0.79091
Root Mean Square Error	5.488198
Mean of Response	41.5
Observations (or Sum Wgts)	15

Analysis of Variance

Source	DF	Sum of Squares	Mean Square	F Ratio
Model	8	1836.0381	229.505	7.6196
Error	6	180.7219	30.120	Prob > F
C. Total	14	2016.7600		0.0117

Parameter Estimates

Term	Estimate	Std Error	t Ratio	Prob>|t|	Lower 95%	Upper 95%	VIF
Intercept	1187.141	63792601	0.00	1.0000	-1.5609e8	156096058	.
DCD	0.4615045	0.126447	3.65	0.0107	0.1520987	0.7709103	1.0100952
CS	-54.10517	13290125	-0.00	1.0000	-32519819	32519711	0
TP	-175.8462	56.95373	-3.09	0.0215	-315.2069	-36.48541	1.1846154
AIR	0.21	0.388074	0.54	0.6079	-0.739583	1.1595834	1
DT	-4.118444	0.895171	-4.60	0.0037	-6.308848	-1.928041	1.3763302
(DCD-52.4867)*(DCD-52.4867)	-0.020103	0.007694	-2.61	0.0400	-0.038928	-0.001277	1.3087076
(AIR-40)*(AIR-40)	-0.040538	0.045665	-0.89	0.4089	-0.152276	0.0711987	1.2
(DT-215.867)*(DT-215.867)	-0.01641	0.192998	-0.09	0.9350	-0.488659	0.4558384	1.6052191

Effect Tests

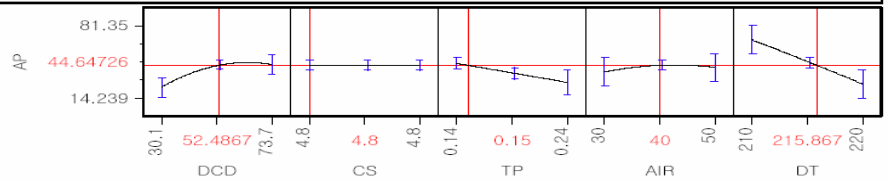
Source	Nparm	DF	Sum of Squares	F Ratio	Prob > F
DCD	1	1	401.22802	13.3208	0.0107
CS	1	1	0.00000	0.0000	1.0000
TP	1	1	287.13165	9.5328	0.0215
AIR	1	1	8.82000	0.2928	0.6079
DT	1	1	637.54999	21.1668	0.0037
DCD*DCD	1	1	205.64216	6.8274	0.0400
AIR*AIR	1	1	23.73752	0.7881	0.4089
DT*DT	1	1	0.21776	0.0072	0.9350

Scaled Estimates

Continuous factors centered by mean, scaled by range/2

Term	Scaled Estimate	Std Error	t Ratio	Prob>|t|
Intercept	44.647263	1.525965	29.26	<.0001
DCD	10.060798	2.756555	3.65	0.0107
CS	0	0	0.00	1.0000
TP	-8.792308	2.847686	-3.09	0.0215
AIR	2.1	3.880742	0.54	0.6079
DT	-20.59222	4.475854	-4.60	0.0037
(DCD-52.4867)*(DCD-52.4867)	-9.553639	3.656306	-2.61	0.0400
(AIR-40)*(AIR-40)	-4.053846	4.566457	-0.89	0.4089
(DT-215.867)*(DT-215.867)	-0.410256	4.824945	-0.09	0.9350

Prediction Profiler

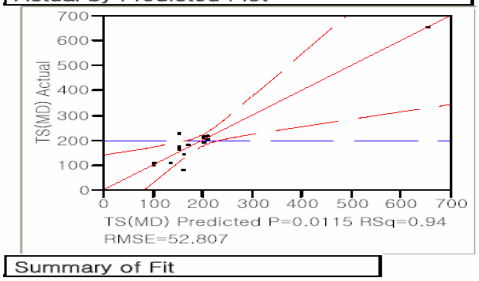


Tear strength of TPU_{280}

58280-MD- Fit Least Squares

Response TS(MD)

Actual by Predicted Plot



Summary of Fit

RSquare	0.944997
RSquare Adj	0.845993
Root Mean Square Error	52.80721
Mean of Response	196.6667
Observations (or Sum Wgts)	15

Analysis of Variance

Source	DF	Sum of Squares	Mean Square	F Ratio
Model	9	239554.33	26617.1	9.5450
Error	5	13943.01	2788.6	Prob > F
C. Total	14	253497.33		0.0115

Lack Of Fit

Source	DF	Sum of Squares	Mean Square	F Ratio
Lack Of Fit	1	11139.840	11139.8	15.8961
Pure Error	4	2803.167	700.8	Prob > F
Total Error	5	13943.007		0.0163
				Max RSq
				0.9889

Parameter Estimates

Term	Estimate	Std Error	t Ratio	Prob>|t|	Lower 95%	Upper 95%	VIF
Intercept	-1856.197	6.1381e8	-0.00	1.0000	-1.5778e9	1.57785e9	.
DCD	-0.017858	1.216917	-0.01	0.9889	-3.146043	3.1103269	1.010502
CS	137.42727	1.2788e8	0.00	1.0000	-3.2872e8	328718471	0
TP	181.37772	560.6772	0.32	0.7594	-1259.889	1622.6444	1.2400297
AIR	-27.6	3.734034	-7.39	0.0007	-37.19864	-18.00136	1
DT	8.337408	9.865008	0.85	0.4366	-17.0214	33.696218	1.8054227
AT	2.7018678	6.645943	0.41	0.7012	-14.38207	19.785809	3.0875426
(DCD-52.4867)*(DCD-52.4867)	0.1118392	0.076897	1.45	0.2056	-0.085831	0.3095097	1.4121395
(AT-232.733)*(AT-232.733)	-0.134958	0.733712	-0.18	0.8613	-2.021023	1.751108	4.0962116
(AIR-40)*(AIR-40)	2.2444814	0.450347	4.98	0.0042	1.0868271	3.4021358	1.2606386

Effect Tests

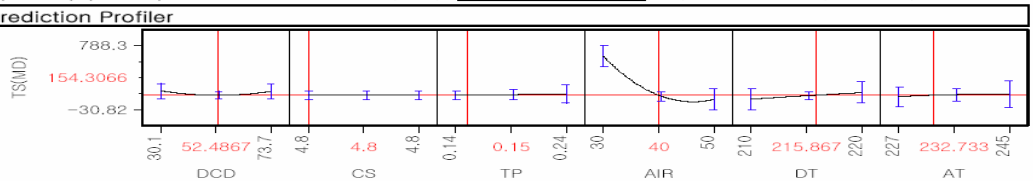
Source	Nparm	DF	Sum of Squares	F Ratio	Prob > F
DCD	1	1	0.60	0.0002	0.9889
CS	1	1	0.00	0.0000	1.0000
TP	1	1	291.83	0.1047	0.7594
AIR	1	1	152352.00	54.6338	0.0007
DT	1	1	1991.84	0.7143	0.4366
AT	1	1	460.89	0.1653	0.7012
DCD*DCD	1	1	5898.66	2.1153	0.2056
AT*AT	1	1	94.35	0.0338	0.8613
AIR*AIR	1	1	69266.55	24.8392	0.0042

Scaled Estimates

Continuous factors centered by mean, scaled by range/2

Term	Scaled Estimate	Std Error	t Ratio	Prob>|t|
Intercept	154.30665	22.45798	6.87	0.0010
DCD	-0.389303	26.52879	-0.01	0.9889
CS	0	0	0.00	1.0000
TP	9.0688862	28.03386	0.32	0.7594
AIR	-276	37.34034	-7.39	0.0007
DT	41.68704	49.32504	0.85	0.4366
AT	24.316811	59.81349	0.41	0.7012
(DCD-52.4867)*(DCD-52.4867)	53.150455	36.54462	1.45	0.2056
(AT-232.733)*(AT-232.733)	-10.93157	59.43064	-0.18	0.8613
(AIR-40)*(AIR-40)	224.44814	45.03472	4.98	0.0042

Prediction Profiler

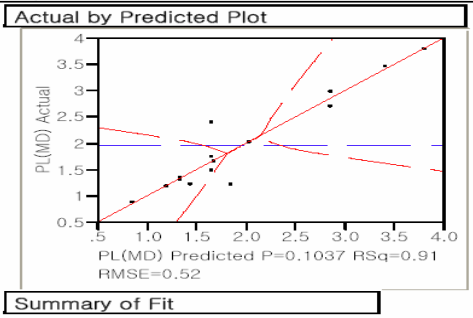


Peak force of TPU_{280}

58280-MD- Fit Least Squares

Response PL(MD)

Actual by Predicted Plot



Summary of Fit

RSquare	0.905476
RSquare Adj	0.669167
Root Mean Square Error	0.520005
Mean of Response	1.958
Observations (or Sum Wgts)	15

Analysis of Variance

Source	DF	Sum of Squares	Mean Square	F Ratio
Model	10	10.361220	1.03612	3.8317
Error	4	1.081620	0.27041	Prob > F
C. Total	14	11.442840		0.1037

Parameter Estimates

Term	Estimate	Std Error	t Ratio	Prob>|t|	Lower 95%	Upper 95%	VIF
Intercept	−32.79051	6044326	−0.00	1.0000	−16781773	16781708	.
DCD	−0.033834	0.011984	−2.82	0.0477	−0.067107	−0.000561	1.0106279
CS	−0.263245	1259235	−0.00	1.0000	−3.4962e6	3496195.7	0
TP	−1.535004	18.17018	−0.08	0.9367	−51.98351	48.913504	13.430629
AIR	−0.1305	0.03677	−3.55	0.0238	−0.23259	−0.02841	1
DT	0.1329751	0.097621	1.36	0.2448	−0.138066	0.4040158	1.8232505
AT	0.0611079	0.06547	0.93	0.4035	−0.120665	0.2428808	3.0899502
(DCD−52.4867)*(DCD−52.4867)	0.0008768	0.000766	1.15	0.3160	−0.001249	0.0030029	1.4441424
(TP−0.15)*(TP−0.15)	67.19234	238.0263	0.28	0.7917	−593.6746	728.05929	12.620367
(AIR−40)*(AIR−40)	0.0084904	0.004468	1.90	0.1302	−0.003914	0.0208943	1.2794008
(AT−232.733)*(AT−232.733)	0.0029006	0.007271	0.40	0.7103	−0.017286	0.0230878	4.1483356

Effect Tests

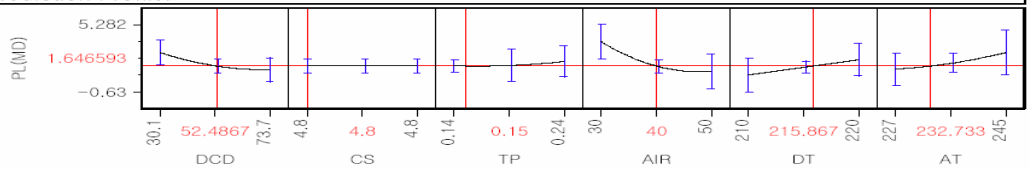
Source	Nparm	DF	Sum of Squares	F Ratio	Prob > F
DCD	1	1	2.1552902	7.9706	0.0477
CS	1	1	0.0000000	0.0000	1.0000
TP	1	1	0.0019298	0.0071	0.9367
AIR	1	1	3.4060500	12.5961	0.0238
DT	1	1	0.5017242	1.8555	0.2448
AT	1	1	0.2355750	0.8712	0.4035
DCD*DCD	1	1	0.3545472	1.3112	0.3160
TP*TP	1	1	0.0215479	0.0797	0.7917
AIR*AIR	1	1	0.9766300	3.6117	0.1302
AT*AT	1	1	0.0430358	0.1592	0.7103

Scaled Estimates

Continuous factors centered by mean, scaled by range/2

Term	Scaled Estimate	Std Error	t Ratio	Prob>|t|
Intercept	1.6465929	0.21849	7.54	0.0017
DCD	−0.737572	0.261251	−2.82	0.0477
CS	0	0	0.00	1.0000
TP	−0.07675	0.908509	−0.08	0.9367
AIR	−1.305	0.367699	−3.55	0.0238
DT	0.6648757	0.488107	1.36	0.2448
AT	0.549971	0.589227	0.93	0.4035
(DCD−52.4867)*(DCD−52.4867)	0.4167096	0.363918	1.15	0.3160
(TP−0.15)*(TP−0.15)	0.1679808	0.595066	0.28	0.7917
(AIR−40)*(AIR−40)	0.8490383	0.446755	1.90	0.1302
(AT−232.733)*(AT−232.733)	0.2349513	0.588939	0.40	0.7103

Prediction Profiler

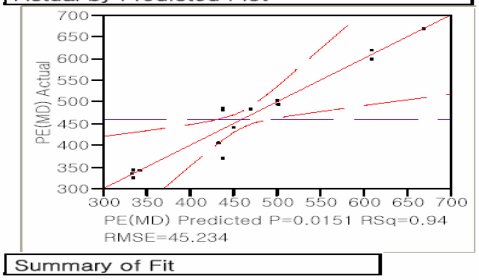


Peak elongation of TPU_{280}

58280-MD- Fit Least Squares

Response PE(MD)

Actual by Predicted Plot



Summary of Fit

RSquare	0.938304
RSquare Adj	0.827252
Root Mean Square Error	45.23363
Mean of Response	458.8
Observations (or Sum Wgts)	15

Analysis of Variance

Source	DF	Sum of Squares	Mean Square	F Ratio
Model	9	155589.99	17287.8	8.4492
Error	5	10230.41	2046.1	Prob > F
C. Total	14	165820.40		0.0151

Lack Of Fit

Source	DF	Sum of Squares	Mean Square	F Ratio
Lack Of Fit	1	1267.740	1267.74	0.5658
Pure Error	4	8962.667	2240.67	Prob > F
Total Error	5	10230.407		0.4938
				Max RSq
				0.9459

Parameter Estimates

Term	Estimate	Std Error	t Ratio	Prob>|t|	Lower 95%	Upper 95%	VIF
Intercept	-4200.98	5.2578e8	-0.00	1.0000	-1.3516e9	1.35155e9	.
DCD	-6.236204	1.042388	-5.98	0.0019	-8.915746	-3.556661	1.010502
CS	453.97797	1.0954e8	0.00	1.0000	-2.8157e8	281574206	0
TP	635.83251	480.2652	1.32	0.2428	-598.7286	1870.3936	1.2400297
AIR	-16.35	3.198501	-5.11	0.0037	-24.57201	-8.127992	1
DT	17.419535	8.450174	2.06	0.0943	-4.302329	39.1414	1.8054227
AT	-1.769317	5.692786	-0.31	0.7685	-16.40309	12.864456	3.0875426
(DCD-52.4867)*(DCD-52.4867)	0.0606269	0.065869	0.92	0.3996	-0.108694	0.2299476	1.4121395
(AIR-40)*(AIR-40)	0.6781938	0.385759	1.76	0.1391	-0.313431	1.669818	1.2606386
(AT-232.733)*(AT-232.733)	0.1059636	0.628483	0.17	0.8727	-1.509604	1.7215309	4.0962116

Effect Tests

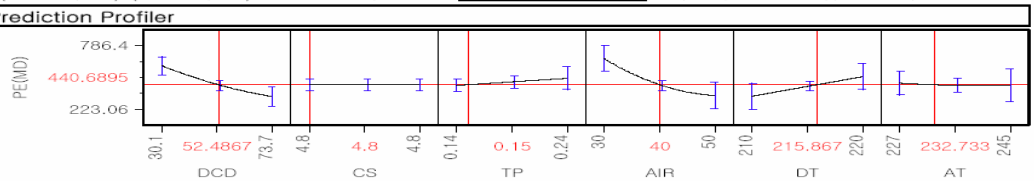
Source	Nparm	DF	Sum of Squares	F Ratio	Prob > F
DCD	1	1	73232.708	35.7917	0.0019
CS	1	1	0.000	0.0000	1.0000
TP	1	1	3586.295	1.7528	0.2428
AIR	1	1	53464.500	26.1302	0.0037
DT	1	1	8694.902	4.2495	0.0943
AT	1	1	197.644	0.0966	0.7685
DCD*DCD	1	1	1733.387	0.8472	0.3996
AIR*AIR	1	1	6324.105	3.0908	0.1391
AT*AT	1	1	58.163	0.0284	0.8727

Scaled Estimates

Continuous factors centered by mean, scaled by range/2

Term	Scaled Estimate	Std Error	t Ratio	Prob>|t|
Intercept	440.68949	19.23707	22.91	<.0001
DCD	-135.9492	22.72405	-5.98	0.0019
CS	0	0	0.00	1.0000
TP	31.791625	24.01326	1.32	0.2428
AIR	-163.5	31.98501	-5.11	0.0037
DT	87.097677	42.25087	2.06	0.0943
AT	-15.92386	51.23508	-0.31	0.7685
(DCD-52.4867)*(DCD-52.4867)	28.812305	31.30341	0.92	0.3996
(AIR-40)*(AIR-40)	67.819376	38.57587	1.76	0.1391
(AT-232.733)*(AT-232.733)	8.5830526	50.90713	0.17	0.8727

Prediction Profiler



VITA

Youn Eung Lee was born in Daejeon, Republic of Korea, on April 24, 1972. He went to Chungnam National University in 1991 and received a B.S. of Textile Engineering in 1998. He continued his study at Chungnam National University at Daejeon, Republic of Korea, and gained M.S. of Textile Engineering in 2000. He went to the University of Tennessee, Knoxville, USA, in January 2001 and received a Ph.D. degree in Materials Sciences and Engineering as Textile Science concentrated in the summer 2004.